Moscow International School of Earth Sciences - 2016

Moscow (23-28 May 2016)

ABSTRACTS

Vernadsky Institute of Geochemistry and Analytical Chemistry RAS

Vernadsky State Geological Museum RAS

Lomonosov Moscow State University

RSF | Russian Science Foundation

Supported by RSF №15-17-30019

Vernadsky Institute of Geochemistry and Analytical Chemistry RAS

Vernadsky State Geological Museum RAS

Lomonosov Moscow State University

Moscow International School of Earth Sciences - 2016

Moscow (23-28 May 2016)

ABSTRACTS

ГЕОХИ

UDC 55

Editor-in-chief
Academician L.N. Kogarko
Reviewers:
Ph.D. V.N. Ermolaeva
Ph.D. N.V. Sorokhtina
Ph.D. V.A. Zaitsev

All papers are presented in author's edition.

Moscow International School of Earth Sciences - 2016. Abstracts of International conference. 23-28 May 2016/ Editor-in-chief L.N. Kogarko. – M.: GEOKHI RAS, 2016. 136 с. – ISBN 978-5-905049-13-2.

Supported by Russian Foundation for Basic Research (№15-17-30019)

The Organising Committee of Moscow International School of Earth Sciences - 2016

Prof. Dr. Kogarko L.N. (GEOKHI RAS)	Chairman of the Conference
Dr. Plechov P.Y. (MSU)	Scientific coordinator of International School
Ph.D. Gerasimova E.I. (SGM RAS)	Coordinator of International School
Acad. Galimov E.M. (GEOKHI RAS)	Organizing Committee Member
Acad. Pushcharovsky D.Y. (MSU)	Organizing Committee Member
Acad. Malyshev Y. N. (SGM RAS)	Organizing Committee Member
Acad. Ryabchikov I.D. (GEOKHI RAS)	Organizing Committee Member
Dr. Kostitsyn Y.A. (GEOKHI RAS)	Organizing Committee Member
Ph.D. Cherkasov S.V. (SGM RAS)	Organizing Committee Member
Ph.D. Aksenov S.M. (GEOKHI RAS)	Organizing Committee Member
Ph.D. Sorokhtina N.V. (GEOKHI RAS)	Organizing Committee Member
Ph.D. Zaitsev V.A. (GEOKHI RAS)	Organizing Committee Member

ISBN 978-5-905049-13-2

Content

Moon rediscovered

Bagdassarov N.B.
Institut für Geowissenschaften, Goethe-Universität, Frankfurt am Main, Germany

Recent oxygen isotopic studies of lunar samples contrained a realistic model for primordial oxygen isotopic reservoirs. These results favor vigorous mixing during the giant impact and therefore a high-energy, high-angular-momentum impact between Theia (LV) and the proto-Earth[1].

Lunar reflectance spectra of the near and far lunar sides explain a dichotomy of topography, crustal thickness, mare volcanic activity and elemental concentrations. This dichotomous difference in mafic mineral abundance between the near and the far sides may have originated from the solidification stage of the crust from the lunar magmatic ocean (LMO)[2].

From other side, there are new constrains of mineralogical and thermal structure of the Moon based on the analysis of Love-number and magneto-electric observations on the lunar surface. Therefore the thermal evolution of the moon beginning from the moment of the complete differentiation till today may be modeled using a finite difference code. For the thermal evolution model the parameters of thermal conductivity, heat capacity and density are taken as temperature and pressure dependent, resulting in a time-dependence of these properties during cooling of the Moon. Furthermore, the convection inside the Moon can be implemented using an effective thermal conductivity based on Nusselt number.

Melting processes and the related latent heat of iron and silicate melting are taken into account using an effective heat capacity. The radiogenic heat production is modelled including a fractionation of incompatible radioactive elements into a temporally growing lunar crust. The derived selenotherm is used for the modeling of elastic deformation response due to the Earth-Moon-tides in a form of the k_2 Love number and the tidal dissipation factor Q. The electrical conductivity of the lunar rocks is evaluated from the temperature profile in order to calculate the lunar day side magnetometer transfer function located on the Moon. Additionally, the electrical conductivtity measurements of lunar analogue materials have been carried out. The modelled results are compared with the observed lunar mass, moment of inertia, recently monitored k_2 Love number and magnetometer transfer-function. The parameters of mineralogical boundaries between crust/upper-mantle, upper/lower mantle and core/mantle, the lunar minerals water content and the initial temperature after differentiation are constrained by applying a fitting procedure to choose "the best possible" lunar model. The obtained results imply that the lunar near side crust has a thickness of 40 ±3 km, the internal-mantle boundary lies in a depth of 930 ±14 km below the surface and the radius of the solid core is 475 ±9 km. Further the initial temperature after differentiation is found to be likely 2910 ±40 K. The amount of water in the lunar mantle minerals is about 15 ±3 ppm.

The lunar crust, especially on the near side, experienced a significant global stress resulted from relaxation of early lunar tidal and rotational bulges from despinning and orbital recession[3]. Diurnal tidal stresses on the lunar surface are small relatively small in comparison with global contraction stress, but still result in a net non-isotropic compressional stress field. This non-isotropic compressional stress is expected to result in thrust faulting with preferred orientations on the near lunar side[4].

References:

1. Young et al., Science, 2016, 351(6272): 493-396.
2. Ohtake et al., Nature Geoscience, 2012, 5: 384-388.
3. Melosh, 1980, Icarus, 43: 334–337 4. Watters et al., Geology, 2015, 43(10): 851–854).

Modern methods of igneous petrology

Blundy J.
Professor at School of Earth Sciences of the University of Bristol, UK

It is approximately 100 years since the pioneering work of N.L. Bowen established the idea of a magma chamber, a predominantly liquid-filled, crustal vat in which magmas undergo crystallisation and degassing, and where most magmatic differentiation occurs. Magma chambers have remained a central concept in our understanding of how magmatic systems work and how volcanic eruptions are driven. Recently it has become clear that the magma chamber concept is no longer consistent with many features of magmatic systems, petrologically, thermally and geophysically. Seismic and magnetotelluric surveys have failed to find any liquid-rich cavities of significant volume beneath active volcanoes, and most igneous rocks show a complex, polybaric evolution. It seems likely that magmatic systems are in a mushy, partially-molten state throughout most of their lifetimes. Such systems may be very long-lived and traverse much of the continental crust. Periodic destabilisation of mush systems is predicted from a thermal and mechanical standpoint and may be critical in triggering volcanic eruptions. I will review some aspects of mush-rich magmatic systems and explore their physical and chemical consequences with reference to volcanoes in the Cascades, Andes and Lesser Antilles.

Multivalent elements in magmatic melts with special emphasize on ferric/ferrous ratio

Borisov A.A.
Institute of Geology of Ore Deposits, Petrography, Mineralogy, and Geochemistry (IGEM), Russian Academy of Sciences, aborisov@igem.ru

The effect of SiO_2 (Borisov and McCammon, 2010), TiO_2, P_2O_5 (Borisov et al., 2013), total FeO, Al_2O_3, MgO (Borisov et al., 2015), CaO, Na_2O and K_2O (Borisov et al., in prep.) on the ferric/ferrous ratio in silicate melts was investigated in model silicate melts in the temperature range 1400-1550°C at 1 atm total pressure. The experiments were done mostly in air and partially in pure CO_2.

It is demonstrated that an increase in Al_2O_3 content in a basic melt results in a moderate decrease of Fe^{3+}/Fe^{2+} ratio. In contrast, the increase in Al_2O_3 in more silicic melts results in a much more pronounced decrease of Fe^{3+}/Fe^{2+} ratio. The increase of MgO content in a basic melt results in a moderate increase of Fe^{3+}/Fe^{2+} ratio but has a negligible effects in more silicic melts. The different behavior of Al_2O_3 and MgO in basic and silicic melts indicates that at constant T-fO_2-conditions the effects of melt composition on ferric/ferrous ratio cannot be predicted accurately with Sack's et al. (1980) model, that is as a function of $\Sigma d_i X_i$ where d_i are empirical coefficients and X_i are mole fractions of the main oxide component in silicate melts. We suggest an alternative approach which accounts for the interaction of cations in complex silicate melts.

We also found that an increase in K_2O content results in essential increase of Fe^{3+}/Fe^{2+} ratio both in peralkaline and peraluminous melts. It contradicts to previous results obtained by Dickenson and Hess (1981) in SiO_2-Al_2O_3-"Fe_2O_3"-K_2O system.

References:

1. Borisov A., McCammon C. (2010) The effect of silica on ferric/ferrous ratio in silicate melts: An experimental investigation using Mössbauer spectroscopy. American Mineralogist 95, 545-555.
2. Borisov A., Behrens H., Holtz F. (2013) The effect of titanium and phosphorus on ferric/ferrous ratio in silicate melts: an experimental study. Contribution to Mineralogy and Petrology 166, 1577-1591.
3. Borisov A., Behrens H. and Holtz F. (2015) Effects of melt composition on Fe^{3+}/Fe^{2+} in silicate melts: a step to model ferric/ferrous ratio in multicomponent systems. Contributions to Mineralogy and Petrology 169, Article 24.
4. Dickenson M.P. and Hess P.C. (1981) Redox equilibria and the structural role of iron in aluminosilicate melts. Contributions to Mineralogy and Petrology 78, 352-357.
5. Sack R.O., Carmichael I.S.E., Rivers M.L., Ghiorso M.S. (1980): Ferric-ferrous equilibria in natural silicate liquids at 1 bar. Contribution to Mineralogy and Petrology 75, 369-376.

Large Igneous Provinces: links to supercontinent breakup, climate change, including extinction events, and major ore deposits

Ernst R.E.
Department of Earth Sciences of Carleton University, Canada

A Large Igneous Province (LIP) represents a large volume (>0.1 Mkm^3; frequently above >1 Mkm^3), mainly mafic (-ultramafic) magmatic event of intraplate affinity, that can occur in both a continental and oceanic setting, and is typically of short duration (<5 m.y.) or consists of multiple short pulses over a maximum of a few 10s of m.y. A LIP comprises volcanic packages (flood basalts), and a plumbing system of dykes, sills and layered intrusions. LIPs can also be associated with silicic magmatism, carbonatites and kimberlites. LIPs occur throughout the Phanerozoic and Proterozoic, at a rate of about 1 event per 20 to 30 m.y. Archean examples are known (as well as planetary analogues). LIP events are linked with mantle plumes, continental breakup, global climate change including extinction events, and represent significant reservoirs of energy and metals that can either drive or contribute to a variety of metallogenic systems (for example, the Ni-Cu-PGE ores of the Norilsk region as part of the 251 Ma Siberian Trap LIP). In addition, LIPs can also affect hydrocarbon and aquifer systems.

Reference:

1. Ernst, R.E. (2014) Large Igneous Provinces. Cambridge University Press, 653 p.

Seismological and Geophysical Studies around Cairo area, Egypt

Hassan G.S.

Egypt, Minia University, Faculty of Engineering, Petroleum Engineering Department gseliem@yahoo.com

Cairo area plays an important role in both historical and recent seismicity. Seismic activities in and around Cairo suggest interested geodynamic behavior of this area due to the existence of local seismo- active tectonic from one side. On the other side, its location indicates the effect of the regional tectonic between the African plate and both the Eurasian and Arabian plates on it.

The main target of this study was to delineate the crustal deformation in this area using geophysical and geodetic measurements. These measurements over the geodetic points are carried out in the same time. The calculated deformation analysis shows accumulated stress and strain covered the south and southeast of the area. Thus, it was important to determine subsurface structures attributed to the stress-strain accumulation and its relation to the earthquake occurrence. Temporal gravity variations could deliver important information about the mass redistribution attributed to the seismological activities and can be considered as important integration of the geodynamic studies of this area. Local seismic activity at the southern part of Cairo is triggered under the effect of the regional tectonic setting around Cairo especially from the Gulf of Suez at the East and slightly from the northern Mediterranean. Also it is affected by the regional tectonic settings around Cairo. This conclusion was agreed very well with the geodetic and geophysical results.

Key words:

African plate, Regional tectonic setting, Arabian plate, Crustal deformation

Tectonic setting:

The study area is situated in the northern part of the African plate. The distribution of the major fault trends in Northern Egypt, as well as the volcanic outcrops close to Dahshour area were shown in Fig.(1) . The first trends WNW–ESE, while the second trends NW-SE. The WNW - ESE faults are of diagonal-slip movements, where the horizontal sense of dislocation is always of right- lateral type and the vertical displacements are of normal type.

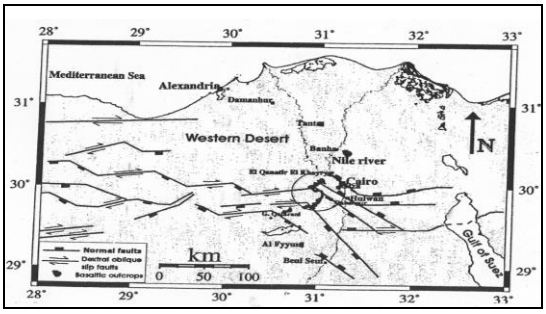

Fig.1 The distribution of major fault trends in northern Egypt as well as the basement outcrops close to Dahshour area, the down circle points to the major faults intersections close to Dahshour area, modified (after Hussein and Abd-Allah 2001).

Seismicity:

The activity along the NW-SE trend is mainly attributed to the Red sea rifting and characterized by shallow earthquakes and micro- earthquakes (Kebeasy,1990). The high level of seismic activity in the Cairo-Suez district is interpreted to be a result of the interaction between the African, Arabian and Eurasian plates.

The focal mechanism solutions of the strong seven earthquakes, that occurred during this period, have been determined form the P-wave first onsets at the different Egyptian National Seismic Network (ENSN) stations (Badawy et al.,2003) . All solutions show normal faulting mechanism with strike-slip component (Fig.2).

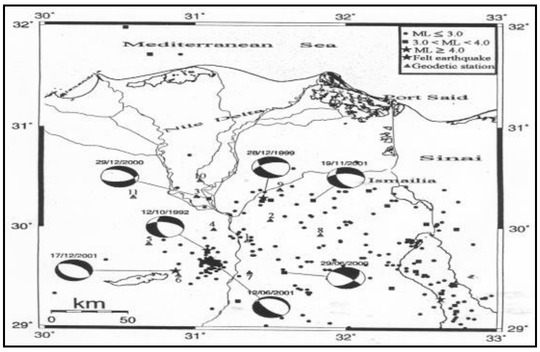

Fig.2 Earthquake fault plane solutions of strong seven earthquakes around Cairo region.

New models for kimberlite parental melts: composition, temperature, ascent and emplacement

Kamenetsky V.S.[1], Golovin A.V.[2], Maas R.[3], Yaxley G.M.[4], Kamenetsky M.B.[1]

1 -University of Tasmania, Hobart, Australia, Dima.Kamenetsky@utas.edu.au

2 -V.S. Sobolev Institute of Geology and Mineralogy, Novosibirsk, Russia

3 -University of Melbourne, Melbourne, Australia

2 -Australian National University, Canberra, Australia

Kimberlites represent magmas derived from great mantle depths and are the principal source of diamonds. Kimberlites and their xenolith cargo have been extremely useful for determining the chemical composition, melting regime and evolution of the subcontinental mantle. Significant effort has gone into characterizing styles of emplacement, ages, petrography, mineralogy, textural and compositional characteristics, and the tectonic setting of kimberlites. However, a full understanding of kimberlite petrogenesis has been hampered by effects of pre-emplacement contamination, syn-emplacement stratification and syn/post-emplacement alteration of kimberlite rocks, all of which tend to hinder recognition of primary/parental kimberlite magma compositions. The prevailing practice of using bulk kimberlite compositions to derive parental compositions has been challenged by research on the Devonian Udachnaya-East pipe and other relatively fresh kimberlites worldwide.

Since its discovery in 1956, the Udachnaya kimberlite pipe has become a “type locality” for geochemists and petrologists studying mantle rocks and mantle physical-chemical conditions. Apart from hosting a diverse suite of extremely well-preserved mantle xenoliths, the host kimberlite (East body) is the only known occurrence of fresh kimberlite, with secondary serpentine almost absent and uniquely high Na_2O and Cl (up to 6.2 wt.%) and low H_2O (< 1 wt.%) contents. The discovery of such compositional features in the only unaltered kimberlite has profound implications for models of parental kimberlite magma compositions, and the significance of the high Na and Cl abundances in the Udachnaya-East pipe has therefore been subjected to vigorous criticism. The main argument against a primary magmatic origin of high Na - Cl levels involves the possibility of contamination by salt-rich sedimentary rocks known in the subsurface of the Siberian platform, either by assimilation into the parental magma or by post-intrusion reaction with saline groundwaters.

The main evidence against crustal contamination of parental kimberlite magmas is that the serpentine-free varieties of the Udachnaya-East kimberlite owe their petrochemical and mineralogical characteristics to a fortuitous lack of interaction with syn- and post-magmatic aqueous fluids. The groundmass assemblage of this kimberlite, as well as earlier-formed melt inclusions, contains alkali carbonate, chloride and other Na- and Cl-bearing minerals. This mineralogy reflects enrichment of the parental melt in carbonate, chlorine and sodium. The combination of low H_2O, high alkali-Cl abundances, lack of serpentine, and the presence of alteration-free mantle xenoliths all indicate that the Udachnaya-East kimberlite preserves pristine compositions in both kimberlite and mantle xenoliths. Evidence for broadly similar chemical signatures is found in melt inclusions from kimberlites in other cratons (South Africa, Canada, Finland and Greenland). We demonstrate that two supposedly “classic” characteristics of kimberlitic magmas - low sodium and high water contents - relate to postmagmatic alteration. The alkali- and volatile-rich compositions of melt inclusions is responsible for low-temperature phase transformations during heating experiments, melting at <600°C, carbonate-chloride liquid immiscibility and homogenisation temperatures at ~650-800°C, well below the solidus of the high-Mg melt that is traditionally inferred to be primary kimberlite composition. Notably, records of heating stage experiments with melt inclusions from different kimberlites are broadly similar.

Previously inferred high liquidus temperatures (>1400°C) are inconsistent with geological evidence (e.g., absence of thermometamorphic effects), temperatures in the potential mantle source and melt inclusion data. We consider the protokimberlite liquid to be low temperature near the surface (<800°C), virtually anhydrous, aluminosilicate-poor, Na-Ca carbonate, enriched in lithophile trace elements, halogens, and sulphur. Although kimberlite magmas are dense in crystals and deeply-derived rock fragments, they ascend to the surface extremely rapidly, enabling diamonds to survive. The unique physical properties of kimberlite magmas depend on the specific compositions of their parental melts. We explain exceptionally rapid ascent of kimberlite magma from mantle depths by combining empirical data on the essentially carbonatite composition of the kimberlite primary melts and experimental evidence on interaction of the carbonate liquids with mantle minerals. Our experimental study shows that orthopyroxene is completely dissolved in a Na_2CO_3 melt at 2.0 to 5.0 GPa and 1000-1200°C. The dissolution of orthopyroxene results in homogeneous silicate-carbonate melt at 5.0 GPa and 1200°C, and is followed by unmixing of carbonate and carbonated silicate melts and formation of stable magmatic emulsion at lower pressures and temperatures. The dispersed silicate melt has a significant capacity for storing a carbonate component in the deep mantle (13 wt% CO_2 at 2.0 GPa). This component reaches saturation and is gradually released as CO_2 bubbles, as the silicate melt globules are transported upwards through the lithosphere by the carbonatite magma. The globules of unmixed, CO_2-rich silicate melt are continuously produced upon further reaction between the natrocarbonatite melt and mantle peridotite. On decompression the dispersed silicate melt phase ensures a continuous supply of CO_2 bubbles that decrease density and increase buoyancy and promote rapid ascent of the magmatic emulsion, and ultimately drives crack propagation and emplacement of kimberlite with its load of entrained ultramafic and crustal material into the crust. The melt saturation in olivine at low pressure prompts olivine crystallisation, which drives the residual melt towards the initial (protokimberlite) carbonatite composition.

The solubilities of H_2O and CO_2 in the model (ultramafic/ultrabasic) kimberlite melt at emplacement pressures are not as high, as measured abundances of these volatiles in kimberlite rocks. The low H_2O content of the kimberlite melt, as at least during emplacement in the crust, do not support fluidisation mechanism (i.e., rapid degassing and expansion of magmatic volatiles in an open system) of the kimberlite emplacement. Furthermore, a number of studies have convincingly demonstrated that kimberlite explosions were unexpectedly powerful for such small magma volumes. The evidence was interpreted as excavation and even emptying of pipes from top down to significant depths (up to 1 km), prior to filling with juvenile material and pulverised country rocks. Notably, eruptive activity was shown to be polyphase and span considerable time with intermittent episodes of violent venting out and periods of quiescence and sedimentation in crater lakes. Moreover, as manifested by the presence at significant depths in some pipes of relatively fresh, often uncharred wood fragments, plant leaves, animal and fish parts, the venting juvenile material was likely cold and even solid.

If the kimberlite magma does not experience H_2O and CO_2 degassing and is disrupted at subsolidus conditions, what causes the kimberlite explosive eruption? We hypothesise that emplacement of the kimberlite magma as subsurface dykes is followed by gravitational separation and sinking of dense olivine and xenoliths, whereas the buoyant carbonatitic liquid is squeezed to the top of intrusive bodies. Olivine-rich cumulates with interstitial carbonate-rich melt form the “root zones” of hypabyssal kimberlites, whereas the upper parts of dykes are composed of the carbonatite with scattered silicate minerals. The olivine-rich rocks worldwide are prone to intensive serpentinisation and associated production of H_2 and CH_4 through the Fischer-Tropsch synthesis. The amount of hydrogen produced is ~10% of the volume of serpentinised olivine. Thus the serpentisation may explain spontaneous outgassing of the UE kimberlite (~10^5 m^3/day at 50-70 atm; 52% H_2) recorded in the boreholes at the level of the lower aquifer.

We envisage that degrading water-soluble carbonatite in the upper parts of kimberlite intrusions was turned into a cavernous system that provided initial storage to the hydrogen- and methane-rich gases derived from serpentinisation of olivine cumulates in the kimberlite “root zone”. The oxidation of these flammable gases and/or their pressurisation in a single spot resulted in a powerful detonation and destruction of surrounding rocks, and possibly caused “chain reaction” by sending shock waves through the cavernous system and thus triggering numerous explosions. Subsequent detonation activity resulted in vertical and lateral explosive boring, and further fragmentation inside the dyke system and surrounding country rocks. This was followed by collapse of rocks from the top and walls and related growth of a carrot-shaped “diatreme” by excavation from top down and fragmentation on the contacts between the kimberlite and country rocks (i.e. in-situ “contact breccia”). While the idea of post-magmatic brecciation of kimberlite rocks is not entirely new, the role of combustible gases in the formation of kimberlite diatremes and their pyroclastic and volcaniclastic kimberlite facies is proposed for the first time.

We invite collaborations on microanalysis of individual mineral phases and phenocryst-hosted melt inclusions in the least altered kimberlite samples from different localities. It is important to maintain an open mind, to not doggedly stick to increasingly untenable orthodox views, and to analyse emerging evidence on merit.

Ore potential of critical metals in alkaline magmatism and plume connection

Kogarko L.N.*

**V.I. Vernadsky Institute of Geochemistry and Analytical Chemistry, Russian Academy of Sciences, Moscow, Russia*

kogarko@geokhi.ru

The world’s largest deposits of REE, Nb, Ta, Sr, Al, P are related to alkaline rocks and carbonatites. The interest to alkaline rocks and carbonatites has grown significantly due to the increasing consumption of strategic metals in industry. This is well illustrated on an example of rare earth elements during the last several years. This is related to the extension of the utilization of REE in nuclear industry, in the production of high precision weapons and in the productioon of pure energy. In the center part of Kola Penunsula (Russia) there is ultramafic alkaline province comprising carbonatites , ultramafic rocks and two largest of the Globe layered peralkaline intrusion Khibina and Lovozero (370 Ma age [1,2]).

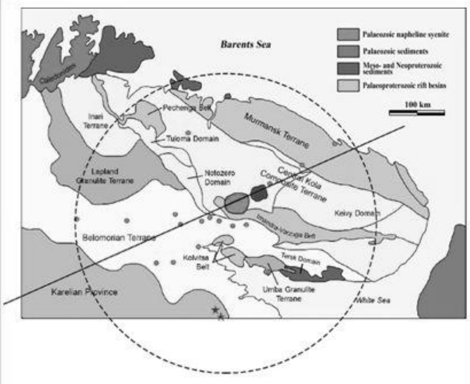

Fig.1 Lovozero massif

The Lovozero massif, contains super-large loparite (Na, Ce, Ca)$_2$ (Ti, Nb)$_2$O$_6$) rare-metal (Nb, Ta, REE) deposit and eudialyte

$(Na_{13}(Ca,Sr,REE)_6Zr_3(Fe,Nb,Ti)_3(Si_3O_9)_2[Si_9O_{24}(OH,Cl,S)_3]_2$ ores-the valuable source of zirconium, hafnium and rare earth.Khibina apatite and Lovozero loparite had been mined during many years and constitute a world class mineral district. The Lovozero Pluton [1] consists of three intrusive phases: [1] medium-grained nepheline and hydronosean syenites; [2] differentiated complex of urtites, foyaites, and lujavrites; and [3] eudialyte lujavrites.

The main ore mineral is loparite (Na, Ce, Ca)$_2$ (Ti, Nb)$_2$O$_6$, In the deepest zone of the intrusion loparite forms anhedral grains confined to interstitial spaces. Above 800m in stratigrafic section loparite makes up euhedral crystals which were formed at the early stage of crystallization. Therefore the initial magma was undersaturated with loparite. After the formation of approximately one-third of the volume of the Lovozerointrusion, the melt became saturated with loparite and this mineral accumulated in ore layers. The composition of cumulus loparite changed systematically upward through the intrusion with an increase in Na, Sr, Nb, Th, U and decrease in REE, Zr, Y, Ba and Ti. Our investigation indicates that the formation of loparite ore was the result of several factors including the chemical evolution of high alkaline magmatic system and mechanical accumulation of loparite as a heaviest phase at the base of convecting unit (Fig. 2).

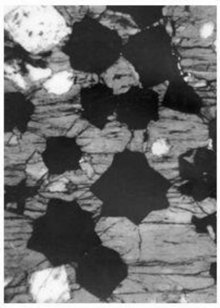

Fig.2 Loparite ore

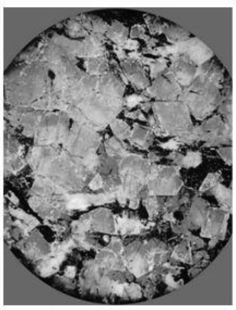

Fig.3 Loparite ore

Zirconium-hafnium-rare-earth deposit is situated in the upper part of Lovozero intrusion as horizontal lenticular bodies. The amount of Zr in eudialyte is very hight -up to 14 wt % and total REE up to 4 wt %. (fig.3) Morfology of eudialyte grains is changed with depth of Lovozero intrusion. (fig.) In the lower part of the intrusion eudialyte forms anhedral interstitial crystals and crystallised when rock-forming minerals generated well-developed framework when convection ceased and accumulation of eudialyte is impossible. In the upper part of Lovozero stratigrafic section eudialyte forms euhedral grains which were formed at the early stage of crystallization. Thus the initial magma of Lovozero complex was undersaturated with this mineral. The melt became saturated with eudialyte after the approximately two-third of the volume of the massif solidified. Compositional evolution of eudialyte has been investigated through a 2.35 km section of the Lovozero massif using CAMECA microprobe and LA-ICP-MS.

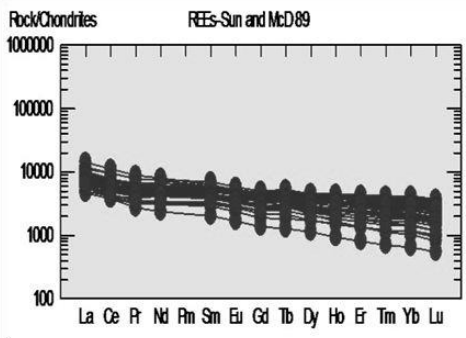

Fig.4 REE pattern of eudialyte

There is hidden layering in eudialyte in the crossection of the intrusion. The composition of cumulus eudialyte changed systematically upward through the third intrusion with an increase in Na, Sr, Nb, Th, Mn/Fe, Nb/Ta, U/Th and decrease in REE, Zr, V, Zn, Ba and Ti. The specific gravity of eudialyte is much higher then initial alkaline melt.

Nevertheless eudialyte accumulated in the very upper zone of Lovozero intrusion. We suggest that eudialyte formed very small crystals (nanoctystals) (fig.) which were stirred in melt and under the conditions of steady-state convection eudialyte emerged upward. Later eudialyte crystals recrystallized and increased in size (fig.).

The Khibina alkaline massif (Kola Peninsula, Russia) hosts the world's largest and economically most important apatite deposit. The Khibina massif is a complex multiphase body built up from a number of ring-like and conical intrusions. The apatite bearing intrusion is ring-like and represented by a layered body of ijolitic composition with a thickness of about 1-2 km. The upper zone is represented by different types of apatite ores. This rocks consists of 60-90% euhedral very small (tenths of mm) apatite crystals.

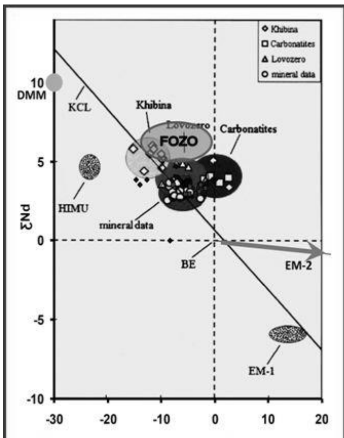

Fig.5 εNd versus εSr isotopic composition of Lovozero and Khibina rocks

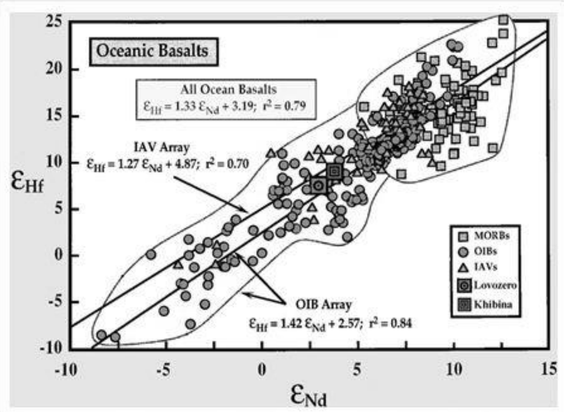

Fig.6 εNd versus εHf isotopic composition of the Lovozero and Khibina ore minerals

The lower zone is mostly ijolitic composition. The lower zone grades into underlying massive urtite consisting of 75-90% large (several mm) euhedral nepheline. Our experimental studies of systems with apatite demonstrated the near-eutectic nature of the apatite-bearing intrusion, resulting in practically simultaneous crystallization of nepheline, apatite and pyroxene.

The mathematical model of the formation of the layered apatite-bearing intrusion based on the processes of sedimentation under the conditions of steady state convection taking account of crystal sizes is proposed. Under the conditions of steady-state convection large crystals of nepheline continuously had been settling forming massive underlying urtite when smaller crystals of pyroxenes, nepheline and apatite had been stirred in the convecting melt. During the cooling the intensity of convection decreased causing a settling of smaller crystals of nepheline and pyroxene and later very small crystalls of apatite in the upper part of alkaline magma chamber.

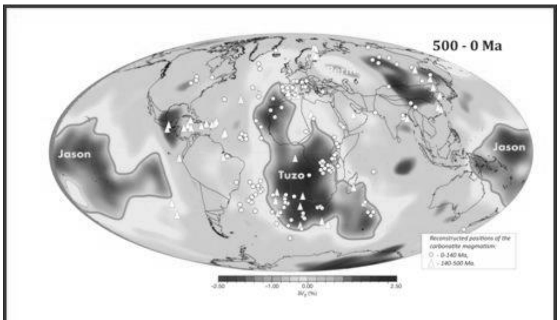

Fig. 7 Reconstructed localities of the Phanerozoic carbonatites

Geodynamic position of the alkaline rocks and carbonatites is actively discussed question during the last decades. Some researches link their formation with ascend of the large volumes of mantle melts from the CMB. There is certain evidence for temporal and spatial correlation of the carbonatites and LIPs, whose origin is certainly related with mantle plumes [4], as it was shown for carbonatites of the Polar Siberia (Maymecha-Kotuy province) which were formed simultiniusly with the Siberian superplume 250 Ma [5].

We used the recent absolute plate kinematic model [6] to reconstruct locations of Phanerozoic carbonatites at the time of their origin (Fig. 7). We have found that 118 out of 180 carbonatites (66%) are projecting onto central or peripheral parts of African Large Low Shear-wave Velocity Province and this can be viewed as an evidence for linking the carbonatites with mantle plumes.

References:

1. Kogarko L.N., Kononova V.A., Orlova M.P., Woolley A.R., 1995. Alkaline rocks and carbonatites of the world: Part 2. Former USSR. Chapman and Hall, 225 p. (London)
2. Kramm U., Kogarko L.N., 1994. Nd and Sr isotope signatures of the Khibina and Lovozero agpaitic centers, Kola Alkaline Province, Russia. Lithos. v. 32, p. 225-242.
3. Kogarko L. N., Lahaye Y. & Brey G. P., 2010. Plume-related mantle source of super-large rare metal deposits from the Lovozero and Khibina massifs on the Kola Peninsula, Eastern part of Baltic Shield: Sr, Nd and Hf isotope systematic. Miner Petrol. v. 98, p. 197-208.
4. Ernst R.E. Large Igneous Provinces. Cambridge University Press. 2014. 666 p.
5. Kogarko L., Zartman R.(2007) Min Petrol.89,113-132.
6. Torsvik T.H. et al. (2014) Proceedings of the National Academy of Sciences of the United States.111, 8735-8740.

Supported by RSCF grant 15-17-30019.

Isotopic constraints on the bulk silicate Earth (BSE) composition

Kostitsyn Y.A.

Vernadsky Institute of Geochemistry and Analytical Chemistry (GEOKHI) RAS

Analysis of published worldwide isotopic data for various terrestrial rocks permits to make an assessment of the isotopic and elemental ratios $^{143}Nd/^{144}Nd$, $^{176}Hf/^{177}Hf$, $^{87}Sr/^{86}Sr$, $^{206}Pb/^{204}Pb$, $^{207}Pb/^{204}Pb$, $^{208}Pb/^{204}Pb$ and Sm/Nd, Lu/Hf, Rb/Sr, U/Th/Pb in the primitive mantle.

The model of chondritic uniform reservoir (CHUR) of DePaolo and Wasserburg (1976) cause many unresolvable contradictions: (1) high magmatic productiveness of the depleted mantle without any clear isotopic signal from the primitive mantle; (2) most of geochemically enriched rocks, specifically alkaline basalts, have isotopic characteristics of a depleted source; (3) HIMU source is depleted enriched in U-Th-Pb isotopic system but depleted in Rb-Sr and Sm-Nd systems; (4) mass-balance calculations for Sm-Nd isotopic system constraints a size of depleted mantle as a crustal source by 1/4 to 1/5 part of the overall mantle mass, but in this case it is impossible to balance Rb, K, U, Th, Pb between the depleted mantle and the crust; (5) direct melts from chondritic mantle source must have neodymium isotopic composition and Sm/Nd ratios close to their source composition, but rocks with $e_{Nd} \approx 0$ and Sm/Nd ≈ 0.325 simultaneously are not known till now.

These contradictions may be resolved in assumption that Sm/Nd ratio of the primitive mantle is higher than chondritic value by 8% and $^{143}Nd/^{144}Nd$ is higher by 8 – 9 epsilon units. Correlations between neodymium, strontium, hafnium and led isotopic ratios aid to find other isotopic ratios of the primitive mantle and then calculate elemental ratios using isotopic ratioa as a proxy:

$\varepsilon_{Nd} = +9$, $^{143}Nd/^{144}Nd = 0.51309$, Sm/Nd = 0.350;

$\varepsilon_{Hf} = +14$, $^{176}Hf/^{177}Hf = 0.28318$, Lu/Hf = 0.268;

$\varepsilon_{Sr} = -22$, $^{87}Sr/^{86}Sr = 0.7029$, Rb/Sr = 0.0206;

$^{206}Pb/^{204}Pb = 18.37$; $^{207}Pb/^{204}Pb = 15.49$; $^{208}Pb/^{204}Pb = 37.97$;

$^{238}U/^{204}Pb = 8.82$, U/Pb = 0.1405; $^{232}Th/^{238}U = 3.81$, Th/U = 3.68.

Possible uncertainty of the neodymium isotopic ratio assessment is probably about $\pm 1\ \varepsilon_{Nd}$.

The primitive mantle composition in terms of some other elements could be found from element correlations in various mantle-derived rocks.

Lighting up the subsurface

Ludden J.

Executive Director, British Geological Survey, UK. Jludden@bgs.ac.uk

Global energy security throughout the next century will continue to depend significantly on fossil fuel and nuclear, while also unlocking the potential of renewable as well as unconventional sources. Many government's industrial strategies highlight the importance of continuing support for the oil and gas and nuclear sectors, while at the same time being required to meet ambitious emissions targets.

As geologist we will be increasingly required to work with the subsurface both as a source of energy and also a repository for waste products (CO2, nuclear waste) and also for storing energy (compressed air, heat etc.)

To facilitate the above we propose the creation of infrastructure "The Energy Test Bed" , shown in Figure 1, to allow the subsurface to be monitored at time scales that are consistent with our use of the subsurface, to increase efficiency and environmental sustainability, but also to act as a catalyst to stimulate investment and speed new technology energy options to commercialisation.

It will thus act as a bridge from ideas to application and would attract support and possible co-funding from oil and gas companies, utilities and energy and environment consultancies.

An integrated multicomponent sub-surface monitoring infrastructure linked with the European Plate Observing System (EPOS) and the global energy test beds this infrastructure would underpin the following:

1. the impact of deep shale gas drilling and hydraulic fracturing on shallow groundwater and surface water, on seismic activity, and on ground stability and subsidence;
2. processes relating to the containment, confinement, and rates of solution and carbonation of subsurface stored CO2 in carbon capture and storage;
3. processes relating to the containment and confinement of subsurface nuclear and other types of waste; movement of fluids (gas, water, solutes);
4. studies on the impact of coal combustion products on the environment both from surface and subsurface operations (e.g. underground coal gasification);
5. the role of biological mediation in the subsurface in shallow to deep environments;
6. processes at basin and reservoir scale in reservoir stimulation and enhanced oil recovery (EOR);

7. Ground deformation and induced seismicity associated with enhanced geothermal systems in hot-rock-dry-rock environments.
8. The possibility of supercritical geothermal in high geothermal gradient environments
9. Subsurface storage of potential energy (compressed air, water) and heat

In the UK and worldwide we need would develop a unique package of monitoring capability where monitoring at the surface and in the critical zone will be coupled with deep borehole monitoring of variables such as pressure, temperature, heat flow, seismicity, tilting, strain accumulation, fluid chemistry, pH and biological properties. Monitoring will also include satellite and remote sensed data such as InSAR (Interferometric synthetic aperture radar) and gravity, electrical, spectral and magnetic data.

Fig. 1: The Geological Environments for Energy Test Beds

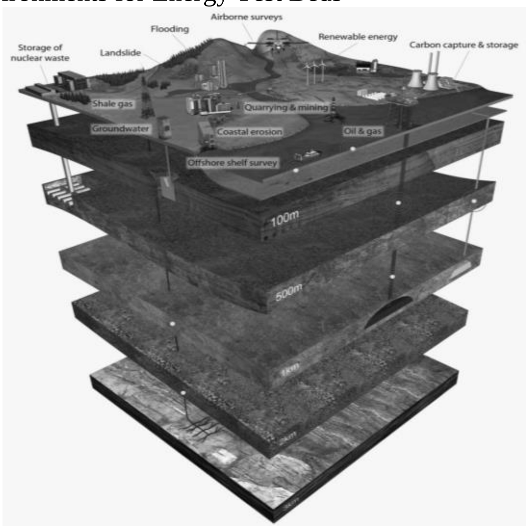

As geologists we will be in a position to reassure the public that we are able to use the subsurface and the infrastructure that underpins this will make us better at monitoring and managing these new and continuing activities safely and sustainably, including optimising exploration practices. Industry would benefit in being able to access state-of–the–art monitoring data to maximise efficiency of extraction and subsurface management, as well as maximising environmental sustainability.

Links:

1. BGS energy test bed http://www.bgs.ac.uk/research/energy/shaleGas/esios.htm, Energy Security and Innovation Observing System for the Subsurface (ESIOS).
2. European Plate Observing System http://www.epos-eu.org/
3. British Geological Survey http://www.bgs.ac.uk/home.html

Structural and chemical complexity of minerals and their evolution with time

Krivovichev S.V.
St.Petersburg State University University Emb. 7/9 199034 St.Petersburg Russia
s.krivovichev@spbu.ru

Complexity is one of the most interesting and rather unexplored themes in modern mineralogy. Recently, complexity of crystalline solids received a renewed attention from the various points of view, including its role in the interpretation of energy landscapes in solids [1], mathematical description of complex alloys [2], analysis of disordered materials [3], etc.

According to the information-theoretic approach developed in [4-7], complexity of a crystal structure can be quantitatively characterized by the amount of Shannon information it contains measured in bits (binary digits) per atom (bits/atom) and per unit cell (bits/cell), respectively. For a crystal structure, the calculation involves the use of the following equations:

$$IG = -\sum_{i=1}^{k} p_i \log_2 p_i \text{ (bits/atom) (1),}$$

$$IG,total = -v \sum_{i=1}^{k} p \quad IG = -vi \log2 pi \text{ (bits/cell)} \quad (2),$$

where k is the number of different crystallographic orbits (independent crystallographic Wyckoff sites) in the structure and pi is the random choice probability for an atom from the ith crystallographic orbit, that is:

$$pi = mi / v \quad (3),$$

where mi is a multiplicity of a crystallographic orbit (i.e. the number of atoms of a specific Wyckoff site in the reduced unit cell), and v is the total number of atoms in the reduced unit cell. It has recently been shown [77] that the IG value provides a negative contribution to the configurational entropy (Scfg) of crystalline solids in accordance with the general principle that the increase in structural complexity corresponds to the decrease of the Scfg value.

Shannon information can also be used to estimate chemical complexity of minerals.

The fundamental questions of interest for mineralogy are: (i) how are structural and chemical complexities of minerals related to each other? (ii) does structural complexity influence the processes of mineral crystallization? (iii) how structural complexity of minerals and mineral associations changes with temperature and/or pressure? (iv) how structural and chemical complexity of minerals (crystalline solids of natural origin) evolves through the age of the Universe? These questions will be considered in our contribution.

References:

1. Oganov, A.R. & Valle, M. (2009): How to quantify energy landscapes of solids. J. Chem. Phys. 130, 104504.
2. Hornfeck, W. & Hoch, C. (2015): Structural chemistry and number theory amalgamized: crystal structure of Na11Hg52. Acta Cryst. B71, 752-767.
3. Varn D.P. & Crutchfield J.P. (2016): What did Erwin mean? The physics of information from the materials genomics of aperiodic crystals and water to molecular information catalysts and life. Phil. Trans. R. Soc. A 2016 374 20150067 DOI: 10.1098/rsta.2015.0067
4. Krivovichev, S.V. (2012): Topological complexity of crystal structures: quantitative approach. Acta Cryst. A68, 393-398.
5. Krivovichev, S.V. (2013): Structural complexity of minerals: information storage and processing in the mineral world. Mineral. Mag. 77, 275-326.
6. Krivovichev, S.V. (2014): Which inorganic structures are the most complex? Angew. Chem. Int. Ed. 53, 654-661.
7. Krivovichev, S.V. (2016): Structural complexity and configurational entropy of crystalline solids. Acta Cryst. B72, 274-276.

Petrological ore content peculiarities of the Mesozoic magmatism of Lesser Caucasus

Mammadov M.N., Babayeva G.J., Gasanguliyeva M.Ya., Abasov K.F.

Institute of Geology and Geophysics of the Azerbaijan National Academy of Sciences

musamamedov@rambler.ru

Mesozoic magmatic complexes within the Lesser Caucasus have mainly developed in the Lok-Gafan structural-formational zone.

This zone on the outer periphery of Lesser Caucasus and parallel to the south board of the Kura intermountain trough is traced from the west of Lok crystalline core-area in the east direction up to Araz River. This structural-formational zone according to Shikhalibeyli (1994) is separated into Lok-Agdam, Geycha-Garabag and Gafan subzones. Within Lok-Agdam subzone Mesozoic magmatic complexes are mainly developed in Alaverd, Shamshadin, Murovdag and Agdam anticlinoria and in Gazakh, Dashkesan, Aghjakend and Agderin synclinoria.

Mesozoic magmatic complexes are characterized as Middle Jurassic, Late Jurassic, Early Cretaceous and Late Cretaceous development stages of Lok- Agdam structural-formational zone and as the part of the above-mentioned structures.

The earliest magmatic processes within Lok-Agdam zone in effusive-pyroclastic facies were manifested in Early Bajocian. The vulcanites are mainly composed by pyroclastic andesite-basalts, andesites and subordinate lava sheets of these rocks overlie unconformably on the sandy-clay deposits of Aalenian stage. These vulcanites are conformably overlain by Late Bajocian marked lava-pyroclastic facies of quartz-plagioporphyries.

The volcanic process was accompanied by sedimentation at the Bathonian development stage of Lok-Agdam subzone. The part of sedimentary and volcanogenic-sedimentary formations increases sharply at the end of Bathonian time. The vulcanites of Bathonian complex are composed by sequentially differentiated basalts, andesites, dacites and rhyolites.

Plutonic comagmatites of Upper Bajocian and Bathonian volcanic complexes have been represented by Atabek-Slavyan, Gilanbir, Mekhrab, Akhnat plagiogranite and Blyuldyuz gabbro-plagiogranite intrusives.

The plagiogranites are characteristic and most distributed petrographic rocks types of the above-mentioned intrusives. The granophyric, porphyry, aplite-like leucocratic differences of plagiogranites are differed in the structural and textural peculiarities and the quantitative content of intermediate orthoclase among them.

The quartz, oligoclase and albite plagioclase take part predominantly in the composition of the mentioned rocks types (An_{6-15}).

Generally intermediate orthoclase (2V = 80-87, dhk_{l201} = 4.223-4.236Å, Or_{83-96}) as xenomorphic segregation is situated in the range of quartz and plagioclase. Hornblende and biotite are participated as the individual grains. The accessory minerals content aren't more than 1-3% which are formed by orthite, epidote, magnetite, ilmenite, apatite, zircon, sphene and etc.

However the orthoclase content increase in the composition of subalkalic aplite-like pegmatite and leucocratic granite as well as the presence of tourmaline in the contact zone indicate that accompanying volatile components barium, potassium, rubidium, boron, flor and other were accumulated in the residual melt.

In this regard the copper-molybdenum mineralization is observed in areola of Atabey-Slavyan intrusive among the metasomatic formations. Unlike the previous one Late Jurassic-Early Cretaceous magmatic complexes are the most productive ore-bearing. They are well represented in the Lok-Agdam, Geycha-Akeri and Gafan subzones of Lok-Gafan structural-formational zone.

The intrusives are characterized by clearly defined facial and phase diversities here. Within each phase the transition between petrographic rocks types is gradual i.e. due to crystallization differentiation the gabbroids are changed to diorite, quartz diorite. In the second phase the quartz diorite changes gradually to granodiorite, tonalite, banatite. Finally granites, pegmatites, alaskites are appeared in the next phase.

Along with them picrites and picrobazalts appear within Murovdag anticlinorium. It is necessary to note that in the most cases diorites and their quartz differences are often changed to monozo-diorite, monzonite and even to syenite. More likely gold-sulphide, copper-sulphide mineralizations are connected with hydrothermal solutions of quartz-diorite phase of the mentioned intrusives.

It seems likely that copper-polymetallic, barite-metallic and copper-molybdenum mineralizations are connected with monzonite, monzo-diorite and syenite.

Later Cretaceous gold-polymetallic fields of Gazakh, Aghjakend and Bolnis troughs spatially are closely associated with albitized rhyolite and porphyric subalkalic diorite and granite. Obviously the in-coherence of subalcalic elements was ore parent factor here as in the previous ones. In this regard they have also concentrated in the composition of hydrothermal solutions besides residual liquid thereby barite-copper polymetallic mineralizations were formed in the aureolas of subalcalic porphyric quartz diorites, granites and albitized rhyolites.

In the a result of the separation of the Lok-Gafan zone into Lok-Agdam, and Gafan subzones such graben-shaped troughs as Khojakend, Azykh, Gochas were formed during subduction process in the south-western and south-eastern shoulders of the mentioned zone. The alkalic and subalkalic magmatism of the main and intermediate composition were manifested in these troughs in Late Cretaceous time (Santonian-Maastrichtian).

With petrological viewpoint the ore-forming potential of the considered intrusives, in all probability, is closely connected with sufficient concentration of these elements in the composition of the initial melts. In this regard (the accumulation of the main concentration) of the ore-forming elements in hydrothermal solutions can be leading factor in the evolution process of the initial melts which are controlled by different physical-chemical and geological-geodynamic conditions.

Mineralogy of volcanic fumarole deposits: an overview and geochemical insight

Pekov I.V.

Faculty of Geology, Moscow State University

Fumarolic formation is very specific in its mineralogy and geochemistry as well as in crystal chemistry of the minerals. More than 300 mineral species are known in volcanic fumarole deposits. About 180 from this number were first discovered there and the majority of them are endemic for this formation. The originality of fumarolic mineralization is caused by unusual for natural, mineral-forming systems conditions, namely combination of high temperature (from 70-100 to 1000-1100ºC) with low pressure (close to atmospheric pressure) and gas transport of the most important chemical constituents (that causes, in particular, strong fractionation of elements). Crystallization of minerals typically happens under extremely nonequilibrium conditions. The most prolific in mineral diversity fumaroles can be distinctly subdivided to two main types: reducing and oxidizing. The brightest examples of the former type are fumaroles related to the volcanoes Vulcano (Aeolian archipelago, near Sicily, Italy) and Kudryavyi (Iturup island, Kurily archipelago, Russia) while of the latter type are fumaroles located at the volcanoes Vesuvio (Capmania, Italy) and Tolbachik (Kamchatka, Russia). Tolbachik is the world "record-holder" in the diversity of fumarolic minerals: >200 including 85 (!) described as new species. Strongly oxidizing conditions are caused by the mixing of hot volcanic gas with atmospheric air. For such fumaroles, minerals with chemical elements in highest oxidation degrees are characteristic: S^{6+}, Fe^{3+}, V^{5+}, As^{5+}, Mo^{6+}, Tl^{3+}, *etc*. The most important indicator minerals there are sulfates and oxides; in some fumaroles arsenates, vanadates and/or molybdates are common. For fumaroles of the reducing type, sulfides are indicator minerals. Chlorides, fluorides and high-temperature silicates occur in fumarolic systems of both types. Thus, the main constituents of volcanic gases that form anions it fumarolic minerals are O, S, Cl and F (note: CO_2 and H_2O remain volatile at temperatures higher than 100-150ºC under low pressures and are not fixed in high-temperature fumarole minerals). Strong fractionation of chemical constituents causes the formation of minerals of rare elements (including ones with minor concentrations in volcanic gases): Re, In, Se, Bi, Cd, Tl, Cs, Br, I, *etc*. Some of them form extremely rich mineralization unknown for other genetic types. Common components of fumarolic deposits at some volcanoes (at the first place, Tolbachik) are Cu, Zn, Pb, As, V, K and Na. Besides direct deposition from volcanic gas, the gas-rock interaction (so-called gas metasomatism) is very important mechanism of formation of fumarolic minerals. This process involves the constituents of host rocks having low volatilities, such as Al, Si, Mg, Ca, and Ti, and their minerals, including highly-alkaline silicates and aluminosilicates, are closely associated with compounds of chalcophile elements in fumarolic incrustaitions.

The work was supported by the Russian Science Foundation, grant no. 14-17-00048.

Iron stable isotope fractionation: driver forces, regularities and geochemical applications

Polyakov V.B.

Institute of experimental mineralogy, RAS

142432, Academician Osypyan str. 4, Chernogolovka, Moscow region, Russian Federation

Iron stable isotope fractionation factors for minerals and Fe-aqua complexes obtained by experimental and theoretical approaches are discussed. Dependence of iron isotope fractionation factors on oxidation state is elucidated in terms of difference in chemical bond energy of Fe atoms in ferric and ferrous species. Applications of stable iron isotopes to reduction-oxidation geochemical processes occurring at wide-range P – T conditions are reviewed. In particular, the use of iron isotope as an indicator of the oxidation state is considered on the example of the redox evolution of the ocean (Rouxel et al. 2005). The enrichment of pyrite in light iron isotopes is discussed basis on the modern seafloor hydrothermal vents (Rouxel et al. 2008, Polyakov and Soultanov, 2011). Iron isotope implications to the problem of genesis of band iron formations are presented following to Johnson et al. (2008) and Dauphas et al (2007). Iron isotope fractionation at high and ultra-high pressures applied to core-mantle differentiation in planetary bodies.

Parameters of processes in deep geospheres assessed from mineral inclusions in sublithospheric diamonds

Ryabchikov I.D.

Russian Academy of Sciences, IGEM, E-mail: iryab@igem.ru

Mantle is a silicate shell situated between the Earth's crust and metallic core, and it comprises about 70% of the mass of the Earth. According to geophysical data mantle is divided into 3 parts: upper mantle (lower boundary at 410 km), transition zone (410 – 670 km) and lower mantle (670 – 2900 km). Upper mantle is sampled by xenoliths in alkaline basalts and kimberlites, as well as by the large blocks uplifted to the surface by tectonic processes. An important information concerning the composition of lower mantle and transition zone is provided by mineral inclusions in a rare variety of diamonds transported from sublithospheric depths.

The most common minerals in such inclusions, demonstrating that they come from the lower mantle, are bridgmanite (metasilicate $(Mg,Fe)SiO_3$ with perovskite crystalline structure), $CaSiO_3$ with perovskite structure and ferropericlase (Mg,Fe)O). Comparison of the composition of these minerals with the results of experiments, conducted at high pressure and temperature, shows that in many cases the bulk composition of their primary source is similar to peridotites from the upper mantle.

An important problem concerns the presence of metallic alloy in the rocks of lower mantle. It stems from experimental data demonstrating, that at pressures above 30 GPa FeO in peridotitic phase assemblage should disproportionate forming Fe_2O_3 entering bridgmanite solid solution and Fe^0 forming metallic phase. A number of geochemists suggested that disproportionation reaction is the main cause of the redox evolution of mantle during the early stages of the formation of the Earth.

To assess the redox conditions and possible presence of Fe-rich alloy in the domains of lower mantle where sublithospheric diamonds originated I estimated position of the stability fields of carbon-bearing crystalline compounds coexisting with rock-forming minerals of the pyrolitic lower mantle. This diagram demonstrates that the field of diamond stability is separated from that of Fe-rich metallic alloy by the field of co-existence of iron carbides with prevailing silicates and oxides. It implies that the formation of diamond in lower mantle requires more oxidizing conditions by comparison with the predominant part of this geosphere.

Oxidizing conditions in some zones of lower mantle are supported by measurements of valence state of Fe in ferropericlase from lower mantle. f_{O2}-values were estimated from measured $Fe^{3+}/\Sigma Fe$ ratios in ferropericlases included in diamonds from lower mantle, based upon experimental data. Estimated values confirm relatively oxidizing conditions in the zones of diamond formation. Some fall into field of carbonates.

It is possible that the leading role of the relatively oxidizing conditions in diamond-forming parts of lower mantle belongs to the effect of increasing temperature on redox reactions. This hypothesis is corroborated by thermodynamic calculations. It in turns supports the idea that substrate containing sublithospheric diamonds belonged to mantle plumes which transported heat and material from deep levels of the Earth.

Financially supported by RScF, project no. 15-17-30019.

Paleoproterozoic history of assembly of the East European Craton: Evidence from basement of the Russian Platform

Samsonov A.V.[1], Spiridonov V.A.[2], Larionova Yu.O.[1], Larionov A.N.[3], Bibikova E.V.[4], Gerasimov V.Y.[5]

*1-Institute of geology of ore deposits, petrography, mineralogy and geochemistry of Russian Academy of Sciences (IGEM RAS) Staromonetny 35, 119017 Moscow, Russia (*correspondence: samsonovigem@mail.ru)*

2 -VNIIgeosystem, Moscow, Russia

3 - VSEGEI, St. Petersburg, Russia

4 -GEOHI RAS, Moscow, Russia

5 -GIN RAS, Moscow, Russia

Main volume of the Earth continental crust was formed in the Early Precambrian before 1.7 Ga. Tectonic processes and history of growth of this early crust are the most debated questions in geological sciences. In the talk, these questions will be discussed for the East European Craton (EEC) – large early Precambrian lithosphere block, basement of the East European (or Russian) Platform.

Available data suggest that the EEC consists of three autonomous crustal megablocks: Fennoscandia, Sarmatia and Volgo-Uralia (Bogdanova et al., 2008). Two of them, Fennoscandia (exposed on the Baltic Shield) and Sarmatia (exposed on the Ukrainian Shield and Voronezh Massive), had fundamentally different Archean and Early Paleoproterozoic history that allows us to consider these megablocks as fragments of Archean supercratons Superia and Vaalbara.

History of assembling the Archean blocks of the EEC is recorded in adjacent Paleoproterozoic fold belts.

The Volgo-Don Belt (VDB) located between Sarmatia and Volgo-Uralia megablocks in the southeast of the EEC. This well-studied accretional type orogenic belt consists of 2.20–2.10 Ga island-arc related volcano-sedimentary sequences and igneous complexes of collision (about 2.07 Ga) and post-collision (2.07–2.05 Ga) stages.

The Central Russian Belt (CRB) separates the Fennoscandia and Volgo-Uralia megablocks in the central part of the EEC. The belt is covered by a thick sequence of platform sediments. We will report the results of interpretation of geophysical data, and of petrographic, geochemical, isotopic and geochronological studies of core samples from 25 deep boreholes.

The southern part of CRB consists of Paleoproterozoic (1.95 - 2.00 Ga) juvenile volcano-sedimentary rocks and various granitoids with island arcs affinities. These rocks are similar in age and composition with the adjacent Osnitsk-Mikashevichy belt, and as the latter, it was probably formed in an active margin setting on the edge of the Volga-Sarmatia megablock.

The northern part of CRB consists of Archean (3.2 to 2.7 Ga) gneisses and granitoids and numerous ca. 2.5 Ga intrusions of high-Ti monzodiorites and metagabbro. These intrusions have geochemical and isotope features typical of Phanerozoic LIPs, particularly of the Parana province, and it could be considered as an indicative for a 2.5 Ga rifted margin of the southern edge of the Fennoscandian megablock.

The boundary of Archean and Paleoproterozoic domains of the CRB is marked by a wide mylonite zone of granulite facies rocks that could be a result of collision of the Fennoscandia and Volgo-Sarmatia megablocks at 1.8- 1.7 Ga.

Lapland-Kola-Dvina Belt (LKDB) locates within the Fennoscandia megablock. The belt is well studied on the Baltic Shield and traced to the Arkhangelsk province under the sedimentary platform cover using drill-hole samples.

In the Arkhangelsk province the LKDB consists of a juvenile Paleoproterozoic diorites, granodiorites, granites and calc-alkaline metagabbros (T = ca 1980 Ma, ε_{Nd}(T) from +1.70 to +3.50) similar with rocks of the Tersk terrane of the Baltic Shield. Subordinated Sill-Gar-Bi metasedimentary gneisses also had a Paleoproterozoic source (T_{DMNd} =2.33-2.38 Ga), and they are similar to kondalitic gneisses of the Umba terrane of the Baltic Shield. The Nd model age of felsic and mafic crustal xenoliths from kimberlitic pipes, located in the LKDB, vary from 1.99 to 3.13 Ga. The $^{207}Pb/^{206}Pb$ ages of zircon xenocrysts from porphyric kimberlite of V.Griba and Pionerskaya pipes vary from 2.7 to 0.9 Ga, and zircons of age ca 1.8, 1.5 and 1.2 Ga prevail.

It should be noted that localization of all industrial diamondiferous kimberlites within the Paleoproterozoic collisional belt is an additional example of exclusion from the “Clifford rule”.

Conclusions:

1. EEC includes heterogeneous Archean blocks, which can represent pieces of different Archean continents.
2. Assembling the Archean blocks into Paleoproterozoic continent Colombia includes at least two stages.

The first stage includes 2.2-2.1 Ga subduction processes in the Volga-Don Ocean, and its closure at 2.07-2.05 Ga resulted in the convergence and amalgamation of the Sarmatia and Volga-Uralia megablocks.

The second stage includes subduction processes in the Central Russian ocean that form ca. 2.00-1.95 Ga active margin at the edge of the Volga-Sarmatian megablock, which then collided with 1.7-1.8 Ga southern passive margin of Fennoscandia.

Subduction history of the Lapland-Kola-Dvina and Central Russian orogens overlaps in time 1.95-2.00 Ga and it possibly occurring in a single ocean basin, which opened ca 2.5 Ga ago and edged Fennoscandia megablock on the south and north-east. Several questions about the unity of Archean history of the Archean Karelian and Kola-Murmansk cratons, separated by the Lapland-Kola-Dvina orogen, as well as for the Karelian Craton and adjecent Volga-Uralia block, separated by the Central Russian orogen remains unresolved. These issues will be the subject of our future research.

References:

1. Bogdanova et al., 2008. The East European Craton (Baltica) before and during the assembly of Rodinia. Precambrian Research 160, 23-45

Ultrahigh resolution mass spectrometry to unravel the chemical space of terrestrial and meteoritic organic matter

Schmitt-Kopplin Ph.

Helmholtz Zentrum München, German Research Center for Environmental Health,
Research Unit Analytical BioGeoChemistry (BGC),
Ingolstaedter Landstrasse 1, 85764 Neuherberg, Germany
schmitt-kopplin@helmholtz-muechen.de

In terrestrial environments natural organic matter (NOM) occurs in soils, freshwater and marine environments, in the atmosphere and represents an exceedingly complex mixture of organic compounds that collectively exhibits a nearly continuous range of properties (size-reactivity continuum). In these materials, the “classical” biogeosignatures of the (biogenic and geogenic) precursor molecules, like lipids, glycans, proteins and natural products have been attenuated, often beyond recognition, during a succession of biotic and abiotic (e.g. photo- and redox chemistry) reactions. Because of this loss of biochemical signature, these materials can be designated non-repetitive complex systems.

(Ultra) High resolution analytical approaches will be presented in their application to unravel the chemical nature and organic signatures in terrestrial bio-geosystems and in extraterrestrial material especially in selected meteorites. We will focus on thermal effects in CM types of materials and describe the effect of Shock events on the changes in chemodiversity and the formation of unique novel organic compounds using high magnetic field ultrahigh resolution mass spectrometry (12 Tesla ion cyclotron resonance Fourier transform mass spectrometry – ICR-FT/MS) and nuclear magnetic resonance spectroscopy (Cryo 800MHz NMR).

References:

1. Hertkorn N., M. Harir, K. M. Cawley, Ph. Schmitt-Kopplin, R. Jaffé, Molecular characterization of dissolved organic matter from subtropical wetlands: a comparative study through the analysis of optical properties, NMR and FTICR/MS. Biogeosciences Discuss., 12, 1–55, 2015.
2. Meckenstock, R.U., F. von Netzer, C. Stumpp, T. Lueders, A.M. Himmelberg, N. Hertkorn, Ph. Schmitt-Kopplin, M. Harir, R. Hosein, S. Haque, D. Schulze-Makuch Water droplets in oil are microhabitats for microbial life. Science Magazine (2014), 345(6197) pp. 673-676.
3. Gonsior M., N. Hertkorn, M.H. Conte, W.J. Cooper, D. Bastviken, E. Druffel, Ph. Schmitt-Kopplin Photochemical Production of Polyols arising from Significant Photo-transformation of Dissolved Organic Matter in the Oligotrophic Surface Ocean, Marine Chemistry, 2014, 163, 10-18.
4. Popova O., P. Jenniskens, V. Emel'yanenko, A. Kartashova, E. Biryukov, S. Khaibrakhmanov, V. Shuvalov, Y. Rybnov, A. Dudorov, V.I. Grokhovsky, D.D. Badyukov, Q.Z. Yin, P.S. Gural, J. Albers, M. Granvik, L.G. Evers, J. Kuiper, V. Kharlamov, A. Solovyov, Y. S. Rusakov, S. Korotkiy, I.Serdyuk, A.V.Korochantsev, M.Y. Larionov, D. Glazachev, A.E. Mayer, G. Gisler, S.V. Gladkovsky, J. Wimpenny, M.E. Sanborn, A. Yamakawa, K.L. Verosub, D.J. Rowland, S. Roeske, N.W. Botto, J.M. Friedrich, M. Zolensky, L. Le, D. Ross, K. Ziegler, T. Nakamura, I. Ahn, J. Ik Lee, Q. Zhou, X.H. Li, Q.L. Li, Y. Liu, G.Q. Tang, T. Hiroi, D. Sears, I.A. Weinstein, A.S. Vokhmintsev, A.V. Ishchenko, Ph. Schmitt-Kopplin, N. Hertkorn, K. Nagao, M.K. Haba, M. Komatsu, T. Mikouchi (The Chelyabinsk Airburst Consortium). Chelyabinsk Airburst, Damage Assessment, Meteorite Recovery and Characterization. Science 2013, 342, 1069-1073.
5. Schmitt-Kopplin, Ph., Z. Gabelica, R.D. Gougeon, A. Fekete, B. Kanawati, M. Harir, I. Gebefuegi, G. Eckel, N. Hertkorn, High molecular diversity of extraterrestrial organic matter in Murchison meteorite revealed 40 years after its fall., 2010, PNAS, 107(7), 2763-2768.

Geotectonic position and features of magmatism of porphyry copper deposits of Central Kazakhstan

Serykh V.I., Makat D.K.

Karaganda state technical university, dastankgtu90@mail.ru

Polycyclic of Central Kazakhstan (Fig. 1) causes repeated manifestation at different times of porphyry copper deposits (PCD) that has been stated by I.V. Orlov in 1986. There were established the PCD of the following age levels: O_3, O_3-S_1, D_1, C_1, C_2, C_3 (Orlov, 1989, p.86, p.98).

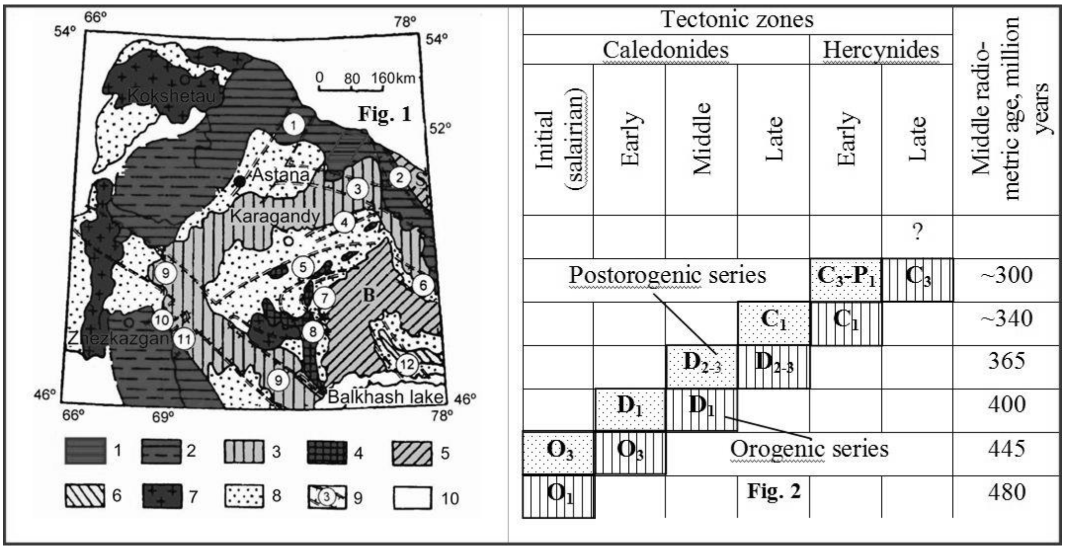

Fig. 1 The main geological-structural zones of Central Kazakhstan: **1-6** – orogenic volcano-plutonic belts (VPB): **1** – initial Caledonian, "Salairian", $Є_3$-O_1 - O_3; **2** – early Caledonian, O_{2-3}-D_2; **3** – middle Caledonian, "Devonian", D_1-D_3; **4** – late Caledonian, D_2-C_1; **5** – early Hercynian, "Balkhash-Iliysky" (B) and "Saursky" C_1-P_1; **6** – late Hercynian "Sayaksky", C_2-P_2; **7** – fragments of the Proterozoic base; **8** – Phanerozoic sedimentation basins; **9** – Hercynian tectonomagmatic reactivation zones (TMR, number of zones in circles): 1 – Koytasskaya, 2 – Tleumbetskaya, 3 – Bayanaulskaya, 4 – Spasskaya, 5 – Uspenskaya, 6 – Yuzhnochingizskaya, 7 Vostochno-Zhamansarysuyskaya, 8 – Akbastau-Akzhalskaya, 9 – Zhailma-Karaobinskaya, 10 – Uytas-Zhezkaz-ganskaya, 11 – Kenzhebay-Zhamanaybatskye, 12 – Susyzkarinskaya. **10** – MZ-KZ platform cover.

Fig. 2 Diagram of the age ratio of Paleozoic orogenic and postorogenic plutonic series of Central Kazakhstan

By now there has been significantly improved the region geology: there have been preparated the maps of comagmatism of VPB (Devonian and late Paleozoic), and new geological map of the 1:500 000 scale, the Salair stage in the caledonides with its PCD Bozshakol of Є$_3$-O$_1$ age (Serykh, 2009), there has been established the natural ratio of ore-bearing orogenic and ore-free postorogenic plutonic series (Fig. 2), made more exact PCD ages.

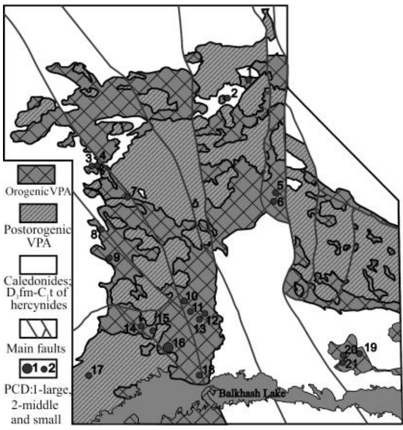

PCDs:	
1- Ozernoe	11-Kepsham
2-Baiskoe	12-Kaskyrkazgan
3-Olginskoe	13-Kenkuduk
4-Almaly	14-West Borly
5-Shatyrsha	15-Borly
6-Besshoky	16-Konyrat
7-Korgantas	17-Karatas
8-Altuait	18-Pribrezhnoe
9-Zhekeduan	19-Moldybai
10-Auezbaky	20-South Berkara
21-Zhambas	

Fig. 3 Scheme of locating orogenic and postorogenic VPAs and PCDs in north part of the Dzhungaro-Balkhashsky foldbelt.

The PCD position relative to plutonic series is shown on the example of the Hercynian series (Fig. 3). The orogenic volcanic-plutonic association (VPA) is presented by comagmatic complexes here: essential volcanic Karkaralinsk suite of C_1v-s (basalts, andesite-basalts, andesites, Na dacites, plagioriodacites) and plutons of the Balkhash intrusive C_1v-s complex (gabbro, diorites, q. diorites, Na granodiorites, plagiogranites). The orogenic stage comes to the end with the Keregetasskaya suite C_2 (rhyolites) and the East Kounrad intrusive C_{2-3} complex (leucogranites). The postorogenic comagmatic association includes the Arkharlinskaya suite C_3-P_1 (trachybasalts, trachyandesibaslats, trachyandesites, trachydacites, trachyriodacites) and the Kokdombaksky and Kokdalinsky intrusive P_1 complexes (syenogabbro, monzonites, q. monzonites, granosyenites, syenogranites). The association comes to the end with the Ayulyozekskaya suite P_1 and the Kyzylraysky intrusive P_1 complex (alaskites).

PCD in Central Kazakhstan are connected genetically only with calc-alkalic plutons of the orogenic granodioritic formation. Independent of the age (see Fig. 2) plutons are constructed similarly: the initial phase – diorites (+ gabbro sometimes), I – q. diorites, II – granodiorites, tonalites, III – plagiogranites. PCD are directly connected with a special type of porphyric intrusions – plutonic porphyries which are in their geological position additional intrusions of the II phase (Serykh, Egorychev, 1978). There is observed the certain dependence of the composition of porphyric intrusions on their form: plagiogranite-porphyries are characteristic of the bodies similar to dikes (PCD Bozshakol, Koktaszhal, Borly, etc.), plagiogranodiorite-porphyries have formed cupola-stock bodies (Konyrat, Aktogai, etc.). In the TMR zones (Fig. 1, 3) there are spread kali-soda and potassic granitoids with the porphyries corresponding to them in alkalinity (Almaly, Baiskoe, etc.).

References:

1. Orlov I.V. Geology of the USSR, v.20, book 1. Alma-Ata, 1989. 543 p.
2. Serykh V.I., Egorychev L.G. Genetic linkages of porphyry copper mineralization in the Balkhash region//Geol. of ore deposits, 1978, No. 6, p. 35-45.
3. Serykh V.I. Geology, petrology and metallogeny of ultraacidic granitoids of Central Kazakhstan. Karaganda, 2009. 318 p.
4. Serykh V.I. Orogenic magmatism and metallogeny // "Smirnovsky sbornic-2012", p. 167-199. OP Prod.-publish. complex VINITI combine. - Nauka, M., 2012.

The temperature and H_2O contents of mantle derived magmas and their sources

Sobolev A.V. [1,2]
1 -Russian Academy of Sciences, Vernadsky Institute of Geochemistry and Analytical Chemistry, Moscow, Russian Federation.
2 -ISTerre, University J. Fourier, Grenoble, France alexander.sobolev@ujf-grenoble.fr

The compositional and thermal heterogeneity of convecting mantle critically affect magma production and compositions and cannot be easily distinguished from each other. The way to resolve this ambiguity is an independent estimation of temperature and composition of mantle sources of various types of magma.

Here we report application of olivine-spinel-melt geothermometers based on partition of Al, Cr, Sc, Y, Fe and Mg as well as direct measurement of H_2O concentrations in melt for olivine hosted melt and spinel inclusions from different primitive lavas of MORB, OIB, LIP, Archean komatiites and SSZ. The results suggest significant variations of crystallization temperature for the same Fo of high magnesium olivines from different types of mantle-derived magmas: from the lowest (down to 1220^oC) for MORB and SSZ to the highest (up to over 1500^oC) for komatiites and Siberian meimechites. These results confirm the relatively low temperature of the mantle source of MORB and SSZ magmas, low to moderate amount of H_2O in komatiites, high H_2O contents of SSZ magmas and higher temperatures in the mantle plumes.

The established liquidus temperatures and compositions of primary melts allow estimating potential temperatures of their mantle sources. The highest potential temperatures over 1800 ^oC are characteristic for Archean komatiites. For Phanerozoic age the highest potential temperatures (1650^oC) are found for the largest LIPs: Siberian, North Atlantic and Caribbean. The sources of OIBs yield significant range of potential temperatures: 1400-1600^oC, positively correlated with magma production rate. MORBs yield potential temperature between 1350-1400^oC except those from ultra slow spreading ridges (e.g. Knipovich ridge), which display potential temperatures down to 1250 ^oC. Potential temperatures of SSZ mantle sources are typically within the range for MORB, suggesting origin of SSZ primary melts by H_2O fluxing of convecting mantle wedge. Exceptions are some boninites, which require higher temperature and plume related sources.

The results strongly confirm mantle plume theory and external source of H_2O in SSZ mantle. The H_2O in komatiites could be incorporated in the transitional zone.

In particular in our recent paper [1] we report measurements of the content of water and other volatile components, and of major and trace elements in melt inclusions in exceptionally magnesian olivine (up to 94.5 mole per cent forsterite). This information provides direct estimates of the composition and crystallization temperature of the parental melts of Archaean komatiites. We show that the parental melt for 2.7-billion-year-old komatiites from the Abitibi belt in Canada contained 30 per cent magnesium oxide and 0.6 per cent water by weight, and was depleted in highly incompatible elements. This melt began to crystallize at around 1,530 degrees Celsius at shallow depth and under reducing conditions, and it evolved via fractional crystallization of olivine, accompanied by minor crustal assimilation. As its major- and trace-element composition and low oxygen fugacities are inconsistent with a subduction setting, we propose that the high water content resulted from entrainment into the komatiite source of hydrous material from the mantle transition zone[2,3]. These results confirm a plume origin for komatiites and high Archaean mantle temperatures, and evoke a hydrous reservoir in the deep mantle early in Earth's history.

References:

1. Sobolev A.V et al. Komatiites reveal an Archean hydrous deep-mantle reservoir. Nature 531, 628-632.(2016).
2. Bercovici, D. & Karato, S. Whole-mantle convection and the transition-zone water filter. Nature 425, 39–44 (2003).
3. Pearson, D. G. et al. Hydrous mantle transition zone indicated by ringwoodite included within diamond. Nature 507, 221–224 (2014).

Mafic layered intrusions and related ore deposits

Veksler I.V. [1,2]
1 -German Research Centre for Geosciences GFZ Potsdam, Germany, veksler@gfz-potsdam.de
2 -The Department of Mineralogy, Perm State University, Russia

Layered igneous rocks have attracted much attention and have been a topic of extensive multidisciplinary research since pioneering studies of the Skaergaard intrusion in East Greenland by L.R. Wager and his co-workers in the 1930's [1]. Magmatic layering of various types is a characteristic feature of many mafic-ultramafic intrusions, which are believed to represent fossilized magma chambers at the roots of magmatic systems. Studies of magmatic layering have provided important insights to processes of magma crystallization and differentiation, and key results of the studies were summarized in several special volumes, the most recent of which published in 2015 [2, 3, 4, 5]. Layering in plutonic bodies is observed as succession of layers differing in terms of crystal size (grain-size layering), mineral modes (modal layering), crystal shape (textural layering) or mineral compositions (cryptic layering). Despite significant efforts and decades of active research, the origin of magmatic layering remains poorly understood and, in view of the great diversity of types and forms of layering, there is probably more than one mechanism of its formation.

Of special interest, for reasons not only theoretical but also practical, is the formation of layers enriched in valuable minerals such as chromite, magnetite and apatite. In terms of economic geology layers strongly enriched in Cr-spinel with chromite modes up to 90 wt. % are synonymous to stratiform chromite deposits. The deposits are the main world's reserve of chromium for metallurgy and alumina-rich chromite for refractory ceramics. Some of the massive chromitite layers, such as the UG2 layer of the Bushveld Complex in South Africa or the J-M Reef of the Stillwater Complex in Montana, USA contain very important resources of platinum-group elements (PGE), which greatly exceed chromite in economic value. In addition to that, magnetite layers in the upper part of the Bushveld Complex host the world's greatest resources of vanadium.

Early theories of magmatic layering emphasized the importance of crystal settling and sorting by gravity, and the origin of layering was viewed as a process similar to deposition of layered clastic sediments [2]. At the end of the 1970's those views were challenged by new petrographic observations and more accurate experimental measurements of magma density. New models, which were developed at that time, emphasized the importance of *in situ* crystallization and often referred to the process of double diffusive convection [3, 4]. Much attention in recent years has been given to processes at advanced stages of crystallization in magmatic crystal mush [5]. Current progress in studies of igneous layering heavily relies on new analytical methods and instruments, such as laser ablation mass spectrometry (LA ICP-MS) and X-ray computer tomography, and new mathematical approaches, such as statistical analysis of rock textures and numerical models of magma dynamics. Revived interest in magmatic ore deposits, and the need for better methods of ore prospecting and beneficiation also contributes to the growing activity in studies of layered mafic intrusions.

References:

1. Wager, L. R. & Deer, W. A. (1939). Geological investigation in East Greenland, Part III, The petrology of the Skaergaard intrusion, Kangerdluqssuaq, East Greenland. *Meddelser om Grønland* 105(4).
2. Wager, L. R. & Brown, G. M. (1968). *Layered Igneous Rocks*. Edinburgh: Oliver & Boyd.
3. Parsons, I. (ed.). *Origins of Magmatic Layering*. D. Reidel, Dodrecht, 1987.
4. Cawthorn, R.G. (ed.) *Layered Intrusions*. Elsevier, Amsterdam, 1996.
5. Chariler, B., Namur, O., Latypov, R. & Tegner, C. (eds). *Layered Intrusions*. Springer, Dordrecht, 2015.

Variation of gas content layer K_7 of Kuzembayeva coal mine of Karaganda coal basin

Amangeldykyzy A.[1],Filimonov E.N.[2],Portnov V.S.[1]

1 -Karaganda State Technical University, Republic of Kazakhstan, amangeldykyzy@inbox.ru

2 -Coal devision degassing department, Republic of Kazakhstan, Karaganda

The efficiency of performed degassing procedures is determined by gas condition of unworked coal (pressure, gas temperature and gas capacity), properties (openness, porosity, gas discharging option, gas capacity and etc.), coal structure, technology of performing the mining works and economic feasibility.

When developing beddings with gas content 15-20m^3/t high-performing mining faces by loadings more than 2000t/d, there is the significant delay of preparation works from working face that leads to demurrage of gas. With increasing of mining works depth the natural speed of gas evolution in methane drainage boreholes does not provide the required level of gas extraction from bedding. It relates to low natural filtration and diffusion permeability, high gas capacity and low (comparing to gas collecting mains) coal porosity.

The general mechanisms of changing the methane content are its increasing with the growth of stratigraphic depth of beddings and in the direction of coal rank increasing [1] (Fig 1).

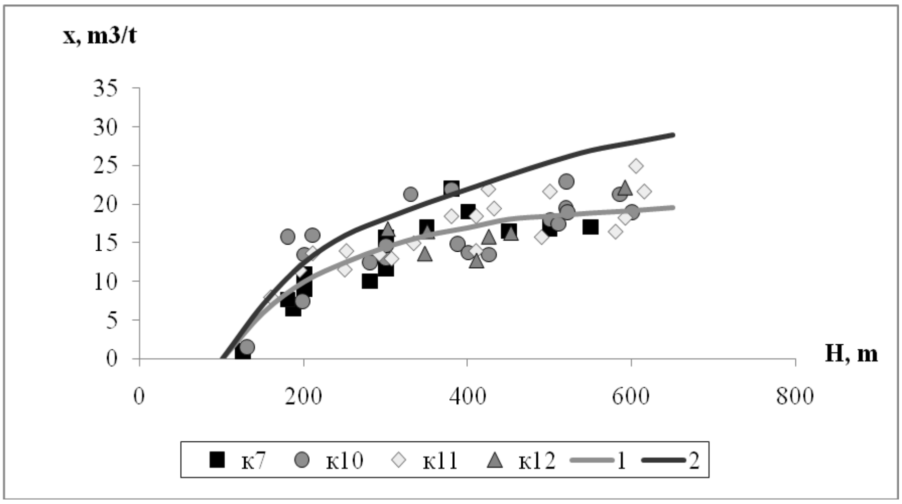

Fig. 1 Seam gas content K_{12} – K_7 depending on the depth of its bedding in Churubai –Nurinskiy district: 1 – average values, 2 – top compound curve.

The majority of researchers think that gas content increases with depth according to hyperbolic law and in general case it looks like Langmuir equation [2].

$$X = X_г \frac{100 - W - A_з}{100}, \ \text{m}^3/\text{t} \tag{1}$$

where $X_г$ - methane content of dry ash-free matter, m^3/t s.b.m. W - natural coal humidity, %; $A_з$ - ash content of coal, %.

Natural methane content of dry ashe-free coal content ($X_г$, m^3/t s.b.m.) is defined by means of statement:

$$X_г = \frac{1{,}3c(H - H_0)}{1 + b(H - H_0)}, \ \text{m}^3/\text{t} \tag{2}$$

where H – mining depth, м; H_0 – depth of gas slacking area, м; c,b – coefficients of Langmuir equation.

The meaning of equation parameters (2) are accepted according to «Classifier of gas content of coal beds in Karaganda coal-mining field».

The value of residual methane content of coal is defined according to formula:

$$X_0 = 0{,}001\, X_{o.г.} (100 - W - A_з), \ \text{m}^3/\text{t} \tag{3}$$

where $X_{o.г}$ – residual gas content of dry ash-free mass of coal in case of air pressure, m^3/t s.b.m.

If before the coal development or brought closer together to beds (layers) were overworked or snubbed, then in calculating formula instead of natural methane content bed (X) the residual methane content is placed (X_{res}).

Based on flattening of gas content isotherm of coal with high pressure of methane it can be assumed that with increasing the bedding depth the growth tempos of gas content slow down.

Theoretically (I.M. Pechuk, L.N. Bykov, A. I. Pokrovskiy, M.A. Yermekov and others) and experimentally it was defined that methane pressure in coal beds increases in conformity with the law, close to hydrostatic:

$$p_г = 10^{-2} \cdot (H - H_0), \ Мпа. \tag{4}$$

Dependence (4) reflects the main pressure build-up-up of gas with increasing of depth of bedding. At the same time, in the field there were cases of significant methane emanation from feeder of gas coal beds that proves the existence in coal-bearing strata of local areas with anomalous increasing of gas pressure and gas content comparing to adjoining sectors.

Calculated change of natural seam gas content k_7 taking into account ash-content and humidity is presented in Picture 2. When calculating Langmuir coefficients c and b consequently were taken 0,195 and 0,01032, H_o – 87м, A^c – 28,7%, W – 4,2% .

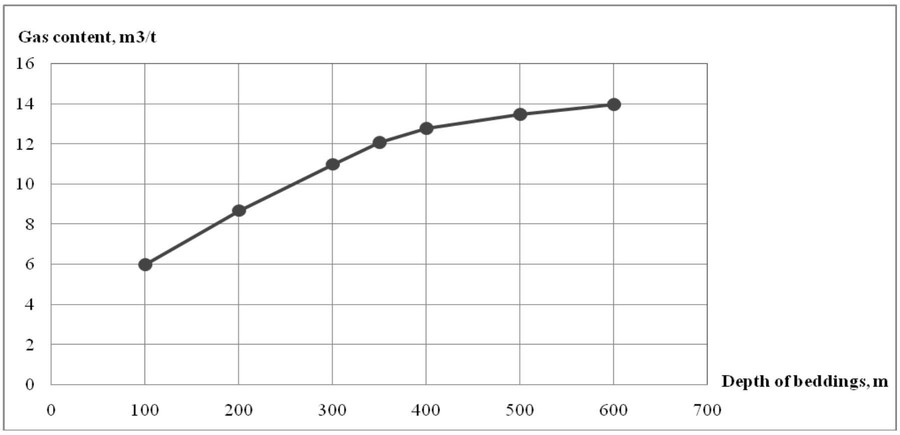

Fig. 2 Calculated change of seam gas content k_7 from stratification depth at Kuzembayev mine*:* where *X* – natural seam gas content considering the humidity and ash-content, m3/t; *H* – the depth of bedding, м; *A, B, C* – empirical coefficients.

Regularity of enlargement of the k_7 foulness layer was determined , with the depth of 100m to 600m, whereas foulness level varies from 6 to 14 m^3/t , which requires adoption of technological solutions during the degassing and coal mining of this layer.

References*:*

1. V.A. Kolmakov Methane-selection and their prevention in mines. M: Nedra, 1981. 46-54 p.

Groundwater quality assessment of oued rmal aquifer (Northeastern of Tunisia) for agricultural irrigation uses, using gis technology

Ameur M., Hamzaoui–Azaza F., Gueddari M.

Research Unit of Geochemistry and Environmental Geology, Faculty of Science of Tunis, University of Tunis El Manar, 2092 University campus Farhat Hached, Tunis

Due to its location between the Mediterranean and the Sahara, Tunisia is a country with semi-arid to arid climate over most of its territory.

Today, demand on groundwater resources is becoming higher and higher, mainly related to the socio-economic development, high urbanization, population growth and widespread irrigation. Moreover, climate change and natural conditions variations are added.

Among the main issues related to this precious resource quality are salinization, solidification process and soils alkalizing. Oued Rmal groundwater, which is situated in the north-east of Tunisia, in Zaghouan governorate, is essentially exploited for irrigation.

A total of twenty-three water samples were taken in 2013 winter, so as to cover the maximum of the aquifer area. These samples were subjects of in field-measurements, of some physicochemical parameters (temperature, pH and salinity) and laboratory analysis of major elements. Several parameters were used to assess the quality of water designed for irrigation among others Electrical conductivity (Ec) and sodium adsorption ratio (SAR).

56% of water points of Oued Rmal aquifer present low alcalinization risk which SAR is between 2 and 10 whereas 44% have high soil destabilization risks (10 $<SAR<26$). Water samples for irrigation present a medium to high sodicity and alcalinization risk. As part of this work, we have elaborated a GIS to study spatial distributions of sodium adsorption ratio (SAR), the percentage of Sodium (% Na) and the Residual sodium carbonate (RSC) and therefore, the evaluation of water quality of Oued Rmal (good, fair and poor) regarding irrigation.

Keywords: GIS, Water resources, Water quality for irrigation, Oued Rmal groundwater, Tunisia.

Early seawater-brine contamination of 3.3-3.5 GA komatiite melts inferred from melt inclusions

Asafov E.V.[1], Sobolev A.V.[1,2], Gurenko A.A.[3], Arndt N. T.[2], Batanova V.G.[1,2], Krasheninnikov S.P.[1], Wilson A.H.[4] and Byerly G.R.[5]

1 -Vernadsky Institute, Moscow, Russia; evasafov@gmail.com

2 -ISTerre, France; alexander.sobolev@univ-grenoble-alpes.fr

3 -CRPG, Nancy, France, agurenko@crpg.cnrs-nancy.fr

4 -University of the Witwatersrand; Allan.Wilson@wits.ac.za

5 -LSU, Baton Rouge, USA; glbyer@lsu.edu

Komatiites are the ultramafic rocks (MgO>18wt.%) that result from a high degree of mantle melting (commonly >30%) under extreme P-T conditions and hence represent its composition. However, the most of known komatiites are highly altered, and this prevents the use of their compositions to directly estimate the volatile and mobile element contents of their mantle source. A recent research of melt inclusions in highly magnesian olivines (Fo 92.4-Fo 94.2) in 2.7 Ga komatiites of the Abitibi Greenstone Belt, Canada [1] demonstrated an early contamination of melts by seawater inferred from the high Cl concentrations. Yet the most magnesian olivines (Fo 94-94.5) hosted melt inclusions unaffected by the interaction with seawater that contained up to 0.8 wt.% H_2O pointing towards the presence of a hydrous reservoir in the Neoarchean deep mantle.

Here we report the new data on the water contents, other volatile elements, major and trace elements concentrations of melt inclusions in a range of olivines Fo 93-95.8 and, Fo 91-92 from the komatiites of the 3.3Ga Weltevreden Formation and 3.5Ga Komati Formation respectively in the Barberton Greenstone Belt, South Africa.

Fresh olivine grains 0.2-0.5 mm across were heated for 5 minutes at 1400 ^oC and 1450^oC according to their composition at the QFM buffer and quenched. Exposed melt inclusions were analysed by SIMS and EPMA and contain 0.2-0.8 wt.% H_2O, 60 ppm to 0.22 wt.% Cl (Fig. 1B) and 130 to 420 ppm K_2O at MgO concentrations between 23-29.6 wt.%. For chlorine that is significantly higher than in the melt inclusions from 2.7 Ga komatiites of the Abitibi Greenstone Belt[1] and Belingwe Greenstone Belt [unpublished data]. Melt inclusions with high Cl contents (>0.1 wt.%) demonstrate positive correlation between chlorine and water contents pointing towards a possible seawater contamination whereas inclusions with lower Cl contents (0.03-0.1 wt.% of Cl) do not show any correlation between these components and thus may represent water from the 3.3-3.5 Ga mantle source. However all the inclusions with Cl over 100 ppm were affected by seawater or seawater-derived brine contamination [2,3], which is indicated by the decrease of Na/Cl ratio together with the increase of K_2O content, see Fig. 1A.

Two series of melt inclusions, one with extremely high chlorine reaching 2.8 wt.% (not shown on Fig.1B) at moderately high K_2O (0.05-0.11 wt.%) and the other with high K_2O contents (0.1-0.4 wt.%) at Cl up to 0.36 wt.% hosted in Fo 95-95.3 comprise the contaminant that affected komatiite melts at an early stage. The First series of inclusions have Cl/K_2O between 10.5-32.4 and relatively low Na/Cl (0.2-0.8 versus average of 2-12 for the other melt inclusions in the same samples) and the Second series (Cl/K and Na/Cl ratios ~1) both fall in the seawater-brine field (Fig.1A) thus referring to a high degree of contamination.

The majority of analyzed melt inclusions demonstrates contamination with seawater brines and cannot be used for an accurate reconstruction of the source water contents but still, a number of inclusions with the lowest Cl contents (<100 ppm) occur in the most Mg-rich olivines from the Weltevreden Formation (Fo 95.3-95.8) and in olivine Fo 91-92 of Komati Formation. These melts were not affected by seawater contamination and record the composition of primary melts and their mantle sources.

This paper was supported by the RSF grant 14-17-00491

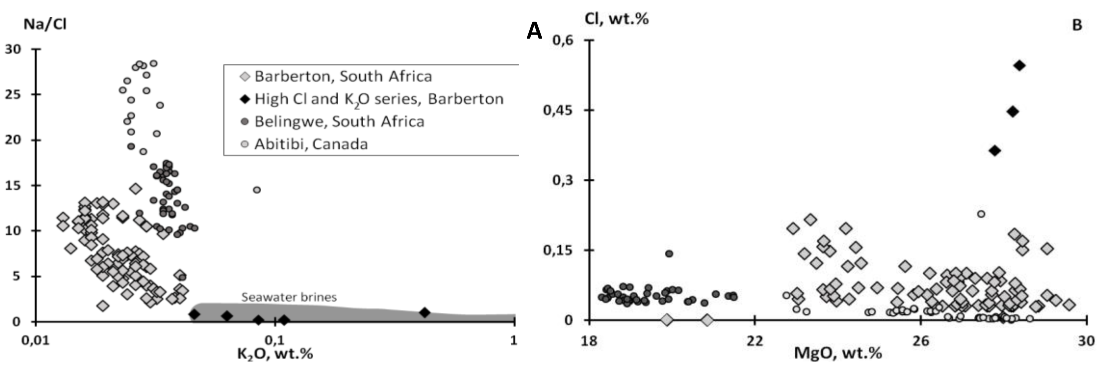

Fig. 1 Composition of komatiite melt. A. Na/Cl versus K_2O with seawater brines field [2,3]. B. Cl versus MgO contents, EPMA data.

References:

1. Sobolev A., Evgeny V. Asafov, Gurenko A, Arndt N., Batanova V., Portnyagin M., Garbe-Schönberg D. & Krasheninnikov S., Komatiites reveal a hydrous Archaean deep-mantle reservoir// Nature, 2016, V. 531, p. 628-632.
2. Holland H., Lazar B. & McCaffrey M., Evolution of the atmosphere and oceans// Nature, 1986, V. 320, p. 27-33
3. Fontes J., Matray J., Geochemistry and origin of formation brines from the Paris Basin, France: 1. Brines associated with Triassic salts// Chemical Geology, 1993, V. 109, I. 1-4, p. 149-175.

Nanoscale Gas Flow in Shale Gas

Banerjee S. and Banerjee M.

Geophysics,BHU,varanasi-221005,India

Sunjay_sunjay@yahoo.com,manasgp@yahoo.co.in

Nanoscale imaging visualizes shale gas plays - nanoscale gas flow in shale gas sediments. Diameter of pores in shale gas sediments range from a few nanometres to a few micrometres. In shale gas systems, nanopores play two important roles. First, for the same pore volume, the exposed surface area in nanopores is larger than in micropores.The phenomena of gas storage and flow in shale gas sediments are a combination of different controlling processes. Gas is stored as compressed gas in pores, as adsorbed gas to the pore walls and as soluble gas in solid organic materials, i.e., kerogen and clays. Gas flows through a network of pores with different diameters ranging from nanometres (nm = 10^{-9}m) to Micrometres(μm=10^{-6}m). In shale gas systems, nanopores play two important roles. First, for the same pore volume, the exposed surface area in nanopores is larger than in micropores. This is because surface area is proportional to $4/d$, where d is the pore diameter. At the nanoscale most continuum equations, e.g. Darcy equation, may not be valid. Characterizing nanopores and obtaining new sets of governing equations to describe gas desorption from nanopores and gas flow in nanopores are major research work for shale-gas reservoirs. Nanologging (nanorobots) play a pivotal role in measurement while drilling.Modern fluid dynamics Knudsen law diffusion become dominant mechanism in shale gas reservoir. Shale rock properties are being studied by AFM.Nanoparticles are also used to obtain better quality images with several imaging methods currently in use, such as computed tomography scans (CT scans), Magnetic Resonance Imaging (MRI) and ultrasound imaging. The way in which nanoparticles help is largely by improving the contrast in the images.This large exposed area permits large volumes of gas desorption from the surface of the kerogen in nanopores. Consequently, higher mass transfer of gas molecules occurs inside the bulk kerogen. Secondly, gas flow in nanopores is different from the Darcy flow. Compares the pore distribution in conventional and unconventional (shale) reservoirs. As shown in this schematic figure, the number of nanopores is higher in unconventional shale gas sediments. Diameter of pores in shale gas sediments range from a few nanometres to a few micrometres. Probing Nano-Scale Forces/Mechanochemistry:AFM(Atomic Force Microscopy) to study interactions of nano-scale particles with fluid mixtures. The ability of the atomic force microscope (AFM) to create three-dimensional micrographs with resolution down to the nanometer and Angstrom scales has made it an essential tool for imaging surfaces in applications. In addition to this topographical imaging, however, the AFM can also probe nanomechanical and other fundamental properties of sample surfaces, including their local adhesive or elastic (compliance) properties. Nanoscale imaging visualizes shale gas plays - nanoscale gas flow in shale gas sediments. Diameter of pores in shale gas sediments ranges from a few nanometres to a few micrometres. In shale gas systems, nanopores play two important roles. First, for the same pore volume, the exposed surface area in nanopores is larger than in micropores. Probing Nano-Scale Forces/Mechanochemistry: AFM (Atomic Force Microscopy) to study interactions of nano-scale particles with fluid mixtures. The ability of the atomic force microscope (AFM) to create three-dimensional micrographs with resolution down to the nanometer and Angstrom scales has made it an essential tool for imaging surfaces in applications. In addition to this topographical imaging, however, the AFM can also probe nanomechanical and other fundamental properties of sample surfaces, including their local adhesive or elastic (compliance) properties. Syntactic/structural pattern recognition techniques can recognize the structural seismic patterns and improve seismic interpretations. Combinatorial Image Analysis, Image structure analysis are employed for nanoimaging. Third generation wavelet transform are employed in nano imaging.

Key words:

Shale gas, Atomic Force Microscope for investigation of nano-pores, Knudsen law diffusion, nanoimaging, MRI, Wavelet Transform, NanoFludics

Correlation of ignimbrite deposits from Verhneavachinskaya Caldera (Eastern range, Kamchatka)

O.V. Bergal-Kuvikas[1], V.L. Leonov[1], A.N. Rogozin[1], I.N. Bindeman[2], E.S. Kliapitskiy[1]

1 -Institute of Volcanology and Seismology, Petropavlovsk-Kamchatsky, Russia
olgakuvikas@gmail.com, lvl@kscnet.ru, rogozin@kscnet.ru, Kliapich@gmail.com
2 -University of Oregon, USA bindeman@uoregon.edu

During 2009, 2010, 2014 field works the new obtained caldera complex descripted in springheads of Levaya Avacha and Kavycha rivers (Eastern Range, Kamchatka) (Kuvikas & Rogozin, 2009; Leonov et al., 2011). Natural outcrops represented by thick interbedded layers of welded tuffs and ignimbrite (>500 meters thickness). The interbedded layers cover nearly 10 km area (Fig. 1). Volume of pyroclastic deposits was calculated as 220-230 km^3, based on size of caldera (Mason et al., 2004). These ejected volumes correspond to strong explosive eruptions with VEI 7 or more. The age of caldera-forming eruption was determined by Ar-Ar method to be of Late Miocene (5.78~5.58 Ma BP).

Detailed descriptions of the numerous thin sections and whole-rock geochemistry allows us to correlate sections of exposed outcrops from Verhneavachinskaya caldera (Fig. 2). We distinguished four main types of the rocks, which are characterized by different major and trace element composition, colors, textures, mineralogical and geochemical compositions. First types of the layers is ignimbrite of basaltic andesitic composition. Columnar jointing occurs at the most of the ignimbrite, exposed by active erosion process. Pyroclastic texture characterize most ignimbrite layers: microtexture represents by fragments of plagioclase, pyroxene phenocrystalls, and matrix of the rocks contains lithified welded tuffs with numerous fiammes. Second type of the layers is black, dense basaltic andesite less-changed ignimbrite layers. Structure of rocks contents fragments of plagioclase, pyroxene phenocrysts. Matrix of rocks represents by oriented plagioclase microlites. Third type is altered tuffs with yellow-orange tone. These rocks characterized by significant secondary hydrothermal alteration of rock`s matrix with quartz micro veins. Fourth type of the layers is volcanic breccias, which composed of broken different sizes rocks fragments with cemented tuffs matrix.

Whole-rock geochemistry of ignimbrite changes from basalt to andesite (SiO_2 51.2-59.5 wt. %), with corresponding natural decreasing FeO*, CaO, MgO, TiO_2. Across the outcrops from lower to upper ignimbrite layers the decreasing contents of SiO_2, MgO, Na_2O are observed with minimum on the top of outcrop. In comparing with another ignimbrite fields on Kamchatka the rocks from Verhneavachinskaya caldera characterized by higher contents of Nb, Ta, TiO_2 and MgO, lower contents of Na_2O, SiO_2 (Kliapitskiy, 2014).

New discovery of the Late Miocene Verhneavachinskaya caldera is as one of the older and mafic complex on Kamchatka opens many questions for origin and evolution magma in active island arc system: which are features of Late Miocene volcanism and how it correlate with geodynamic setting, e.g. with slab jumping and originated transform faults (Avdeiko, Bergal-Kuvikas, 2015).

Reference:

1. Avdeiko, G. P., Bergal-Kuvikas, O. V.. The geodynamic conditions for the generation of adakites and Nb-rich basalts (NEAB) in Kamchatka. Journal of Volcanology and Seismology, 2015. 9(5), 295-306.
2. Kliapitskiy E.S. New data of geochemistry of ignimbrites in Verhneavachinskaya caldera. Material of XIII Regional young scientist conference. Nature of Kamchatka. 15 April 2014. Petropavlovsk-Kamchatsky. 81-90 p.
3. Kuvikas O. V., Rogozin A. N. First results of study 500-meters section of ignimbrite deposit (Kavycha river, Eastern Kamchatka). Material of VII regional conference for young scientists. 29th November 2009. Petropavlovsk-Kamchatsky. p. 39-49.
4. Leonov V.L., Rogozin A.N., Bindeman I.N., Kuvikas O.V., Kliapitskiy E.S. Determination of new caldera on Kamchatka: boundary, ages, complex of inside caldera deposits, unsolved problems. Material of conference to volcanologist day "Volcanism and depended processes". Petropavlovsk-Kamchatsky. 2011. 53-56 p.
5. Mason B.G., Pyle D.M., Oppenheimer C. The size and frequency of the largest explosive eruptions on Earth. Bull. Volcanol. 2004. V.66. p. 735-748.

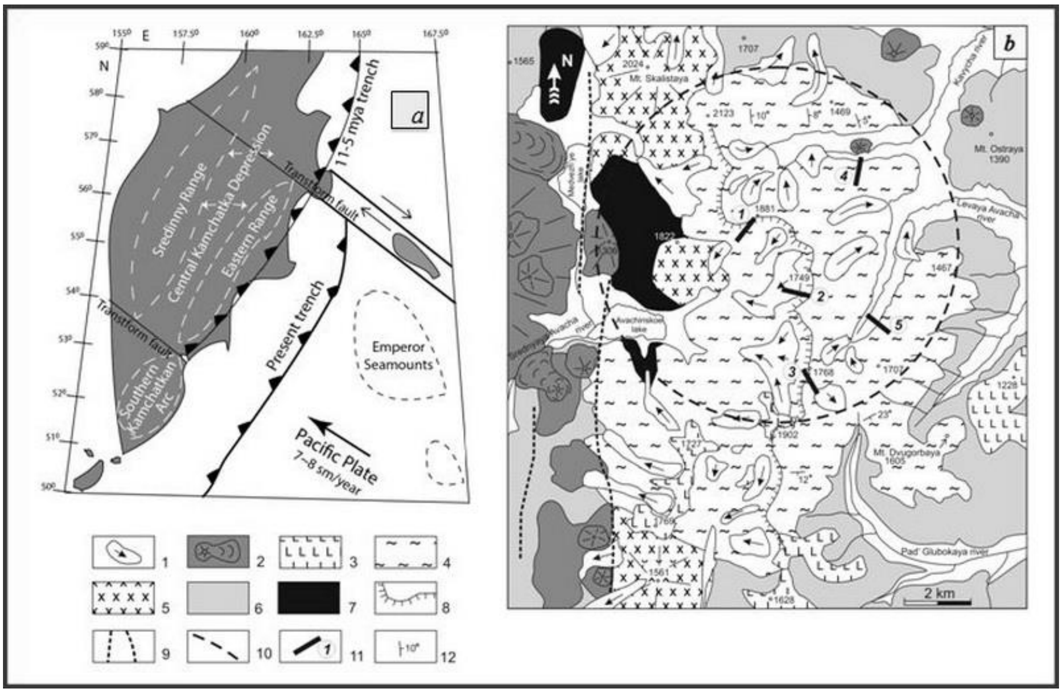

Fig. 1 a) General plate tectonic position of the Kamchatka and location of the Verhneavachinskaya caldera (black square).

b) Scheme of geological structure of springheads of Levaya Avacha and Kavycha rivers (Leonov et al., 2011). Note: 1 - Late Pleistocene-Holocene alluvium, glacial and debris deposits, arrows indicate movement of landslides, 2 - Pleistocene cinder comes and related lava flows, 3 – Pliocene-Early Pleistocene andesitic lava flows, 4 – Late Miocene ignimbrite deposits, 5 – Latter Miocene diorite intrusions, 6 – Miocene porphyritic basalts, agglomerate tuff, 7 - Late Cretaceous siltstones, argillites, 8 – cliffs of Avachinsky range, 9 - faults which are boundary graben of Srednyaya Avacha river, 10 - boundary of new-discovered caldera, 11- location of studied outcrops of ignimbrites (1-L-2010, 2-L-2014, 3-L-2012, 4- R-2009, 5-L-2009, please see details on Fig. 2), 12 – dip of the ignimbrite layer.

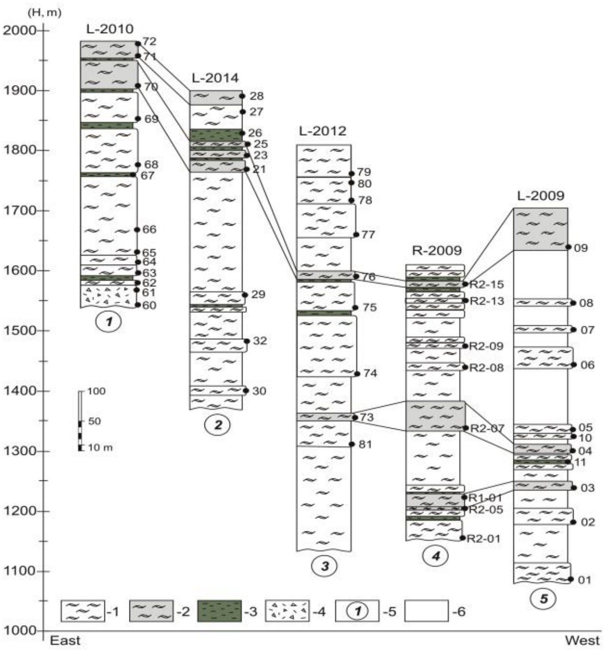

Fig. 2 Correlation of stratigraphic sections. Note: 1- ignimbrite layers, 2- marked ignimbrite layers, which are correlated on the sections, 3- altered tuffs with yellow-orange tones, 4-volcanic breccia, 5- numbers of the section are showed on Fig. 1, 6 – sodded outcrope area.

Steps and stages of ore mineralization of barite – polymetallic deposits at Zmeinogorsk Ore district (rudny Altai)

Bestemianova K.V., Grinev O.M.

National Research Tomsk State University, KsenijaVT@mail.ru

Barite - polymetallic deposits of Zmeinogorsk ore district consist of five commercially important components: copper, lead, zinc, gold and silver. The main ore minerals are pyrite, chalcopyrite, sphalerite, galena, minor fahl ores, bornite, chalcocite, acanthite, native gold, electrum, an amalgam of gold and silver. The ore – hosting rocks are devonian igneous – sedimentary rocks

The process of ore mineralization had polietly and polyphasic character. However, the process which was prior to the step of sediment of the main mass of sulfides, was the process of metasomatic or wallrock alteration of enclosing rocks with the formation of quartz – chlorite – sericite, quartz – chlorite and quartz – sericite rocks. The rock-forming minerals of the wallrock alteration rocks are quartz, chlorite, sericite; accessory minerals are - rutile, apatite, zircon. Also, sulphide mineralization represented by pyrite, to a lesser extent galena, chalcopyrite and sphalerite is observed. As for mineralogy the peculiar feature of the wallrock alteration rocks of deposits under study is the presence of rare earth mineralization [1,2]. Chlorite, which is part of the rock-forming minerals, was used as a natural geothermometer. The approximate temperature of its formation, was calculated using chemical composition as described in [3], and it ranged between 210-255 ° C.

As a result, based on a detailed study of ore structures and textures, their spatial distribution, typomorphic properties as well as varied isotopic composition of the major sulfide minerals two steps of mineralization and five basic mineral complexes were identified in the barite – polymetalic ores. The first step of mineralization was obviously short-termed, and went back to the end of the Ems - top Eiffel (D_1). It was characterized by intense tectonic movements.

The mineral complex of the first step of mineralization is represented by pyrite, chalcopyrite, sphalerite and galena (hereinafter minerals are listed in the order of allocation and distribution). Breccia and disseminated textures, structures – of crushing, substitution (sulfides formed in this step are often replaced by sulfides of the second step) are typical of the first mineral complex. Ores of the first stage compose no more than 10 ... 15% of the total mineralization.

The second step of mineralization was the most long - termed and productive – the sediment of about 80% of the ores occurred. The formation dates probably from Eifel (D_2). It was accompanied by tectonic syn - and to post-ore shifts with recovery of faults and fractured zones.

First mineral complex (first stage of the second step) is composed of chalcopyrite, sphalerite, galena and less pyrite. Ores of the second step is characterized by the following textures: interspersed, vein - interspersed, massive; as well as the following structures - inequigranular, small-, medium- and coarse-grained, emulsion, collomorphic, corrosion, crushing, shearing, to a lesser degree of substitution. The microstructure indicates that the ore formation was accompanied by tectonic shifts.

The average chemical composition of the sulfide minerals in the complex (was determined by the electron microscope «VGA II LMU» blended with energy dispersive spectrometer Oxford INCA Energy 350, the analytical center of "Geochemistry of natural systems" NR TSU). According to the data obtained the content of the elements in the minerals makes up (in weight%): chalcopyrite Cu 35.1%, Fe 29.76%, S 34.26%; sphalerite Zn 64.98%, S 35.02%; galena, Pb 86,06%, S 13,86%. Average sulfur isotopic composition of sulfides of complex (isotopic compositions were determined in the laboratory of stable isotope FEGI RAS, Vladivostok), is δ34CDT, ‰. It is shown that the average isotopic composition of sulphides of the first complex is characterized by the following values: to -0.2 ‰ pyrite, chalcopyrite to 0 ‰, for galena + 0.5 ‰ for sphalerite -1,2 ‰.

The two pairs of sulfides were chosen at the mineral complex first stage of the second step, which made it possible to calculate the temperatures based on their near simultaneous formation and deposition of equilibrium conditions of their sediment determining their fractionation of stable isotopes. By isotopic data approximate temperatures of the mineral complex were calculated, for a pair of pyrite II / II chalcopyrite (300 ... 340°) C; for a couple of sphalerite II - galena II 300 ... 320° C, calculation methodology described in [4].

The second mineral complex of the second step consists of barite, sphalerite, galena, chalcopyrite, tetrahedrite, arsenopyrite, acanthite. The average chemical composition of the main sulphides of the second mineral complex sphalerite Zn 64.16%, Fe 0.29%, Cd 1.28%, S 34.27%; galena, Pb 85.84%, Se 1.05%, Fe 0.72%, S 13.23%; chalcopyrite Cu 33.78%, Fe 31.12%, S 34.81%; tetrahedrite Cu 38.66%, Fe 1.21%, Sb 23.75%, As 4.32%, Zn 7.34%, S 24.72%. By the end of this stage in tetrahedrite silver content is up to 17%.

The average isotopic composition of sulfides of the second complex of the second step: chalcopyrite - 1.9 ‰, galena -3,4 ‰, sphalerite -2.3 ‰, tetrahedrite -3,7 ‰. To calculate the temperature of mineralization pair of sphalerite - galena was selected for this complex. The temperatures ranged between of 280 ... 320 ° C

The third mineral complex of the second step consists of bornite, tennantite, chalcocite, galena, to a lesser extent. The average chemical composition of the main sulfides is bornite Cu 62.86%, Fe 11.36%, S 25.51%; tennantite Cu 40.34%, As 15.47%, Sb 5.96%, Zn 7.0%, Fe 0.63%. S 30.98%; galena, Pb 84.17%, Ag

1,2%, S 14.63%; chalcosine Cu 78%, S 19.8%, Ag 2.2%. The average isotopic composition of sulfides third complex: tennantite -12,8 ‰, bornite -8,9 ‰.

The fourth mineral complex of the second step is composed primarily of non-metallic minerals, namely quartz, barite, calcite, hematite and gypsum. Minerals composing complex heal veins and oral dissolution.

The studied variations of the isotopic composition of sulfur sulphides, which are included in allocated mineral complexes, justify inhomogeneities of the source of ore material, and had mantle - crustal character. So, in the process of mineralization (from the initial stages to the final ones) the change of the dominant mantle source of the initial stage of phase to substantially crust occurred, by the end of the process the ore mineralization. The origin of the crust component might be heterogeneous - both due to the borrowing of sulfur from the enclosing sedimentary rocks, and by meteoric waters, given the near-surface (volcano - tectonic) type of hydrothermal - metasomatic ore systems.

The temperature is changed abruptly. Thus, at the beginning of the second step it changed from 300 to 340 ° C, then it fell to the mid stages up to 280 ° C and raised again to 320 ° C, which may be associated with entering fresh portions solutions in to the mineral system.

References:

1. Bestemianova K.V., Grinev O.M. Mineral composition of the wallrock metasomatites of barite – polymetalic deposits at Zmeinogorsk ore district (Rudny Altai) // The fourth Russian youth school with international participation "New at perception of ore genesis proceses".- M.: IGEM RAS, 2014. P.67 - 72.
2. Bestemianova K.V. The wallrock alteration rocks of barite – polymetallic deposits at Zmeinogorsk ore district (Rudny Altai) // Baikal youth scientific conference of geology and geophysics. Gorjachinsk, 2015. P 190 – 194.
3. Kranidiotis P., MacLean W.H. Systematics of chlorite alteration at the Phelps Dodge massive sulfide deposit, Matagami, Quebec // Econ. Geol. 1987. V. 82. P. 1898-1911.
4. Seal R.R. Sulfur isotope geochemistry of sulfide minerals // Mineralogy and Geochemistry. - 2006. - V. 61. P. 633 - 677.

Reconstuction of the melt composition and crystallization conditions for magnesial basalts of shiveluch volcano (Kamchatka Peninsula)

Bondar D.B.[1], Nekrylov N.[1], Plechov P.Y.[1]

1 -Lomonosov MSU, geolog.bondar@yandex.ru

Shiveluch - one of the most active andesitic volcanoes of the Kamchatka Peninsula. Over the past few centuries, there are more than ten of its eruptions. In Holocene recorded several basalt eruptions atypical for this volcano [7], the largest of them are the eruption of high-potassium (3600 years ago) and the eruption of moderate-potassium (7600 years ago) magnesia basalts, about which this work was written. The material is presented by olivine-clinopyroxene scoria. Reconstruction of the melt composition and crystallization conditions for this eruption can characterize parental melts for Shiveluch volcanic eruptions which relate to moderately potassium series and have more acidic composition. For this reconstruction was used method of melt inclusions.

The study of inclusions was conducted in olivine grains, as the best mineral container in this case. For olivine selection, sample was crushed to the fraction of 0.5-1 mm, because most of it grains belongs to this range. In olivine grains was noted the presence of all types of inclusions: melt, solid, fluid and combined. For the purpose of the melt composition study primary inclusions with a diameter not less than 30 microns are suitable. It's necessary in order to minimize the distorting effects of the real composition of the melts. In this sample, melt inclusions in olivine are crystallized. To determine the temperature of homogenization was conducted the experiment with visual inspection on the Linkam TS1500 stage. Complete melting of the daughter phases in inclusions occurred at temperatures up to 1180°C. Further inclusions were heated to this temperature and quenched without visual control.

The composition of the quenched melt inclusions glasses and their host-olivine was analyzed with the JEOL JSM-6480 in the Department of Petrology of the Moscow State University. Reconstruction of the melt composition was conducted using Fe-loss correction [2] on the basis of olivine-liquid equilibria model [4]. The initial content of iron in melt were taken as its maximum value measured in host-rock, which is 9 wt. % [6]. The equilibrium temperature for the melt in equilibrium with host-olivine reconstructed for dry conditions is 1320 ± 5°C. According to the literature, the water content in the parental melts Klyuchevskoy group of volcanoes can reach up to 4-5 wt. % [5], which according to the model [1] should reduce the equilibrium temperature to 1200 ± 5°C. All calculations were made using the Petrolog3 software [3].

A comparison of the reconstructed melt composition, scoria of the eruption (7600 years ago) [6, 7] and all igneous rocks of the volcano Shiveluch showed that the reconstructed melt may be parental for rocks of the volcano Shiveluch (Fig. 1). The difference between the composition of the rocks and reconstructed melt conditioned by the processes of magmatic evolution.

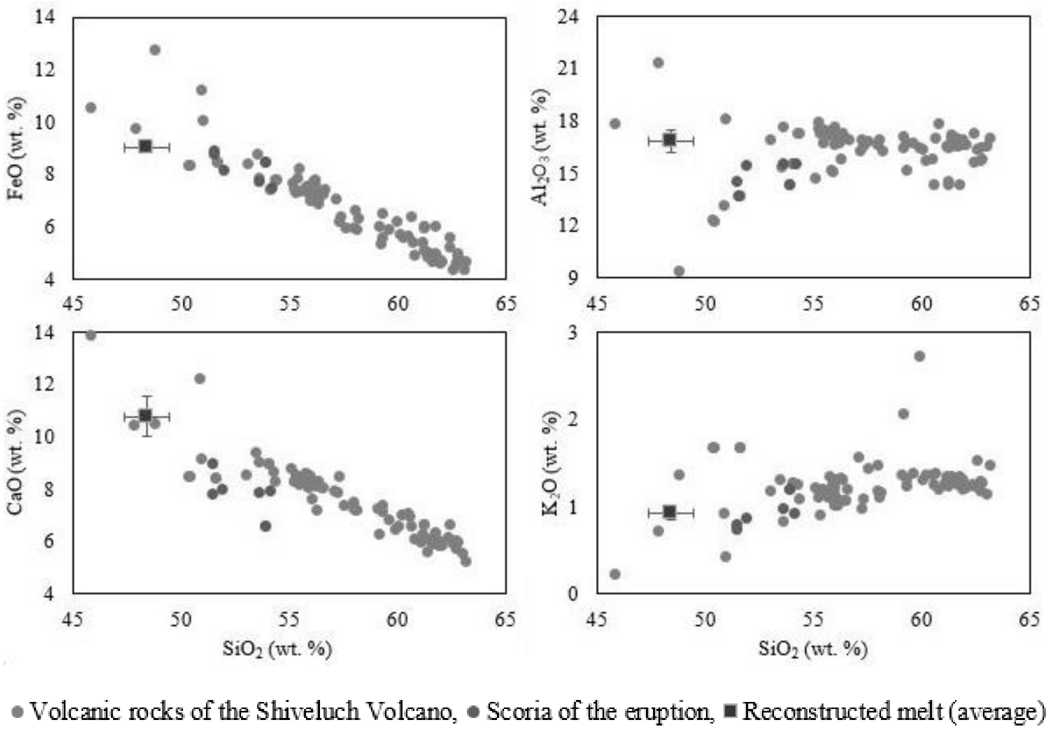

Fig. 1 Harker diagrams involving composition of the reconstructed melt and rocks of Shiveluch Volcano

References:

1. Almeev R. R. et al. The effect of H2O on olivine crystallization in MORB: experimental calibration at 200 MPa //American Mineralogist. – 2007. – Т. 92. – №. 4. – С. 670-674.
2. Danyushevsky L. V., Della-Pasqua F. N., Sokolov S. Re-equilibration of melt inclusions trapped by magnesian olivine phenocrysts from subduction-related magmas: petrological implications //Contributions to Mineralogy and Petrology. – 2000. – Т. 138. – №. 1. – С. 68-83.
3. Danyushevsky L. V., Plechov P. Petrolog3: Integrated software for modeling crystallization processes //Geochemistry, Geophysics, Geosystems. – 2011. – Т. 12. – №. 7.
4. Ford C. E. et al. Olivine-liquid equilibria: temperature, pressure and composition dependence of the crystal/liquid cation partition coefficients for Mg, Fe2+, Ca and Mn //Journal of Petrology. – 1983. – Т. 24. – №. 3. – С. 256-266.
5. Mironov N. et al. Quantification of the CO2 budget and H2O–CO2 systematics in subduction-zone magmas through the experimental hydration of melt inclusions in olivine at high H2O pressure //Earth and Planetary Science Letters. – 2015. – Т. 425. – С. 1-11.
6. Tolstykh M. L. et al. Types of parental melts of pyroclastic rocks of various structural–age complexes of the Shiveluch volcanic massif, Kamchatka: Evidence from inclusions in minerals //Petrology. – 2015. – Т. 23. – №. 5. – С. 480-517.
7. Volynets O.N., Ponomareva V.V., Babansky A.D. Magnesian Basalts of Shiveluch Andesite Volcano, Kamchatka. Petrology, Vol. 5, No. 2, 1997, pp. 183–196.

New seismic reflection imaging of active faults and their tectonic behavior in the Southern Alboran basin (Moroccan Margin). Is the nekor fault a pure strike-slip?

Bouskri G.[1] , Elabbassi M.[2] , Ammar A.[2] , El Ouai D.[1] , Harnafi M.[1] , Villaseñor A.[3]

1 -Department of Geology, Scientific Institute of Rabat, Mohamed V University, Ibn Battouta Avenue, P.B. 703, Agdal 10106, Morocco, ghizlane.bouskri@gmail.com ; harnafimimoun@gmail.com

2 -Department of Geology & Faculty of Sciences, Mohamed V University, 4 Ibn Battouta Avenue P.B. 1014 RP, Agdal, Morocco, elabbassimohammed@hotmail.fr ; siadammar@fsr.ac.ma

3 -Institute of Earth Sciences Jaume Almera, ICTJA-CSIC, 08028 Barcelona, Spain, antonio.villasenor@csic.es

The study of 1000km industrial seismic reflection profiles, carried out on the Northern Moroccan margin (Fig.1), allowed browsing new details on the regional geological structures and their functioning. For this, we elaborated a high-resolution depth model and a global tectonic sketch of the whole study zone, by combining seismic lines (Fig.2) to two of the most prominent and robust methods: seismicity analysis (Fig.1) and field data selected in the onshore part of the Nekor fault, that is the major transforming fault in the area. The idea of regional influence of a recent tectonic activity has been rejected for the transforming Miocene faults in several works, however, we found out that it is still active and manifested by normal and strike-slip faults, trending mainly N070° and N125° in the study zone. In this segment, we found that the Nekor fault is clearly continuous but suddenly changes direction from N30° to N70°, and changing behavior from pure strike-slip to left-lateral strike-slip fault with normal component (Fig.3). Field data confirms also the extension of Miocene faults through quaternary deposits. This is also confirmed by analysis of local seismic activity recorded from 1990 to 2014 with moderate magnitudes activity that shows alignments in clear superposition with the active faults we detected in the region.

Keywords: Active tectonics, Nekor fault, Seismic reflection, Seismicity, Alboran Sea, Rif belt, Morocco.

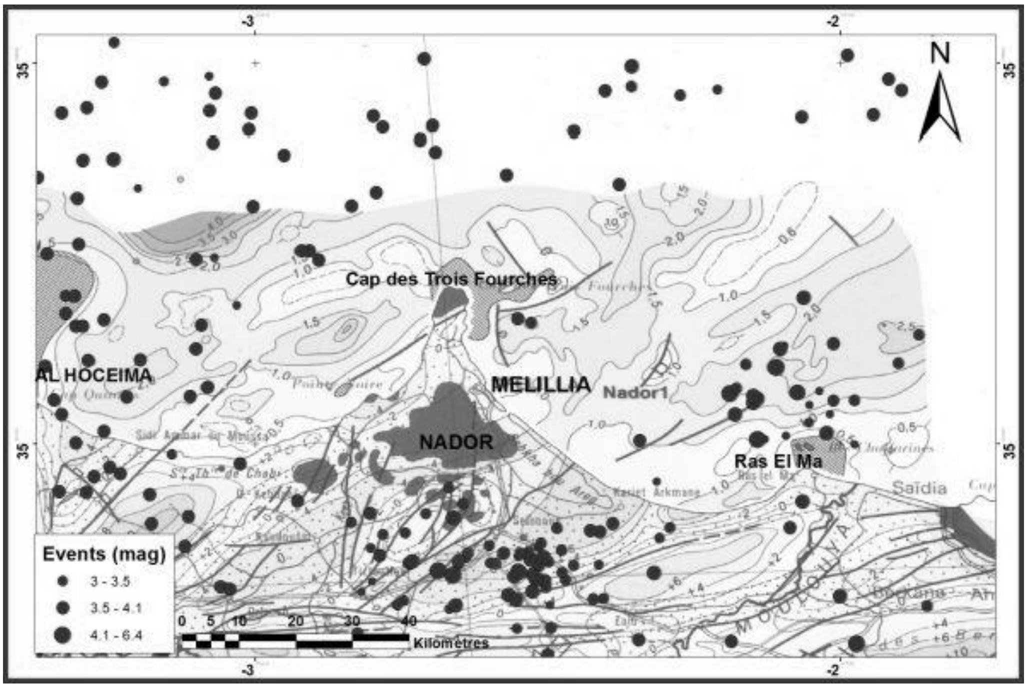

Fig. 1 Recent shallow seismicity from 1990 to 2014 with magnitudes going from 3 to 6.4. Important concentration of seismicity is the indicator of faulting activity in the region. Background map is a fragment of Moscow International School of Earth Sciences - 2016. May 23-28, 2016 Moscow, Russia

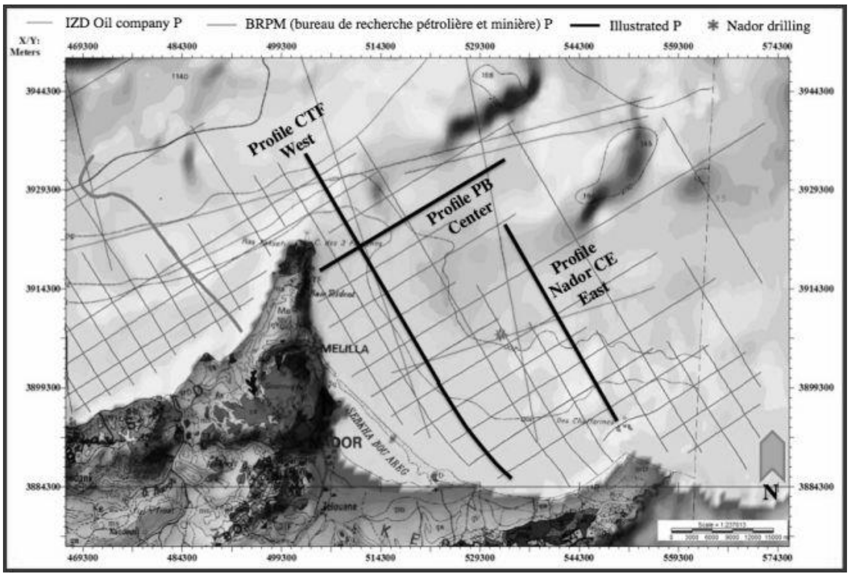

Fig. 2 Position plan of seismic profiles. 50 seismic lines were used in this study, bold lines in the map are seismic lines shown in fig. 2 to illustrate the main tectonic features detected in the area

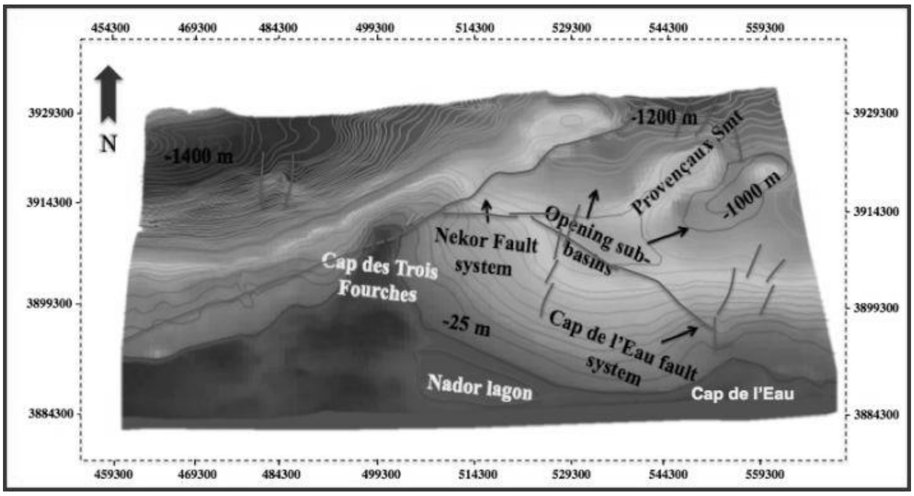

Fig. 3 Global interpretation map, two opening basins are sourrounded by strike-slip faults with normal component and normal faults that are represented with dark blue bold line

Ree mineralogy of the malmyzh cu-au porphyry deposit, Rassian Far East

Bukhanova D.S.[1], Chubarov V.M.[1]
1 -Institute of Volcanology and Seismology FEB RAS, dasha-snejinka@yandex.ru

The proximity of the rare earth elements (REE) chemical properties is unique. They are responsive to redox environments, therefore a comprehensive study of the REE behavior in natural processes allows to use them as indicators of geochemical substance sources and mechanism of hydrothermal ore-forming processes [Rogulina et al., 2013].

The study of rare earth minerals in the ores Malmyzh gold-copper porphyry deposit probably formed by mixing of high-temperature hydrothermal solutions is submitted relevant allows to assume the mechanism of accumulation [Bukhanova, 2015].

Malmyzh deposit is located in Far East Russia, approximately 220 km northeast from the Khabarovsk city. The project has excellent logistics and infrastructure, including high voltage power lines and a paved national highway. As well, the Amur River lies within 2 km of the project boundary and is directly linked to major shipping ports. Malmyzh deposit porphyry centers occur as Cretaceous age diorite and granodiorite stocks that intruded in hornfels-altered siltstone and sandstone sedimentary sequences.

By the resource potential the deposit is comparable to the giant world-class projects, such as the Oyu Tolgoi (Mongolia, South Gobi), Pebble (United States, Alaska), and others. Total estimated resources (category P1 + P2) based on published data make up 4.9 million tons of copper and 266 tons of gold at an average grade of 0.3-0.4% Cu and gold 0.1-0.3 g/t [Chitalin et al., 2013].

The dominant ore minerals are pyrite and chalcopyrite which presented as finely-dispersed phenocrysts, nesting separateness, veinlets and significant clusters in rare veins. Sometimes complemented by bornite and arsenopyrite. There are sulphides of lead, zinc and silver as secondary components [Ivanov et al., 2013].

A detailed study of ores and host altered rocks of the Malmyzh gold-copper porphyry deposit Central district carried out at the analytical center of the Institute of Volcanology and Seismology FEB RAS using the optical apparatus and a scanning electron microscope TescanVega-3 with an energy spectrometer Oxford Instruments X-Max 80 mm^2 showed therein rare earth mineralization (Fig.1). It is represented by anhydrous phosphates (monazite – $REE(PO_4)$, xenotime – YPO_4, REE-apatite – $[Ca,REE]_5(PO_4)_3[F,OH]$), silicates (allanite – $CaREEFe^{2+}Al_2(Si_2O_7)(SiO_4)O(OH)$, huttonite – $ThSiO_4$), fluorocarbonates (synchysite – $Ca(Ce,La,Nd)(CO_3)F$) and oxides (davidite – $Ce,La,Y,U)_2Fe^{3+}{}_2(Ti,Fe^{3+},Cr,V)_{18}(O,OH,F)_{38}$) [Vlasov, 1964].

Figure 1 shows some forms of REE minerals occurrence. For example monazite fills pores in pyrite as well as chalcopyrite and galena (Fig. 1*a*). This pyrite grain flanked by chlorite and potassium feldspar which contains a grain of xenotime. In figure 1*b* allanite crystals are observed in the pores in the chalcopyrite jointly with sericite. It should be noted that in allanite also observed cavities filled by sericite, indicating the later appearance of the latter. Frequently observed zoned crystals of epidote with transitions to allanite where allanite sometimes forms a radiant zones (Fig. 1*d*). The formation of synchysite often occurs on the rim of rutile replacing it (Fig. 1*c*). Advantageously synchysite occurs in areas of intense sericite-chlorite alterations.

As a result of the study of mineral composition of the Malmyzh deposit rocks identified that the main minerals, which include REE are allanite, monazite, xenotime, synchysite, REE-apatite, huttonite and rare davidite. They are not just form independent individuals, but also the form reactionary relations with each other and ore containing altered rocks. Therefore, rare earth minerals of the Malmyzh deposit Central district the actively participated in the metasomatic processes, rather than remain inert and are likely have a hydrothermal origin.

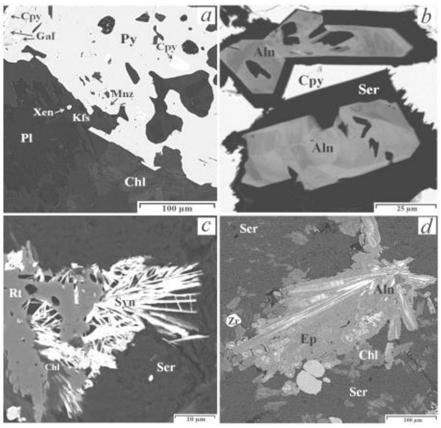

Fig. 1 Photomicrographs of REE minerals occurrence.

Notes: Mnz – monazite, Xen – xenotime, Aln – allanite, Syn – synchysite, Py – pyrite, Cpy – chalcopyrite, Gal – galena, Pl – plagioclase, Kfs – potassium feldspar, Chl – chlorite, Ser – sericite, Rt – rutile, Ep – epidote, Zr – zircon.

References:

1. Bukhanova D.S. Malmyzhskoe Au-Cu-porphyry deposit (Khabarovsky Krai): the genesis of the Central district by the fluid inclusions study // Proceedings of the XIII regional youth conference «Research in Earth Sciences», IV&S FEB RAS. 2015. P. 4-16.
2. Chitalin A.F., Yefimov A.A. Voskresensky K.I., Ignatyev Y.K., Kolesnikov A.G. Malmyzh - a new large world-class porphyry copper-gold system in Sikhote Alin // Mineral Resources of Russia. Economics and Management. 2013. № 3. P. 65-69.
3. Ivanov V.V., Kononov V.V., Ignatiev E.K. Mineralogical and geochemical features of ore
4. mineralization in metasomatites from Malmyzh gold-copper ore field (Lower Priamurye) // Proceedings of the All-Russian Conference: VIII Kosygin's readings Tectonics, deep structure and minerageny of East Asia. 2013. P. 258-261.
5. Rogulina L.I., Voropaeva E.N., Ponomarchuk V.A. Rare earth minerals in ore of Berezitovoye gold-polymetal deposit (Upper Priamuruye) // Advances in current natural sciences. 2013. №11. P.117-120.
6. Vlasov K.A. Geochemistry, mineralogy and genetic types of deposits of rare elements. Vol 2. Mineralogy of rare elements. Publishing house "Science. 1964. 830 p.

Lamproite magma as parental melt for Inagli Massif (Central Aldan)

Chayka I.F.

V.S. Sobolev Institute of Geology and Mineralogy, Siberian Branch of the Russian Academy of Sciences; Novosibirsk State University, ifc02@yandex.ru

Central-Aldan high-potassic magmatic system is a unique formation, combining several magmatic associations of different features, formed one by one at the second half of Mesozoic. It's very interesting to study and investigate it, because its objects can be considered as «models» of ore-forming-systems, and researching them, we can learn much about processes that form ore deposits, especially gold, REE, PGE and uranium deposits.

Inagli is a ring-massif, consisted of a dunite core and potassic-rock periphery, considered by some researchers (Laurent Guillou-Frottier, 2014) as Ural-Alascan type. It is situated 30km west from Aldan town, eastern Siberia. It is an important sourse of PGE and jeweler Cr-diopside. Inagli massif was studied by many researchers, but the properties of its parent-melt are still unknown. Some researchers (Mues-Schumacher, 1995) say that the parent-melt was very magnesian (MgO ~ 25%) and add that it can be close to lamproites of Jakokut massif or Ryabinoviy massif (Okrugin, 2014), which are also situated in this area. What is more, lamproites and lamprophyres of Tobukian dyke complex (Ryabinoviy massif) and Inagli dunites have the similar age: 132±2Ma and 134±2Ma respectively (Shatov, 2015; Ibragimova, 2015). Our purpose is to investigate, can dunites of Inagli massif and lamprophyre dykes of Ryabinoviy massif have similar parent melts. This question becomes more reasonable, because 1) rocks of Tobukian dyke complex contain xenoliths of clinopyroxenites, very similar to Inagli ones, 2) there are many lamprophyre bodies all around the Central Aldan of this age 3) according to documents, there are some lamproite bodies around Inagli massif.

In order to goal this purpose we investigated a full series of Tobukian complex rocks (Ol-Di-Phl-lamproites, Di-Bt-lamproites, minettes and syenite-porphyres) and some main types of rocks of Inagli massif (dunites, wherlites, shonkinites, alkali syenites), also data of some previous researches was taken into account. Bulk chemical compositions of the rocks, composition of rock-forming minerals were investigated and compared. Also, the feature of our research is an investigation of chromites and crystallized inclusions in them as a sourse of information about the earliest stages of melt evolution.

Mineral composition of the rocks of Tobukian dyke complex changes from olivine-diopside-phlogopite-K-feldspar (Ol-Di-Phl-lamproites) through diopside-biotite-K-Feldspar (Di-Bt-lamproites), biotite-aegirine-diopside-K-Feldspar (minettes) to biotite-K-Feldspar (syenite-porphyres). Apatite and magnetite are abundant in lamproites and minettes respectively. Composition of Inagli rocks is more complicated, it is considered in details by previous researchers (Mues-Schumacher, 1995, Korchagin, 1996). Comparing mineral composition of rocks and chemical features of minerals, it can be seen, that they are very close for both Inagli and Tobukian rocks. We compared compositions of olivine and Cr-spinel, which are the earliest minerals and clinopyroxenes, which are «through» ones. Composition of olivine cores of Ryabinoviy lamproites and Inagli dunites varies from #Mg = 90 to #Mg = 95. Clinopyroxenes in both Tobukian and Inagli rocks evolves from Cr-diopside, with Cr_2O_3 up to 2%, through diopside-hedenbergite to aegirine. Although composition-fields of pyroxenes from Inagli syenites and Tobukian syenite-porphyres and minettes seem to be different, early stages of their evolution (more magnesian) are very close. Aegirine in both series contains 0,5-2,1% TiO_2. Also in some Tobukian minettes there is high-Ti aegirine-diopside (TiO_2 – 1-4%).

In lamproites of Tobukian complex Cr-spinel is presented by small euhedral grains in olivine phenocrysts and by grains in groundmass, which contain more Fe2O3, then the first ones, evolving to Cr-magnetites. Also, in one dyke of lamproite (sample I58-12) we found big subhedral grains of Cr-spinel, which are very similar to the ones from Inagli dunites. It can sign, that magma captured cumulatic rocks with cromite, passing through a crystallization camera. Studied dunites and wherlites contain cumulative Cr-spinel, spread between olivines. The results of chemical analysis show, that the composition of Cr-spinels from Tobukian lamproites in general evolves from Mg-chromite (in cores of olivine phenocrysts) to Cr-magnetite (in the groundmass). Cr-spinel from Inagli dunites and wherlites show a similar evolution, although they contain a bit less Al_2O_3 (Fig.1). However, their compositions are very close especially, for fresh Inagli dunites and sp. I58-12 (Tobukian lamproite). Thus we can conclude, that their melt compositions were quite similar at early stages of crystallization, the difference of Al_2O_3 contents can be due to different pressure conditions.

Crystallized inclusions were studied in chromites from Inagli dunites and wherlites and Ryabinoviy lamproite, which contained big grains of chromite (I58-12) (other samples contained chromites too small to be observed). The research shows that mineral compositions of crystallized inclusions both in Ingali and Ryabinoviy chromites are *practically the same*. They contain phlogopite (#Mg -- 96-97, TiO_2 – 0,4-0,8), diopside (#Mg – 94-100), minor apatite and sulphides (chalcopyrite, pentlandite). We tried to estimate composition of parent-melt of Inagli dunites and wherlites, considering it as an average bulk composition of these inclusions. According to this estimation, main petrogenic contents in the parent-melt are: SiO2 – 41-44%, MgO ~ 25-27%, K2O ~ 6-8%, CaO ~ 4-5%. This data coincides with previous researchers' estimation, where MgO content is about 25% (Mues-Schumacher, 1995).

In order to compare chemical trends of Tobukian and Inagli rock series, bulk major-elements compositions of them were studied. Also, we included results of some previous researches for Inagli (Okrugin, 2014, Korchagin, 1996) and for Tobukian (Sharygin, 1996) rocks. The results show, that both Inagli and Tobukian series have very close MgO/Na_2O+K_2O, MgO/Al_2O_3, MgO/TiO_2, MgO/Fe_2O_3+FeO distributions on variation plots. Although CaO content in Inagli series is higher than in Ryabinoviy one, it can be due to cumulation of clinopyroxenes in Inagli clinopyroxenites and shonkinites. The estimated composition of parent-melt for Inagli ultramafites and compositions of Tobukian lamproites and Inagli ultramafites lie on a one line on MgO/CaO plot (Fig.2). It shows, that Inagli dunites and wherlites can be obtained, crystallizing olivine and some diopside from the estimated parent melt, while the residual melt has the composition, close to Tobukian lamproites.

Summing-up all obtained results, we can make following conclusions and supposions.

1. Such series of ultramafite, mafite and potassic rocks, like in Inagli massif, can be obtained by fractional crystallization of *lamproite* magma with MgO~25-26%.
2. Major-element composition of this magma is very close to the parental melt of the dykes of Tobukian complex (Ryabinoviy massif).
3. We can suppose, that under Tobukian dyke complex there are cumulative ultramafic rocks, which are similar to Inagli ones.

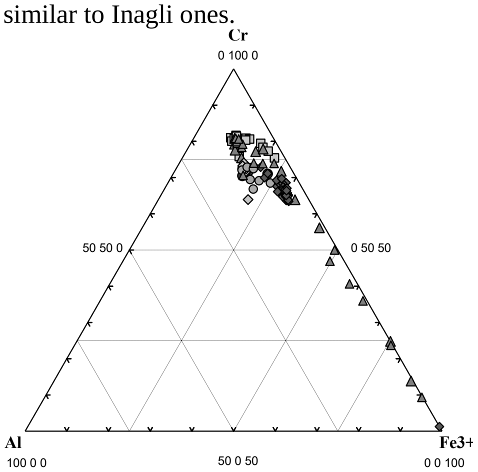

Fig. 1 Compositions of Cr-spinels of Inagli (blue) and Ryabinoviy (orange) rocks.

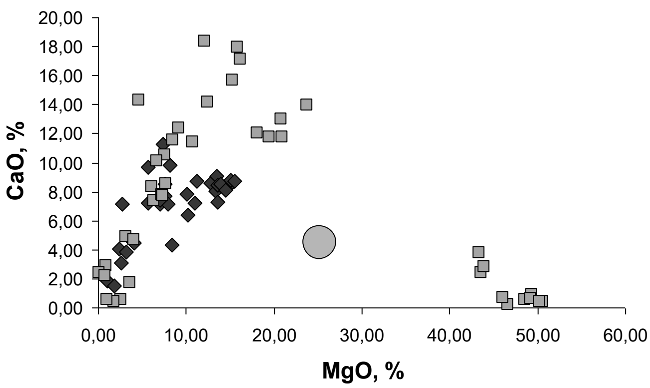

Fig. 2 CaO/MgO distribution plot for Inagli (blue), Ryabinoviy (red) rocks and estimated parent-melt composition for Inagli dunites (green).

References:

1. Ibragimova E.K., et.al, 2015 The results of U-Pb (SHRIMP) dating of zircons from dunites of Inagli massif (Aldan shield) and problem of genesis of concentrically-zoned magmatic complexes [in Russian], Regional'naya Geologiya I Metallogeniya (Regional Geology and Metallogeny) , 62.
2. Korchagin A.M., 1996, Inagli pluton and its minerals [in Russian], Nedra.
3. Laurent Guillou-Frottier, et.al, 2014, Rheological conditions for emplacement of Ural–Alaskan-type ultramafic complexes, Tectonophysics, 631, 130-145.
4. U. Mues-Schumacher, J. Keller, 1995, Mineral chemistry and geochronology of the potassic alkaline ultramafic Inagli complex, Aldan Shield, eastern Siberia, Mineralogical magazine, 60, 711-730.
5. Okrugin A.V., 2004, Crystallizational-immiscibility model of forming of PGE-cromitite ores in mafic-ultramafic complexes [in Russian], Tikhookeanskaya Geologiya, 23 (2), 63-75
6. Sharygin V.V., 1993, K-alkaline picrites of Ryabinoviy massif (Central Aldan), Geologiya I Geofizika, 4, 60-70.
7. Shatov V.V. et.al, 2012, Petrography, geochemistry and isotopic (U-Pb and Rb-Sr) dating of alkaline magmatic rocks of Ryabionoviy massif (Southern Yakutia) [in Russian], Regional'naya Geologiya I Metallogeniya (Regional Geology and Metallogeny), 51, 62-78.

Compositional and internal structure features of pyrochlores from carbonatites of the Chuktukon carbonatite complex

Chebotarev D.A.

The Sobolev's Institute of Geology and Mineralogy of SB RAS, chebotarev@igm.nsc.ru

Attention to the studies of carbonatites is caused by the fact that they are a source of the world's largest deposits of REE, Nb, Zr. One of the most important mineral concentrators of Nb in carbonatites is pyrochlore. Therefore, investigation of its chemical composition and textural features is important for determination of the acceptable options of niobium extraction.

The Chuktukon carbonatite complex is part of the structure of the Chadobets uplift located on the south-western margin of the Siberian platform and represents one of the platform areas of alkaline-ultramafic magmatite formation. The Chadobets uplift has the shape of an ellipse with the axes sizes 45 and 35 km. There are two ledges forming the uplift core – the northern (Terinovskiy) and the southern (Chuktukon). In the uplift core, the upper Proterozoic deposits are exposed, and Cambro-Riphean deposits are exposed at the periphery of the complex: slates, soapstones, aleurolites, sandstones, calciferous, dolomitic-calciferous, dolomitic, sideritic deposits, pebbles, coal interlays. The external frame of the uplift consists of the Permo-Carboniferous and lower Triassic deposits (tuffs) and fields of subgorizontal early Triassic traps. Rocks of the carbonatite complex are presented by the ultramafic alkaline rocks (melilitite-nepheline and pyroxene micaceous peridotites, picrites, alneites, melteygites), carbonatites, kimberlites composing veins, dykes, stocks from several ten to several hundred meters (Kirichenko, etc., 2012; Lapin and Lisitsyn, 2004; Lapin, 2001, 1997).

Several stock-like carbonatite bodies with the sizes of 1,2x0,7 km are mapped at the area of the Chuktukon ledge, (Kirichenko, etc., 2012; Lapin and Lisitsyn, 2004; Lapin, 2001, 1997). Almost the whole other part of the ledge represents stockwork of veins and streaks of carbonatites with different thickness in Proterozoic deposits. Among the carbonatites composing stock-like bodies and large veins, the fine- and medium-grained varieties are prevailing. They are the rocks of white and brown color of different shades with massive, spotty and less frequently banded texture. The main mineral is calcite, minor and accessory minerals are dolomite, pyrochlore, Nb-rutile, sulfides, rippeite, tayniolite, ankilit-(Ce), K-feldspar. The carbonatites have undergone hydrothermal changes from weak to very intensive, which had led to the formation of quartz, barite, goetite, romanechite, parisite-(Ce), sinchysite-(Ce), monazite-(Ce), carbonate-fluorapatite, aegirine. In the weathering crusts of carbonatites, considerable resources of niobium and REE concentrating in goetite, monazite-(Ce), florensite-(Ce) are revealed.

Pyrochlore forms octahedral light brown, brown to black crystals 0,2-1,0 mm in size. In the crushed parts of rocks, pyrochlore forms crystalline aggregates and veinlets of small crystals and fragments up to 0,1 mm.

The pyrochlore crystals have two types of zoning: oscillating and spotty-mosaic. The spotty-mosaic zoning might be combined within one crystal with the oscillating one. Inclusions of calcite, strontianite, barite, fluorapatite, carbonate-fluorapatite, baddeleyite and columbite are observed in large crystals and in their fragments.

According to the classification proposed by D. Atensio (to Atencio et al., 2010), the studied pyrochlores are fluorine- and oxycalciopyrochlore and kenopyrochlore.

In crystals with oscillation zonality variations in contents (in terms of oxides) of niobium (from 65 to 73 wt. %), titan (from 2,8 to 3,1 wt. %), calcium (from 16 to 17 wt. %), sodium (from 7 to 8 wt. %) and fluorine (from 4,7 to 5,6 wt.% F) are observed.

In the areas with the spotty-mosaic zonality, the following features are noted. In the dark parts of the back scattered electron images, in comparison with the light parts, higher content of silicon (up to 4,6 wt.% SiO_2) and titanium (up to 6,14 wt.% TiO_2) are observed. Niobium content (up to 60-65 wt.% Nb_2O_3) and A-site vacancies (0,12 against 0,16 apfu) are lower. At the same time, there are the areas enriched in barium (up to the 3 wt.% BaO), lead (up to the 2 wt.% PbO), containing large amounts of strontium (up to the 10 wt.% SrO) and depleted in calcium (from 5,6 to 14 wt.% CaO), fluorine (up to 2 wt.% F) and sodium (up to 2,5 wt.% Na_2O).

Thus, oscillation zonality is connected with the rhythmical variations of chemistry of the mineral-forming environment during the formation of pyrochlore. The spotty-mosaic zonality is a consequence of the hydrothermal process that had led to the change of the chemical composition of the certain parts of the crystals. The alteration process has affected the external areas and sites associated with the borders of crystal defects (cracks and weakened zones along the borders of inclusions).

Pyrochlore alteration process resulted in its enrichment in strontium, barium, lead, silicon, titanium, and depletion of fluorine, sodium, calcium and niobium according to the following substitution reactions (Nasraoui, Bilal, 2000):

$Ca^{2+} + Ti^{4+} = Na^{+} + Nb^{5+}$,

$Na + F^{-} = VA + VY$, $Ca + O = VA + VY \rightarrow VA + VY = Sr + O$,

where VA and VY are A- and Y-site vacancies, respectively.

These exchange reactions between pyrochlore and hydrothermal fluids are possible at relatively low pH, low $a_{Ca^{2+}}$, a_{HF}, $a_{Ca^{2+}}$ and increased $a_{Sr^{2+}}$ and a_{LREE} (Nasraoui, 1996; Nasraoui, Bilal, 2000). The formed spotty-mosaic zonality is likely caused by the tendency to accumulation of one or another element by different parts of pyrochlore crystals.

References:

1. Kirichenko V. T., Zuev V. K., Perfilova O. Yu., Sosnovskaya O. V., Smokotina I. V., Markovich L. A., Borodin V. P., Mironyuk E. P. "The state geological map of the Russian Federation. Scale 1: 1 000 000 (third generation). Angaro-Eniseysky series. The sheet O-47 – Bratsk. Explanatory note." - SPb.: VSEGEI cartographical factory, 2012, 470 pages (163-179 pp). (In Russian).
2. Lapin A. V., Lisitsyn D. V. "About a mineralogical typomorphism of alkaline ultramain magmatites of the Chadobetsky raising."//Domestic geology, No. 6, 2004, page 83-92. (In Russian).
3. Lapin A. V. "About kimberlites of the Chadobetsky raising in connection with a problem of the formational-metallogeny analysis of the platform alkaline-ultramain magmatites."//Domestic geology, No. 4, 2001, pp. 30-35. (In Russian).
4. Lapin A. V. "Structure, formation conditions and ore-bearing of the main types of REE in the carvonatite weathering crusts."//Domestic geology, No. 11, 1997, pp. 15-22. (In Russian).
5. Lapin A. V., Tolstov A. V. "New unique deposits of rare metals in the carbonatite weathering crusts."//Investigation and protection of the Earth’s interriors, No. 3, 1993, pp. 7-11. (In Russian).
6. Atencio D., Andrade M. B., Christy A. G., Giere R., Kartashov P. M.. «The pyrochlore supergroup of minerals: nomenclature.» // The Canadian Mineralogist, v. 48, 2010, pp. 673-698.
7. Nasraoui M., Bilal E. «Pyrochlores from the Lueshe carbonatite complex (Democratic Republic of Congo): a geochemical record of different alteration stages» // Journal of Asian Earth Sciences, v. 18, 2000, pp. 237-251.
8. Nasraoui, M.. «Le gisement de Nobium de Lueshe (Nord Est du Zaire): evolution geochimique et mineralogique d'un complexe carbonatitique en contextes hydrothermale et supergene». // Ph.D. thesis, Ecole des Mines de Paris/Ecole des Mines de Saint Etienne, 1996.

Content and position in physical fields of Paleozoic volcanic constructions of the Sukhoi Log Zone (The Middle Urals)

Chervyakovskiy V.S.[1], Volchek E.N.[1], Ogorodnikov V.N.[2], Slobodchikov E.A.[2]

1 -Institute of geology and geochemistry of RAS, volchek@igg.uran.ru

2 -The Urals state mining university, fgg.gl@m.ursmu.ru

In the East of the Middle Urals in a number of places the products of ancient volcanic eruptions are of good preservation and comprise a major part of geological sections. This made it possible for the researchers to reconstruct paleovulcanos when fulfilling geologo-surveying works. According to the available geologo-geochemical data the fragments of three volcano-tectonic structures of central type with the features of caldera-formation and the system of radially-arc faults have been preserved in sections along the banks of the r. Pishma and its tributaries [2, 3, 4]. Here it is marked the location of paleovulcanos “Dalniy”, “Diviy Kamen”, “Shata”. Their geological structure and the obtained by us petrochemical data have a great importance for the establishing of paleogeological environments of the vulcanite formation. In different time these formations have been mapped and studied by a number of researchers: T.V. Dianova [1975], V. A. Koroteev et.al [1979], V.N. Ogorodnikov et.al [2002] and oth.

Geomorphologically these paleoconstructions present themselves a series of uplifts, separated by ravines and rivers. The fragments of paleovolcano Dalniy are traced from the mouth of the r. Reft downstream the r. Pishma and along the river Brusyana. The lower series of this paleoconstruction is composed of slope-occurring basalt lavas with uneven-waving surface.

For several lava flows it is typical clear pillow separation. The pillows are of flatten form, it is seen abut them the crust of chilling with parallel to it distribution pores and amigdules. The upper part of the series is associated with vulcanites of andesibasalt content and tuff-breccias. The funnel facies formations basalts are fixed in big rock exposure one kilometer of the r. Reft mouth downstream the r. Pishma. The rock central part is composed of almond-shaped basalts with good porphyry structure. In basalts of marginal parts the porphyry structure is weaker displayed. The lower marginal part of is composed of lavabreccia of the same basalts, including angular fragments and rounded huge blocks and bombs in lava stream. In some places the basalt flows are overlapped by agglomerate bomb-clumpy tuffs. The agglomerate tuffs are gradually changed into coarse- and middle-fragmental tuffs of basalt and andesibasalt content. The basalt flows in a number of exposures are dissected by subvulcanic bodies of acid vulcanites of thickness from 1 to 3 m. Sometimes subvulcanic formations present themselves the protruding over basalts ridges of height for about 1-1.5 m with subhorizontal columnar jointing. The series of volcavogenic-sedimentary rocks in profile are presented by tuffoconglomerates, tuffosandstones, tuffites, jaspers.

The paleovolcano “Diviy Kamen” has been reconstructed in the interfluve of the river Pishma, along its left bank. Its age was determined as D_2 on the Eifelian fauna in limestones fragments from tufoconglomerates and clumpy tuffs of the section lower horizons [2]. The remains of this paleovolcano are presented by a complex association of basalt lavas, andesibasalts, andesites, andesidacites, rhiodacites. Also are widely spread tuffs of different content. In a number of exposures one can observe the lava flow contact of almond-shaped andesibasalts and mid-fragmental tuffs. The main relict of paleovolcano is the rock massif of size 220x55 m with steep slopes. The massif is composed mostly of pyroclastic rocks. These are middle- and coarse-fragmental rocks crystalloclastic tuffs of andesitebasalt and andesite content. The section is penetrated with subvulcanic bodies of dacites, rhiodacites and dolerite dykes.

The remains of one more volcano are in the valley of the river Shata. Here come out into the surface the horizons of tuff-sandstones and tuff-conglomerates, as well as lava flows of basalts, andesibasalts and their tuffs with limestone fragments. The age of these formations has been accepted as D_2 since above the andesibasalts and their tuffs are occurring rifogenic limestones with the Eifelian fauna, forming here numerous rocks. Lava flows are traced on both banks of the river and have pillow structure. The pillow size comprises 0.5 m, sometimes reaches 2-3 m. It is typical for them a clear zone of chilling in marginal parts. The lavas are overlapped by clumpy agglomerate and psephitic tuffs. The fragments in agglomerate tuffs are presented by blocks and basalt and andesibasalt bombs. The size of volcanic bombs reaches 30 cm. Almond-shaped basalts break with subvulcanic body of rhiolite content.

Lava morphology, wide development of pyroclastic rocks, the presence of near-funnel, funnel and extrusive formations in association with limestones and terrigene deposits made it possible for the researchers to conclude that the paleovolcano formation occurred under marine conditions at small depths [2, 3].

The paleovolcanos find their reflection in magnetic field. Funnel formations and subvulcanic bodies possess close magnetic field of intensity for about 400 nTl and the framing them lava flows, composing their slopes, form the stripes with higher values of magnetic field intensity (to 500 nTl). A wide development of pyroclastic rocks caused the appearance of differentiated magnetic field with interval of values from - 400 to +100 nTl [3, 4].

On the obtained by us petrochemical data the paleovolcano Dalniy rocks are presented by andesibasalts, in lower degree – basalts, dacites and rhiodacites. Volcanites of different alkalinity are moderately-potassic. On FeO/MgO and SiO_2 rato they refer to calcareous-alkaline series. Basalts, andesibasalts, andesites and dacites of paleovolcano Diviy Kamen form calcareous-alkaline series. Vulcanites are moderately-potassic, with small titanium presence. On the value of the aluminiferousness coefficient they refer to moderately- and high-aluminiferous (al 0.8-2.7). The observed growth of value of the aluminiferousness coefficient from basic to acid members reflects the increasing of the rock differentiating degree. In effusive rocks of the paleovolcano Shata predominate andesibasalt compositions. Acid rocks are presented by dacites. The alkaline metal sum in all rocks does not accede 5 wt %, K_2O composition 0.5-1.1 wt %. These are low-titanium, moderately aluminiferous rocks.

The study of element-impurities in vulcanites distribution made it possible to suppose in which geodynamical environments they could have been formed. The character of REE distribution in basaltoids of Dalniy and Divyi Kamen paleovolcanos is similar and typical of supersubductional formations. Is characteristic for them the prevalence of light lanthanoids over the heavy ones (La/Yb 2.8-4.5) and the expressed europium deficit. In the Shata andesibasalts the REE composition is not high, lower, than in analogical on composition formations of other paleovulcanos. The lanthanoid fractioning is weak (La/Yb 1.2-1.6).

In comparison with middle oceanic tholeiites (N-MORB) the basalts are enriched with big-ion elements (Rb, Ba, Sr, Th) and impoverished with high-charge elements. It makes them close to the island-arc basalts [5]. The microelement distribution curves for andesites and dacites repeat the plots for basalts, but have less deep Ta and Nb minimums and Sr minimum.

The volcanites of these paleostructures have geochemical features characteristic for the complexes of island arc environments.

References:

1. Dianova T.V. About primary forms of occurring of Paleozoic volcanogenous formations in the Alapaevsk-Kamensk zone of the Urals. Sverdlovsk: USC AS USSR, 1975. P. 181-184.
2. Koroteev V.A., Dianova T.V., Kabanova L. Ya. Middle -Paleozoic volcanism of the Urals Eastern zone. L.: Nauka, 1979. 129 p.
3. Ogorodnikov V.N., Polenov Yu. A., Sazonov V.N., Shevalev V.P., Slobodchikov Ye. A., Dubeikovsky S.G. Geological routs on the Sukhoi Log and Kamensk polygons. Ekaterinburg: Publ. USMGA, 2002. 296 p.
4. Educative geologo-surveying practice. The Sukhoi Log polygon: educative-methodical handbook/ V.A. Dushin, V.A. Ribalko, K.B. Alyoshin: edited by V.A. Ddushin, Ur.st. mining un. Ekaterinburg: Publ. USMU, 2012. 240 p.
5. Frolova T.I., Burikova I.A. Magmatic formations of modern geotectonic environments: Ed. handbook, M.: Publ. MSU. 1997. 320 p.

Oktyabr'sky PGE-Cu-Ni Deposit, Western Flank (Norilsk Area): geology and ore types

Chikatueva V.[1], Krivolutskaya N.[2], Lebedev A.[1]

1-Lomonosov MSU

2 -Vernadsky Institute of Geochemistry Russian Academy of Science

The problem. Norilsk deposits have large resources of Pt-Cu-Ni ores, very important not only in Russia but across the world. Many geologists are looking for similar deposits in other areas, that is why geological structure of these deposits cause a great amount of interest. At the present time, two main models of the formation of the Norilsk ores are known. The first model is based on an suggestion that sulfides were formed open system when magma rised to the surface (Rad'ko, 1991; Naldrett, 2003); the second model supposes the ore formation in closed magmatic system (Dyuzhikov, etc., 1988; Likhachev, 2006; Krivolutskaya, 2014). The main task of this study is to verify these hypothesis based on study the western flank of the Octyabr'sky deposit in the Norilsk district.

Results. The Octyabr'sky deposit is related to the Kharayelakh basic-ultrabasic massif. The massif is located in the Devonian sedimentary rocks inside the southern part of the Kharayelakh Trough. The Kharayelakh intrusion has the differentiated structure in its central part and consists of a gabbro-dolerites of different composition varying from the picritic gabbro-dolerites to gabbro-diorites. The intrusive body has a thickness 100-150 m (Dodin, Batuyev, 1971; Likhachev, 2006). Disseminated mineralization is located in picritic and the taxitic horizons. Sulfide veins are concentrated in the bottom of intrusion and sometimes in its top in outer-contact zone.

During the field work, we have studied cores of boreholes ZF-9, ZF-10, ZF-12 and ZF-18 drilled by Ltd. Norilskgeologiya in the western flank of the Octyabr'sky deposit. Based on these data it has been established that the western flank of deposit consist**s** of numerous small intrusive bodies (from the first meters to 75 meters in thickness). Bodies of gabbro-dolerites are concentrated in the contact zone of Manturovsky and Razvedochninsky Formations. They consist of middle- and coarse-grained olivine and olivine-free gabbro-dolerites with poikilithic texture. The content of MgO varies from 5.37 to 8.2 mas. % in the olivine-free gabbro-dolerites and from 8.6 to 10 mas. % in olivine gabbro-dolerites. The highest concentration of the Cu and Ni are 15805 ppm and 12886 ppm correspondingly. The picritic gabbro-dolerites are located above the olivine-free gabbro-dolerites and have low Cu and Ni and the high MgO contents reaching up 23.49 mas. %. Contactic gabbro-dolerites are characterized by fine-grained texture and low MgO content (0.75 -1.4 mas.%. They contain interlayers with higher MgO concentrations (up to 4 mas.%). The disseminated sulfide mineralization belongs to the lower part of olivine-bearing intrusive body. Composition of sulfide minerals (chalcopyrite, pyrrhotite, pentalandite, cubanite) have been investigated by electron microprobe Cameca SX 100 in GEOKHI of the Russian Academy of Sciences (analyst N. N. Konokova). The study shows that the composition of ore-forming minerals has no essential differences from ones located in the central parts of the deposit.

Conclusions. This study has demonstrated that western part of the Octyabr'sky deposit has a very different structure in comparing with its central part. There are many small intrusive bodies (cores ZF-10 and ZF-12) are located here. They consist of picritic, olivin-free, olivine-bearing and olivine gabbro-dolerites. The sulfide mineralization are concentrated in olivine and olivine-free gabbro-dolerite while picritic gabbro-dolerites are practically free. This is the most essential difference between the western flanks of the field and its central parts.

This study was financially supported by Russian Foundation for Basic Research (project N 15-05-09250).

References:

1. Dyuzhikov, O.A., Distler, V.V., Strunin, B.M., et al., 1988. Geology and Ore Potential of the Noril'sk Region, Moscow: Nedra [in Russian].
2. Krivolutskaya, 2014. Siberian Traps and Pt-Cu-Ni Deposits in the Noril'sk Area, KMK Scientific Press Ltd 320 pp. [in Russian]
3. Naldrett, A.J.,2003. Magmatic Sulfide Deposits of Nickel-Copper and Platinum Metal Ores, ISBN 5-902260-02-7, St Petersburg University 400 pp [in Russian].
4. Rad'ko, V.A., 1991. Model of geodynamic differentiation of the intrusive traps in the northwestern Siberian Platform, Geol. Geofiz. no. 11, pp. 19–27. [in Russian]

Melt inclusion studies implications to magmatic processes of the Wai subgroup, Deccan Volcanic Province (Western India)

Choudhary B.R.[1]

1-Indian Institute of Technology Bombay (IITB) Mumbai, India, choudhary.r.babita@gmail.com

Introduction: Melt inclusions represent melt trapped by minerals during their growth in magma chambers and during magma ascent to the surface. Several studies of melt inclusions in Large Igneous Province (LIPs) in different parts of world had been documented. The geology of Deccan LIP possesses potential published data sets on geochronology and geochemistry; the apparent lack of significant work on Deccan LIP is intriguing. Melt inclusions in Deccan LIP in minerals of mafic volcanic are the best prospects to acquire information on physio-chemical conditions and evolutions of Deccan LIP.

Geological setting: The Deccan LIP lava cover an area about 518,000 km^2 and formations are relatively evolved, as demonstrated by their low MgO and high FeO contents. The Deccan LIP includes a embraces thick sequence of nearly horizontal basalt flows that erupted at the Cretaceous-Tertiary boundary. This volcanic episode was dominated by fissure eruption and occurred repetitively from 63 to 69 Ma [1]. The Deccan LIP rocks belonging to different formations are geochemically different in Western Ghats section. On the basis of major and particularly trace element studies the sequence can be divided into a number of packages with distinct chemostratigaphic character [2]. To identify the reasons accountable for the diversity in geochemical composition and volatile enrichment/ degassing of Deccan LIP rocks from the Western Ghats section (India) melt inclusions studies have carried out in clinopyroxene and plagioclase feldspar. This study signifies the first melt inclusion study of magmas from the Western Ghats Section of Deccan LIP.

Results: This study includes geochemical analyses of rocks, minerals and melt which are well-preserved within the inclusions. The inclusions are primary and range in shape from irregular to elliptical. Their size varies from few to 100 microns. In both clinopyroxene and plagioclase phenocrysts the inclusions are mainly partly crystalline, and are composite with daughter phases. Some are glassy with or without a shrinkage bubble, brownish to murky in color with opaque phases. Among the daughter phases there are ore phases (clinopyroxene, ilmenite, magnetite and titanomagnetite). Shrinkage bubbles are usually distorted due to pressure inside the inclusion generally growing during post-entrapment cooling; fundamentally because of a pressure drop in the inclusion [3]. The inclusions are significantly enriched in TiO_2 (3.68 to 0.08 wt%) and FeO (18.3 to 2.63 wt%). Homogenization experiments were performed, melt inclusions were partially homogenized upon heating and some burst after homogenization, though crystalline phases were incompletely dissolved. Upon overheating up to 1250°C for a longer time some inclusions did not decrepitate.

Volatiles are determined to have a wide range in composition in both plagioclase- and pyroxene-hosted melt inclusions by using FTIR: H_2O at 1630 cm-^{I} (2.04 to 3.76 wt%), total dissolved water peak at 3550 cm-I (0.94 to 2.05wt %) and CO_2 (1808 to 428 ppm). A range of processes are responsible for the variation in the concentrations of volatiles in inclusions, e.g. degasing and diffusion [4]. The variability, particularly of MgO, Al_2O_3, TiO_2, and K_2O in the inclusions explains the differentiated and late stage evolved magma. Post-entrapment crystal aggregates contributed to a change of the parental composition [5]. Compositional concentrations are affected by diffusion from the host into the inclusion, e.g. caused the high Al_2O_3. The melt inclusions exhibited high Fe and Ti contents similar to the bulk composition of the lava of Deccan LIP; i.e. fractionating tholeiitic lava follow a trend that is reflected by iron saturation until Fe-Ti oxides start to precipitate. Fe-Ti oxides that were trapped along with the melt show inconsistent high temperature homogenization (i.e are off-track from the basaltic melt temperature and retain un-melted crystals in partially homogenized melt inclusions).

Representative analyses (wt.%) of melt inclusions

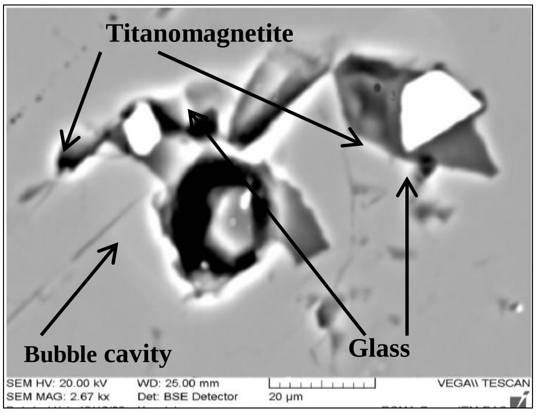

Oxides	Wt%	Wt%
SiO_2	66.8	43.4
TiO_2	3.68	0.08
Al_2O_3	9.7	17
FeO	18.3	2.63
MgO	18.3	1.6
CaO	15.83	3.38
Na_2O	5.92	0.27
K_2O	2.62	0.02
P_2O_5	3	0.1

Discussion: The melt inclusions characterise genetic relationships between magmatic flows of the upper formations of the Deccan LIP (Wai subgroup) and allow elucidation of their mantle source and the influence of differentiation and fractionation on magma composition. Studied melt inclusions are rich in volatile components. The shift of the melting sequence (recorded in the inclusions) towards higher temperatures can also probably be explained by post-entrapment changes and re-equilibration with the host crystal with dropping of temperature.

References:

1. Ernst.E.R (2014) Large Igneous Provinces. Cambridge University Press
2. Mahoney et al. (2000) J. Petrology 47: 1099-1120
3. Wallace P. J et al. (2015) American Mineralogist 100: 787-794
4. Sobolev A.V et al. (2015) In: Volcanism and Global Environmental Change: Cambridge University Press, 147-163
5. Danyushevsky et al. (2002) Chemical Geology 183: 5-24

On mathematical modeling of regularities of geodynamic process

Dolgaya A.A.[1,2], Vikulin A.V.[1], Gerus A.I.[1,3]

1 -Institute of volcanology and seismology FEB RAS, adolgaya@kscnet.ru

2 -Kamchatka State Technical University

3 -Vitus Bering Kamchatka State University

Planetary geodynamic process is manifested mainly in the form of seismic and volcanic events occurring within the most active regions of the Earth: the margin of the Pacific Ocean, the Alpine-Himalayan belt and the Mid-Atlantic Ridge. The importance of studying patterns of seismic and volcanic processes is explained by the necessity to understand and, as a result, to be able to reduce the tragic consequences of the catastrophic earthquakes and volcanic eruptions.

The research conducted by the authors is based on an integrated approach to the study of the laws of planetary geodynamics (seismic and volcanic) process. Information basis of the study is database [7], compiled and registered by the authors. This database contains data on earthquakes over the last 4.1 thousand years and volcanic eruptions over the last 12 thousand years represented in a common format. As energy characteristics we use magnitude M for earthquakes and explosivity index W for eruptions. Database format allows us to explore the features of the distributions of seismic and volcanic activity within a single view using a well-known and new, developed by the authors, methods.

Research of laws of seismicity and volcanism of geodynamic active regions of the planet includes the study of their temporal and spatio-temporal patterns.

To study the temporal regularities authors used the methods of spectral, spectral-correlation analysis of time series and the method of “quasi-phase plane” [3] developed by the authors. These techniques have been formalized in the form of algorithms and automated with the help of specialized computer information systems [1, 2]. Study showed the existence of common for seismic and volcanic processes main period $T_0 \approx 250 \pm 30$ years, and even periods multiples of it: $T_2 \approx 2T_0 \approx 500 \pm 50$, $T_4 \approx 4T_0 \approx 1000 \pm 100$ and $T_8 \approx 8T_0 \approx 2000 \pm 200$ years. According to the authors, the existence of periods common for both processes allows us to consider seismic and volcanic processes as components of a uniform wave geodynamic process.

To investigate the spatial and temporal patterns of the geodynamic process authors constructed the mathematical model of migration of earthquakes foci and volcanic eruptions. The model is based on the description of the seismic and / or volcanic processes as the sum of one-dimensional sequences of events taking place along the axial line of the belt during the reporting period. In theory of stochastic processes this model corresponds to a one-dimensional random walk, which is generated by a sum of mutually independent and identically distributed variables, or Markov chains. To study the spatial and temporal distributions of earthquakes foci and erupting volcanos within the framework of proposed approach computational method for studying the migration of seismic and volcanic activity (IMSiVA) [4] was developed and automatized in software application [8].

Important results have been obtained using this approach.

Firstly, within large energy ranges for the most active zones we obtained a significant statistical data on the velocities of migration of earthquakes foci and volcanic eruptions, which allows to consider the migration process as a characteristic property of seismic and volcanic activity of the Earth.

Secondly, the existence of relationships between the velocities of migration of earthquakes foci and volcanic eruptions (*V*) and their energy characteristics (*M*, *W*) was established. This allowed the authors to assume the wave nature of migration.

Thirdly, it was found that the slopes of the curve defining the relationship between the velocities of migration of seismic and volcanic activity (*p*-value) are "sensitive" to the tectonic setting in the zone. *P*-value for "seismic" dependencies of the Pacific Ocean and the Alpine-Himalayan belt (compression zones) are positive; *p*-values for "seismic" dependency of Mid-Atlantic Ridge and all the "volcanic" dependencies (stretching zones) are negative [6].

Analysis of values of parameter *p* showed that it is a persistent vector, which can be regarded as an analogue of the angular momentum of geodynamic process.

According to the rotational model the motion of block chain and geodynamic properties of geomedium can be described with sine-Gordon equation and one of its solutions in the form of a solitary wave – soliton [5]. This solution in physically understandable way depends on the modulus of momentum. Direction (sign) of the momentum corresponds to the geodynamic conditions in the zones: compression (positive) and stretching (negative). This makes it possible within the framework of physical concepts to model the migration of seismic and volcanic activity as the wave-particle process with the properties of short- and long-range actions.

The following results were obtained during the research:

1. Mathematical, based on the theory of Markov processes, model of migration process of earthquakes foci and volcanic eruptions was constructed.
2. Numerical methods for the study of spatio-temporal patterns of distribution (migration) of seismic and volcanic activity (IMSiVA method) and temporal patterns of seismic process (method of “quasi-phase plane”) were developed.
3. Algorithmic and software implementation of the set of used computational methods was performed. This software is focused on short-term computer simulations, which allows the use standard user computing resources in geodynamic problems under study.
4. The proposed model and developed methods and computer programs made it possible to get data for explanation of the available evidence of the patterns of temporal, spatio-temporal (migration) and energy distributions of seismic and volcanic activity within tectonically active zones of the Earth.
5. A physical model of the geodynamic process as a wave process was proposed. This model is based on concepts of migration and cyclicity (quasi-periodicity) of seismic and volcanic activity, and the geodynamic parameter that is sensitive to the tectonic setting in the active zones and near them. Model consequences are confirmed by physics of solid state, physical (non-linear) acoustics and materials science [5].

References:

1. Dolgaya A.A., Ankvab A.A. Computer information system "Periodicity" // Computer program. Reg. No. 2013661747, 16.12.2013.
2. Dolgaya A.A., Nikolaev A.N. Computer information system "Quasi-periodicity" // Computer program. Reg. No. 2013661748, 16.12.2013.
3. Dolgaya A.A., Vikulin A.V. Quasi-periodicity of geodynamic process and conservation laws // Academic Journal of Western Siberia. 2013. V. 9. No. 6 (49). P. 6–7. (in Russian)
4. Dolgaya A.A., Vikulin A.V., Gerus A.I. Modeling of spatio-temporal regularities of geodynamic processes with the help of IMSiVA method // Volcanism and related processes. XVIII annual scientific conference, devoted to the Day of Volcanology. Abstracts. Petropavlovsk-Kamchatsky, 2015. P. 135-139. (in Russian)
5. Vikulin A. V., Makhmudov Kh. F., Ivanchin A. G. et al. On Wave and Rheidity Properties of the Earth’s Crust // Physics of the Solid State, 2016. V. 58, No. 3. P. 561-571.
6. Vikulin A.V., Akmanova D.R., Vikulina S.A. et al. Migration of seismic and volcanic activity as display of wave geodynamic process // Geodynamics & Tectonophysics. 2012. V. 3. № 1. P. 1–18.
7. Vikulin A.V., Melekestsev I.V., Akmanova D.R. et al. Catalog of seismic and volcanic events // Data base. Reg. No. 2014620569, 17.04.2014.
8. Vikulin A.V., Melekestsev I.V., Akmanova D.R. et al. Information-computational system for modeling of seismic and volcanic processes as a foundation of research on wave geodynamic phenomena // Computational technologies. 2012. V. 17. No. 3. P. 34-54. (in Russian)

Alkaline ultrabasic carbonatitic magmatism of the Chadobets upland

Doroshkevich A.G., Chebotarev D.A, Sharygin V.V.

V.S. Institute of Geology and Mineralogy SB RAS, doroshkevich@igm.nsc.ru

The Chadobets alkaline ultramafic carbonatite complex (Chuktukon and Terinovskiy ledges) is located within the Chadobets upland (water-collecting area of the Chadobets River, Krasnoyarsky krai, Russia). The country rocks are Precambrian and early Cambrian sedimentary terrigene and carbonate rocks. All igneous rocks within the Chadobets upland are not opened on the surface and recovered by alluvial sediments. The complex comprises the following sequence of rocks from the earliest to the latest: ultrabasic rocks (alkaline picrites), carbonatites and kimberlites (Sklyarov et al., 1962). Picrites and carbonatites form stock-like massifs (up to 2.3 km in diameter), dykes and sills. Kimberlite pipes (several tens) occur in a central part of the upland and cut ultrabasic rocks and carbonatites. All igneous rocks of the complex are sometimes deeply altered (goethitization, silicification). Weathering crust (iron-rich laterites) is developed on the various rocks of the upland (sometimes up to 480 m).

This investigation has been motivated by unusual rock association and the order of their emplacement, but the main characteristics of the alkaline picrite, carbonatite and kimberlite are limited (eg: Slukin, 1992; Lapin, Pyatenko, 1992; Lapin, Lisitzyn, 2004). In this study, we present mineralogical and geochemical (including stable isotopes (O, C data) data for the alkaline picrite, carbonatite (unaltered and hydrothermally altered) and kimberlite samples taken from drill cores of the Chuktukon ledge.

The picrites consist principally of phenocrystal olivine (?) set in a fine-grained groundmass. Olivine (?) is highly altered to minerals of chlorite group. The groundmass is composed of mainly of calcite and minerals of chlorite and clay groups. Perovskite, tetraferriphlogopite, fluorapatite, minerals of spinel group and garnet (andradite-grossular) are common. Barite, quartz, titanite, romanéshite, monazite-Ce, Zr- and Nb-bearing rutile (up to 1.2 wt. % of ZrO and up to 1.6 wt. % of Nb_2O_5), calzirtite, minerals of cancrinite group are accessory. Spinels are chromites in the core and evolve toward titanomagnetites at the rims. Their composition is consistent to “titanomagnetite trend” for the minerals from orangeites and lamproites (Mitchell, 1995). Tetraferriphlogopite contains a negligible amounts of F (bdl) and enriched in BaO (1.1-3.2 wt. %) and TiO_2 (2.6-3.7 wt. %). $\delta^{18}O_{SMOW}$ and $\delta^{13}C_{PDB}$ values of calcite are 12.2-12.7 and (-3.5)…(-5) ‰, accordingly.

Carbonatites are calciocarbonatites. Primary mineral assemblage in these rocks includes calcite, fluorcalciopyrochlore, rippeite ($KNbSi_2O_7$), Mg-F-rich mica (tainiolite or yongzhumingite), fluorapatite, fluorite, Nb-rich rutile (up to 17 wt. % of Nb_2O_5), K-feldspar, aegirine, dolomite, ancylite-Ce, strontianite, olekminskite, sulphides. Barite, quartz, goethite, bernalite (?), monazite-(Ce), Ca-REE-fluorcarbonates (parisite-Ce, synchysite-Ce), Sr-Ba-rich hydropyrochlore, Sr-rich francolite (up to 7 wt. %) and romanéshite are related to a stage of metasomatic (hydrothermal) alteration of carbonatites. Calcite is speckled with dolomite spots and fine dispersions of ancylite-Ce, strontianite, olekminskite. Sr concentration in calcite is up to 0.8 wt. %; mineral became depleted in SrO (bdl) in hydrothermally altered parts of the carbonatites. The coexistence of calcite and dolomite (dolomite inclusions in calcite grains) assumes a temperature about of 837°C for crystallization of the primary paragenesis. $\delta^{18}O_{SMOW}$ and $\delta^{13}C_{PDB}$ contents (7…7.7 and -5…-4.8 ‰) in calcite from unaltered carbonatites fall into PIC box of Taylor et al. (1967). The mineral from hydrothermally altered carbonatites is most enriched in $\delta^{18}O_{SMOW}$ (11.8-12.4 ‰). Similar $\delta^{18}O_{SMOW}$ values were obtained for quartz, romanéshite and goethite (12.1-13.8, 12.7-15 and 12.3-15 ‰).

The kimberlites have brecciated textures with clasts of basement rocks and mantle xenoliths (peridotites, eclogites). Phlogopite, dolomite and olivine (? replaced by dolomite-quartz) macrocrysts set in interstitial fine-grained matrix of dolomite, calcite, potash feldspar, with minor and accessory phlogopite-tetraferriphlogopite, fluorapatite, sulphides, rutile, minerals of spinel group, quartz, fluorcalciopyrochlore, ilmenite, diopside, strontianite, daqingshanite-Ce, barite. The rocks are characterized by an abundance of pelletal lapilli in which kernels of phlogopite, dolomite and olivine (?) macrocrysts are surrounded by dolomite-rich microlithic material with rutile, magnetite and phlogopite. Chromites (up to 3 wt. % of TiO_2) occur as small discrete euhedral crystals (fractions of mm) and exhibit an atoll texture with surrounded thin rings of titanomagnetite (up to 13 wt. % of TiO_2). Their compositions are in good agreement with the published compositional trend of spinels from orangeites and lamproites (Mitchell, 1995). Primary dolomites of groundmass, lapilli and macrocrysts are Sr-bearing (0.3 to 0.6 wt.% of SrO). Late dolomite that grew over primary dolomite and replaces olivines (?) has lower SrO (bdl) with SiO_2 concentrations reaching 3 wt.%. Macrocrysts of phlogopite contains a low concentration of F (bdl) and enriched in TiO_2 (4.5-8 wt. %) and Cr_2O_3 (0.5-1.5 wt. %). In contrast, the minerals from groundmass are richer in F (2-4.5 wt. %) and contain much less TiO_2 and Cr_2O_3 (bdl). Compositions of groundmass mica are consistent to Al-enrichment trend for orangeites of Mitchell (1995). Phlogopite macrocrysts and apatite have $\delta^{18}O$ values (5.5-5.7 and 4.8-5.8 ‰) similar to those typical of the mantle-derived igneous rocks.

The picrites and kimberlites are strongly silica undersaturated (19-26 and 14-16 wt. % SiO_2, accordingly). The rocks are enriched in CaO (up to 27 wt. %), MgO is variable (8-18 wt. %). Kimberlites contain less TiO_2 (2-2.5 vs 3-3.5 wt %), Al_2O_3 (3-4 vs 5-6 wt %), FeO (9-10 vs 11-14 wt %), and more K_2O (3-3.5 vs 0.3-0.9 wt %) than picrites. The incompatible trace element abundances show a significant enrichment in most elements, particularly Nb and REEs and pronounced troughs at Rb, Ta, Pb. Zr, and Hf. The kimberlites have higher normalized REE contents than those of the picrites, but the patterns are all remarkably similar and show strong LREE enrichment with La_n/Yb_n between 33-60.

Carbonatites are characterized by low SiO_2 (up to 3.3 wt. %), MgO (0.4-3 wt. %) and alkali contents (Na_2O+K_2O-0.n wt. %). The hydrothermally altered carbonatites are strongly variable in SiO_2 (up to 80 wt. %), P_2O_5 (0.1-16 wt. %), and CaO (13-42 wt. %). The last have higher Nb (up to 2700 vs 1350), REE (3200-13500 vs 2700 ppm) and Zn (1900 vs 270) contents than the unaltered carbonatites. Chondrite-normalized REE profiles are similar for both types of carbonatites with strong LREE enrichment and La_n/Yb_n between 80-120. Compared to picrites and kimberlites, the carbonatites have relatively low concentrations of Rb, Ta, Zr, Hf, and higher REE and Y content, but nevertheless all Chuktukon lithologies have similar relative enrichments and depletions of trace elements. This implies their parental magmas are related and, of course, were strongly silica undersaturated and enriched in CO_2.

Alkaline picrites and carbonatites were formed by successive magma pulses from subvolcanic intermediate magmatic chamber. The presence of the chamber at a depth of 4 km is conformed by the geophysical data (Kirichenko et al., 2012). The final stage of picrite and carbonatite evolution starts from the interactions of earlier-formed assemblages with hydrothermal fluids and formation of calcite-chlorite and barite-goethite-romanéshite-quartz associations. The hydrothermal processes were responsible for the positive shift relative to the primary $\delta^{18}O$ values and deep alteration of the primary magmatic mineral assemblages. Formation of kimberlites most probably was from a deeper chamber, at least eclogite and diamond stability field (according to presence of eclogite xenoliths and diamonds in kimberlites (Kirichenko et al., 2012)). Can be assumed that despite on the different deeps of the chambers, the melts most probably were generated from a single primary mantle source.

The studies were supported by the Russian Science Foundation (RSF), Grant No. 15-17-20036.

References:

1. Slukin A.D. (1994) Bauxite deposits with unusually high concentrations of REE, Nb, Ti, and Th, Chadobets uplift, Siberian platform, International Geology Review, 36:2, 179-193
2. Lapin A.V., Pyatenko I.K. (1992) Chadobets complex of ultrabasic alkaline rocks and carbonatites: new data about composition and condition of formation, Doklady of Earth Sciences, 6, 88-101 (in Russian)
3. Lapin A.V., Lisitzyn D.V (2004) About mineralogical typomorphism of alkaline ultrabasic magmatic rocks of Chadobets upland, Otechestvennaya geologiya, 683-93 (in Russian)
4. Mitchell, R.H. (1995) Kimberlite, Orangeites and Related Rocks. Plenum Press, New York. 410 pp.
5. Kirienko V.T., Zuev V.K., Perfilova O.Yu., Sosnovskaya O.V. G (2012) State geological map of the Russian Federation. Scale 1: 1 000 000 (third generation). Series Angara-Yenisei. Sheet G-47 - Bratsk. Explanatory letter. - SPb .: Cartographic Factory VSEGEI, 470 p. (in Russian)

Structural and compositional evolution of rocks of an ophiolite association from the Barkhatnaya Mountain (Kuznetsk Alatau)

Dugarova N.A., Gertner I. F., Krasnova T. S.

National Research Tomsk State University, nadyadugarova@mail.ru

Ophiolites from the northern slope of the Kuznetsk Alatau (NW sector of the Altay-Sayan folded area) are the most typical fragments of suboceanic crust, which was formed in the Riphean (T (Sm-Nd) = 950±59 and 937±50 Ma) [1]. They are characterized by a belt development along the main lineament of the ridge, and are represented by semi-circle zones. Their external zone is composed by metamorphic ultramafic rocks, whereas center zone consists of magmatic complexes of different depth facies (starting with cumulative one to volcanogenic) [2].Nowadays the most preserved and studied ophiolite paragenesis is the association of Barkhatnaya, Zayachia, Severnaya and Zelenaya Mountains. It is assumed that this association had at least three stages of exhumation to the modern surface, which reflect main phases of tectonic evolution of the folded band in the region.

During the first stage an accretionary prism of an active island arc forms, where oceanic lithosphere fragments obduct preserving NW-trends in central blocks of the ultramafic bodies from Severnaya and Barkhatnaya Mountains. This stage corresponds to the highest-temperature processes of plastic deformations of olivine and development of isoclinal folding in ultrabasites. These events last from the Late Riphean to the Middle Cambrian.The second stage is controlled mainly by vertical movements along submeridional tectonic fissures with extensive development of recrystallization on the flanks of ultrabasic units at relatively moderate temperatures and pressures. It is accompanied by linear type intrusions of large basites, syenitoids and granitoids; geodynamic setting for their formations correspond to the stage of Altai-Sayan superterrane's collisional accretion in the Late Cambrian - Ordovician.The third stage correlates to the Devonian rifting and is accompanied by formation of some depressions and grabens composed by high-alkaline volcanics and "red-colored" terrigene sediments. In the studied ophiolite paragenesis, actual tectonic events of this stage were shown in turning a core block of basic rocks southward with respect to hyperbasite sides. Other tectonic events were a formation of a serpentinite melange on Zayachia Mountain and in zones of intensive gabbro schistosity on the eastern slope of SevernayaMountain, and activation of crosscutting faults in massifs of Severnaya and Barkhatnaya Mountains with NE and NW trends respectively. These deformations mostly corresponded to dynamic metamorphic alterations of rocks in upper crust levels, and were characterized by low temperatures and locally raised pressures. Another indicator of late events is formation of Barkhatnyi-Kiysk intrusive of subalkali gabbroids and pulaskites, whose rocks "break" through ultrabasites of Barkhatnaya Mountain and Early Devonian effusive rocks of the Rastaysk graben.

Additional research in mineralogy and geochemistry of basites from Barkhatnaya and Zelenaya Mountains confirm multistage metamorphic transformations at different P-T conditions and different stages of obduction of oceanic fragments.On the western slope of Barkhatnaya Mountain, prevailing rocks are homogeneous fine- and medium-grained gabbro and gabbro-diabases pierced through by numerous dyke and vein bodies of microgabbro, microgabbrodiorits and rarely dacite porphyries. By petro- and geochemical characteristics, these rocks correspond to moderate and high-Ti and low-Mg mafites, which are widely spread in upper parts of the gabbroid section and in a parallel dike complex. On the eastern slope of Severnaya and Zelenaya Mountains, basites are represented by gabbroids with various melanocraticity and with signs of differentiation and banded structures, which belongs to upper series of the plutonic complex [3]. All basites have signs of superimposed metamorphic changes (up to the epidote-amphibolite facies).

During studying of mineral composition of metabasites, we found that feldspars are represented by a wide range of minerals from albite to bytownite. Basic plagioclases form prismatic elongated grains, whichare replaced by secondary minerals (sericite, zoisite and calcite) to some extent. Andesines are found in diabases from Barkhatnaya Mountain; they have elongated rectangular shape and irrational orientation. Acid plagioclases are seen in all samples and are characterized by replacement structure, where albite develops in medium and basic plagioclases forming irregularly shaped grains. This type of plagioclase demonstrates metamorphogenic, quite low-temperature transformations of parental rocks.

Other widely spread minerals are amphiboles,whose composition ranges a lot (ferro-edenit, ferropargasite, magnesiohastingsite, actinolite, magnesio- and ferrohornblende). They form slightly elongated or very elongated grains, sometimes with hexagonal section. We can often see irregularly shaped aggregates. In some crystals, zonal structure of a mineral is clear optically and compositionally. Central parts are usually composed by ferropargasite, whereas external zones consist of actinolite and ferrohornblende.

Data obtained from studying phase relationships and changes in chemical composition of the mineral pair "plagioclase - amphibole" suggest several stages of transformations for studied rocks with signs of progressive and retrograde metamorphism. Using a bimineral geothermobarometer [4] we established two stages: progressive metamorphism peak occurs at T = 540-680 °C and P = 2-6 kbar, and regressive stage occurs at T = 450-510 °C and P = 2-8 kbar. This is also confirmed by the results of amphibole geothermobarometer [5], where minerals of marginal parts formed at T = 340-440 °C and P = 1kbar, being superimposed over higher-temperature amphiboles from central parts, which were generated at T = 550-650 °C and P = 2-7 kbar.

Another proof of multi-stage exhumation of ancient oceanic crust fragments into upper crust levels is isotope-geochemical analyses on these rocks and their composing minerals performed by us within last few years. The earliest stage of obduction of restitic ultrabasites, which occurred during formation of "Riphean" oceanic island arc, may be associated with episodes of regional metamorphism at epidote-amphibolite facies.This process was registered based on the results of Sm-Nd isotope analyses of amphibolites from the Tomsk Salient, which yield an isochronous age of 703 ± 63 Ma [6], and 676 ± 16 Ma for metabasalt dike (microgabbro-amphibolite)"breaking" through the southern end of the Barkhatny ultramafic massif. As of now, we have a wide range of ages for different magmatic complexes, which reflects different stages of tectonic evolution in the Kuznetsk Alatau. However, the most recent fragment of magmatic activity in this region is still activation at the age of 265 Ma, which was noted in alkaline rocks from the Goryachegorsk massif [7]. For magmatic peridotite from the western slope of Barkhatnaya Mountain, Sm-Nd mineral isochrones yield the age of 244 ± 37 Ma, which reflects the most recent tectonic movements along the boundary of the Rastayskii graben.

Thus, structural and compositional evolution of the basic component of ophiolite association from Barkhatnaya, Severnaya and Zelenaya Mountains correlates to the stages of plastic deformation of restitic ultramafic rocks, and in some cases fulfills it.

Research carried out with the financial support of the project 8.1.14.2015 (program for improving of competitiveness of the Leading research Tomsk State University)

References:

1. GertnerI.F., BayanovaT.B., KrasnovaT.S., Vrublevskii V.V., SayadyanG.R. Age and matter sources of ophiolites of the Kuznetsk Alatau, SW Siberia: new Sm-Nd isotope data // Mineralogical Magazine, 2013. V. 77, N 5. P. 1159.
2. KonovalovaO.G., PrusevichN.A. Dunite-harzburgite massifs of the Kuznetsk Alatau and Salair. Novosibirsk: Nauka, 1977. 166 P.
3. KrasnovaT.S., UtkinYu.V., Rikhvanov L.P. Geochemistry of gabbroids of ophiolite association from the Barkhatnayamountain (Kuznetsk Alatau) // Magmatism and geodynamics of Siberia: proceeding of the conference. Tomsk, 1996. P. 27-29.
4. MishkinM.A. Amphibole geothermobarometr for metabasites // DAN SSSR, 1990. V. 321,N 4. P. 944-946.
5. Plyusnina L.P. Experimental study of metabasite equilibria, geothermobarometry // Experiment in solving actual problems of geology: proc. scient. works. M .: Nauka, 1986. P. 174-183.
6. PlotnikovA.V., StupakovS.I., BabinG.A., Simonov V.A. Age and geodynamic nature of ophiolite from the KuznetskAlatau // DAN, 2000. V. 372,N 1.PS. 80-85.
7. GertnerI.F., Vrublevskii V.V., Tishin P.A.,GrinevO.M., Gutierrez-Alonso G., BayanovaT.B., Serov P.S. Formational status of goryachegorskii complex: material composition, geochronological attestation and structural position of typomorphic massif // Second Russian-Kazakhstan international scientific meeting "The correlation of altaides and uralides". Novosibrsk: IGM SB RAS, 2014. P. 35-37.

Geochemical zonation of the Porphyry-Epithermal systems of the Baimka trend, Chukchi Peninsula

Dzhedzheya G.T., Sidorina Yu.N.

Lomonosov Moscow State University, bobbin@yandex.ru

Porphyry-epithermal systems (PES) are defined as large volumes of hydrothermally altered rock that may host: porphyry Cu±Au±Mo deposits centered on intrusions; Cu, Au and Zn skarns along the periphery of magmatic bodies; distant subepithermal Zn-Cu-Pb-Ag±Au veins; and Au±Ag±Cu IS and HS epithermal orebodies. PES commonly occur as grouped in linear trends or isometric clusters a few tens to hundreds of km long (Sillitoe, 2010). The models of the mineralogical and geochemical zonation may contribute significantly to the estimation of the erosion level and ore potential at the early stages of PES exploration.

Major resources of porphyry copper in Russia have been discovered in the Baimka trend, Chukchi Peninsula, which includes the known Peschanka deposit and the Nakhodka ore field and other less explored prospects. The region comprises J_3 tuffaceous-terrigeneous sequence intruded by the bodies of J_3 gabbro, K_1 diorite porphyry, and productive K_1 monzodiorite, syenite and quartz monzonite porphyry. The porphyry Cu-Mo mineralization is spatially controlled by the stocks and large dikes of the monzodiorite and quartz monzodiorite phase.

At the Peschanka deposit porphyry ore mineralization is represented by bornite, chalcopyrite, pyrite, and tennantite-tetrahedrite and molybdenite which are minor. Subepithermal sphalerite, Se-bearing galena, tennantite-tetrahedrite, altaite, hessite, and native gold were determined sporadically. There are three stockworks discovered at the deposit — Main, Central and North — producing secondary halos of ore metals of extremely high intensity (up to 1% Cu, 0.5% Mo and 1 g/t Au in soils).

The Nakhodka ore field includes the porphyry Cu-Mo stockworks of the Nakhodka, III Vesenny, Pryamoy, and Malysh and the Vesennee Au-Ag IS epithermal deposit. The major ore minerals are pyrite, chalcopyrite, bornite, tennantite-tetrahedrite, molybdenite, and high fineness native gold. Subepithermal and epithermal IS mineralization, which has economical significance only at the Vesennee deposit, is abundant in all areas to various degrees. It includes the quartz-carbonate veins with As-rich pyrite, galena, sphalerite, chalcopyrite, tennantite-tetrahedrite, as well as minor enargite, electrum, native gold, hessite, altaite, clausthalite, and occasional petzite, pearceite, acanthite.

To determine geochemical zonation the results of core sampling from 175 drill holes within the Nakhodka ore filed and 270 drill holes within the Peschanka deposit were used. The database included such records for the core intervals of an average length of 2 m as (1) the results of fire assay for Au, (2) ICP-OES analysys results for 40 elements, (3) mineralogical description, specifically proportions of the sulfides.

After statistical analysis of the elemental distribution and delineation of the anomalous geochemical areas it was revealed that the highest degrees of concentration are typical of Mo, Au, Ag, Bi, Se, Te, As, Sb, Zn, Pb, Cd, Fe, and Mn, which are incorporated in the minerals of porphyry copper, subepithermal, and epithermal ores.

The geochemical data were processed by the factor analysis of major components using Statistica software. As a result, we obtained factors, in which elements were grouped according their weight into geochemical associations. Significant correlation between factor values and concentration of given sulfides allowed us to treat factors as ore stage associations (Table 1).

Contouring of factor allocation allowed to identify lateral geochemical zoning of the objects of research.

The MnFe and FeMnAu associations spatially correspond to the pyrite zones and forms the outer shell in the structures of the studied PES. It is indicative that the Nakhodka ore filed pyrite shell demonstrates higher gold enrichment than one of the Peschanka deposit.

The MoCuAgSb & AuCuAgAs and MoCu factors refer to the chalcopyrite-molybdenite assemblage of the porphyry Cu-Mo stockworks and determines the embedded area. The stockwork bornite cores can be revealed by the development of the Bi or CuBiSe associations. Bornite cores at the Peschanka deposit are cut only at the Central and Main stockworks while the North one is believed to be less eroded so its rich Cu core might be discovered at depth.

Table 1. Geochemical associations distinguished by the factor analysis and related minerals in accordance to the assumed stages of ore formation

Geochemical association (factors)		Correlating sulfides	Ore stage
Peschanka deposit	Nakhodka ore field		
MnFe	FeMnAu	py*	porphyry (Au)-pyrite
MoCuAgSb & AuCuAgAs	MoCu	chp, bo, mol	porphyry Cu-Mo
Bi	BiCuSe	bo, chp	bornite
SbAsAg	SbAsCuSe	fh	tennantite-tetrahedrite
ZnPbCdAgMn	ZnPbCdMnAgAu	spl, gn	subepithermal base metal
	TeAuSeAg	bo, py, spl	epithermal Au-telluride

*bo — bornite, chp — chalcopyrite, fh — tennantite-terahedrite, gn — galena,
mol — molybdenite,py — pyrite, spl — sphalerite

The SbAsAg and SbAsCuSe associations are linked to the tennantite-tetrahedrite minerals generated both at the porphyry and (sub)epithermal stages. They are superimposed on the associations mentioned above.

The same distribution is shown by the ZnPbCdAgMn and ZnPbCdMnAgAu and TeAuSeAg factors.

The former complies with the subepithermal and epithermal types of the Ag – base metal mineralization. These types can be distinguished by the mineralogical markers. The northern part of the Peschanka deposit lacks this type of mineralization, while the southern flank is believed to be a lens out of the Peschanka PES due to abundant base metal distribution.

The latter corresponds to the Au-Ag mineralization of the Nakhodka ore field and coheres with the data on coexisting of low-fineness gold and hessite. To discriminate between the subepithermal and epithermal TeAuSeAg association one should apply to mineralogical data.

Contouring of the revealed factors within cross-sections will allow us to build model of the vertical geochemical zonation.

The reported study was funded by RFBR according to the research project No. 16-35-00296 мол_а.

References:

1. Sillitoe R.H. Porphyry copper systems // Economic geology. 2010. Vol. 105. P. 3-41.

Boron-bearing igneous complexes of East Sikhote-Alin volcano-plutonic belt and boron source of the Dal'negorsk skarn deposit in the Sikhote-Alin

Eliseeva O.A., Ratkin V.V.

Far East Geological Institute, Far Eastern Branch of the Russian Academy of Sciences, okaras@yandex.ru

The Dal'negorsk ore district occupies central and eastern parts of the Lower Cretaceous Taukha terrane, with the Early Cretaceous-Paleocene volcanites of the East Sikhote-Alin volcano-plutonic belt (ESAVPB) and the Eocence volcanic rocks of the Khasan-Amur areal lying over. The district is known for Pb, Zn and Ag-containing deposits as well as for a unique borosilicate skarn deposit. Researches on the Pb-Zn deposits generated a recognized conception asserting that there is a relation between the Maastrichtian-Paleocene magmatic complexes and ore formation. The opinions about the nature of borosilicate ores and the formation time of large Dal'negorsk boron deposit are discrepant and described in several publications [1, 3, 5, 6, 7]. Our data on the formation time of the borosilicate ores show that it was the final stage of Cenomanian - Campanian volcanism. Boron can be sourced from the Early Cretaceous sandstones of the Taukha terrane, which were involved in a process of magmatic chambers formation in the upper mantle.

The borosilicate deposit is situated in the center of the Dal'negorsk ore district, 27 km from the Sea of Japan coast. It is a giant, more than 1 cubic kilometers, zone of skarned (volume of substitution makes up 70%) Triassic limestones representing a steeply-dipping stratum in the Early Cretaceous olistostrome body of the Taukha terrane. At a depth, the skarned body of limestones abuts on the late Paleocene intrusion.

Several stages in the deposit formation are distinguished [8]. In the beginning, during the Campanian Age, a huge olistolith of the Triassic limestones underwent changes resulted in the formation of grossular-wollastonite skarns with danburite crystals. Another change of the same limestone body took place in the late Paleocene, with the formation of ilvaite-andradite-hedenbergite skarns and replacement of danburite by silicates, quartz and calcite. Boron was redeposited in the form of datolite and axinite.

Between these stages of skarning intervenes intrusion of basaltic bodies, which were also transformed in the process of late skarn-hydrotermal phase. The intruded bodies by their chemical composition are referred to subalkaline rocks of calk-alkali series, with dominat amount of K_2O, high contents of Rb (about 200 g/t), B (up to 25 g/t) and relatively low contents of Sr (less than 400 g/t). The age of the basaltic intrusions is estimated as near 78 Ma [4]. We suggest that intruding was caused by the closing stage of the Turonian-Campanian magmatism; that is the formation of the skarns with danburite crystals occurred in the plateau ignimbrites of the Primorsky Complex formation final.

Chemically, the plateau ignimbrites of the Primorsky Complex correspond to high-alumina series of rocks with high alkalinity. Based on [9] data, they have signs of S-type acid magmas distinguished by characteristic values of $^{87}Sr/^{86}Sr$ - more that 0.707. Production of acid melts that brought about ignimbrite layers is associated with the zones of metasedimentary rocks anatexis [2]. The ignimbrite layers are characterized by the abnormal concentration of boron (up to 220 g/t) [9].

Analyses of melt inclusions in quartz from the ignimbrites yielded parameters of the anatectic magmatic melts: temperature - 950ºC, pressure – 0.6-1 bar, water concentration – up to 5 mass%. According to the data of Raman spectroscopy, there are traces of CO_2 in the gas phase of melt inclusion, and H_2O in the glass. Solid phases are represented by the Ba-bearing potash feldspar, titanite and hornblende. Microprobe analysis has shown that the initial melt was super normally enriched with Al, Ba and Ti.

An ore-magmatic system of the early stage of skarning can be imagined as a succession of generation and uploading of the magmatic chambers during the process of volcanism (Primorsky Complex). Boron was sourced from the Taukha terrane-related boron-bearing Early Cretaceous arkosic rocks with clastic tourmaline. As reported in [5], boron in danburite from the early skarn associations is isotopically heavy ($\delta^{11}B$ = +17.7‰) that corresponds to marine evaporates. The similar isotopic composition of boron is inherent in tourmalinite from the feeding zone of the Early Cretaceous basin, where Taukha sandstones were formed. Comparison of the microelemental compositions of ignimbrites and the Early Cretaceous arkosic sandstones, both have similar contents of majority elements (Sn, Zn, Pb, Ba, Rb, Sr, Nb, Sm, Eu, Th, etc.), confirms an idea about the involving of the Early Cretaceous sedimentary rocks in the process of anatexis.

It appears that formation of the early skarns with danburites was associated with near-surface hearths of magmatic activity at the late stage of Primorsky Complex volcanism. The melts underwent magmatic differentiation causing separation and accumulation of a fluid rich in silicic acid, aluminum and boron. Modeled magmatic chamber with silicic melts of volume 100 cubic kilometers and initial boron content of 150 g/t, common lithostatic pressure about 100 MPa (depth 3.5-4.0 km) and appropriate boron redistribution ratio in favour of the fluid phase at level 2.0 [10] ensure fluid detachment with boron content comparable to reserves of the Dal'negorsk deposit – no less than 50 million tons of B_2O_3.

References:

1. Baskina V.A., Dubinina E.O., Avdeenko A.C. About the nature of ore-bearing fluids at the Dal'negorsk borosilicate deposit (Primorye) // Proceeding of the Academy of Sciences. 2011. V. 436. N.3. P. 363-367 (in Russian).
2. Grebennikov A.V., Popov V.K. Petro-geochemical aspects of Late Cretaceous and Paleogene ignimbrite magmatism in the Eastern Sikhote-Alin // Pacific Geology. 2014. V. 33. N.1. P. 41-57 (in Russian).
3. Govorov I.N. Geochemistry of ore districts of Primorye. Moscow: Nauka. 1977 (in Russian).
4. Dubinina E.O., Baskina V.A., Avdeenko A.C. Nature of ore-forming solutions of the Dal'negorsk deposit: isotopic and geochemical parameters of the altered host rocks //Geology of Ore Deposits. 2011. V.53, N.1. P. 65-82 (in Russian).
5. Karas O.A., Ratkin V.V. The Dal'negorsk skarn deposit: staging and sources of matter in borosilicate ores (Sikhote-Alin) // Proceedings of the Academy of Sciences. 2014. V. 455. N. 4. P. 444-446 (in Russian).
6. Malinko S.V. Origin of the unique bodies of borosilicate ores at the Dal'negorsk deposit in Primorye // Mineralogical Journal. 1992. V.14, N. 5. P. 3-11 (in Russian).

7. Nosenko N.A. Geology and genesis of the Dal'negorsk boron deposit / Candidate's thesis. Vladivostok, 1986. 308 p. (in Russian).
8. Nosenko N.A., Ratkin V.V., Logvenchev P.I. et al. The Dal'negorsk borosilicate deposit - a result of polychronic processes of skarning // Proceedings of the Academy of Sciences of the USSR. 19990. V. 312. N. 1. P. 178-182 (in Russian).
9. Sakhno V.G. Late Mesozoic – Cenozoic volcanism in East Asia continental margin. Vladivostok: Nauka. 2002. 336 p. (in Russian).
10. Hervig R.L., Moor G.M., Williams L.B. et al. Isotopic and elemental portioning of boron between hydrous fluids and silica melt // American Mineralogist. 2002. V. 87. P. 769-774.

Spatial variations of thermal conductivity of marine sediments in high latitudes

Ermakov A.V. [1,2]
1 -Geological Institute RAS,
2 -Lomonosov MSU, e-mail: a.v.ermakov@gmail.com

Thermal conductivity (TC) of rocks is the one of measured parameters together with temperature gradient in the terrestrial heat flow density (HF) equation. In simplest case HF defined as: $q=k\cdot(dT/dz)$, where q is HF in mW/m^2, k is TC in W/m·K and dT/dz is gradient in mK/m. In marine HF studies practice one usually use 2-10 m long probes to measure gradient with limited temperature points (2 to 15 temperature sensors). At such shallow sediment depth gradient may be strongly affected by exogenous factors e.g. bottom temperature variations. TC is often measured onboard on sediment cores from nearby corings, and more rarely *in situ*. Cores length is also does not exceed 10 m. Porosity, water content, mineral composition and grain size of unlithified sediments are varying significantly as dependent TC values. Thereby TC errors considerably affect HF values.

TC of marine sediments varies in range 0.6 – 1.8 W/m·K. It is believed to change moderately within the limits of basin area, for this reason before development of *in situ* measurement devices one value of TC were used to calculate HF at a number of stations sometimes very distant from each other. Estimation of TC by water content or other sediment properties was widely used.

We analyzed published TC data in Eurasian an Norwegian-Greenland basins, among them data taken by author in 25-27 cruises of R/V "Akademik Nikolaj Strakhov". The dataset consist of 218 values. Selection of data was geographical – area bounded 74-86N and 10W-60E includes continent-ocean transition zone. Main geomorphologic features in the region are northern Barents sea shelf, continental slope and foot, Knipovich and Gakkel spreading riges with flanks. Figure 1A shows fairly representative depth range of all points in the dataset. Most selected TC values were measured on sediment cores by needle probe and a little part by HF probes *in situ*. For each station we use mean value whether published by consequent works authors or calculated from their data.

Data analysis makes us conclude that vertically in cores TC increases with depth or changing chaotically. Linear trend when recognized connected to porosity/water content decrease in compacted sediments. Changes in grain size and mineral form local departures from main trend. Several distant stations of TC with frequent measurements show apparently similar curves. That is in agreement with suggestion of moderate TC lateral changes. But in the all-data scale mean values of TC are statistically independent from sea depth or lat long position of stations. Averaging of TC in depth intervals in fig. 1B shows tendency to decrease from shelf break to ~1800 m and following increase with deepening of sea bed. Main factors that control spatial variance of TC probably are rock composition at nearby source of sedimentary material and major oceanic currents.

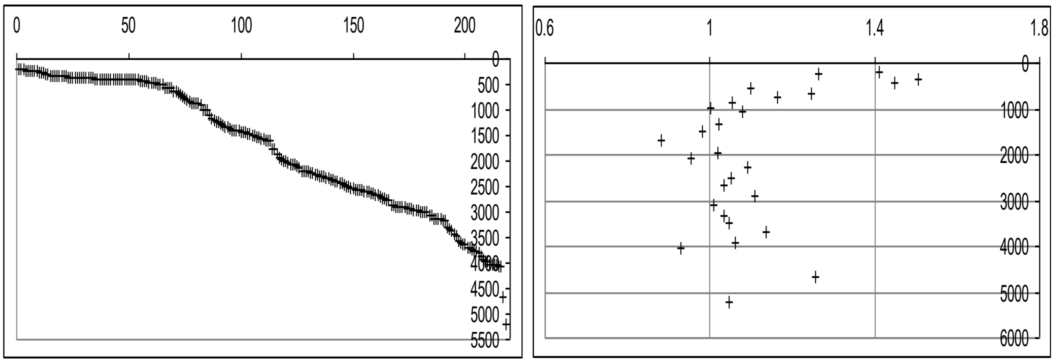

A B

Fig. 1 A – water depth vs. point number in dataset; B – averaged water depth vs. averaged mean TC, depth intervals 200 m.

References:

1. Levitan M.A., Lavrushin Yu.A., Shtein R. Outlines of sedimentation history of the Arctic Ocean and Subarctic Seas for the last 130 ka. GEOS, 2007. 400 p.
2. Merkushev V.N., Podgornykh L.V., Smirnov Ya.B., Trotsyuk V.Y. Arctic Ocean. In: Methodological and experimental fundamentals of Geothermal. Nauka, 1983. 232 p.
3. Scientific Report of 25 cruise R/V "Akademik Nikolaj Strakhov". GIN RAS, 2007. 145 p.
4. Khutorskoy M.D., Akhmedzyanov V.R., Ermakov A.V., Leonov Yu.G., Podgornykh L.V., Polyak B.G., Sukhikh E.A., Tsybulya L.A. Geothermics of the Arctic seas. GEOS, 2013. 232 p.
5. Berndt, C., Feseker, T., Treude, T., Krastel, S., Liebetrau, V., Niemann, H., Bertics, V.J., Dumke, I., Dunnbier, K.,Ferre, B., Graves, C., Gross, F., Hissmann, K., Huhnerbach, V., Krause, S., Lieser, K., Schauer, J. and Steinle, L. Temporal Constraints on Hydrate-Controlled Methane Seepage off Svalbard // Science. 2014. V. 343 (6168). P. 284-287.
6. Bullard, E. C., and A. Day, The flow of heat through the floor of the Atlantic Ocean // Geophys. J., 4 (spec. vol.), 282-292, 1961.
7. Crane K., Eldholm O., Myhre A.H., Sundvor E. Thermal implications for the evolution of the spitsbergen transform fault // Tectonophysics. 1982. V. 89. Issues 1–3. P. 1–32.
8. Crane K., Sundvor E., Buck R., Martinez F. Rifting in the northern Norwegian-Greenland Sea: Thermal tests of asymmetric spreading // J. Geoph. Res.-Solid Earth. 1991. № 96(B9). Pp. 14529-14550
9. Crane K., Sundvor E., Foucher, J.P., Hobart M.A., Myhre A.M., LeDouaran S. Thermal evolution of the western Svalbard margin // Marine Geoph. Res. 1988. № 9 (2). Pp. 165-194.
10. Jackson H.R., Johnson G.L., Sundvor E., Myhre A.M. The Yermak Plateau: Formed at a triple junction // J. Geoph. Res. 1984. № 89(B5). Pp. 3223–3232.
11. Lachenbruch A., Marshall V. Heat flow through the Arctic Ocean floor: the Canada Basin-Alpha Rise Boundary // J. Geoph. Res. 1966. V. 71. Issue 4. P. 1223-1248.
12. Langseth M., Zielinski G. Marine Heat Flow Measurements in the Norwegian-Greenland Sea and in the Vicinity of Iceland // Geodynamics of Iceland and the North Atlantic Area. 1974. Pp. 277-295.
13. Ratcliffe, E. B., The thermal conductivities of ocean sediments // J. Geoph. Res. 1960. V. 65(5). Pp. 1535-1541.
14. Spielhagen R., Pfirman S., Thiede J. Geowissenschaftlicher Bericht über die ARK-IV/3 Expedition des PFVS Polarstern im Sommer 1987 in das zentrale oestliche Arktische Becken. Berichte-Reports № 24. Geologisch-Paläontologisches Institut der Universität Kiel. 1988. 166 p.
15. Stein R., Grobe H., Wahsner M. Organic carbon, carbonate, and clay mineral distributions in eastern central Arctic Ocean surface sediments // Marine Geology. 1994. V. 119. Pp. 269-285.
16. Sundvor E. Heat Flow Measurements on the Western Svalbard Margin. University of Bergen, Seismological Observatory. Internal Report. 1986.

Compositional evolution in pyroxenes of the peralkaline nepheline syenite (Kola Peninsula, Russia)

Filina M.I., Kogarko L.N.

Vernadsky Institute of Geochemistry and Analytical Chemistry RAS, makimm@mail.ru

Explore pyroxenes from peralkaline nepheline syenite from the Niva intrusion and peralkaline dyke [1,2]. There are located of the northwestern part of the Belomorian mobile belt (Kola Peninsula, Russia). Among the major minerals of the syenite are nepheline (10–15 vol %), orthoclase (15–20 vol %), lamprophyllite group minerals (15–20 vol %), titanian egirine–augite (10–15 vol %), enigmatite (10–15 vol %), alkaline amphibole (5–10 vol %), natrolite (5-10 vol %), and astrophyllite (up to 5 vol %).

Pyroxene, forms a small (0.5 - 1.3 mm), needle-like or prismatic crystals, often zoned with green-yellow core and green rim, there is a weak pleochroism. Investigated pyroxenes relate to diopside-hedenbergite-aegirine series, typical for peralkaline rock. The central part of the crystal composition correspond to augite, marginal parts aegirine-augite sometimes almost completely corresponds aegirine composition (Fig. 1).

Most pyroxene grains are zoned, from the core to the rim increases the contents of sodium, iron and titanium, and a decrease of the content of magnesium and calcium (Table. 1). Pyroxenes contain titanium up to 6.05 wt. % TiO_2 in the marginal parts of the crystal, as shown previously, titanium is present in the pyroxene in the form of $NaTiSiAlO_6$, and partly in the form neptunite $Na_2FeTiSi_4O_{12}$ [3], the presence of the neptunite molecule can be confirmed Na-Ti positive correlation.

Table 1. Chemical composition of zoned pyroxenes from peralkaline dyke and Niva intrusions.

	zone	SiO_2	TiO_2	Al_2O_3	FeO	MnO	MgO	CaO	Na_2O	K_2O	V_2O_5	Cr_2O_3	ZrO_2	Total
1	core	50.57	3.18	0.72	19.36	0.39	4.79	10.12	7.65	0.01	0.36	0.02	1.26	98.44
2	rim	50.94	4.67	0.89	19.49	0.29	4.06	8.06	9.09	0.05	0.41	B.d.l.	0.44	98.35
3	core	50.63	1.83	0.90	14.14	0.41	8.91	17.66	3.70	0.06	0.13	0.03	0.27	98.66
4	rim	51.70	5.99	0.57	22.95	0.23	1.41	2.17	12.29	0.05	0.08	0.04	0.45	97.94
5	core	50.59	2.75	1.03	13.94	0.43	8.4	16.41	4.23	0.02	0.46	B.d.l.	0.22	98.48
6	rim	51.26	6.05	0.81	18.37	0.33	3.4	6.4	10.16	0.05	0.53	B.d.l.	0.27	97.63
7	core	50.76	1.64	0.6	14.15	0.64	8.68	17.23	3.69	0.01	0.26	B.d.l.	0.56	98.21
8	rim	51.12	5.57	0.78	18.72	0.36	4.06	7.81	9.02	0.06	0.6	0.03	0.34	98.47

Note. 1-4 - pyroxenes from peralkaline dyke, 5-8 - pyroxenes from intrusions Niva. B.d.l., below the detection limits.

To evaluate the evolution of pyroxenes used Na-Mg parameter Stevenson [4], the main direction of the evolution of the composition of pyroxene is to increase aegirine (Na, Fe^{3+}) component and decrease diopside (Ca, Mg) and hedenbergite (Ca, Fe^{2+}) component this trend is parallel to the increase in Ti content. Content of Al, Mn content shows a slight variation.

Investigated pyroxene are similar in chemical composition to the pyroxene of the Khibiny and Lovozero alkaline massifs [5, 6], they show a continuous evolution towards aegirine components (Fig. 1), while the pyroxene of Ilimaussaq alkaline massif [7,8] especially in early evolution shows growth hedenbergite component of this difference in the trend of the evolution of the composition of pyroxene, primarily depends on the fugacity of oxygen in an alkaline melt [9].

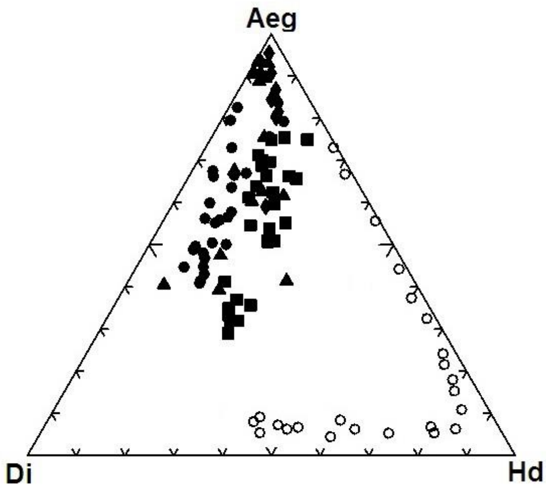

Pyroxene composition plotted in terms of diopside (Di), hedenbergite (Hd) and aegirine (Aeg). The shaded circles - peralkaline dike; shaded squares - intrusion Niva, unpainted circles - Ilimaussaq intrusion [7,8], shaded triangle - Khibiny massif [6], shaded rhombus - Lovozero massif [5].

This study was supported by the RSF (No. 15-17-30019)

References:

1. Akimenko M. I., Kogarko L. N., Sorokhtina N. V., Kononkova N. N., Mamontov V. P.. A New Occurrence of Alkaline Magmatism on the Kola Peninsula: An Agpaitic Dyke in the Kandalaksha Region // Doklady Earth Sciences. 2014, Vol. 458, Part 1, p. 1125–1128.
2. Arzamastsev A.A., Belyatsky B.V., Arzamastseva L.V. Agpaitic magmatism in northeastern Baltic Shield: A study of the Niva intrusion, Kola Peninsula, Russia // Lithos. 2000, V. 51, № 1, p. 27.
3. Ferguson A.K. The natural occurrence of aegirine-neptunite solid solution // Contributions to Mineralogy and Petrology, 1977, 60, p. 247-253.

4. Stephenson D., Alkali clinopyroxenes from nepheline syenites of the South Qoroq Centre, South Greenland // Lithos, 1972, № 5, p. 187-201.
5. Kogarko L.N., Williams C.T., Wooley A.R. Compositional evolution and cryptic variation in pyroxenes of the peralkaline Lovozero intrusion, Kola Peninsula, Russia // Mineral. Magazine. 2006, V. 70, p. 347-359.
6. Yakovenchuk V.N., Ivanyuk G.Y., Pakhomovsky Y.A., Menshikov Y.P., Konoplev N.G., Korczak Yu., Pyroxenes Khibiny alkaline massif (Kola Peninsula, Russia) // Russian Notes Mineralogical Society, 2008, № 2. p. 96-113.
7. Larsen L.M. Clinopyroxenes and coexisting mafic minerals from the alkaline Ilimaussaq intrusion, South Greenland // Journal of Petrology, 1976, № 17, p. 258-290.
8. Marks M., Markl G., Fractionation and assimilation processes in the alkaline augite syenite unite of the Ilimaussaq intrusion, South Greenland, as dedused from phase eguilibria // Jornal of petrology, 2001, № 10, p. 1947-1969.
9. Mann U., Marks M., Markl G., Influence of oxygen fugacity on mineral compositions in peralkaline melts: The Katzenbuckel volcano, Southwest Germany, Lithos, 91 (2006) 262–285.

Carbonate-dyke and related pyroxenite xenoliths from Val Mastallone (Ivrea Verbano zone, Italy): evidence of carbonatite formation by liquid immiscibility?

Galli A.[1], Grassi D.N.[1], Gianola O.A.[1]

1 -Department of Earth Sciences, ETH Zurich, Sonnegstrasse 5, 8092 Zurich, Switzerland

andrea.galli@erdw.ethz.ch

The Ivrea Verbano Zone (Italy/Switzerland) represents one of the best exposed mantle-crust sections worldwide. Its geological evolution has been governed by the Permian underplating of mantle-derived basic magmas („Mafic Complex") into the high-grade basement of the Southern Alps ("Kinzingite Formation").

In the Ivrea Verbano Zone (IVZ), marble occur as concordant bodies or partly discordant carbonate-dykes. Generally, these dykes are constituted of calcite, diopside, scapolite, contain enclave of the host rocks and display sharp contacts to the host lithologies, without evidences of alteration zones. In Val Mastallone an up to 40 m thick carbonate-dyke with different characteristics occurs within mafic granulites. This dyke is composed of calcite, clinopyroxene and subordinate allanite and zircon. No scapolite is observed. The contacts to the host granulites are characterized by a greenish alteration zone composed of actinolite, chlorite, clinozoisite, plagioclase and calcite.

The carbonate-dyke bears xenoliths of phlogopite-amphibole-apatite-rutile-ilmenite ± garnet, corundum or spinel clinopyroxenites. These rock types are not outcropping elsewhere in the proximity of the dyke, suggesting a significant transport. Calcite dykelets rich in zircon, baddeleyite and other Ba, U, Th, REE-rich phases, as well as corundum and apatite bearing, plagioclase rich veinlets cut across the enclave.

The carbonate-dyke shows an enrichment of LREE over HREE ($(La/Yb)_N = 14$), with a Σ REE = 95-115 ppm and Y/Ho = 26-33. On the chondrite-normalized REE abundances diagram, no Eu anomaly is observed. Mantle-normalized pattern shows strong negative anomalies at Cs, Rb, K, Pb, P, Zr, Hf and Ti and positive Ba, Th, Sr, Nd anomalies, similarly to the "world average carbonatites". Measured absolute trace element concentrations are lower than average carbonatites but significantly higher than typical limestones and similar to cumulate carbonatites found elsewhere in the world.

Grt-bearing clinopyroxenite enclave have a X_{Mg} of 0.50, $K_2O + Na_2O$ of 1.01 and are rich in TiO_2 (3.40 wt%) and P_2O_5 (0.93 wt%). Grt-free clinopyroxenites show higher X_{Mg} values of 0.61-0.73 and are alkali, TiO_2 and P_2O_5 poorer ($K_2O + Na_2O$ of 0.21-0.59 wt%, TiO_2 of 1.16-2.72 wt% and $P_2O_5 < 0.20$ wt%). On the mantle-normalized trace element diagram, the enclave display a nearly antithetic pattern in respect to the enclosing carbonates, with positive anomalies at Cs, Rb, U, Pb, Zr, Hf, Ti and negative anomalies at Ba, Th, Sr and Nd. Melt composition calculated using the partitioning coefficients between carbonatites and silicate melts reproduces the trace element patterns displayed by the pyroxenite enclave. This suggests that the carbonate-dyke and the enclosed clinopyroxenites may originated by liquid immiscibility, probably from a parental K-rich, ultramafic melt, similar to the alkaline ultramafic intrusions occurring as pipes in the IVZ.

This carbonatitic magmatism is probably related to the Triassic CO_2-bearing alkaline magmatism occurring during the early stage of the opening of the Thetyan Ocean.

Structure, whole-rock and mineral compositions of Layered Rocks in the East Pana Intrusion, Kola Peninsula, Russia

Alikin O.V[1], Asavin A.M.[1,2], Gorbunov A.A.[1], Khasiiatov D.F.[1] and Veksler I.V.[1,3]

1 -Perm State University, Perm, Russia, art.gor.psu@ya.ru

2 -The Vernadsky Institute of Geochemistry RAS, Moscow, Russia

3 -German Research Centre for Geosciences GFZ Potsdam, Germany

East Pana intrusion is a part of the Fedorovo-Pana massif in the central part of the Kola Peninsula, Russia. The massif is a mafic-ultramafic layered intrusion of Paleoproterozoic age [1]. The massif was affected by postmagmatic modifications such as tectonic movements and metamorphism. The Fedorovo-Pana massif hosts economic platinum-group elements (PGE) mineralization of low-sulphide type.

The layered sequence of East Pana intrusion comprises gabbro, gabbronorite and norite. Gabbro is more common in the upper part of the intrusion, gabbronorite and norite – in the lower part. The PGE mineralization is concentrated in three layers or zones labelled as A, B and C.

Our present study has been focused at the mineralized zone B, where we have carried out detailed petrographic and mineralogical study on a set of drill core samples using electron microprobe and X-Ray computer tomography (XRCT) [2]. The rock sequence across zone B mostly comprises meso-gabbronorite and pegmatoidal leucogabbro. Characteristic feature of meso-gabbronorite is that it contains porphyre quartz.

According to conventional terminology, there are four types of layering that are related (1) to the appearance or disappearance of liquidus phases (phase layering), (2) variations in grain size and crystal shapes (grain-size or textural layering), (3) mineral modes (modal layering), or (4) mineral compositions (cryptic layering) [3]. Drill core logging [4], petrographic studies of thin sections and XRCT results for samples through zone B revealed no prominent phase or modal layering such as described at Skaergaard, Bushveld, Stillwater and other classical layered intrusions. Only one sample showed signs of textural layering at mm- to cm-scale (Fig. 1). The stratigraphic section through the mineralized zone B (Fig. 2) is characterized by interbedding of gabbronorite and pegmatoidal leucogabbro. Overall, the results imply the existence of only minor modal and textural layering.

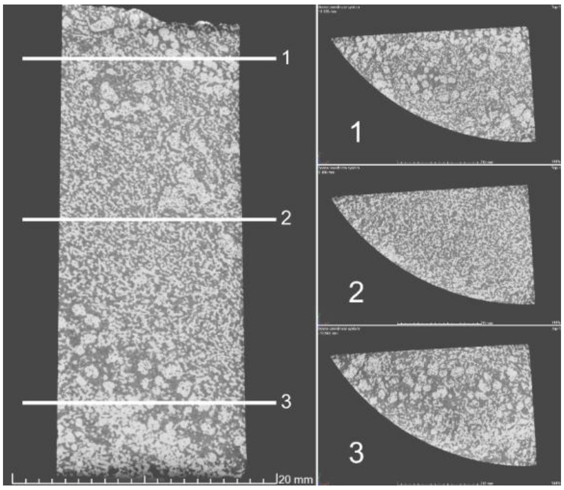

Fig. 1 XRCT images of a texturally layered drill core sample. The longitudinal section (left) and three transverse sections (right).

Electron microprobe analyses revealed significant variations of mineral compositions, both within a single sample and along the vertical profile through the mineralized zone B (Fig. 2). Some compositional zoning of minerals is due to metamorphic alteration. However, there are compositional variations of clinopyroxene and plagioclase compositions that are probably of primary magmatic origin and can be classified as cryptic layering.

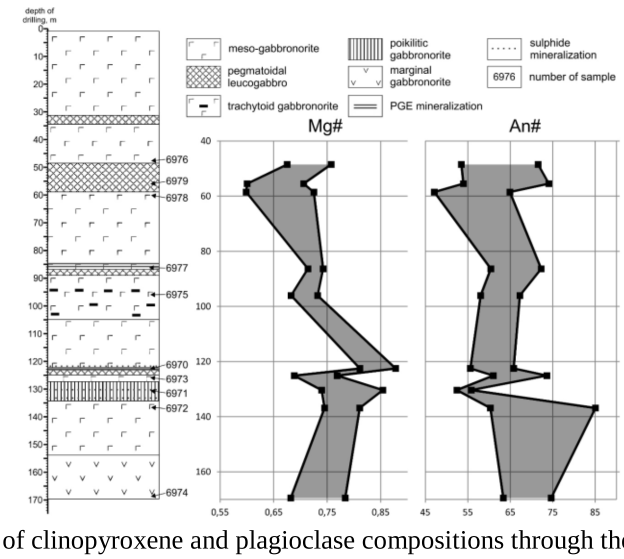

Fig. 2 Variations of clinopyroxene and plagioclase compositions through the mineralized zone B

Conclusions. Our study revealed the existence of minor modal and textural layering in a 170-m long vertical drill core profile through the mineralized zone B. Cryptic primary magmatic layering characterized by correlated variations of clinopyroxene and plagioclase compositions is partly obscured by metamorphic alteration of the rocks but is evident in the results of microprobe analyses.

The authors thank the staffs of Central Kola Expedition.

This work was supported by the Russian Science Foundation, grant No. 14-17-00200.

References:

1. Serov P.A., Nitkina E.A., Bayanova T.B. and Academician of the RAS Mitrofanov F.P. Comparison of New U–Pb and Sm–Nd Isotope Data on Rocks of the Early Barren Phase and Basal Ore-Bearing Rocks in the PGE-Bearing Fedorovo–Pana Layered Massif, Kola Peninsula // Doklady Earth Sciences. Vol. 416.No. 7. 2007. P. 1125-1127.
2. Gorbunov A.A., Asavin A.M., Veksler I.V. Studying rocks of East Pana intrusion (Fedorovo-Pana massif, Kola peninsula) // The problems of mineralogy, petrology and metallogeny. Scientific Readings in Memory of N.P. Chirvinskiy. Perm, 2016. Ed. 19. P. 307-314.
3. Charlier B., Namur O., Latypov R., Tegner Ch. Layered Intrusions, 2015. 749 p.
4. Kalinin A.A., Voytechovich V.S., Kazanov O.V. The report on the results of the survey and assessment work on the PGE mineralization of the Eastern Part of the Pana Tundra Massif in 2006-2008 years // Kola Mining and Geological Company, Apatity, 2008. 202 p.

Atomistic modeling of $MgSiO_3$ post-perovskite rheology

Goryaeva A., Carrez P., Cordier P.

Unité Matériaux et Transformations, CNRS UMR 8207, Université des Sciences et Technologies de Lille 1, 59655 Villeneuve d'Ascq, France alexandra.goryaeva@ed.univ-lille1.fr

In contrast to the lower mantle, the D″ layer exhibits significant seismic anisotropy both at the global and local scale [1]. Located right above the CMB, the D" represents a very complex region and the causes of its pronounced anisotropy are still debated (CPO, oriented inclusions, layering, thermo-chemical heterogeneities etc). Among them, contribution of the $MgSiO_3$ post-perovskite rheology is commonly considered to be substantial. However, for this high-pressure phase, information about mechanical properties, probable slip systems, dislocations and their behavior under stress are still extremely challenging to obtain directly from experiments [3, 4]. Thus, we propose employing full atomistic modeling (based on the pairwise potential previously derived by [2]) to access the ability of $MgSiO_3$ post-perovskite to deform by dislocation glide at 120 GPa.

Lattice friction opposed to the dislocation glide in $MgSiO_3$ post-perovskite is shown to be highly anisotropic. Thus, remarkably low values of Peierls stress (1 GPa) are found for the glide of [100] screw dislocations in (010), while glide in (001) requires almost 18 times larger stress values. In general, (010) plane is characterized by the lowest lattice friction which suggests (010) deformation textures. Comparison of our results with previous study of $MgSiO_3$ perovskite (bridgmanite) [5], based on similar simulation approach, clearly shows that monotonous increase in Peierls stress of bridgmanite will be followed by a dramatic drop after the phase transition to the post-perovskite phase, which consequently suggests the D″ located at the CMB to be weaker than the overlying mantle. In addition to that, the observed evolution of CRSS with temperature clearly demonstrates that post-perovskite deforms in the athermal regime which backs up it to be a very weak phase and indicates its deformation by dislocation glide in contrast to high-lattice friction perovskite (bridgmanite) phase deformed by climb only.

References:

1. Panning M. and Romanowicz B., Geophys. J. Int., (2006), 167:361–379.
2. Oganov A. *et al.*, Phys. Earth Planet. Int. (2000), 122:277-288.
3. Merkel S. *et al.* Science (2007), 316:1729-1732.
4. Miyagi L. *et al.* Science (2010), 329:1639-1641.
5. Hirel *et al.*, Acta Mater (2014), 79:117–125.

The Extended Phenotype of Chemolithoautotrophs as an Object of Physical Geochemistry and Structural Biogeochemistry in the Framework of V.I. Vernadsky Concepts

Gradov O.V.
INEPCP RAS

This report considers the effect of the geochemical environment on the evolutionary morphology of the chemoautotrophic prokaryotes coupled by a dual feedback with the effect of the prokaryotic microorganisms on geomorphology and the chemical composition of their environment. It is shown that the environmental changes are usually accompanied by the evolutional changes in prokaryotic organisms, and *vice versa*. It is also shown that the emergence of the multiple microbiomorphic structures in the geochemical environment of chemoautotrophs, which are usually poorly distinguishable from their biological prototype due to a high degree of isomorphism, is also determined by the geochemical conditions, their non-equilibrium thermodynamics and the specific response of the soft matter. The above findings are in consistence with the fundamental concepts introduced by V. Vernadsky and S. Winogradsky. We emphasize the mutual nature of determination of the coevolution of microbiota and their environment, which allows to consider the evolutionary morphology of chemoautotrophic prokaryotes and the evolutional biogeochemistry of their phylogeny as a manifestation of the extended phenotype in the framework of the concept proposed by R. Dawkins, with a sufficient remark, that both "biogenic" and "bioinert" matter (terms introduced by Vernadsky) undergo evolution due to the feedback principles. Moreover, here we introduce for the first time a concept of the coevolution of geochemistry, determining the phenotype, and the extended phenotype as a statistical value, formed by a large sample of microorganisms. In this regard we also propose a method of the extended phenotype mapping in correlation with the changing environment using the dynamic colocalization mapping with a number of descriptors, reflecting the state of the environment and of the statistical population sample of the microorganisms, respectively.

Ni,Co,Ag redistribution in the minerals phases during metamorphism Norilsk sulfide ores

Gritsenko Yu.
Lomonosov Moscow state university, geology department
Fersman Mineralogical Museum. Moscow, ygritsenko@rambler.ru

The content of Ni in the Norilsk sulfide ores is usually 2-5 wt. %, Co – 0.1-0.2 %, Ag – 2-100 g/t. Ni, Co, Ag are equally compatible with Mss and Iss. The main Ni and Co mineral-concentrator and carrier is pentlandite; Ag – hessite, electrum, kustelite. The trap formation was undergone low-grade metamorphism of submersion, wherein primary sulfides including pentlandite and other Ni-Co-Ag minerals begun to be replaced by a series of other minerals.

Under high f S_2 millerite-chalcopyrite-pyrite associations were formed during metamorphism (replacement) of exocontact primary ores with an abundance or with a predominance of pyrrhotite. **Millerite** NiS contains up to 9 wt. % Fe, 1,5% Co and forms full or partial pseudomorphs after large crystals of pentlandite and thin lamellae of pentlandite disintegration in chalcopyrite matrix. Thioshpinels – **polydymite** $NiNi_2S_4$, **violarite** $FeNi_2S_4$, **siegenite** $CoNi_2S_4$ developed in this association. They usually replaced pentlandite of primary ores along joints. Ag is part of the mineral series chalcopyrite $CuFeS_2$ **– lenaite** $AgFeS_2$.

Pentlandite is replaced by sulfides in which Ni and Co predominates over S during metamorphism under conditions of sulfide sulfur deficient (log a S_2 -12 – -15) and at high oxidation potential. Chalcopyrite and cubanite are replaced by bornite, then bornite are replaced by chalcosine. **Godlevskite** Ni_9S_8 closely associates with bornite, chalcosite, millerite and forms needle-shaped crystals and pseudomorphs after large pentlandite crystals. **Heazlewoodite** Ni_3S_2 is the most poor of S nickel sulphide. It is also the product of pentlandite and/or millerite substitution. It developed among chalcosine Cu_2S, which is poor of S copper sulfide. **Parkerite** $Ni_3Bi_2S_2$ forms metasomatic ingrowths in primary galena; rims of replacement around intergrowths of Pd and Pt bismuthides, hessite, and borders on native Bi. **Bismutohauchecornite** $Ni_9Bi_2S_8$ and **Shandite** $Ni_3Pb_2S_2$ form small flattened extended xenomorphic segregations in the area of eutectic aggregates Iss-PbSss in bornite. **Argentopentlandite** $AgFe_5Ni_3S_8$ and **Cupropentlandite** $CuFe_5Ni_3S_8$ form amoeba-shaped metasomes and less small crystals in association with chalcopyrite (without disintegration structures), chlorites, magnetite. Ni-Co-Fe arsenides, antimonides and sulphoarsenides are formed in the calcite and anhydrite metamorphogenous-hydrothermal veins under low f S_2. These pisolites involve up to 10-15 zones, formed by different Ni and Co minerals. They are **orcelite** Ni_5As_2, **maucherite** $Ni_{11}As_8$, minerals of **nickeline** NiAs – **breithauptite** NiSb series, split aggregates of **rammelsbergite** $NiAs_2$ – löllingite $FeAs_2$ series, rarer intermediate member of the rammelsbergite – **safflorite** $CoAs_2$ series, sulfurous **krutovite** $NiAs_2$ crystals, triarsenides – **nickelskutterudite** $NiAs_3$, **skutterudite** $CoAs_3$ and ferroskutterudite, rarer sulfoarsenides – minerals of **gersdorffite** NiAsS –

cobaltite CoAsS series, sulfoantimonides – **ullmannite** NiSbS. Ni arsenides predominate in the pisolites, S, Co, Fe content in them is insignificant. Therefore these elements are periodically accumulated in solutions and thin zones of Ni, Fe, Co sulphoarsenides. Ag minerals in the metamorphogenous-hydrothermal veins are **acantite** Ag_2S**, naumanite** Ag_2Se**, stromeyerite AgCuS.**

The word was performed with financial support of the Russian Federation Foundation for Basic Research (grant № 16-05-00241).

Garnets from Odikhincha massif (Siberia)

E.I. Gerasimova[1,2], Yu.D. Gritsenko[3,4], V.V. Korovushkin[5]

1 - SGM RAS, 2 -GEOKHI RAS, 3 -MSU, 4 -FMM RAS, 5 - MISIS

Odikhincha massif is the second largest intrusion in Maimecha-Kotui region (West part of the Siberian platform) and is located 60 km to the east of the Guli complex. The massif has a concentric structure with sequentially located intrusions. The Odikhincha garnets aren't study enough and most of all specimens have traditionally referred to schorlomite. We started comprehensive study of garnets. Some of them are museum quality, as black crystals of garnet reach 40 cm in diameter. We studied 7 samples using electron probe microanalysis of the different zones of pegmatite veins. The analyses calculated on basis of 8 cation per 12 oxygens, the valence of Fe is determined by a balance of charges. Additionally, three samples were studied with Mëssbauer spectroscopy. The study did not identify any actual shorlomite, all the studied samples are of variable composition from andradite $Ca_3(Fe^{3+})_2Si_3O_{12}$ to morimotoite $Ca_3TiFe^{2+}Si_3O_{12}$ (fig.1).

Fig. 1 Big black crystal of garnet is of variable composition from andradite to morimotoite

Study of the properties of seismic process within the concept of block geomedium

A.I. Gerus[1,2], A.V. Vikulin[1]

1 -Institute of volcanology and seismology FEB RAS, gerus@kscnet.ru

2 -Vitus Bering Kamchatka State University

The rotational model of a block-structured geomedium was built to describe seismicity within the Pacific Ocean margin. Block movements in this model are mathematically represented by the sine-Gordon equation (SG) [1, 2]. This equation has solutions in the form of solitons – solitary waves that interact elastically, just like particles do.

Relying to the perturbation theory that was developed by D. McLaughlin and A. Scott [3], we have added the effects of force moments deviation from equilibrium positions μ and boundary friction α to our equation to better describe a real seismic process:

(1) Such equation has no analytical solutions, but we can numerically investigate the dynamics of its single-soliton solution parameters: coordinate X, velocity U and rotary deformation rate .

Velocity and rotary deformation rate become time-dependable in the presence of structural perturbation; the first one always has a local maximum U_{max}, the second – two maximums and one minimum between them. Both parameters reach their asymptotes after the oscillations.

Our numerical investigations allow us to make some conclusions:

1. With increasing the friction rate α the values $U_{\max}$, , , are reduced while their times increase. Thus, the soliton propagation slows down and smoothes
2. With increasing the rotation inhomogeneity rate μ the values $U_{\max}$, , , are increased while their times reduce. Thus, the modeled process goes faster and sharper.
3. When we simultaneously increase or decrease the values of α and μ the time scale of the process also changes.
4. Asymptotic value of X, i.e. $X_{\max}$, corresponds to the equality $X_{\max} \approx R_0$ for any α and μ, where R_0 is the block radius.
5. The wave always reaches its U_{max}, values and the asymptote of X simultaneously, for any α and μ.

In addition, there are other invariant quantities that are independent of α and μ, but typical for the process as a whole:

1. The ratio of the deformation rate maximum values
2. The ratio of the deformation rate maximums durations

These values are very close to the actual parameters of the seismic process [4], which allows us to interpret the graph of the deformation rate as follows: the first and the second maximums correspond to the foreshock and aftershock stages of the seismic process, and the minimum corresponds to an actual earthquake.

Thus, the equation (1) as a part of the rotational model allows to quantitatively describe such important characteristics of a seismic process as its foreshock and aftershock stages and the strongest earthquake between them. Moreover, the results of numerical modeling of a seismic process are consistent with real experimental data.

References

1. Vikulin A. V., Makhmudov Kh. F., Ivanchin A. G. et al. On Wave and Rheidity Properties of the Earth’s Crust // Physics of the Solid State, 2016. V. 58, No. 3. P. 561-571.
2. Vikulin A.V., Ivanchin A.G. Modern concept of block hierarchy in the structure of geomedium and its implications in geosciences // Journal of Mining Science, 2013. Vol. 49, No. 3. P. 395-408.
3. McLaughlin D. W., Scott A. C. Perturbation analysis of fluxon dynamics // Phys. Rev. A, 1978. 18. P. 1652-1680.
4. Vikulin A.V. Physics of wave seismic process. Petropavlovsk-Kamchatsky: KGPU, 2003. 150 p. (in Russian)

Theoretical modeling of crystal morphology of natural compounds according to data of atomistic calculations

Gromalova N.A.[1], Eremin N.N.[1], Nikishaeva N.D.[1]

1 -Lomonosov MSU, gromalnat@mail.ru

Despite the fact that significant progress in forecasting of energetically favorable structures are achieved, unfortunately, much less attention has been paid to the problem of the theoretical forecast of morphology of crystals at the present level. The estimate of the equilibrium habit of crystals is extremely important for the digestion of the physics and chemistry of new materials. Thus, the use of modern atomistic methods of computer modeling for the calculate of the properties of the crystal surfaces and equilibrium morphology of natural compounds is extremely important.

For the first time the thesis about the reference of the equilibrium shape of a crystal with its crystal structure was project in the works of O. Brave, according to which the idealized habit is determined in the simplest case in correspondence with the reticular R_{hkl} individual faces. This approach with all the further introduced corrections does not consider the nature of atoms and characteristic of the chemical bond in crystals.

The atomistic calculations of crystal surfaces are generally performed using the energetic characteristic of faces: the surface energy E_{surf} which is a measure of the thermodynamic stability of the crystal face. The value of the surface energy of faces is calculated based on the developed set of parameters of interatomic potential (Eremin, 2008; Eremin et al., 2009), according to which a theoretical modeling of crystal morphology of natural compounds and the subsequent comparative analysis of morphological features of calculated crystals with the experimental data are implemented. To determine the equilibrium habit, it is necessary to calculate the energies of all possible faces that can be involved in faceting. In addition, we apply an original method for the calculation of the theoretical equilibrium habit - "combined" approach (Gromalova, Urusov, 2011), in which the habit series is formed on the basis of both the E_{surf} values for the face, which were obtained by the atomistic calculations and the values of relative reticular area for this face, which was found during the geometric calculation of the habit. So some faces may be characterized by relatively large values of the reticular area, they do not manifest themselves in crystal faceting, although they have small E_{surf} values in some cases.

Objects of the study were chosen simple and complex oxides, such as chrysoberyl ($BeAl_2O_4$) and isostructural analogs: $BeFe_2O_4$ and $BeCr_2O_4$ (Gromalova et al., 2012), and corundum group minerals: corundum (Al_2O_3), eskolaite (Cr_2O_3), hematite (Fe_2O_3) (Gromalova et al., 2015). The surface energies for different faces of selected natural minerals were calculated using Metadise code (Watson et al., 1996) at P4-3000 personal computer with Windows XP operating system. Time of calculation of one simple form was from 30 minutes to 12 hours.

As can be seen from the comparison of habits, the surface energy is the extremely sensitive parameter for the estimate of the equilibrium habit of crystal despite tendencies the similarity of the morphology of natural and theoretically calculated crystal, and even a small change of energy significantly changes its shape. It can be seen from the reconstruction of the equilibrium habits of crystals of natural compounds that one of the constitutive factors affecting the value of the surface energy E_{surf} in calculations E_{surf} is a choice of potentials model. In turn, the appearance of the different morphological types of crystals is depended of the impurity elements into it. So, small amounts can significantly affect the appearance of crystals and change its morphological features.

References:

1. Gromalova N. A., Urusov V. S. Chrysoberyl and jem variety - alexandrite. Flux growth and complex research of composition, crystallomorfophogy and properties of natural and synthetic crystals. GmbH.: Lambert Academic Publishing. 2011. P.262.
2. Gromalova N.A., Eremin N.N., Dorokhova G.I., Urusov V.S. Chrysoberyl and alexandrite synthetic crystals morphology: experimental data analysis and theoretical modeling //Crystallography. 2012. V. 57. № 4. P. 679-686
3. Gromalova N.A., Eremin N.N., Urusov V.S. Atomistic computer modeling of the crystal-morpology of corundum group minerals // Zapiski RMO. V. 144. №4. 2015. p. 84-92.
4. Eremin N.N., Talis R.A., Urusov V.S. Computer modeling of the local structure, mixing properties, and stability of binary oxide solid solutions with corundum structure. Crystallography Reports. 2008. V.53 №5. P. 755-763.
5. Eremin N. N., Gromalova N. A., Urusov V. S. Atomistic modeling and prediction of the structure, energy characteristics of point defects, and thermodynamic and elastic properties of the simple and complex beryllium oxides//Glass physics and chemistry. 2009. V. 35. №. 6. P. 613–619.
6. Watson G.W., Kelsey E.T., de Leeuw N.H., Harris D.J, Parker S.C. Atomistic simulation of dislocations, surfaces and interfaces in MgO. Journal of the Chemical Society Faraday Transactions. 1996. V.92 P. 433-438.

Paleomagnetism of the Siberian traps: implications for the intrusive magmatic activity in large igneous provinces

A.V. Latyshev[1,2], R.V. Veselovskiy[1,2], A.M. Fetisova[1], V.E. Pavlov[2], P.S. Ulyahina[1], E.M. Mirsayanova[1]

1 -Lomonosov Moscow State University, anton.latyshev@gmail.com

2 -Institute of Physics of the Earth, Moscow

Nowadays the scientific interest in the Siberian Trap province is caused by several reasons. At first, the Siberian Traps represent the classic example of Large Igneous Provinces (LIPs) and are used to be an object for the mantle plume hypothesis testing. Secondly, the idea of the possible causal connection between LIPs emplacement and mass extinctions is widely discussed now. Finally, the unique Cu-Ni and PGE deposits of Norilsk region are localized in Siberian Trap intrusions, and the genesis of such deposits is still debated. Solving all the above-mentioned problems, we have to obtain the detailed and reliable information about the magmatic activity duration and intensity, as well as about the correlation of volcanic sections and intrusive complexes.

The recent U-Pb and 40Ar/39Ar dating established that the main phase of most LIPs formation takes about 1 Ma (Burgess, Bowring, 2015; Renne et al., 2015; etc.). The detailed paleomagnetic investigations demonstrated the predominantly “pulsating” style of volcanic activity during LIPs emplacement (Chenet et al., 2009; Moulin et al., 2011). As to Siberian Traps, it was shown that the eruptions of the thickest and most complete volcanic sections of Norilsk and Maymecha-Kotuy regions happened as interchange of brief volcanic pulses and more prolonged period of quiescence (Pavlov et al., 2015). Besides, the systematic paleomagnetic studies of intrusions from the Southern and Eastern periphery of Tunguska syncline revealed several short and powerful magmatic events (Latyshev et al., 2013; Konstantinov et al., 2014). However, it is unclear if this style of magmatic process is dominant for the internal regions of Siberian Traps.

Here we present the results of the detailed paleomagnetic case study of the intrusive complexes from two regions: Angara-Taseeva depression and central part of Tunguska syncline. Two long profiles including about 30 paleomagnetic sites were sampled on distance more than 500 km along the Nizhnyaya Tunguska river (Tunguska syncline) and the Chuna river (Angara-Taseeva depression). All paleomagnetic samples were underwent to the stepwise thermal demagnetization according to the standard procedure; the mean-site directions were calculated. Also, the anisotropy of magnetic susceptibility (AMS) was measured.

The results from Angara-Taseeva depression revealed the existence of extremely tight clusters of paleomagnetic directions corresponding to the discrete short magmatic events (large Padunskiy and Tulunskiy sills). The low amplitude of geomagnetic field secular variations, recorded in these sills and associated intrusions, points out that secular variations are not averaged and, consequently, the duration of these magmatic events didn't exceed 10^4-10^5 years (Tauxe, 2014). These brief episodes of magmatic activity took place simultaneously in the Angara and Chuna rivers valleys (the distance is about 200-250 km). The previous paleomagnetic data from intrusive trap complexes allows to suggest that the "pulsating" character of intrusive magmatism is typical for the periphery of Tunguska syncline (Latyshev et al., 2013; Konstantinov et al., 2014; Pavlov et al., 2007).

The formation of Nizhnyaya Tunguska intrusions was generally less intense comparing with sills of Angara-Taseeva depression. The presence of both normal and reversal polarities, the positive reversal test and the moderate values of the concentration parameter of site-mean paleomagnetic directions indicates the more or less even and prolonged magmatic activity. In addition, the scatter of virtual geomagnetic poles (VGP) is higher than for Angara-Taseeva depression events but slightly lower than expected according to the model TK03 (Tauxe and Kent, 2004).

Further, we tried to correlate distinguished intrusive groups with the volcanic trap sections, using structural relationships, recent paleomagnetic and geochronological data (Burgess and Bowring, 2015). The majority of studied normally magnetized intrusions from the central part Tunguska syncline are likely coeval to the basalts of Kochechumsky formation; the reversally magnetized intrusions cutting the lava pile are younger than the main part of volcanic section (having the normal polarity). Similarly, reversally magnetized Padunskiy sill (Angara-Taseeva depression) was probably emplaced just after the termination of the main phase of volcanic activity on Siberian platform. As to Tulunskiy sill, its age is questionable because of the absence of U-Pb datings.

At last, the results of AMS measurements are performed. In Angara-Taseeva depression the most part of sites demonstrates so-called "normal magnetic fabric" for sills (e.g. Dragoni et al. 1997): the minimal axis of AMS ellipsoid is subvertical and normal to the contact, the two other axis are shallow. Interpreting the orientation of the maximal axis as the magma flow direction, we can determine the feeding zone of sills locating in the central part of Angara-Taseeva depression. In addition, the obtained data does not confirm the idea of single large sills extending over the whole depression: the directions of the AMS lineation form several "half-moons" converging to the discrete centers which could be the local zones of intruding.

The sampled intrusions from the Nizhnyaya Tunguska river demonstrate the wide variety of AMS ellipsoid forms and orientations. This fact could be the evidence of relatively small size (not larger than dozens of km) and various morphology of the intrusions from this region.

Thus, the results of paleomagnetic investigation revealed two different styles of magmatic activity during the Siberian Traps formation. The short and powerful magmatic events expressed in intruding of the large sills are typical for the periphery of Tunguska syncline. More or less even emplacement of local intrusions connected with lava eruptions is the common feature of the central part of the syncline.

This study was funded by RFBR (projects № 16-35-60114, 15-35-20599) and the Ministry of Education and Science RF (project № 14.Z50.31.0017).

References:

1. Burgess S.D. and Bowring S.A. High-precision geochronology confirms voluminous magmatism before, during, and after Earth's most severe extinction. Sci. Adv. 2015. doi: 10.1126/sciadv.1500470.
2. Chenet, A L., Courtillot, V., Fluteau, F. et al. (2009). Determination of rapid Deccan eruptions across the Cretaceous–Tertiary boundary using paleomagnetic secular variation: 2. Constraints from analysis of eight new sections and synthesis for a 3500-m-thick composite section. Journal of Geophysical Research, 114(B06103), doi:10.1029/2008JB005644.
3. Dragoni M., Lanza R., Tallarico A. Magnetic anisotropy produced by magma flow: theoretical model and experimental data from Ferrar dolerite sills (Antarctica). *Geophys. J. Int.* (1997) 128, p. 230-240.

4. Konstantinov K.M., Bazhenov M.L., Fetisova A.M., Khutorskoy M.D. Paleomagnetism of trap intrusions, East Siberia: Implications to flood basalt emplacement and the Permo–Triassic crisis of biosphere. Earth and Planetary Science Letters. 394. 2014. P. 242–253.
5. Latyshev A.V., Veselovsky R.V. Ivanov A.V. Fetisova A.V. Pavlov V.E. 2013. Evidence of brief intense peaks of magmatic activity in the south Siberian platform (Angara–Taseeva Basin) as indicated by paleomagnetic studies. Physics of the Solid Earth, vol.5, pp.1–14.
6. Moulin, M., Fluteau, F., Courtillot, V. et al. (2011). An attempt to constrain the age,duration, and eruptive history of the Karoo flood basalt: Naude's Nek section(South Africa). Journal of Geophysical Research, 116(B07403), doi:10.1029/2011JB008210
7. Pavlov V., Courtillot V., Bazhenov M., Veselovskiy R. Paleomagnetism of the Siberian traps: new data and a new overall 250 Ma pole for Siberia. - Tectonophysics 443 (2007), p. 72–92
8. Pavlov V., Fluteau F., Veselovskiy R., Fetisova A., Latyshev A., Elkins-Tanton L.T., Sobolev A.V. and N.A. Krivolutskaya (2015). Volcanic pulses in the Siberian Traps as inferred from Permo-Triassic geomagnetic secular variations. Chapter 5 in "Volcanism And Global Environmental Change", Cambridge University Press, pp. 63-78.
9. Renne P.R., Sprain C.J., Richards M.A., Self S., Vanderkluysen L., Pande K. State shift in Deccan volcanism at the Cretaceous-Paleogene boundary, possibly induced by impact. 2015, Science, Vol. 350, I. 6256, p. 76-78.
10. Tauxe L. Essentials of Paleomagnetism. California university Press. 2014. 512 p
11. Tauxe L., Kent D.V. A simplified statistical model for the geomagnetic field and the detection of shallow bias in paleomagnetic inclinations: Was the ancient magnetic field dipolar? in: Timescales of the paleomagnetic field. American Geophysical Union. 2004. V. 145. P. 101–116.

Long lived episodic magmatic history in the Variscan belt of Western Europe

Gutiérrez-Alonso G.[1, 2], López-Carmona A. [1, 2], Fernández-Suárez J. [3]

1 -University of Salamanca (Spain), alioli@usal.es; gabi@usal.es

2 -Tomsk State University, labspm@ggf.tsu.ru

3 -Departamento de Petrología y Geoquímica, Universidad Complutense and IGEO, CSIC, 28040 Madrid, Spain, jfsuarez@geo.ucm.es

One of the main characteristics linked to the amalgamation of Pangea in the western European Variscan belt is the presence of a large amount of igneous intrusive and volcanic rocks spanning in age from 350 to 295 Ma. Nowadays the time constraints and their relation with the collisional processes are subject of intense debate. New LA-U-Pb-ICP-MS geochronological data from the Tormes Dome, the Toledo Migmatitic Complex and the Cantabrian Zone in Iberia, toghether with other recent available ages in surrounding realms, provide important constraints in understanding the timing and the involved large-scale processes that shaped Pangea. The recent new geochronological data suggest the episodicity of the main igneous pulses present in Iberia which can be correlated to major tectonic events during Pangea amalgamation. The three main identified pulses range in age from: i) 350-335 Ma, recording the effects of the onset of theVariscan collision and the exhumation of the subducted passive margin of Gondwana: ii) 325-318 Ma, reflecting the orogenic collapse of the Variscan orogen that stitched Pangea; and iii) 310-290 Ma, related to the magmatic effects of the orocline development and coeval mantle replacement in the core of Pangea. In addition, the abundance of inherited xenocrystic zircons present in the analysed samples shed light in the tectonic events that pre-dated the Variscan collision and also in the nature of the different terranes involved.

Imperial topaz from the Capao Mine, Minas Gerais, Brazil

Gvozdenko T.A.[1]

1 -Vernadsky State Geological Museum of Russian Academy of Sciences, t.gvozdenko@sgm.ru

Brazil has been known for centuries for its significant and outstanding gem deposits, included topaz. The Ouro Preto area, Minas Gerais is one of the richest and most famous region in Brazil producing topaz and its most desirable variety – Imperial topaz. Known since 1768, nowadays the Ouro Preto Imperial Topaz district consists of two major mining sites, one of them – Capao mine.

The geology of region has been discussed by many scientists – Keller (1983), Pires (1983), Oliveira (1984), Hoover (1992); etc. By now there are two hypothesis for the topaz formation: the first one considers the topaz mineralization as the consequence of the intrusive process. About 1300 million years ago the intrusion had caused the fluorine-rich hydrothermal solutions that invaded the rocks through fractures with topaz formation resulted; the second opinion based on the hydrothermal process that took place during or shortly after a period of intense metamorphism.

Besides the gemological identification of gemstone (here topaz) and its variety (Imperial topaz), the most important question is the gem source. The key point is the price – topazes refer to as "Ouro Preto's" achieve the highest prices on the world jewelry market.

Seven orange-yellow, pinky-orange and orange rough topazes, suspected with Brazilian origin, was studied. Gemological tests determined refractive indices of n_p = 1.625 (min) and n_g = 1.641(max); birefringence$_{(midvalue)}$ = 0.006; specific gravity of 3.49-3.53. All of the samples were fluoresced faint orange to both short-wave and long-wave ultraviolet radiation. The pleochroism of the samples was orange, yellowish-orange, barely noticeable. According to the X-ray fluorescence the samples contain trace amount of Fe, which is relate to the internal inclusions of hematite. On the other hand the chromium was not detected (colour agent), but it can be possible in Brazilian Imperial topazes (nature of the colour caused by F-centers). The internal examine displayed liquid and mineral inclusions - two-phase and three-phase; internal fractures, which is typical for topaz from this area. The research should be continued.

References:

1. Keller P.C. The Capao topaz deposit, Ouro Preto, Minas Gerais, Brazil.// Gems and Gemology. 1983 – Vol.19, №1. - P.12-20
2. Olsen R.D. Origin of topaz deposits near Ouro Preto, Minas Gerais, Brazil//Economic Geology.1972 – Vol.67. – P. 119-123
3. Sauer D., Keller A., McClure S. An update on Imperial topaz from the Capao mine, Minas Gerais, Brazil// Gems and Gemology. Winter 1996. – P. 232-241
4. B.W. Anderson Gem testing// Moscow, Gemstone's world, 1996

Morphological, structural and dimensional features of the mineral composition of iron meteorites

Hontsova S.S.[1], Maksimova E.M.[1], Nauhatsky I.A.[1], Milyukova E.T.[1]

1 -Physical-Technical Institute, Vernadsky CFU, email: sgoncova@gmail.com

Meteorites are major source of information about the composition of matter of the Solar system and the only source of information about the early stages of its development and further evolution. The long evolution and nonuniformity processes of cosmic mineralogenesis caused emergence different genetic types of mineral formations – condensation, metamorphism and exogenetic. The first were formed as a result of condensation in the gas-dust cloud, second – at a thermal, a aqueous and a shock metamorphism in the parent bodies of meteorites and third – as a result of terrestrial weathering processes of meteorites [1]. Essentially, all the meteorites can be regarded as a combination of metal and silicate phases, sometimes with an admixture of sulphide – phase of troilite. Stony meteorites are composed mainly of silicate minerals. The foundation of iron and stony-iron meteorites is an alloy Fe-Ni-Co. It should be noted that iron meteorites contain information about the processes proceeding the chemical differentiation of meteorite parent bodies and planets.

It was investigated three samples of iron meteorites by X-ray diffraction, X-ray fluorescence analysis and scanning electron microscopy: Campo del Cielo, first discovered in 1576 in northern Argentina; Sikhote-Alin, fell 12 February 1947 in the vicinity of ridge the Sikhote-Alin and Dronino, found in 2000 in the Ryazan region, fig. 1.

a) b) c)

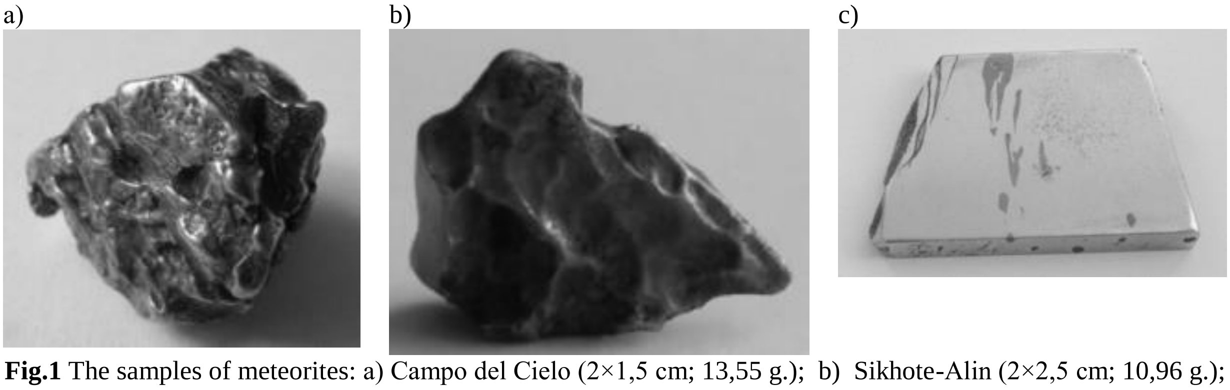

Fig.1 The samples of meteorites: a) Campo del Cielo (2×1,5 cm; 13,55 g.); b) Sikhote-Alin (2×2,5 cm; 10,96 g.); c) Dronino (1,8×3 cm; 16,35 g.)

It was found that the surface of the fragments of the Sikhote-Alin meteorite and meteorite Campo del Cielo consists on 90% of iron with a small <7% nickel content. The composition of the meteorite Dronino another: 80% of iron and ~ 18% of nickel.

The crystal structure of the samples were examined on diffractometer «DRON-3» by powder method with copper radiation (Cu). Survey was carried out in the range of angles from 10° to 100°. The study showed that in all samples is dominated by mineral of kamacite α-(Fe, Ni) – body-centered phase of nickeliferous iron, which has condensation origin. Meteorites are experiencing load at collisions with other bodies or with the Earth. The surface of kamacite is covered by numerous groups of parallel strips – so called Neumann lines formed as a result of shock loading, fig.2.

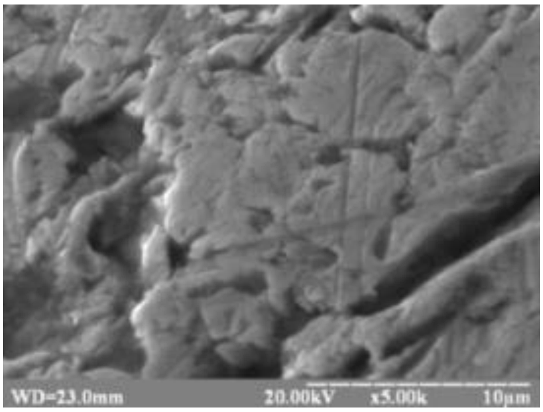

Fig.2 Microphotographs of surface of the Campo del Cielo meteorite
(scanning electron microscope SEM-106).

In all samples are presented high-temperature phases high-nickeliferous iron (taenite) and sulphides - the structures of shock melting (the formations of shock metamorphism). Shock load also leads to numerous deformations mineral schreibersite Fe_2NiP which refers to the condensation minerals. Was found in meteorites Campo del Cielo and Sikhote-Alin in as sufficiently clear facetted rod-shaped crystals of rhabdite $Fe_{1,5}Ni_{1,5}P$, [2], fig. 3.

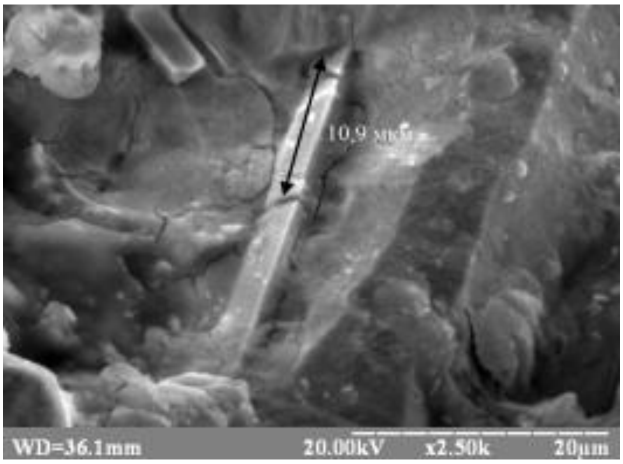

Fig. 3 Crystals of rhabdite (from 10 to 17 μm) on the surface of the Sikhote-Alin meteorite.

Among the most interesting metamorphic formations cause the graphite grains sizes from 1 to 5 μm. Graphite grains was found in a meteorite Campo del Cielo at the boundaries of silicate inclusions, [3, 4]. Also discovered numerous globular formation of different mineralogical compositions, formed at average thermal metamorphism, [5].

In the studied meteorites are presented also secondary minerals formed by as a result of terrestrial weathering. Mainly it is a various of morphological types of crystals of iron oxides found in all the samples studied meteorites, fig.4.

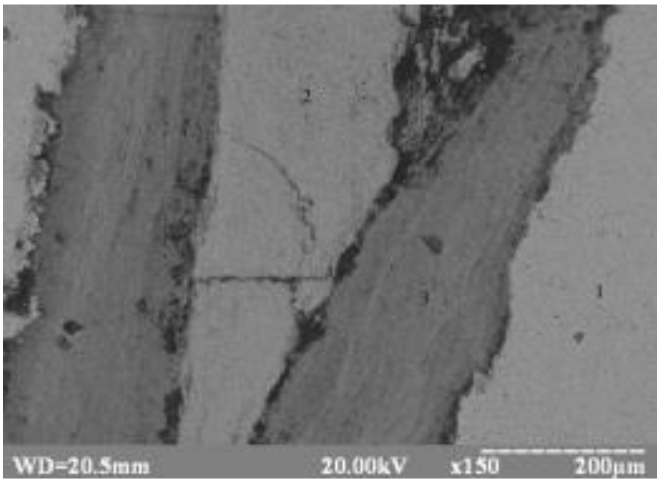

Fig. 4 Surface of the meteorite Dronino in the reflected electrons: 1 – matrix of iron-nickel, 2 – troilite, 3 – a transition zone with oxides kamacite.

Minerals chukanovite and droninoite – the unique products of weathering, first found in a meteorite Dronino.

The presence in meteorites of different genetic types of mineral formations points to a fundamental process in nature, beginning from the process of accretion of stellar material and finishing processes of weathering minerals of meteorites in terrestrial conditions.

References:

1. Dodd R.T. Meteorites, a petropogic-chemical synthesis. New York: Cambridge University Press, 1981. 384 p.
2. Maksimova E.M., Nauhatsky I.A, Hontsova S.S., Milyukova E.T. Petrography of iron meteorites on the case study of the Sikhote-Alin meteorite fragments // Scientific Notes of Taurida V.I. Vernadsky University – Series – Physics and Mathematics Sciences. 2014. V.22 (66). No. 2. pp. 99-106.
3. Maksimova E.M., Hontsova S.S., Nauhatsky I.A, Milyukova E.T. The Study of Nanometer Mineral Formations in the Campo del Cielo Meteorite// The 12th Young Scientists Conference «Fundamental and Applied Space Researches». 2015. p. 91-96 [In Russian].
4. Hontsova S.S., Maksimova E.M., Nauhatsky I.A. The study of thin crystalline structure of meteorite Campo del Cielo // Physical education in higher education institutions. 2015. V.21. No. 1C. pp. 18-19 [In Russian].
5. Semenenko V.P., Girich A.L., Shirinbekova S.N., Horovenko T.N., Kichanov N.V. Genetic types of nanometer grains of minerals in meteorites // Nanosystems, Nanomaterials, Nanotechnologies. 2012. V.10. No. 1. pp. 1-10 [In Russian].

Tektonophysic conditions and geodynamic condition of formation of Daugyztau gold ore deposit (Central Kyzyl Kum)

Janibekov B.O.[1], Turapov M.K.[1], Dulabova N.Ju.[2], Ummatov N.F.[3], Shofaiziev H.H.[3]

1 -“Scientific – Research Institute of Mineral Resources”State Enterprise Tashkent, Uzbekistan. E-mail: gpniimr@evo.uz

2 -State Committee of the Republic of Uzbekistan on Geology and Mineral Resources. Tashkent, Uzbekistan

3 -Tashkent State Technical University. Tashkent, Uzbekistan

1. According to prospecting works Daugyztau deposit is located within the ore field of the same name. The geological and structural position of the Daugyztau ore field defined by its predisposition to a zone of crossing of the Yasvay-Daugyztausky ribbon, a dislocation on Beltauskaya folded - ruptural structure of deep (2) deposit. The Daugyztau depositis dated for a site of interface of Daugyztausky and Asaukaksky faults which are considered as ore control. The deposit position in relation to folded structures is defined by a confinedness to axile part of the southern wing of an anticline. In a structure of a deposit two structural floors are allocated: the lower Paleozoic is put by thickness of besapanskaya suite (€3-O2) and the upper Meso-Cainozoic platform cover is put by terrigenous and sedimentary formations.

2. Formations of besapanskaya suite (sandstones, aleurolites, soapstones) are ore-hosting and widespread everywhere. Along with structures (folds, faults) and magmatic formations of formation of besapanskaya suite are the major geological factors of the gold objects controlling formation and placements of an ore in them. The structural factor consists in control of an ore by faults (downthrows, robbles, overfaults) NE and NW spreading, a crumpling of ore-hosting thicknesses in small folds. The ore field is over the intrusion a syenite-diorite-granophyric complex. Consensus is not present about age and genesis of a deposit, as well as, in general, for all gold objects of Central Kyzyl Kum. Many researchers (I.H. Hamrabayev, H.R. Rakhmatullayev, M. M. Mansurov, A.V. Korolev, V.D. Tsoi, etc.) hold take the view about hydrothermal genesis of a deposit and define age - the Upper Carbon - Lower Perm. The deposit represents a mineralization zone (length of 2,4 km, width - 4-100m and more) where more than ten gold deposits from tens to several hundred meters long are concentrated.

3. One of physical features of crust is tectonic intensity and a deformation under which geological phenomena including ore formation take place. Therefore between a physical condition (density, deformation) of crust and geological processes there has to be a certain interrelation. It is necessary for definition of this interrelation: 1) to define all data of the main geological phenomena (in this case - geological data of Daugyztau deposit) and 2) to define tectonic tention of the area of the geological phenomena occurrences in the period of its occurrence. The first task is solved in the course of carrying out of prospecting works. For the solution of the second task experimental works on modeling of tectonic tension in structures of a field on the basis of M. V. Gzovsky's technique and D. V. Osokina's compounding are carried out [1, 2]

4.The structural position of a Daugyztau deposit is defined by its confinedness to a zone of junction of Daugyztausky and Asaukaksky faults with formation of wedge-shaped structure. In a preore stage for the area of a deposit it was typical the contrast of magnitude of stress spreading caused by clockwise shift of the Asaukaksky fault. Activity of a fault caused shift of the wedge-shaped block in the southwest direction that led to formation of a cavity of a opening in a zone of junction of Daugyztausky and Asaukaksky breaks. In further development in this cavity of a opening it was a formation of the mineralized zone to ore deposits up to one hundred meters long. Asaukak deposit, located in the north from the Daugyztausky fault have the same mechanism of formation, and Vysokovoltnoe - is in the south of the Daugyztausky ore field. In this situation the Daugyztausky fault can be considered as ore distributing, and areas of junction with NE faults – ore-hosting.

By the ore formation period the area of an ore field got a block structure. Each block had the scheme of a structural framework, therefore a picture of distribution of tectonic tension. The tectonophysical condition of each block is defined by their boundary faults, their morphology, a spatial arrangement in relation to the direction of tectonic efforts of compression. Distribution of tension in the block also depends on intra block structures.

5. The geodynamic condition of the period of ore formation was defined due to the influence of regional tectonic movements of mainly horizontal direction. The regional movements caused activity of NE ore control faults which are at the same time boundary elements of tectonic blocks. Activity of breaks caused shift of blocks that led to migrations of efforts of compression and tectonic intensity, therefore there were changes in deformation of the background medium. There was a redistribution of tension. Zones of local compression and stretching were formed, concentration of tension is noted in areas of faults junction, in zones of local compression. All these phenomena are directly connected with morphological features, spatial position of ruptural structures and they in turn defined a block structure of an ore field. Activity of faults was caused by shift of blocks in geological space.

6. Dynamics of faults and blocks, zones of local change of deformation in the form of stretching promoted formation of cavities of opening of faults edges, formation of zones of a cleavage and rock breaking, ruptures, etc. that led to decrease to a minimum of tectonic intensity and to increase of openness of the background medium. Such geological and structural stress-deformed and geodynamic characteristics belong to the areas of occurrences of a ore-grade gold of the Daugyztau ore field to which number it is necessary to refer also Daugyztau deposit.

References:

1. Gzovsky M. V. Bases of tectonophysics. - M.: Science, 1975.-536 pages.
2. Osokina D. N. Questions of studying of hierarchical structure of a tectonic field of tension, criteria of allocation of fields of various levels and interrelation between them on the basis of modeling and theoretical calculations//Experimental tectonics in the solution of tasks of theoretical and practical geology: Tez. dokl. - Novosibirsk: IGIG FROM Academy of Sciences of the USSR, 1982. - C11-12.

Anhydrite and gypsum on gold-sulphide deposit Raduzhnoe (Northern Caucasus).

Kaigorodova E.N.[1]
1 -IGEM RAS, katmsu@mail.ru

The gold ore occurrence Raduzhnoe is located in the mountainous part of the republic of Kabardino-Balkaria in Hulamo-Bezengi gorge (Northern Caucasus). Ore mineralization in the Raduzhnoe spatially associated with subvolcanic bodies of Jurassic potassic rhyolites and trachytes. The ore bodies and mineralized zones often are represented by vein-like and stok-like bodies, explosive-hydrothermal breccia zones and siliceous breccias, disseminated sulfide ores in polygenic breccias, lenticular bodies of massive sulphide ores and rich-impregnated ores and different in composition veins and veinlets.

Gypsum and anhydrite are widespread in the massive sulphide deposits of the Lesser Caucasus, but almost never occur in the deposits of the North Caucasus. In the ores of massive sulphide deposits sulfates are widespread, they occur in bajocian volcanic suites (Shamlugh, Alaverdi deposits) and the Upper Cretaceous ones (Madneuli, Tsitelisopeli deposits) with mostly average composition with the subordinate significance of acidic and basic rocks [Gogishvili, 1969]. In the North Caucasus hydrothermal anhydrite and gypsum are described only in the deposit Raduzhnoe [Koptyukh et al, 1985; Grigorchuk et al., 1980].

Gypsum association with sulfides and link between sulfates and the processes of mineralization were studied on the Raduzhnoe deposit. Sequence anhydrite - gypsum – bassanite was determined. Anhydrite deposition occurred at an early stage of the productive hydrothermal process (table 1). Under the influence of surface water anhydrite was hydrated to gypsum. Finding bassanite confirms its formation from hydrothermal solutions with temperatures above 100^0 C. The sulfur isotopic composition of sulphides and gypsum indicates a homogenous igneous and sedimentary sulfur sources.

Table 1. Mineral sequence and ore composition of Raduzhnoe deposit.

Metallogenic epoch	Cimmerian (Early Alpine)				
Mineralization Stage	Prior-productive	Early productive		Late productive regenerated	Post-productive
Mineral assemblage (complex)	premineral metasomatites	Gold-sulphide	Galena-sphalerite	Gold -silver	Supergene weathering products
Mineral association	quartz-chlorite-hydromica, hydromuscovite -quartz-pyrite	Quartz-carbonate-pyrite with anhydrite, gold-pyrite-galena-chalcopyrite with gold	Galena-sphalerite-quartz-carbonate	Gold-silver, kustelite-carbonate-barite with gray ores	Gold-acanthite with hydroxides of Fe, Mn, sulphosalts of Ag, Pb, Zn, Cu
Minerals	Quartz, carbonate, chlorite, sericite, hydromica, hydromuscovite, pyrite, arsenopyrite, anatase.	Pyrite, marcasite, chalcopyrite, sphalerite, galena, gold isomorphic in pyrite and chalcopyrite, barite, anhydrite, gypsum, quartz	Sphalerite, galena, chalcopyrite, pyrite, barite, quartz	Native gold, silver, kustelite, freibergite, bournonite, barite, calcite, chalcedony, adularia	Acanthite, native gold jarosite, beudantite, malachite, azurite, hematite

Gypsum forms both single veins and the network of thick veinlets. The total capacity of gypsum-bearing strata is up to 65-80 m. As a rule, gypsum associated with sulfide bodies.

Conclusions. On the deposit Raduzhnoe anhydride was formed at the early productive stage and gypsum - in the subsurface environments as a result of the hydration of anhydrite. This process has been so intense that it is quite difficult to find a non-hydrated anhydrite. Gypsum association with primary unaltered sulphides explains by the high rate of the hydration reaction, caused to closing of the path of oxygen-rich water circulation, before happen appreciable oxidation of sulfides.

The association of anhydrite to the lower horizons of deposit and the barite to the upper ones is related with a sharp temperature drop established between these horizons at interstratal disruption. Finding the gypsum-anhydrite veins mineralization at the Raduzhnoe is a prospecting indicator for gold-sulfide mineralization.

The work was supported by the program of fundamental researches of RAS (project no. I.4П(P)) "Deposits of strategic raw materials in Russia: innovative approaches to forecasting, evaluation and production."

References:

1. Gogishvili V.G. On the genesis of calcium sulfate in sulfide deposits on the example of Alaverdi-Bolnisi ore field (Lesser Caucasus). Geol. Of Ore Deposits. Volume IX. №6. 1969.
2. Grigorchuk G.Y, Kryzhevich S.S. et al. Prospective evaluation of gold-silver occurrences on Bezengi ore field based on the study of geological, physical and chemical conditions of the mineralization. Interim report on works 1978-79 years. L'vov. 1980.
3. Koptyukh L.M., Semenyuk N.P. et al. Report on economic agreements №3/82 "Study of volcanism and its connection with the processes of mineralization and metasomatism in activation zones of Kabardino-Balkaria." Kiev. 1985.

Silver mineralization in Chuckotka: geochemical prospecting and connection to magmatism

***Kalko I.A.*[1]**

1-Lomonosov MSU, ildarkalko@yandex.ru

The are several evidence of presence silver mineralization throughout Chukotka. Vast areas covered by geochemical data are signs of a silver mineralization anomalies in streams and secondary dispersion halos. Low cost of silver and lack of demand for silver is the reason for their lack of the investigation. There are three types of structures in Chukotka to locate silver ores: volcanic belts (VB), folded sedimentary rocks (FB) and orogenic magmatic (OM) structures. For example, around The Kupol deposit there are several ore prospects with silver ores (VB), in the Anuy folded belt located silver prospects (FB), the Mramorny cluster of prospects (OM). All of those prospects are seems to be connected to intruded rocks or subvolcanic stockworks.

The largest silver deposit in Far East Region is the Dukat (Magadan region), with a cluster of satellite deposits, connected to structure of Okhotsk-Chukotka Volcanic Belt (OCVB). As a rule, the silver deposits are confined to the outputs of volcanic or intrusive bodies. Definition of geochemical characteristics of the host rock and ore-controlling testify in favor of the fact that the source of ore components were they. At The Dukat researchers noted geochemical specialization breeds such that the complex of silver, arsenic, tin, tungsten, lead, copper, which are found in the ore bodies [Konstantinov, 2000]. On fields with tin geochemical specialization rocks indicates the concentration of ore components of the ore-controlling intrusions. Zou Shu pointed out that the tin-bearing granites enriched Sn, Cu, Pb, Zn, and other elements [Zou Shu et all, 1984].

Many researchers have associated silver mineralization at the fields with the characteristics of the rocks. In the works of Cher and Konstantinov has been suggested to the confinement of silver objects subalkalic, alkaline rocks. As a rule, in the vicinity of silver deposits marked rocks with high alkalinity and metasomatic with K-feldspar. Excessive amounts of potassium in the surrounding rocks, sericite, K-feldspar metasomatic, ore in excess of calcite formations.

There are several mistakes in description of silver prospect: main component of silver prospect is gold, severally examples – led and zinc. But silver always play accompanying role. For example, silver-gold prospect: Kapelka, Arykevaam, Shak, Zhilky and many others are divided to the group of the gold deposits, but main role play silver.

This happened due to the fact that the main component in Chukotka has always been gold, and in the presence of a large satellite facility with a predominance of gold over silver, the fate of all other objects were doomed.

Ore deposits of silver are often rife with silver minerals, but the surface is very often plays a major role acanthite and native silver. Primary Is this acanthite: often have questions. Tellurides, selenides, stibnidy arsenides and quickly release the silver as a result of supergene processes, we see the formation of supergene acanthite.

Search stage often provides an answer to the question about the prospects of ore objects, but supergene silver behavior is not simple: sulfide forms disproportionate and formed a water soluble form of silver along with native silver but this can occur electrolytic processes.

The deposits of silver can often be located on the rich stream anomalies (around the Dukat silver concentration in streams was 10 ppm). Ore areas promising for silver can be released in silver anomalies grading 1 ppm. Usually this areal structure, forming clusters of streams.

In soils of Chukotka empirically found that when the content of more than 5 ppm silver content in the primary ores can reach 500 ppm or more. When the content of more than 10 ppm with a probability of detection of ore content 0.1 % of silver. In Dukat secondary halos have a continuous loop anomalies greater than 5 ppm area.

Studying the composition of geological complexes were carried out on Alyarmaut area. Alyarmaut area located to the north of Bilibino. Silver mineralization were found there in last years. Determination of ore elements allowed us to obtain the spectrum of ore elements in the background rocks. Normilized on the content of the upper mantle according to the concentration of the spectra obtained [Rudnick, 2003] elements in the unaltered or weakly altered rocks.

The sedimentary siute are generally not allocated a significant excess over the crust.

Exceptions are Anyui gabbro complex, intensely chloritized buyout. In addition they are set higher copper concentration. In shales pribrezhnenskoy suite installed elevated concentrations of arsenic and antimony.

Intrusive rocks in studied area represented Lower Cretaceous rocks of a broad range of compositions from a normal rock diorite-granodiorite-granite composition tymkiveemsky complex. Individual units of the complex have a higher concentration of silver, antimony, arsenic.

Rocks of suharninsky suites have subalkalic composition and have a higher concentration of Ag, Bi, Mo, Sn, W, Pb (fig.1)

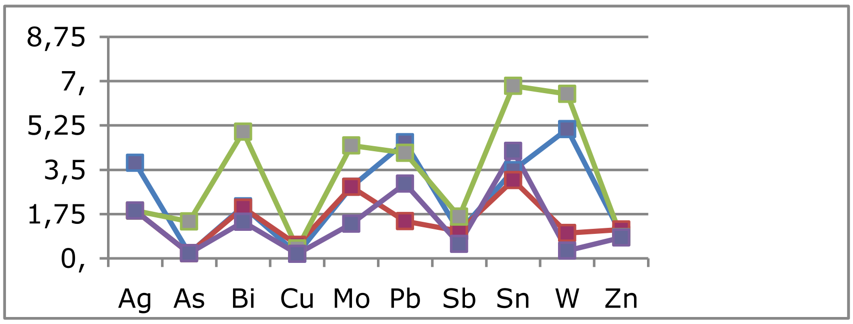

Fig. 1 Normalized concentration of elements in suharninsky suit

Referenses:

1. Zou Shu, Linyongcai And Gao Zepe. An Approach to Ore-Forming Characteristics and Metallogenic Model of the Granites Emplaced Through Tectonic Remelting in the Yunlong Tin Belt, Western Yunnan //Geology of Tin Deposits in Asia and the Pacific: Selected Papers from the International Symposium on the Geology of Tin Deposits, 1984, pp 258-269.
2. Rudnick RL, Gao S. Composition of the continental crust. // The crust. Treatise on geochemistry, vol 3, 2003, pp 1–64 Konstantinov M. M., Vargunina N.P., Kosovetc T.N. et all. Gold-Silver deposits: models of ore deposits of precious metalls (in Russian). 2000, 239 p.

Petro-mineralogical studies of phosphorite deposit of ram ka munna block of Banswara district, Rajasthan, India

Khan S.[1], Khan K. F.[2]

1 -Department of Geology, AMU, Aligarh, India, shamsuddin.amu@gmail.com

2 -Department of Geology, AMU, Aligarh, India, farahimamu@gmail.com

Paleoproterozoic phosphorite deposit at Ram Ka Munna block under Banswara district in Rajasthan is a part of Kalinjara formation of Lunavada group of Aravalli Super Group. This deposit of phosphorite is inherent in dolomite, multicolored chert and calcareous quartzite. Phosphorites occur in form of thin, bluish-grey stringers. These stringers are composed with phosphate, carbonate and siliceous materials.

We have used petrological microscope, X- ray diffractometry, FEG- SEM and EDX for Petro-mineralogical studies of phosphorite samples. The study reveals that Apatite-(CaF) is dominant phosphate mineral which is intermixed with insignificant amount of carbonate material. Infrequent findings of the uniform tiny granules of partially anisotropic Apatite-(CaF) along with dolomite, calcite, quartz, muscovite, zeolite and other gangue minerals have been observed. Further, replacement of phosphate material by quartz and carbonate is noticed.

The presence of microbial filaments of organic, mutual replacement of phosphate-carbonate-quartz indicates that the deposition of the phosphate took place in shallow marine oxidizing environmental conditions. This leads to the formation of phosphorite layers as primary biogenic precipitates by bacterial or algal activities. The different forms and texture of phosphate minerals may due to environmental fluctuations of the time of deposition followed by some replacement processes and biogenic activities.

Key words: Ram Ka Munna, Phosphorites, Apatite-(CaF), Dolomite.

Mineralogically probable synthetic phases obtained in hydrothermal conditions

Kiriukhina G.V.[1], Yakubovich O.V.[2]
1 -Lomonosov MSU, g-biralo@yandex.ru
2 -Lomonosov MSU, IGEM RAN, yakubol@geol.msu.ru

Novel synthetic analogues of minerals in different crystal chemical classes have been obtained hydrothermally (T = 280°C и P = 70 atm) in presence of mineralizers and in conditions approximated to the environments of natural hydrothermal systems. Based on the results of the X-ray spectral and X-ray (or synchrotron) diffraction analyses the products of crystallization were identified as synthetic analogues of minerals elpasolite, niahite, shibkovite and mahnertite, and their crystal structures were found and refined [1-4].

The similarity of structural fragments in a new centrosymmetric modification of niahite $NH_4MnPO_4 \cdot H_2O$ and lithiophilite $LiMnPO_4$ (*TOT*-layers of Mn-octahedra and P-tetrahedra) indicates possible genetic relations between these minerals. The synthesis of "Fe-niahite" under hydrothermal conditions in association with the typical mineral of granitic pegmatites, zwieselite Fe_2FPO_4 suggested that the natural analogue of niahite can be found among the secondary pegmatite phosphates. It can be formed on the basis of triphylite–lithiophilite solid solution under low-temperature reductive conditions provided that ammonium ions are available in the system: $LiMnPO_4 + NH_4OH + H_2O \rightarrow NH_4MnPO_4 \cdot H_2O + LiOH$. This scheme was indirectly confirmed experimentally on the preparation of synthetic analogues of minerals of the triphylite–lithiophilite series based on the "niahite" precursor.

Synthetic shibkovite $K(K_{1.67}H_2O_{0.33})(Ca_{1.3}Na_{0.7})Zn_3[Si_{12}O_{30}]$ is a new water containing variety in milarite group that unites 21 minerals of different origin. The variety of the chemical compositions of minerals crystallized into milarite type structures is primarily related to the large number of isomorphic substitutions in octahedra and tetrahedra forming a mixed type anionic framework. Large voids in the framework are occupied by K atoms in most minerals of the group. Although large cavities in the structures allow for the location of H_2O molecules and the creation of hydrogen bonds with framework oxygen atoms, there are only two minerals and two synthetic (shibkovite and milarite) analogues that contain crystallization water. Only these four phases were grown under soft hydrothermal conditions. It means that the presence or absence of the H_2O molecules in the structures depends mainly on the conditions of formation of minerals and synthetic phases with the milarite structure type.

The Rb_2NaAlF_6 is isotypic with elpasolite K_2NaAlF_6, usually formed as a secondary mineral and often associated with pegmatites. Rubidium belongs to dispersed elements exhibiting a close geochemical affinity with potassium, which is one of the most abundant elements in the Earth crust. Owing to the close dimensions of these monovalent cations, Rb^+ isomorphously substitutes for K^+ in the structures of minerals and it is this substitution that disperses rubidium in nature. The resent discovery of several rubidium minerals in late associations of rare metal granite pegmatites, the isotypy of Rb_2NaAlF_6 and elpasolite K_2NaAlF_6, and the preparation of cubic mixed K,Rb elpasolites in laboratory conditions allow us to suppose an existence of the Rb rich elpasolite in nature.

A new phosphate modification of mahnertite, $K_{2.5}Cu_5Cl[PO_4]_4(OH)_{0.5}(VO_2)H_2O$ is a structural representative of the topology shown by the lavendulan group of secondary copper arsenate and phosphate minerals. We suggest interpreting this group in terms of the modular concept with a synthetic phase $Ba(VO)Cu_4(PO_4)_4$ as a simplest member of the new polysomatic series. The heteropolyhedral slabs with a topology similar to the $[Cu_4Cl(PO_4)_4]^{5-}{}_{\infty}$ layers of our synthetic mahnertite are the basis of all crystal structures even though these minerals differ in symmetry. A main diversity among the lavendulan-group members arises from their slabs' linkage, specifically the second slab alternating along one axis of their unit cells and varying in content.

The authors thank O.V. Dimitrova and A.S. Volkov for the products of hydrothermal synthesis.

References:

1. Yakubovich O.V. *et al.* // Crystal. Reports, 2013. 58(3): 412-415.
2. Kiriukhina G.V. *et al.* // Crystal. Reports, 2015. 60(1): 37-45.
3. Kiriukhina G.V., *et al.* // Crystal. Reports, 2015. 60(2): 198-203.
4. Yakubovich O.V. *et al.* // Z. Kristallogr. - Crystalline Materials, 2015. 230(5): 337-344.

Ir-determination of water abundance in the mantle xenoliths from Udachnaya kimberlite pipe, Yakutia

Kolesnichenko M.V.[1], Zedgenizov D.A.[1,2], Ragozin A.L.[1,2], Litasov K.D.[1,2]
1 -V.S. Sobolev Institute of Geology and Mineralogy SB RAS, Novosibirsk, Russia
2 -Novosibirsk State University, Novosibirsk, Russia
m.kolesnichenko@igm.nsc.ru

Water can change physical and chemical properties of mantle minerals, or the part of the mantle, for instance, the effect of OH on mineral deformation and its impact on mantle rheology [1]. Kimberlites are one of the most important objects for research because they carry mantle xenoliths to the surface. So that kimberlites are the only direct source of information on the petrology and geochemistry of the deep mantle rocks.

We have studied representative collection of the 19 and 25 relatively fresh xenoliths of peridotites and eclogites, respectively. The xenoliths of peridotites are non-deformed and deformed garnet lherzolites, harzburgite and dunite. The studied peridotites contain 45-70% olivine, 10-40% orthopyroxene, 5-25% clinopyroxene and 10-25% garnet. The garnet bearing peridotites have microscopically recognizable deformation textures. The peridotite xenoliths have granular, porphyroclastic, mosaic-porphyroclastic and fluidal textures [2]. Using different degrees of peridotites deformation we identify three types of lherzolites: non-deformed garnet lherzolites, medium-deformed garnet lherzolites and high-deformed garnet lherzolites.

The studied eclogites are bimineralic and contain 40-70 % clinopyroxene (Cpx) and 30-60 % garnet (Grt). Cpx and Grt show wide range of compositions. Clinopyroxenes are characterized by Na_2O (1.7- 7.0 mas.%) and Al_2O_3 (1.9-15.3 mas.%) contents and Mg# 73-92. In garnets almandine component varies from 19 to 48%, pyrope component from 21 to 72%, grossular component from 8 to 33%. All eclogites are divided into three groups by classification scheme of [3], based on MgO and Na_2O contents in Cpx.

Using calibration coefficients [4] we calculated water content in mineral samples. Water contents in peridotites range from 2 to 95 ppm in olivine, 8-61 ppm in orthopyroxene, 7-71 ppm in clinopyroxene. The water in eclogites is mainly stored in omphacite (4-99 ppm). Garnets do not contain measurable OH in both rock types. Taking into account the volume ratios of mineral phases in the studied xenoliths, the water contents vary over narrow ranges, from <1 to 61 ppm in peridotites and from 2 to 55 ppm in eclogites. It should be noted that the high-deformed peridotites have the highest water content and vice versa, low-deformed and non-deformed ones contain the low water amounts (Fig. 1). We suppose that higher water contents in deformed peridotites associate with water enrichment of kimberlite fluid, which infiltrate through the peridotite vein.

Moreover we obtained no correlation between eclogite water concentration and temperature, pressure or composition of the rock. Low amounts of water in eclogites may be related to intensive dehydration during subduction or partial melting of the rock before kimberlite ascent. The former confirm limited water transfer in subducted slab.

This work was partially supported by the Ministry of education and science of Russian Federation, project No. 14.B37.21.0457 and RFBR (projects No 15-55-50033; 15-55-53029; 16-35-00317).

References:

1. Miller G.H., Rossman G.R., Harlow G.E. (1987). Physics and Chemistry of Minerals 14, 461-472.
2. Harte B. (1977). Journal of Geology 85, 279-288.
3. Taylor L. A., Neal C. (1989). The Journal of Geology, 551.
4. Bell D.R., Rossman G.R., Maldner J., Endisch D., Rauch F. (2003). Journal of Geophysical Research 108, 1-9.
5. Brey, G.P., Koehler, T. (1990). Journal of Petrology 31. 1353–1378.

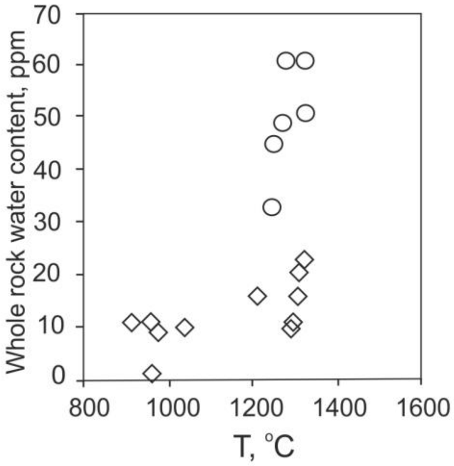

Fig. 1 Whole rock water content versus temperature (calculated using Opx-Cpx 'solvus' by [5]). High-deformed peridotites (circles), medium-deformed and non-deformed peridotites (diamonds)

Type of variation of hydro physical properties of enclosing coal solid at mine field named after Kostenko of Karaganda coal field

Kopobaeva A.N. [1]***, Satibekova S.B.*** [1]***, Toleytai T.A.*** [1]
1 -Karaganda State Technical University, aiman_25.87@mail.ru

Karaganda coal field is located in Karaganda region. Regarding industrial and geological issue it is divided into four districts such as Tentekskiy and Chyurubai-Nurinksiy, located in its western part, Karagandinskiy, located in the center of the coal field, and Verkhnesokurskiy is in the eastern part.

According to geological and field zoning of area, Karaganda coal mine field named after Kostenko is located in eastern part of Industrial district of Karaganda coal region.

The geological structure of the field of mine involved rocks of Carboniferous, Jurassic, Neogene and Quaternary. It is well known that the stability of the rock mass depends on the thickness of the constituent types of rocks and their mineral composition, their capacity and relationships of physical and mechanical properties of the lithologic varieties of mine rocks. Because of this we studied the variability of the volume weight, moisture content and porosity of the host rocks Karaganda sunk [1] with depth, selected from the exploratory boreholes 11405, 22202, 11339, 22180, 20808 section of the intervals for specified sunk.

The dependence of hydro physical properties (volume density, inherent moisture) enclosing coal rocks studied on the test results of core drilling core samples in the exploration of coal seams for above mentioned sunk and is determined separately for different lithological.

The dependence of volume density (d, g/cm^3) lithotypes rocks on the depth of their occurrence (Picture 3) sand rocks is described by the equation:

$$d_n=1,5+1,2xH/H+30$$

where – d_n volume density of sand rocks, g/cm^3.

Mean square deviation is 0,22.

The volume density of silt stones is described by the following equation:

$$d_{aleurolite}=2,6xH/H+10\ ,$$

where – $d_{aleurolite}$ volume density of aleurolite, g/cm^3.

Mean square deviation is 0,14.

For clay rocks the equation is:

$$d_{argillite}=H/0,4xH+5,$$

where – $d_{argillite}$ volume density of argillite, g/cm^3.

Mean square deviation is 0,68.

The dependence of inherent moisture ratio (W, %) of sand rocks on the depth of their occurrence (Picture 4) is described by the equation

$$W_n=H^{0,398}x\ 121/H,$$

where W_n – inherent moisture of sandstone, %;

H – the depth of the surrounding rocks, m.

Mean square deviation is 0,78.

The dependence of inherent moisture ratio of slit rocks on the depth of their occurrence is defined as follows

$$W_{aleurolite}=4H^{0,4}/32H,$$

where $W_{aleurolite}$ – inherent moisture of aleurolite, %;

Mean square deviation is 0,84.

The dependence of inherent moisture ratio (W, %) of clay rocks от on the depth of their occurrence is defined according to the following equation:

$$W_{argillite}=2+100/0,07H^{1,2}\ ,$$

where $W_{argillite}$ – inherent moisture of argillite %;

Mean square deviation is 0,77.

Decreasing of inherent moisture and increasing of sandstones volume density, slit and clay rocks with the depth that corresponds to physical significance of changes for mentioned parameters with the depth of their occurrence.

It is well known fact that porosity correlated with a specific, volume density and inherent moisture breeds.

The sandstones porosity correlates with the dependence of inherent moisture ratio (Picture 5) is described by the following equation:

$$P_s=30-1,1xH^{0,5}$$

where P_s – sandstones porosity, %.

Mean square deviation is 0,32.

The siltstone porosity is defined by the following formula:

$$P_{aleurolite}=30-12xH^{0,48}/1,1\ ,$$

where $P_{aleurolite}$ – aleurolite porosity, %.

Mean square deviation is 0,4.

The clay rocks porosity is defined by the following formula:

$$P_{argillite=}25\text{-}H^{0,45}/0,8$$

where P $_{argillite}$ – argillite porosity, %.
Mean square deviation is 0,89.

Earlier in Karaganda city the Karaganda scientific and research coal institute (KSRCI) had been successfully functioning and it had been providing scientific justification of adopted schemes of opening and development of coal seams Karaganda coal field. Its scientific potential was rather high. Doctors and candidates of science have been studying the physical-and-mechanical properties of coal and enclosing its rocks of Karaganda coal field [1,3,5-7] in order to solve the tasks rock pressure control, questions of mechanization in mining industry or rock rigidity. After liquidation of this institute and the transfer of mines to private owners the studying of the physical-and-mechanical properties of coal and coal-bearing strata of rocks of Karaganda coal field, unfortunately, had stopped.

Besides, water-and-physical properties of enclosing rocks were considered by Yermekov M.A. and Bilyalov B.D. [2] the study of the amplitudes puppy faults with depth for Zavjyalovsky coalfield to subsist the different stress values of locking and central parts of syncline structure, which is reflected in the different gradients of change of the hydro physical properties with the depth of its occurrence.

We consider, similar researches should be held indifferent parts (side and central parts of folds) synclinal and anticlinal structures of second and third order of Karaganda syncline. These researchers will allow identifying different gradients of changes of mentioned hydro physical and physical – and- mechanical properties enclosing rocks coal pays in different parts folds that can be directly used when identifying the sustainability of rock solid or when solving issues of top control the development of coal seams.

As the result of our researches the effect of tangential tectonic and geostatic forces it was defined on changes of volume density, inherent moisture and different lithotypes porosity of enclosing rocks coal pays with depth of its occurrence. This pattern can be used for the forecast the rock solid in the development of coal pays Karaganda near the mine field named after Kostenko mine and adjacent mine fields, located in Industrial district of Karaganda coal field.

References:

1. Altayev Sh.A., Smirnov A.I. About some physical-and-mechanical properties of rocks Karaganda coal field (Saransk district) //Technology issues in mining industry: Works of KSRCI, M.:Nedra, 1966. Edit. 21.
2. Geology of Karaganda coal field //M.: Nedra, 1972.
3. Gumenyuk G.N. Studying the mechanical-and-physical properties of coal of rock formation «Top Marianna» // Research of mechanical-and-physical properties of rocks in relation to the tasks of control rock pressure, M.: Edit. AH USSR, 1962.
4. Yermekov M.A., Bilyalov B.D.. To analysis of changes displacement amplitude faults with depth in the graben structures (using example of Zavyalovsk mine site) // Vetsnik AS of KazSSR, Alma-Ata, 1972, №1.

Distribution of iron minerals in Bauxite-Bearing lateritic profiles formed after dolerites, Republic of Guinea

Korrea Gomesh G.[1] and Makarova M. A.[2]

1 -RUDN University, jolica20@hotmail.com, 2 - Lomonosov Moscow State University

Bauxite deposits of the largest bauxite-bearing province of the Republic of Guinea have essentially originated from the lateritic weathering of basic igneous rocks (dolerites and konga-diabases) of the Mesozoic trap association.

The classic lateritic profile is distinctly zoned, which results from varying physical and chemical conditions of weathering over it. Shown in the table are: lithological horizons forming the vertical lithological zoning; average absolute concentrations of major petrogenic components, calculated with volume weight values of the rocks, and their concentration ratios (R_C) relative to their concentrations in the subjacent zone, as indicators of the matter redistribution; according to the view point shared by a number of researches (Bronevoi, Mamedov, Slukin, *et al*), the lateritic profile is a supergene infiltration metasomatic column with each superposed zone formed after its subjacent zone; primary and neogenic iron minerals of the zones/horizons under consideration.

As evident from the submitted data, iron and iron-containing minerals of the protolith are presented by monoclinic pyroxene (augite), hypersthene, hornblende (uralite), chlorite, and subordinate biotite, ilmenite, and magnetite.

In ***the clayey horizon*** (the decomposition and hydration zone), which is flooded in the rainy season, primary aluminosilicates are substituted by mixed lattice clayey minerals in the lower zone and then by kaolinite in the upper zone. Iron leached with the decomposition of dark-colored aluminosilicates is bound in such a hydroxide as goethite of the first generation. Accessory ilmenite and magnetite are replaced by martite and then hematite of the first generation. Formation of the clayey horizon after dolerites is accompanied by some accumulation of iron, mostly in the upper zone.

The ferruginous lateritic horizon (the transition zone) forms above the clay in the hydrogeological zone of fluctuation of groundwater table, owing to an intense input of iron and its deposition as ferric oxide minerals, which indicates an active oxidation barrier in the weathering profile. Oxygen permeates into this zone with meteoric waters infiltrating down along fractures.

Brought iron impregnates and substitutes the clay and residual quartz and forms ferrigels crystallizing as cryptocrystalline to fine-grained goethite. Though being hardly distinguishable from goethite of the first generation under optic microscope, this goethite is certainly later (1a).

In addition to the above-mentioned goethites there is goethite of the second generation (2). It is cryptocrystalline and forms colloform veinlets, veins, and filling of vugs and pores. The goethite hosts microscopic bands of hematite of the second generation or hydrohematite - hematite of the first generation represents pseudomorphs after magnetite and ilmenite. Evidently, the colloform iron oxyhydroxide aggregates originated from the ferrigels. Nevertheless, the deposition of hematite 2 on the background of dominating goethite seems some uninterpretable.

Maximum iron concentration (the absolute accumulation/input) occurs in the middle and upper parts of transition zone, and ferriplantite plates and lenses form there. Their concentration ratio exceeds 3-4. When calculated for 1 m^3 of the rock the absolute iron accumulation is 1190 kg/m^3. Like other ferruginous laterites, the ferriplantite plates and lenses show the iron oxyhydroxide mineralization including fine- to cryptocrystalline goethite 1 and 1a matrix, pseudomorphous hematite 1 grains, and colloform goethite 2 and hematite 2 (or hydrohematite) aggregates.

In addition to the above-mentioned iron oxyhydroxide varieties there are columnar goethite 3 and hematite 3 aggregates revealed in the ferruginous laterites and ferriplantites, usually as incrustation of pores, with hematite 3 forming peripheral bands of the aggregates.

The bauxite horizon occurring above the ferruginous laterites and confined to the hydrogeological zone of infiltration is characterized by intense leaching of iron (more than a half of the initial iron amount) and by a comparable input of Al_2O_3. This is the replacement zone of iron to aluminum, and hence, the zone of ferruginous metasomatism gives place to the zone of aluminum metasomatism. In the middle and upper parts of this zone CO_2 content increases abruptly by two orders of magnitude, with less intense CO increase and with O_2 decrease by two to three times. As a result the glei geochemical setting arises, favorable for iron reduction and removal. And only along the fractures controlling infiltration of oxygen-bearing meteoric waters down the weathering profile there occur the enrichment in oxygen and the limonitization and replacement of aluminum minerals. Neogenic iron minerals in the fractures are presented by goethite 2a and 3a and by hematite 2a and 3a.

Upwards the horizon, with increasing O_2 and decreasing CO_2 concentrations in the subsurface air, the bauxites become deeper red-colored, and at the surface they are often replaced by brownish-red ferruginous laterites of ***cuirass***.

As evident from the comparison of cuirass to bauxites, a considerable input of iron (to 500 kg/m^3 of Fe_2O_3) and a substantial loss of alumina (about 200 kg/m^3 of Al_2O_3) are needed to for its formation, i.e., ferruginous metasomatism occurs again. Mineralogical data show that the cuirass is distinctly dominated by goethite 2a and 3a with subordinate hematite 2a.

Thus, there are two horizons/zones of absolute iron accumulation distinguishable in the bauxite-bearing classic lateritic profile. Goethite found as several morphologies is the absolutely dominant iron oxyhydroxide. The lower horizon is some richer in neogenic hematites 2 and 3. Note, however, that neither reasons nor mechanism of the formation of dehydrated iron oxides (hematite) from ferrigels are clear yet.

Horizon			Metasomatism	Lithology of horizons/zones	Average values $\frac{kg/m^3}{R_c}$				Primary and neogenic iron minerals
					$\frac{Fe_2O_3}{R_c}$	$\frac{Al_2O}{R_c}$	$\frac{SiO_2}{R_c}$	$\frac{LOI}{R_c}$	
Lateritic profile	Cuirass		Ferruginous	Ferruginous laterites rocky, firm, brecciated and/or structure-relict	$\frac{820}{1.46}$	$\frac{837}{0.97}$	$\frac{82}{3.53}$	$\frac{477}{0.99}$	Goethite[1)] 1; 1a; 2; 2a; 3; 3a Hematite 1; 2; 2a; 3; 3a
Lateritic profile	Bauxites	red-colored	Ferruginous	Bauxites red-colored, low- to medium-grade, rocky, structure-relict and/or brecciated	$\frac{562}{1.83}$	$\frac{864}{0.84}$	$\frac{23}{0.74}$	$\frac{482}{0.88}$	Goethite 1; 1a; 2; 2a; 3; 3a Hematite 1; 2; 2a; 3; 3a
Lateritic profile	Bauxites	light-colored	Aluminum	Bauxites light-colored, medium- to high-grade, rocky, structure-relict and brecciated	$\frac{308}{0.42}$	$\frac{1027}{1.59}$	$\frac{32}{0.41}$	$\frac{550}{1.44}$	Neogenic iron minerals confined to fractures Goethite[1)] 2a and 3a Hematite 2a and less usual 3a
Lateritic profile	Ferruginous laterites	general	Ferruginous	Ferruginous laterites rocky and crumbly, fragmental and structure-relict	$\frac{734}{1.89}$	$\frac{647}{1.33}$	$\frac{77}{0.15}$	$\frac{382}{1.98}$	Goethite (1 and 1a); Hematite (1); Goethite 2 and 2a, 3 and 3a Hematite 2 and 3
Lateritic profile	Ferruginous laterites	ferriplantites	Ferruginous	Ferriplantites rocky, very firm, massive and indistinctly banded	$\frac{1548}{3.98}$	$\frac{507}{1.04}$	$\frac{151}{0.29}$	$\frac{437}{1.87}$	Goethite (1 and 1a), Hematite (1). Goethite (2) and Hematite (2) filling fractures and pores. Goethite (3) and occasional Hematite (3)
Lithomarge and saprolite	Clays		Decomposition and hydration zone	Clays substantially kaolinitic in the upper section and polymineralic in the lower section	$\frac{358}{1.2}$	$\frac{488}{1.13}$	$\frac{516}{0.38}$	$\frac{234}{6.9}$	Goethite (1) after dark-colored minerals Hematite (1) after titaniferous magnetite Goethite (1a) impregnating clays in the upper section
Protolith				Dolerites and konga-diabases, fine- to medium-grained	$\frac{293}{1}$	$\frac{432}{1}$	$\frac{1344}{1}$	$\frac{34}{1}$	Monoclinic pyroxene, hypersthene, uralite, biotite, titaniferous magnetite and less usual magnetite

The test of olivine-liquid thermometry modelling: results of high-temperature one-atmosphere experiments

Krasheninnikov S.P.[1], Sobolev A.V.[1,2], Batanova V.G.[1,2], Kargaltsev A.A.[1], Borisov A.A.[1,3]

1 - V.I. Vernadsky Institute of Geochemistry and Analytical Chemistry RAS, (spkrash09@gmail.com)

2 - Institut des Sciences de la Terre (ISTerre) Université Grenoble Alpes, Grenoble, France

3 - Institute of Geology of Ore Deposits, Petrography, Mineralogy and Geochemistry RAS

Olivine-liquid thermometry is a powerful modelling method in the modern petrology allowing scientists to reevaluate thermic conditions of the mantle [1, 2]. Different calculation models fit better for special types of compositions or temperature values [3]. The most primitive mafic and ultra-mafic melts formed at the highest magmatic temperatures (more than 1400^o C). We propose results of high-temperature one-atmosphere experiments conducted to determine the best model for such type of rocks/melts.

For that study the brand-new high-temperature Nabertherm vertical-tube one-atmosphere furnace (up to 1700^o C) mounted and launched in Vernadsky Institute (Moscow, Russia) for experiments in C-O-H atmosphere (within the range of NNO ±3 log units). Pt/PtRh10 or PtRh6/PtRh30 thermocouples in the working furnace were employed for measuring temperature during experimental runs. Furnace temperature profile at different T values shows 7 cm hot-spot zone ($\Delta T<1^o$ C). Stability of the temperature regime during one experimental run lies within ±1^o C. The "loop" technique chosen to obtain several compositions in one experimental run with the highest sample-container ratio. Fine powder of each sample was mounted on ~2mm Pt loop with an organic glue and placed on the ceramic stick-holder. All experiments were conducted in three steps. The first one is the saturation of the Pt wires with Fe from the sample during several hours at experiment conditions with the following dissolution of the sample in hydrofluoric acid. The second stage aimed to melt and homogenize sample at above liquidus temperature during a few hours. The last step was the experimental run.

20 experiments with natural mafic and ultra-mafic compositions (tab. 1) conducted at high temperatures (1297-1588^o C) and NNO ±2 log units buffer conditions, each experimental run contains 5-6 loops with different composition. Some samples were doped with small amount of oxides (Cr_2O_3, Al_2O_3 & TiO_2) and/or up to 20 wt. % of San-Carlos olivine to increase the olivine liquidus temperature. Major elements in glasses, olivines and spinels from the experiment products were measured by EPMA (ISTerre, France) using precise olivine protocol [4]. Coexisting olivine-liquid compositions calculated using Petrolog 3 software [5] and equations [6, 7 & 8] acknowledged as the most precise models for basaltic magmas [3]. Used models form uniform trend of T_{calc} at lower temperatures (T<1400^o C) and growing difference with the experiment temperature ascent (up to 70^o C at 1550^o C). In-situ temperatures measured with the thermocouple generate average values between chosen models (fig. 1).

Reported data shows that new updated quantitative model of olivine-liquid equilibria should be developed for high-temperature ultramafic melts and that such a study could be done on the base of presented furnace at Vernadsky Institute.

Research made with support of the RSF grant 14-17-00491

Table 1. Natural starting compositions (bulk-rock; wt. %).

Sample	Rock	Locality	SiO2	TiO2	Al2O3	FeO	MgO	CaO
03-122	picrite	Iceland	44.04	0.88	7.42	11.14	29.43	6.25
SR-31	picrite	Hawaii	44.55	0.65	4.99	11.98	32.06	4.36
SR-98	picrite	Hawaii	47.88	1.43	9.00	11.36	20.86	7.13
Pu06-52/4b	pyroxenite	Voykar, Polar Urals	56.65	0.03	1.01	6.75	33.47	1.32
Pu214-6	pyroxenite	Voykar, Polar Urals	56.12	0.04	1.65	5.96	33.19	1.83
SDK-14	picrite	Siberian traps	46.86	1.96	8.31	14.28	18.36	7.90
594	picrite	M-K province	41.08	3.52	3.53	15.09	24.75	9.40
1986-11	meimechite	M-K province	41.39	2.27	3.05	12.64	32.17	6.28
Z6	komatiite	Canada	49.88	0.25	5.59	8.88	30.35	4.93
08-384	picrite	Iceland	45.80	0.33	10.25	9.07	24.27	9.03
08-373	picrite	Iceland	46.65	0.40	12.21	8.42	19.54	11.40

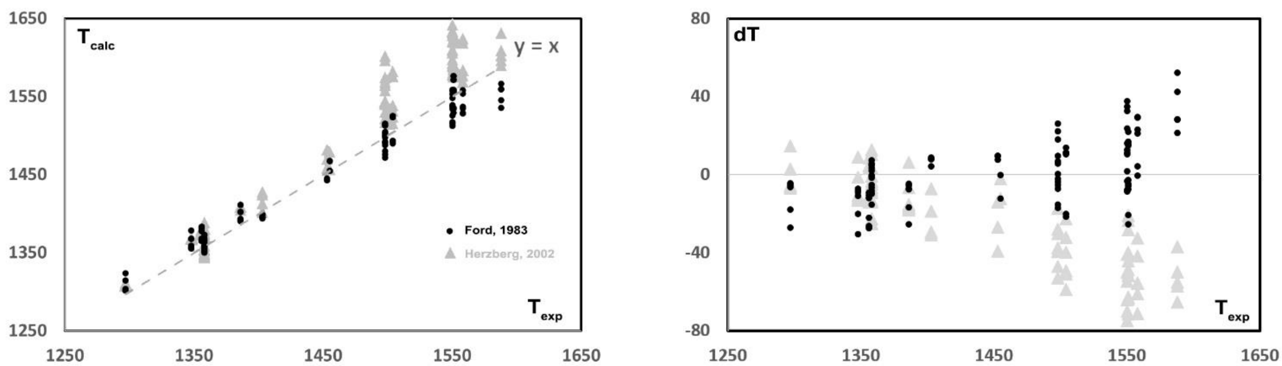

Figure 1. Left – T_{exp} - T_{calc} dependence for equations from [6] black dots and [7] grey triangles, dashed line for 1:1 ratio. Right – increasing difference between T_{Ford} & T_{exp} (black dots) and T_{Ford} & T_{Herz} (grey triangles) with growth of T_{exp}.

References:

1. Sobolev A.V., and Nikogosian I.K. (1994). Petrology of long-lived mantle plume magmatism: Hawaii, Pacific and Reunion Island, Indian Ocean. Petrology, **2**, 111-144.
2. Herzberg, C. (2011), Basalts as temperature probes of Earth's mantle, Geology, 39(12), 1179-1180, doi:10.1130/focus122011.1.

3. Fallon T. J., Danyushevsky L.V., Ariskin A. A., Green D. H., Ford C. E. // Chem. Geol., 2007, V. 241, p. 207-233
4. Batanova, V. G., Sobolev, A. V. & Kuzmin, D. V. // Chem. Geol., 2015, V. 419, p. 149–157.
5. Danyushevsky L.V., Plechov P. // Geochem. Geophys. Geosyst., 2011, V. 12(7), doi: 10.1029/2011GC003516
6. Ford C. E., Russell D. G., Groven J. A., Fisk M. R. // J. Petrol.,1983, V. 24, p. 256–265
7. Herzberg, C., and M. J. O'Hara // J. Petrol., 2002, V. 43, p. 1857–1883, doi:10.1093/petrology/43.10.1857.
8. Beattie, P. // Contrib. Mineral. Petrol., 1993, V. 115, p. 103–111, doi:10.1007/BF00712982

The association of platinum group minerals in Prizhimny Creek Placer (Kamachatka, Russia)

Kutyrev A.V.[1], Sidorov E.G.[2], Antonov A.V.[3], Stepanov S. Yu.[4]
1 – National University of Mineral Resources, kutyrev.geologist@gmail.com
2 – Institute of Volcanology and Seismology, mineral@kscnet.ru
3 – All the Russian state Geological Institute, avlan.online@gmail.com

In last years the great work of studying the concentrically zoned clinopyroxenite-dunite massifs of the Uralian or Ural-Alaskan type, widely distributed in Koryak-Kamchatka region (approximately 30-40 massif). The Tamanvayam group of massifs in one if the latest not very well studied objects of current type in that region. The reason of relatively low interest payed to this massif by the researchers is its low erosion level, which does not allow us to expect the profitable placer deposits associated with it. In the modern erosion outcrop, only gabbro and different clynopyroxenites can be seen, while dunite (the main source for PGM in most Uralian-Alaskan type massifs (Betekhtin, 1935)) was still not found. This makes even the assignment of these massifs to the Ural-Alaskian type not 100% reliable. Therefore, studying of PGM can lift the veil on the origin of Tamanvayam group massifs and the geology of adjacent territory.

Prizhimny Creek drains the satellite massif of Tamanvayam group, situated at Tamanvayam river basin. Small gold placer, located at the alluvium of the Creek was developed at 1999-2003; by the end of mining operations, 850 kg of gold and 50 kg of PGE was obtained. Most of the PGM grains are small-sized (0,1 – 0,2 mm), in this work we used partly the ordinary material, partly – the largest grains we have obtained (2-4 mm).

All of about 25 five PGE-grains, studied by electrone microprobe, are represented by Pt-Fe-Cu alloys (Fig.1), containing inclusions of native osmium, chromite, Cr-rich magnetite, several unnamed phases – sulfides of Pt, Ir and Ru (Fig. 2). Al Pt-Fe-Cu alloys refer to Ir-free native platinum (isoferroplatinum was not met at all). Both these features are typical for the platinum mineralization in clinopyroxenits and olivine clynopyroxenites.

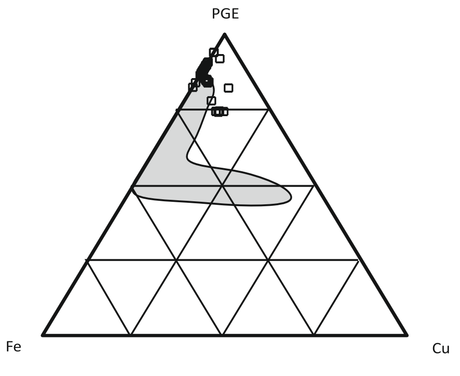

Fig. 1 Composition of PGE alloys from placer of the Prizhimny River in terms of the Fe – Pt – Cu diagram. Gray area – composition of Fe-Pt-Cu alloys of Galmoenan massif (Vildanova et al., 2002)

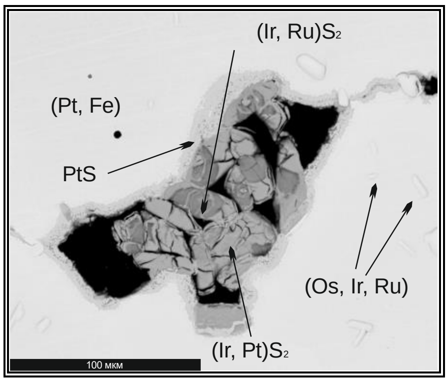

Fig. 2 BSE-image of unnamed sulfide phases inclusions in platinum. The plate-shaped crystals of native osmium with slight impurity of Ir and Ru can be seen

Cr-rich magnetite is typical for olivine-clinopyroxenite and wherlite (Kepezhinskas et al., 1993). We have also found it at olivine clinopyroxenite from Machevna massif – one of the Tamanvayam group. The presence of both chromite and Cr-rich magnetite also shows us, that the source of PGM may be heterogenic – minerals could be extracted partly from olivine clinopyroxenite body and partly – from completely eroded body of dunite of the same massif.

In Kamchatka, the closest to the Prizhimny PGM assotiation was described for Pustaya river, that is also considered to have the outer parts of concentric-zoned massifs (consisting of clinopyroxenite and wherlite) as the source of PGM (Tolstykh et al., 2000). Most feauters – Pt-Fe-Cu alloys composition, inclusions of osmium, absence of Ir impurities in platinum are typical for both placers. The only serious difference is full absence of Pd impurity in platinum of Prizhimny Creek placer.

Summarizing all fact, we can conclude, that the source of PGM in Prizhimny Creek placer was the mineralization in the outer parts of concentric-zoned massifs of Ural-Alaskian type; PGM may origin partly from clinopyroxenite and partly from dunite.

References:

1. Betekhtin, A.G. (1935): Platinum and other Minerals of PGE Group. Akad. Nauk SSSR, Moscow, Russia (in Russ).
2. Vildanova E.Yu. et al. (2002): Koryak-Kamchatka region – new platinum province of Russia. VSEGEI, Saint-Petersburg, Russia (in Russ)
3. Kepezhinskas P.K., Taylor R.N., Tanaka H. (1993): Geochemistry of plutonic spinels from the North Kamchatka Arc: comparisons with spinels from other tectonic settings. Mineralogical Magazine. 57. 575-589.
4. Tolstykh N. D., Sidorov E.G. et al. (2000): The association of platinum-group minerals of the Pustaya River, Kamchatka, Russia. Can. Mineral. 38, 1251-1264.

Thermodynamic modelling of metamorphic processes: Pseudosection approach

López-Carmona A.[1, 2], Gutiérrez-Alonso G.[1, 2], Tishin P.[2]; Gertner I. F.[2]

1 - University of Salamanca (Spain), alioli@usal.es; gabi@usal.es

2 - Tomsk State University, labspm@ggf.tsu.ru

Understanding global-scale orogenic processes related to supercontinents, and their relationship to the secular evolution of the Earth's lithosphere, represent important challenges for Earth scientists today. The record of these processes is preserved in the microstructures, mineral assemblages and mineral compositions of lithospheric rocks exhumed to the Earth's surface. Given a well-characterized microstructural evolution, thermodynamic modelling is the key to quantifying changes in Pressure–Temperature (*P*–*T*), with the rate of these changes being provided by rock-forming and accessory mineral-based geochronology. Thus, metamorphic rocks provide Pressure–Temperature–time–deformation (*P*–*T*–*t*–*d*) data to parameterize orogenic processes.

Equilibrium thermodynamics provides the formal mathematical framework that links measurable variables (whole-rock or domainal compositions, mineral and fluid/melt inclusion compositions) with intensive variables (pressure, temperature and chemical potentials). This approach includes the field of thermobarometry (e.g. Powell & Holland, 2008). Thermobarometry has evolved significantly in the last twenty five years with the development of internally consistent thermodynamic datasets and sophisticated thermodynamic mixing models for phases of interest. These advances have enabled the calculation of equilibrium phase diagrams for complex chemical systems, close to those in nature, for a variety of variables. Such diagrams are called pseudosections for the reasons given by Powell *et al*. (1998; 2005). Critically, inverse modelling using pseudosections allows us to use all available compositional information, both for the system and the individual minerals; this is not the case for conventional thermobarometry, where the chemical system is largely ignored. This development represents one of the most important advances of modern metamorphic petrology. The numerical modelling of phase relations requires a set of thermodynamic data for end-members, a description of the activity−composition ($a-x$) relations (the solid- or liquid-solution models) and software to perform calculations.

In addition to forward modelling of metamorphic processes in general, the ability to model phase equilibria in chemical systems that are close to nature in their complexity, has allowed us to calculate $P-T$ pseudosections for each critical sample in a regional study, and when used in conjunction with microstructural information, has enabled the routine construction of $P-T$ paths. The utility of these phase diagrams lies in the fact that they permit natural observations and interpretations from thin sections to be explained in terms of the evolving *P*–*T* conditions within the context of a structural evolution and from place to place. When combined with petrologically-linked age data (e.g. petrochronology; Kohn, 2016), the resulting *P*–*T*–*t*–*d* paths provide essential input into constraining the processes involved in mountain-building and the evolution of continental lithosphere (e.g. Brown, 2014).

Despite these advances, there remain considerable uncertainties in both, the thermodynamic framework used (end-member thermodynamics and $a-x$ models) and more importantly, in estimating the volume of equilibration and changes in rock composition during metamorphism. These factors require the approach to be used with care. Thus, the results of any calculations are best viewed as an independent theoretical framework in which to interpret a rock rather than an exact reproduction of its evolution (White *et al*., 2014).

In this abstract we have justified the use of $P-T$ pseudosections in regional studies; in the presentation, we will illustrate the application of the pseudosection approach using as an example blueschist-facies rocks from the north Gondwana margin (NW Iberian Massif; Figure 1).

Thermodynamic modelling of petrological systems is merely a tool, but because the pseudosection approach uses the maximum amount of available information, it is extremely useful. Nowadays is an essential tool in the parameterization of metamorphic histories, and in the last decade it has involved an outstanding advance in quantifying orogenic processes.

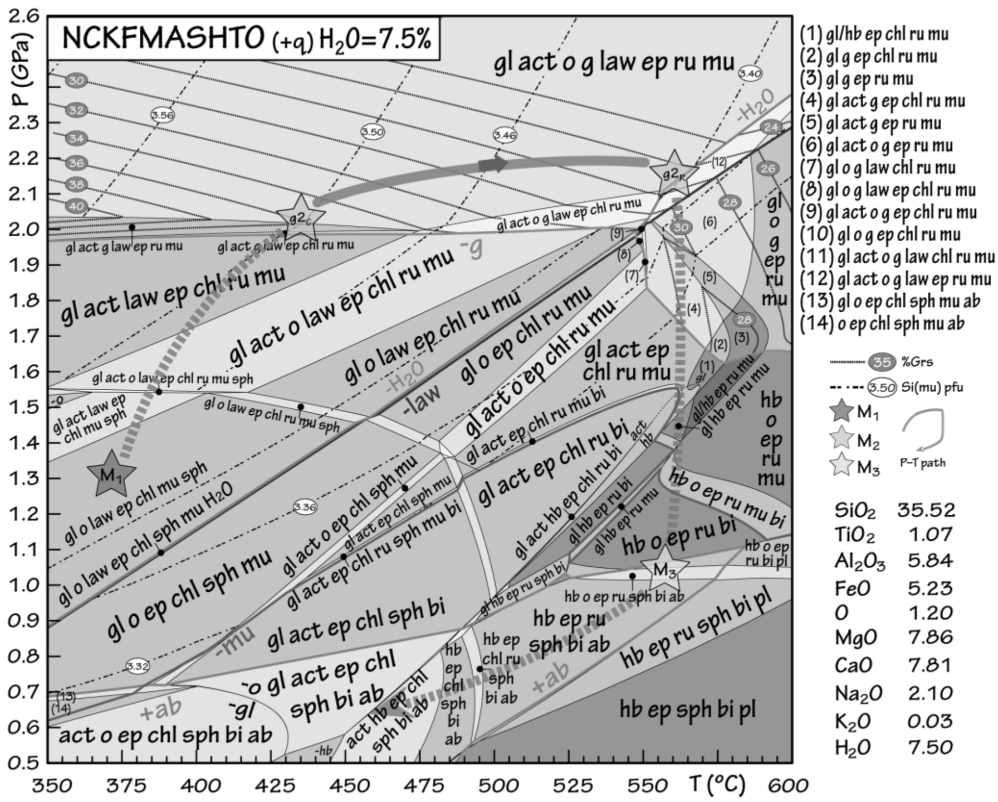

Fig. 1 P–T pseudosection calculated for retrogressed lawsonite blueschists from the NW Iberian Massif (Spain). Dashed blue lines represent the proposed P–T path. The P–T diagram was calculated using THERMOCALC 3.37 and the internally consistent thermodynamic dataset from Holland & Powell (1998; updated Nov. 2003) in the chemical system Na_2O-CaO-K_2O-FeO-MgO-Al_2O_3-SiO_2-H_2O-TiO_2-Fe_2O_3 (NCKFMASHTO). Bulk-rock composition is expressed in mol. %.

References:

1. Brown, M. (2014): The contribution of metamorphic petrology to understanding lithosphere evolution and geodynamics. Geoscience Frontiers 5, 553–569
2. Kohn, M. (2016): Metamorphic chronology−a tool for all ages: past achievements and future prospects. American Mineralogist 101, 25−42
3. López-Carmona, A., Abati, J., Pitra, P. & Lee, J.K.W. (2014): Retrogressed lawsonite blueschists from the NW Iberian Massif: P–T–t constraints from thermodynamic modelling and $^{40}Ar/^{39}Ar$ geochronology. Contributions to Mineralogy and Petrology 167(3), 1–20
4. Powell, R. & Holland, T.J.B. (2008): On thermobarometry. Journal of Metamorphic Geology 26, 155–179
5. Powell, R., Guiraud, M. & White, R.W. (2005): Truth and beauty in metamorphic mineral equilibria: conjugate variables and phase diagrams. Canadian Mineralogist 43, 21−33
6. Powell, R., Holland, T.J.B. & Worley, B. (1998): Calculating phase diagrams involving solid solutions via non-linear equations, with examples using THERMOCALC. Journal of Metamorphic Geology 16, 577–588
7. White, R.W., Powell, R. & Johnson, T.E. (2014): The effect of Mn on mineral stability in metapelites revisited: new a–x relations for manganese-bearing minerals. Journal of Metamorphic Geology 32, 809–828

Chemical composition of major products of dolerite laterization, Republic of Guinea

Makarova M. A.[1], Korrea Gomesh G.[2], and Shipilova E. S.[1]
1 – Lomonosov Moscow State University, frolikovam@gmail.com, 2 – RUDN University

There are large bauxite-bearing districts Boke, Kogon-Tomine, and Fatala in the Futa Jallon-Mandingo Province, the northwest of Guinea.

These bauxites have considerably originated from lateritic weathering of dolerites and konga-diabases of the Mesozoic trap association. The generalized bauxite-bearing profile of weathering on these rocks includes the following units (upwards from above the protolith): the clay horizon (in this paper, without division to polymineralic and kaolinitic clays), the ferruginous lateritic horizon (the transition zone) with almost ubiquitous inclusions of extra-ferruginous plates called ferriplantites, and the bauxite horizon somewhere covered by cuirass unconsidered in this paper.

Abundances of trace elements have been first studied for the districts, in addition to major petrogenic elements. They were determined by ICP-MS, with a devise ELEMENT-2, at the Geological Department of MSU. Samples were prepared by the acid decomposition. The assay results are summarized in Table, shown as relative (ppm and %) and absolute (g/m^3 and kg/m^3, with consideration of volume weight) values.

With no attention to reasons and mechanisms for variation of element concentrations in the lateritic profile horizons (zones), let us note some of evident regularities.

When comparing apodoleritic bauxites to their protolith there are three groups of trace elements distinguishable, namely the following: (1) accumulative elements (Ga, Zr, Nb, Cd, Sn, Sb, Hf, Ta, W, Pb, Bi, and Th) and elements tending to accumulation (V, Cr, Ag, and La), (2) leaching elements (Be, Sc, Co, Ni, Cu, Rb, Sr, Mo, Cs, Ba, Eu, Dy, Ho, and Tl) and elements tending to removal, and (3) the other elements without any distinct variability of concentration. Substantial Al_2O_3 and Fe_2O_3 accumulation in the bauxites and almost complete SiO_2, RO, and RO_2 removal represent the general background of mentioned tendencies.

Zoning of the lateritic weathering profile has originated from the infiltration metasomatism. Therefore, products of each subjacent horizon should be considered as initial for each overlaying horizon.

When compared to the protolith, the clay mostly shows removal of elements or their concentrations keep stable, except for Th, W, Sn, Tl and Pb.

Formation of the ferruginous laterite horizon after the clay is characterized both by an intense absolute accumulation of iron and by an accumulation of V, Cr, Ge, Mo, Nb, Zr, Sb, Hf, Bi, Th, and U. The other elements keep almost stable concentrations or they are leached out. The iron accumulation in this zone is explained by an oxidizing geochemical barrier. The maximum absolute iron accumulation (almost three times, in comparison with the clay) occurs in the ferriplantite formation as a special situation of the transition zone. Accordingly the group of accumulative elements of the ferriplantites is supplemented by Li, Be, Sc, Ni, Cu, Zn, Sr, Cd, REE, Ta, Tl, Pb.

When compared to the subjacent ferruginous laterites, the bauxite horizon (the next zone of the infiltration-metasomatic column) shows the accumulation of Li, Ni, Zn, Ga, Sr, Zr, Nb, Cd, Sn, Cs, Ba, REE, Hf, Ta, and Bi. Hence, when compared to the protolith, the group of accumulative elements is increased by the additional 18 elements.

Thus, changing of physical and chemical conditions in the weathering profile and redistribution of great amounts of petrogenic components is accompanied by the redistribution (often bidirectional) of trace elements.

	Relative values						Absolute values				
	Protolith	*Clay*	*Laterite of transition zone*	*Ferriplantite*	*Bauxite*		*Protolith*	*Clay*	*Laterite of transition zone*	*Ferriplantite*	*Bauxite*
Number of samples	4	12	18	3	40	**Number of samples**	4	12	18	3	40
SiO_2, %	49,77	34,00	5,44	5,60	0,91	SiO_2, kg/m^3	1344	600	103	151	18
Al_2O_3, %	16,01	27,56	33,78	18,77	50,45	Al_2O_3, kg/m^3	432	486	642	507	1009
TiO_2, %	1,21	1,79	2,12	1,35	3,00	TiO_2, kg/m^3	33	32	40	36	60
Fe_2O_3, %	10,86	20,24	38,01	57,32	18,41	Fe_2O_3, kg/m^3	293	357	722	1548	368
FeO, %	7,72	0,45	0,34	0,15	0,20	FeO, kg/m^3	208,4	8,0	6,5	4,0	4,0
CaO, %	9,41	0,21	0,05	0,14	0,05	CaO, kg/m^3	254,1	3,7	1,0	3,9	1,0
MgO, %	5,84	0,41	0,07	0,10	0,06	MgO, kg/m^3	157,7	7,2	1,3	2,7	1,3
MnO, %	0,14	0,12	0,04	0,02	0,03	MnO, kg/m^3	3,8	2,1	0,8	0,5	0,6
K_2O, %	0,71	1,05	0,22	0,31	0,01	K_2O, kg/m^3	19,2	18,5	4,2	8,3	0,2
Na_2O, %	1,78	0,09	0,03	0,06	0,02	Na_2O, kg/m^3	48,1	1,6	0,6	1,7	0,3
P_2O_5, %	0,17	0,18	0,19	0,48	0,12	P_2O_5, kg/m^3	4,5	3,1	3,6	12,8	2,5
Li, ppm	7,95	7,23	2,87	9,67	5,98	Li, g/m^3	21,5	12,8	5,5	26,1	12,0
Be, ppm	0,76	0,98	0,68	1,88	0,41	Be, g/m^3	2,1	1,7	1,3	5,1	0,8
Sc, ppm	38,9	42,0	46,3	37,5	16,1	Sc, g/m^3	105	74	88	101	32
V, ppm	278	386	738	244	501	V, g/m^3	752	682	1403	658	1001
Cr, ppm	262	241	541	409	403	Cr, g/m^3	709	425	1027	1105	806
Co, ppm	33,0	36,0	26,7	23,8	7,54	Co, g/m^3	89,0	63,5	50,7	64,3	15,1
Ni, ppm	61,6	33,0	4,82	207,0	15,9	Ni, g/m^3	166	58,3	9,2	559	31,8
Cu, ppm	106	87,9	62,2	86,9	37,0	Cu, g/m^3	286	155	118	235	74,0
Zn, ppm	90,9	61,5	54,9	234	150	Zn, g/m^3	245	108	104	631	299
Ga, ppm	19,7	40,5	42,8	21,5	54,3	Ga, g/m^3	53,2	71,5	81,3	58,0	109
Ge, ppm	16,4	15,7	54,9	43,2	20,2	Ge, g/m^3	44,3	27,7	104	117	40,4
Rb, ppm	20,4	40,1	9,39	1,65	7,62	Rb, g/m^3	55,1	70,8	17,8	4,4	15,2
Sr, ppm	142	20,2	14,6	78,9	34,9	Sr, g/m^3	382	35,7	27,6	213	69,7
Zr, ppm	117	153	198	47,1	294	Zr, g/m^3	316	271	377	127	588
Nb, ppm	10,7	21,2	23,9	16,5	42,6	Nb, g/m^3	29,0	37,5	45,5	44,6	85,1
Mo, ppm	5,33	1,48	3,22	1,74	2,43	Mo, g/m^3	14,4	2,61	6,12	4,69	4,86
Ag, ppm	0,95	1,64	1,42	1,24	1,86	Ag, g/m^3	2,6	2,9	2,7	3,3	3,7
Cd, ppm	0,11	0,22	0,24	4,23	0,84	Cd, g/m^3	0,31	0,39	0,46	11,4	1,7
Sn, ppm	1,41	4,75	2,74	2,74	4,26	Sn, g/m^3	3,8	8,4	5,2	7,4	8,5
Sb, ppm	0,26	0,48	1,39	0,98	0,98	Sb, g/m^3	0,69	0,84	2,6	2,6	2,0
Cs, ppm	0,94	1,16	0,42	0,43	0,59	Cs, g/m^3	2,53	2,05	0,80	1,17	1,17
Ba, ppm	160	315	47,0	57,7	102	Ba, g/m^3	431	555	89,3	156	204
Y, ppm	18,2	9,17	7,05	63,4	12,8	Y, g/m^3	49,3	16,2	13,4	171	25,5
La, ppm	11,0	16,3	9,39	46,4	23,0	La, g/m^3	29,6	28,7	17,8	125	46,1
Ce, ppm	35,3	58,1	44,3	59,4	49,4	Ce, g/m^3	95,3	103	84,1	160	98,9
Pr, ppm	3,03	3,65	2,15	8,94	4,51	Pr, g/m^3	8,2	6,4	4,1	24,1	9,0
Nd, ppm	13,1	13,7	7,36	36,3	15,7	Nd, g/m^3	35,3	24,2	14,0	98,0	31,3
Sm, ppm	3,20	2,88	1,63	7,50	2,80	Sm, g/m^3	8,6	5,1	3,1	20,2	5,6
Eu, ppm	1,00	0,68	0,45	2,00	0,60	Eu, g/m^3	2,7	1,2	0,9	5,4	1,2
Gd, ppm	3,65	2,84	1,95	8,54	3,55	Gd, g/m^3	9,9	5,0	3,7	23,1	7,1
Tb, ppm	0,60	0,39	0,28	1,47	0,43	Tb, g/m^3	1,6	0,7	0,5	4,0	0,9
Dy, ppm	3,56	2,13	1,65	8,84	2,22	Dy, g/m^3	9,6	3,8	3,1	23,9	4,4
Ho, ppm	0,72	0,41	0,34	1,86	0,45	Ho, g/m^3	1,9	0,7	0,6	5,0	0,9
Er, ppm	2,11	1,32	1,06	5,44	1,48	Er, g/m^3	5,7	2,3	2,0	14,7	3,0
Tm, ppm	0,28	0,22	0,17	0,73	0,21	Tm, g/m^3	0,8	0,4	0,3	2,0	0,4
Yb, ppm	1,94	1,57	1,24	4,78	1,58	Yb, g/m^3	5,2	2,8	2,3	12,9	3,2
Lu, ppm	0,28	0,22	0,19	0,69	0,21	Lu, g/m^3	0,8	0,4	0,4	1,9	0,4
Hf, ppm	3,64	5,38	6,51	4,20	8,86	Hf, g/m^3	9,8	9,5	12,4	11,3	17,7
Ta, ppm	1,12	2,08	1,93	2,10	12,7	Ta, g/m^3	3,0	3,7	3,7	5,7	25,4
W, ppm	0,83	4,26	2,73	1,10	2,17	W, g/m^3	2,2	7,5	5,2	3,0	4,3
Tl, ppm	0,12	0,28	0,11	0,33	0,07	Tl, g/m^3	0,3	0,5	0,2	0,9	0,1
Pb, ppm	6,98	17,0	13,9	16,5	15,4	Pb, g/m^3	18,8	29,9	26,5	44,4	30,8
Bi, ppm	0,12	0,24	0,30	0,32	0,43	Bi, g/m^3	0,3	0,4	0,6	0,9	0,9
Th, ppm	4,30	14,2	19,8	9,02	23,1	Th, g/m^3	11,6	25,1	37,7	24,4	46,3
U, ppm	2,14	2,13	3,26	2,29	2,74	U, g/m^3	5,8	3,8	6,2	6,2	5,5

Two stages of Archaean eclogite-facies metamorphism in the Belomorian mobile belt, Fennoscandian Shield, Gridino structure

Maksimov O. A.[1], Volodichev O. I.[1]
1 - IG KRS RAS, olemaximov@mail.ru

There are two age and genetic generations of eclogites, Archaean and Palaeoproterozoic, in the Gridino structure of the Belomorian mobile belt, Fennoscandian Shield [1, 2]. The metamorphic evolution of Archaean 2720.7±5.8 Ma eclogites [3] consisted of a prograde stage (T = 740–865 °C, P = 14–17.5 кбар) and a retrograde stage (T = 780–630 °C, P = 14.5–6.5 Kbar), which is consistent with their subduction and exhumation stages [1, 2]. However, signs of two-stage eclogite-facies metamorphism have been identified lately in eclogites from some localities [4]. Until now, two-stage eclogite-facies metamorphic events have only been described from the Phanerozoic complex of the Swiss Alps [5]

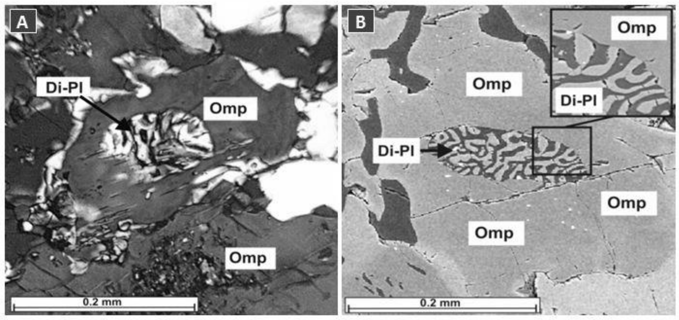

Fig.1. Di-Pl symplectite inclusions in single crystals Omp.
(A) - Nicole crossed. (B) - BSE image.

A new eclogite locality has been revealed on the Samylino Lake shore, north of Gridino Town, where eclogites occur as lenticular fragments in a granitoid matrix. They are comparable in geologo-petrological characteristics to Archaean eclogites [1]. Omphacite is one of rock-forming minerals. Omphacite grains (jadeite content 30-35%) are common in the matrix and in the inclusions in the intermediate zone of garnet (jadeite content >35%). Coarse omphacite crystals are commonly rimmed Di-Pl (±Amph) by symplectite (Jd=6-18%) and amphibole.

Two-stage eclogite-facies metamorphism is usually indicated by:

1. Diopside-plagioclase symplectite inclusions in omphacite monocrystals (Fig. 1A). Symplectites in inclusions display a dactylitic non-zonal structure with sharp cross-cutting contacts at their boundary with omphacite (Fig. 1B). Diopside contains 6-14% jadeite, and plagioclase carries 20-30% anorthite. These ratios suggest that omphacite monocrystals formed later.

2. Variations in the composition of garnet in zonal crystals are associated with the mineral composition of the inclusions (Fig.2 A, B). Garnet crystals in the central portion occasionally contain polymineral symplectite inclusions Cpx-Pl(±Amph). At other localities inclusions contain both Di-Pl symplectites and omphacite with up to 50% jadeite [4]. Omphacite inclusions are widespread in the intermediate zone of garnet. The external zone of garnet grains, affected by retrograde metamorphism, is rimmed by amphibole, plagioclase and quartz. The central portion of garnet typically contains 20-25% pyrope, 52-58% almandine and 20-22% grossular. The zone with omphacite inclusions contains 27-30% pyrope and 48-52% almandine. The grossular content of the central portion of garnet is within the error limit (19-23%). In the margin of garnet pyrope concentration declines markedly to 22-24%, almandine concentration increases to 52-56% and grossular concentration rises to 22%. Such a succession of mineral inclusions and chemical composition for the garnets in Gridino eclogites has been revealed for the first time.

Metamorphic pressures and temperatures in the zones delineated were estimated [6]. The Cpx-Pl-Amph of symplectites from the central portion of garnet were formed at T = 700–760 °C and P = 12.4–14.6 Kbar. Omphacite inclusions in the intermediate zone of garnet were formed at T = 710–820 °C and P = 14–16 Kbar, which is consistent with the peak values of eclogite-facies metamorphism. The subsequent stage in the alteration of eclogites in the marginal zone is associated with a decline in temperature to 650-730 °C and pressure to 10.3-12.7 Kbar – the period of formation of clinopyroxene-plagioclase symplectites and amphibole.

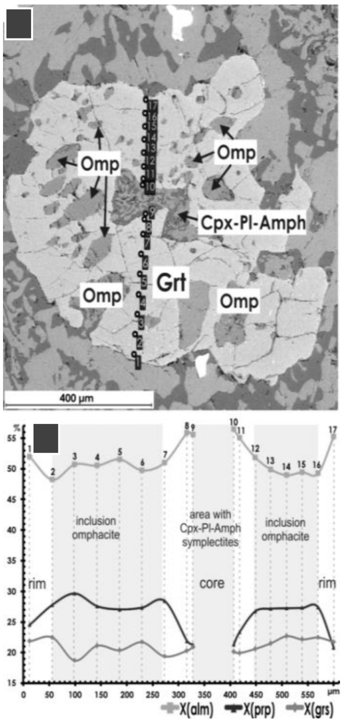

Fig.2 (A) - Changing the composition of the mineral inclusions from the center to the rim in a crystal garnet: Cpx-Pl-Amph → Omp. BSE image. (B) - Diagram of changing the modal composition of the garnet on the profile of 1-17.

Scarce omphacite (Jd=50%) relics in the central portion of garnet were probably formed at the first stage of eclogitization. The presence of Di-Pl symplectites in the central portions of garnet and coarse omphacite monocrystals from the matrix is associated with the decompression period of "early" eclogites. Omphacite grains in the intermediate zone of garnet and monocrystals in the rock matrix mark a second stage in eclogitization. The formation of Di-Pl(±Amph) symplectites at the boundary of coarse omphacite crystals in the matrix is associated with a second stage in the retrograde metamorphism of eclogites. The minerals succeeded each other in the following order: Omp I→Di-Pl I→Omp II→ Di-Pl II.

The study was supported by RFBR grant 15-05-09288

References:

1. Volodichev O.I., Slabunov A.I. Superposition of two age and genetic groups of eclogites in the Gridino area, Belomorian province of the Fennoscandian Shield // Granulite and eclogite complexes in the Earth's history. Proceedings of the international conference and a field guide, Petrozavodsk, p. 46–48, 2011.
2. Volodichev O.I., Kuzenko T.I. Prograde and retrograde trends in the metamorphic evolution of Archaean eclogites and their geodynamic interpretation (Gridno area, Karelia) // RMO Notes, No. 3, p. 28–51, 2013.
3. Volodichev O.I., Slabunov A.I., Bibikova E.V., Konilov A.N., Kuzenko T.I. Archaean eclogites of the Belomorian mobile belt, Baltic Shield // Petrologia. 2004. V. 12. No. 6. P. 609□-631.
4. Volodichev O.I., Maksimov O.A., Slabunov A.I., Kuzenko T.I. Petrological and geochronological indicators of Archaean two-stage (?) eclogite-facies metamorphism in the Belomorian mobile belt, Fennoscandian Shield, Gridino structure // Petrography of igneous and metamorphic rocks. Proceedings of the 12th All-Russian Petrographic Meeting. Petrozavodsk: KarRC, RAS. 2015. P. 394-397
5. Herwartz, D., Nagel, T.J., Munker, C., Scherer, E.E. & Froitzheim, N. Tracing two orogenic cycles in one eclogite sample by Lu-Hf garnet chronometry // Nature Geoscience. 2011. 4. 178-183.
6. Berman, R.G. Thermobarometry using multi-equilibrium calculations: a new technique, with petrological applications; in, Quantitative methods in petrology: an issue in honor of Hugh J. Greenwood; Eds. Gordon, T M; Martin, R F. Canadian Mineralogist 1991.v. 29, 833-855.

Mechanism and kinetics of $CaCO_3$ and $MgCO_3$ interaction with metallic iron: implications for carbonatesubduction into the deep mantle

Martirosyan N.S.[1,2], Yoshino T.[3], Shatskiy A.[1,2], Chanyshev A.D.[1,2], Litasov K.D.[1,2]

[1]V.S. Sobolev Institute of Geology and Mineralogy SB RAS, Novosibirsk, Russia

2Novosibirsk State University, Pirogova st., 2, Novosibirsk 630090, Russia

3Institute for Study of the Earth's Interior, Okayama University, Misasa, Tottori 682-0193, Japan

martirosyanns@gmail.com

Stability of carbonates during subduction is an important issue for the global geodynamic processes, diamond formation and the carbon cycle. The deeper part of the mantle can be too reduced to favor stable carbonates. The details of carbonate reduction processes and their interaction with surrounding mantle are still poorly constrained. The complexity of this system impedes particular reconstruction of redox reaction, so composite systems should be studied.

One of the principal redox exchange reactions at the slab-mantle interface during subduction is carbonate–Fe^0 interaction. Using uniaxial press multianvil apparatus, we have studied interaction of $MgCO_3$ and $CaCO_3$ with Fe^0 at 650–1400 °C and 4–16 GPa. To determine water influence on the reaction, additional experiments were conducted in the $MgCO_3$–Fe–H_2O and peridotite-$MgCO_3$–Fe–H_2O systems.

Following redox reactions have been established:

$3CaCO_3$ (aragonite) + $13Fe^0$ = $3CaFe_2O_3$ (Ca-wüstite) + Fe_7C_3 (1)

$MgCO_3$ (magnesite) + $5Fe^0$ = MgO (wüstite) + 2FeO (wüstite) + Fe_3C (2).

Diffusion of components was suggested to be the major rate – limiting process with the reaction rate constant (k) being log-linear in 1/T (Fig 1, 2). Temperature dependence of k for Ca-carbonate – iron interaction were fit to Arrhenius equations, which can be written as: be k [m^2/s] = $2.8\times10^{-5}\exp(-211/RT)$ at 4-6 GPa and k [m^2/s] =$2.1\times10^{-11}\exp(-56/RT)$ at 16 GPa. Reaction rate constant for magnesite – iron reaction is higher than that for the $CaCO_3$-Fe, and can be presented by following equations: k [m^2/s] =$3.55^x10^{-5x}\exp(-(194)/RT)$ at 6.5 GPa.

Calculations of kinetic parameters clearly detected, that the rate of product formation in the magnesite – iron – water system increases by two orders of magnitude in comparison with the magnesite – iron system. Temperature dependence of k can be written as: k [m^2/s] =$4.8^x10^{-7x}\exp(-107/RT)$ at 4-6 GPa and k [m^2/s] =$3^x10^{-2x}\exp(-259)/RT)$ at 16 GPa. However, in water containing peridotite, reaction rate constant of magnesite reduction was computed to be 10^{-13} m^2/sec at 1100°C and 6 GPa, that is two order of magnitude lower than in the simplified magnesite-iron system.

The experimental results allow to calculate the length scale over which the reaction kinetics between carbonates and metallic iron is likely effective. Using relatively simple relationship between the characteristic distance of diffusion as a function of k and duration of the process, we estimate the length scale of the reaction for time scales 4-16 Myr, which corresponds to subduction rates of 2-8 cm/year from 250 km (metal-saturation boundary) to 470 km, for different slab PT-profiles. Assuming that carbonates are in a direct contact with iron and there is no water in the system, the maximum degree of carbonate reduction can be evaluated using the results of our study and the data on CO_2 distribution in altered oceanic basalts. The estimates suggest that up to 0.5, 12, and 20 vol. % of carbonates can be reduced in such case during subduction down to the mantle transition zone at the conditions of cold, medium and hot geotherms, respectively.

In the other hand, water-containing systems, examined in our investigation reflects that despite the fact that water acts as a transporting agent for the reactants, the reduction of carbonates will increasingly depends on the rate of diffusion in the silicates that is extremely small. The sluggish kinetics of $MgCO_3$-metallic iron interaction in the water-containing peridotites, established in our study suggests that more than 60 % of carbonates could survive during subduction from metal saturation boundary near 250 km depth down to the transition zone and presumably to the lower mantle.

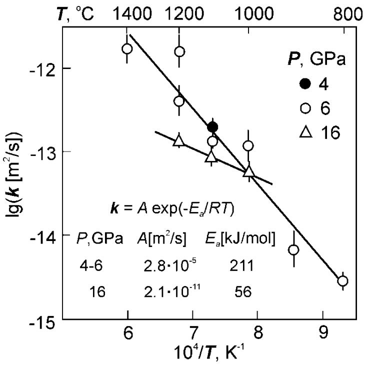

Fig. 1 Logarithm of the reaction rate constant ($k = \Delta x^2/2t$) versus reciprocal temperature 3 $CaCO_3$ (aragonite) + 13 Fe^0 (metal) = Fe_7C_3 (carbide) + 3 $CaFe_2O_3$ (Ca-wüstite). Two solid lines are linear regressions from data at 4-6 GPa and 16 GPa. The error bars show the uncertainties.

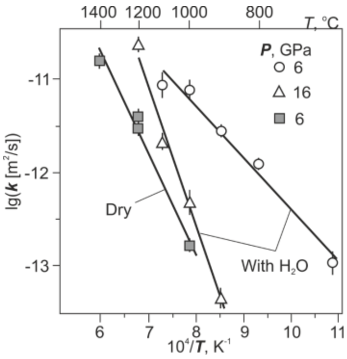

Fig. 2 Logarithm of the reaction rate constant ($k = \Delta x^2/2t$) versus reciprocal temperature for $MgCO_3$+Fe^0 interaction in H_2O- bearing system in comparison with k calculated for the reaction in "dry" conditions based on data from. Solid lines are linear regressions from data at 6 GPa and 16 GPa. The error bars show the uncertainties.

Compositional characteristics of gaussberg phenocrysts (E.Antarctica)

Migdisova N.A.[1], Sushchevskaya N.M.[1], Sobolev A.V.[2], Kuzmin D.V.[3]

1 -Vernadsky Institute for geochemistry and analytical chemistry Russian academy of Sciences, 119991, Russia, Moscow, Kosygin street, 19. +7 495 939 7017, nat-mig@yandex.ru

2 -(ISTerre) Institut des Sciences de la Terre (ISTerre) Université J. Fourier-CNRS Maison des Géosciences, Grenoble, France

3 -V.S. Sobolev Institute of Geology and Mineralogy of the Russian Academy of Sciences (IGM SB RAS)

Olivine leucitites of late Cenozoic age form the Gaussberg extinct volcanic cone on the coast of the Antarctic ice sheet within Gaussberg rift zone possibly being a part of Lambert fracture zone. Samples gathered during 2nd Soviet Antarctic Expedition (1957-1958) are mostly pillow lavas with a well defined black glassy crust. Extinct Gaussberg volcano on the West Antarctic ice sheet coast is composed by lamproiites of the late Cenozoic age (56±5 ky [Tingey et al., 1983]). The origin and evolution of these continental alkaline melts is under discussion since 80th [Foley et al., 1987; Foley, Venturelli, 1989; Mitchell, Bergman, 1991; Foley, 2008]. Gaussberg volcano is a unique object to study alkaline continental magmatism due to its subglacial eruptions and excellent preservation of rocks often containing volcanic glass. Several pulses of such eruptions are expressed by terraces building a 370 m high volcanic edifice. We present here the results of study of olivine (Ol), clinopyroxene (Cpx) and leucite (Lc) phenocrysts from Gaussberg rock samples collected during the 2nd Soviet Antarctic Expedition in 1957-1958. The samples are fragments of glassy rims of pillow lavas [Vyalov & Sobolev, 1959]. Major and trace in the mineral phases were analyzed by electron microprobe at Max-Plank Institute für Chemie (Mainz, Germany).

Mineral phenocryst assemblage of the Gaussberg lamproiites is represented by 20-40% Lc, 10% Ol, and 5% Cpx. Leucite, diopside, phlogopite and apatite microliths are present in glassy matrix. Some samples (e.g. 464 trachy-andesite) contain ortho- and clinopyroxene, magnetite, ilmenite, olivine, pyrrhotite sulfur globules and rare large rounded grains of ilmenite, apatite and zircon in glassy matrix. In this study we report the Gaussberg mineral collection [Vyalov O.S., 1959].

Two types of Cpx phenocrysts were detected in Gaussberg: (1) high TiO_2, low Al_2O_3 group and (2) low TiO_2, high Al_2O_3 group. Detailed electron probe microanalysis (ISTerre Université J. Fourier-CNRS, Grenoble, France) revealed the inverted zone character of Cpx grains – the core is enriched in FeO and depleted in Al_2O_3 while the rim is enriched in Al_2O_3 and depleted in FeO. Obviously Cpx imprinted the mix of two different melts. These melts can indicate the two stages of crystallization in Gaussberg magmatic system. Rare element distribution patterns in Gaussberg clinopyroxenes are higher in MREE and lower in heavy REE than clinopyroxenes from Queen Maud Land and Hobbs Coast provinces. Meanwhile rare element patterns for group (1) demonstrate specific character showing higher LILE values and appreciable lower $D^{Cpx/liq}$ (two orders of magnitude) for LILE than it was proposed in previous studies [Foley and Jenner, 2004]. These features can be a result of fluid impact on magmatic system.

Leucite is the most abundant phenocryst in Gaussberg lavas. Leucite fractionation is restricted in near surface magma chambers. Gaussberg leucite phenocrysts have nearly ideal stechiometry $K[AlSi_2O_6]$. Gauss leucites are enriched in Na_2O (0,1-0,28 wt%) and depleted in K_2O (20,7-20,2 wt%) and FeO (0,7-1,2 wt%) compared to the leucites from another lamproiite provinces.

Gaussberg olivine is high magnesium (up to Fo_{93}). Coefficients of olivine/liquid distribution were calculated based on new high precision data on minor elements (Li, Al, Ca, Cu, Zn, Si, Sc, Ti, V, Cr, Mn, Co, Ni, Ga, Ge, Sr, Y, Zr, Mo, Ce, Nd, Gd, Dy, Er, Yb) in olivine and corresponding quenched glasses. Determined coefficients $K_D^{Ol/Liq}$ are the larger for Ni (73) > Co (5) > Mn (1,2) > Zn (0,8) > Li (0,5) > Cu (0,02) and other non compatible lithophile elements. Gaussberg olivine has high Ni/Co ratios (20-40) implying the melting under the thickened lithosphere [Sobolev et al., 2007]. $K_D^{Ol/Liq}$ in Gaussberg lamroiites differ from those of Toro Ankle region (ugandites from the southern Bunyarunguru field and leucite basanites from the northeast of the Virunga field) [Foley et al., 2011]. Gaussberg olivines have higher K_{Ds} for Li, Mn, Ca and lower K_{Ds} for Al, Cr, Zn, Mo, Ga than mentioned above olivines from East Africa. The most promising trace elements for deciphering the early history of mafic melts are the transition elements and highly charged elements such as phosphorous, niobium, titanium and zirconium, as they better preserve zoning due to their slow but varying diffusion rates [Foley et al., 2011]. The main Gaussberg olivine phenosrysts population show common but relatively subtle zonation for such elements as Ca, Fe, Al, P meanwhile olivine phenocrysts from ugandites and leucite basanites demonstrate zonation for another elements (Mn, Sc, Ni и Cr).

Presented results make a contribution to lamproiite's database expanding the data for weakly studied (due to their rarity) leucitite rocks.

This work is supported by grant RNF 16-17-10139.

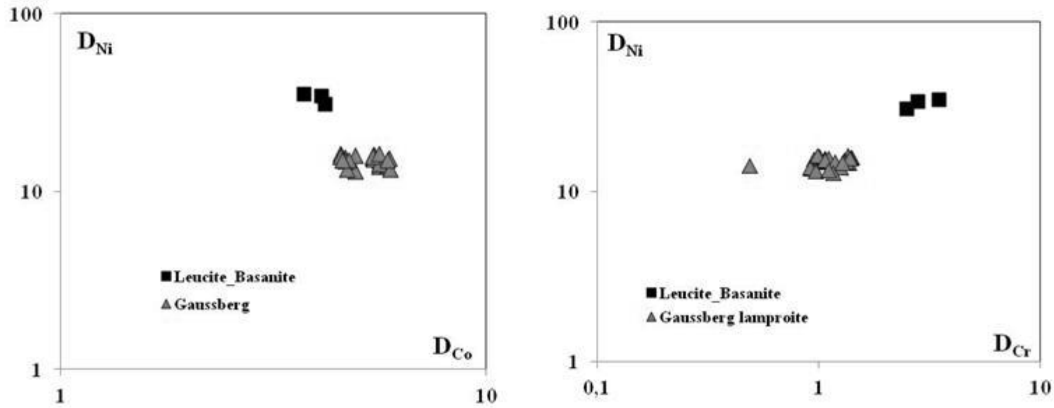

Fig. 1 Distribution coefficients in olivine phenocrysts from Gaussberg Mountain and Toro Ankle region.

References:

1. Foley S. F., Venturelli G. High K_2O rocks with high MgO, high SiO2 affinities // In Boninites and Related Rocks (ed. A. J. Crawford) Unwin Hyman. London. 1989. P. 72–88.
2. Foley S.F. Petrological characterization of the source components of potassic magmas: geochemical and experimental constraints // Lithos. 1992a. V.28. P. 187–204.
3. Foley S.F. Rejuvenation and erosion of the cratonic lithosphere // Nature Geoscience. 2008. V. 1. P. 503–510.
4. Foley S. F., Jacob D.E., O'Neill H.St.C. 2011. Trace element variations in olivine phenocrysts from Ugandan potassic rocks as clues to the chemical characteristics of parental magmas.// Contrib. Mineral. Petrol., 162, pp. 1-20.
5. Mavrogenes, J.A., O'Neill, H.S.C. 1999. The relative effects of pressure, temperature and oxygen fugacity on the solubility of sulfide in mafic magmas. Geochim. Cosmochim. Acta 63, pp.1173-1180.
6. Mitchell R.H., Bergman S.C. Petrology of Lamproites // Plenum Press, New York. 1991. 408 p.

7. Murphy D.T., Collerson K.D., Kamber B.S. 2002. Lamproites from Gaussberg, Antarctica: Possible Transition Zone Melts of Archaean Subducted Sediments. J.Petrol., 43. pp. 981-1001.
8. Sobolev, A.V., Hofmann, A.W., Kuzmin, D.V., Yaxley, G.M., Arndt, N.T., Chung, S.-L., Danyushevsky, L.V., Elliott, T., Frey, F.A., Garcia, M.O., Gurenko, A.A., Kamenetsky, V.S., Kerr, A.C., Krivolutskaya, N.A., Matvienkov, V.V., Nikogosian, I.K., Rocholl, A., Sigurdsson, I.A., Sushchevskaya, N.M., Teklay, M., 2007. Published online 28 March 2007. The amount of recycled crust in sources of mantle-derived melts. Science 316, 412–417. doi:10.1126/Science.1138113.
9. Tingey R.J., McDougall I., Gleadow A.J.W. The age and mode of formation of Gaussberg, Antarctica // Journal of the Geological Society of Australia. 1983. № 30. P.241-246.
10. Vyalov O.S. and Sobolev V.S. Gaussberg, Antarctica // International Geology Review. 1959. № 1 (7). P. 30-40.
11. Сущевская Н.М., Мигдисова Н.А., Антонов А.В., Крымский Р.Ш., Беляцкий Б.В., Кузьмин Д.В., Бычкова Я.В. Геохимические особенности лампроитовых лав четвертичного вулкана Гауссберг (Восточная Антарктида) - результат влияния мантийного плюма Кергелен // Геохимия. 2014. №12. С.1-21.

Partial H_2O loss from melt inclusions in olivine and its initial content in Karymsky volcano magmas, Kamchatka

Nazarova D.P.[1], Portnyagin M.V.[1,2], Krasheninnikov S.P.[1], Grib E.N.[3]

1 – V.I. Vernadsky Institute of Geochemistry and Analytical Chemistry RAS, nazarova2405@rambler.ru

2 – GEOMAR Helmholtz Centre for Ocean Research Kiel

3 – Institute of volcanology and seismology FED RAS

Water plays an important role in formation and evolution of arc magmas.

In this work, we estimated initial H_2O content in primitive magmas of Karymsky Volcano (Kamchatka). We investigated two types of melt inclusions from volcanic bomb collected from the north-eastern side of Karymsky Lake from base of the lower terrace [1]. The first type are natural glassy inclusions consisting of volcanic glass and gas bubble, and the second - partially re-crystallized melt inclusions.

Glassy inclusions were analyzed without experimental re-heating. To eliminate effects of partial crystallization in the second type inclusions, they were homogenized experimentally. Experiments were carried out at 1 atm in a vertical furnace at the Vernadsky Institute, Moscow. The heating was performed in the atmosphere of CO_2 and H_2 gases mixed in proportion corresponding to NNO oxygen buffer. Loose olivine grains with melt inclusions picked under microscope were loaded in unsealed Pt capsule, heated during 5 min at 1300 ^{o}C and then quenched in water. After the experimental treatment, melt inclusions contained glass, gas bubble and occasionally spinel crystal. Major elements in glasses, olivine and spinel were analyzed by electron microprobe at GEOMAR (Kiel). All inclusions were corrected for equilibrium with their host olivine using Petrolog 3.1 software [2]. Initial FeO in the inclusions was assumed to equal FeO (9.86 wt. %) in their host rocks [1].

H_2O content in glasses of melt inclusions were determined by confocal Raman spectroscopy at the Geological Faculty of the Moscow State University, Moscow [3]. The measured H_2O content glassy inclusions is 3.2-4.4 wt. %, in reheated inclusions 2.3-2.4 wt. % (Fig.1). Positive correlation is observed between the H_2O content and inclusion size (Fig.1). This correlation can originate due to partial H_2O loss from melt inclusions in nature and during experiment re-heating [4].

After correction for equilibrium with host olivine, the H_2O contents were estimated to be 2.8-3.7 wt. % and 2.7-3.3 wt. % in the two types of inclusions, respectively (Fig. 2).

The measured H_2O contents were compared to H_2O contents calculated using method from ref. 5 based on comparison of “real” and “dry” crystallization temperatures of olivine. The “real” crystallization temperatures were obtained using geothermometer based on Al partitioning between olivine and spinel [6]. These temperatures were found to be 1114±9 °C (1σ) as calculated for 19 pairs of olivine $Fo_{86\text{-}89}$ and spinel with Cr#=0.6-0.7. “Dry” crystallization temperatures were calculated using the composition of melt inclusions in olivine by model from ref. 7. Difference between real crystallization temperature and “dry” crystallization temperatures of olivine (□T) is 111±10°C (1σ), which corresponds to 4.2±0.6 wt. % H_2O (Fig. 2) according to the model [8].

Measured and calculated initial H_2O content in the largest inclusion are similar within the error. This implies that natural glassy inclusions lost not more than 1 % of initial H_2O (Fig.2).

The research was supported by the Russian Science Foundation, project no. 14-17-00582

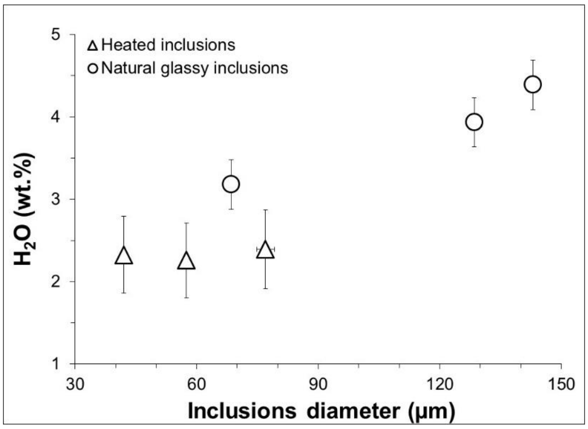

Fig.1 Correlation between H_2O content and size of melt inclusions. Smaller inclusions lose H_2O faster. H_2O content were determined by confocal Raman spectroscopy [3]

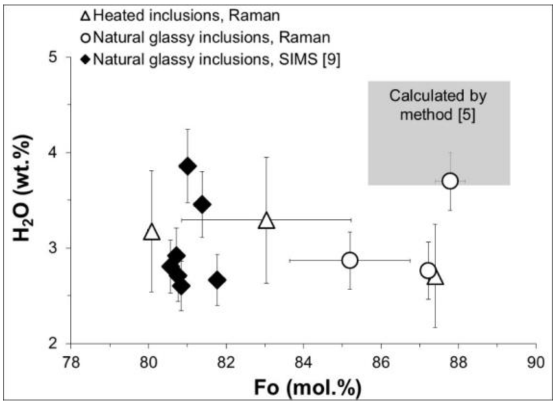

Fig.2 H_2O content in melt inclusions versus Fo content of host olivine. The shaded area shows calculated H_2O content in melt inclusions using method from ref. 5.

References:

1. Grib E.N., Perepelov A.V. // J. Volcanol. and Seismol., 2008, V.2(4), p. 228-247
2. Danyushevsky L.V., Plechov P. // Geochem. Geophys. Geosyst., 2011, V. 12(7), doi: 10.1029/2011GC003516
3. Plechov P. et al. // J. Volcan. Geotherm. Res., 2015, V.307, p. 182-199
4. Qin Z., Lu F., Anderson A.T. // Am. Mineral., 1992, V. 77, p. 565-576
5. Sobolev A.V. et al. // Nature, 2016, doi:10.1038/nature17152
6. Coogan L.A., Saunders A.D., Wilson R.N. // Chem. Geol., 2014, V. 368, p. 1-10
7. Ford C. E., Russell D. G., Groven J. A., Fisk M. R. // J. Petrol.,1983, V.24, p. 256–265
8. Almeev R.R. et al. // Am. Mineral., 2007, V. 92(4), p. 670-674
9. Portnyagin M.V. et al. // Geokhim., 2011, V. 49 (11), p. 1153-1178

Statistics for annually registered signals from the small aperture antenna "Mikhnevo" monitoring

Nepeina K.S.

IDG RAS, nepeina.k@mail.ru

Control of the seismicity level in the major engineering facilities areas is necessary even on a subactive territories. For the implementation of seismic monitoring in the central region of Russia in 2004 the permanent small aperture seismic antenna "Mikhnevo" (SASA) was established [1]. Configuration SASA "Mikhnevo" represents three concentric circles. Annually SASA registers a large number (over 500 events) of different nature signals (natural and anthropogenic). Man-made seismic events from mineral deposits exploration are most common [2]. SASA allows isolate very weak signals and thus significantly increases the number of detectable events [3].

Multichannel processing allows the SASA to ensure the sensitivity of the observations for the sources of seismic events with magnitudes M>2.5 on a distance of 280-300 km with magnitudes M>1,5 - at distances up to 90 km; for weak events with magnitudes M>-0,5 at distances up to 5 km.

For signals with low signal-to-noise even resolution of the antenna is insufficient to uniquely identify the source. For this purpose, all known sources are numbered and digitized, and their azimuthal distribution is presented in figure (a). Registration of weak seismic events (M<3.5) at regional distances allowed to collect representative statistics for plotting the frequency and consequently to estimate the main parameters of technological developments within the mild areas (Figure (b)). Method matched filter with template waveforms, carefully selected from a ten-year archive of digital records SASA "Mikhnevo" [4], allows to create various geostatistics algorithms assisting to relative identification of the quarry blasts. The work is supported by grant of Russian National science Foundation № 16-17-00095.

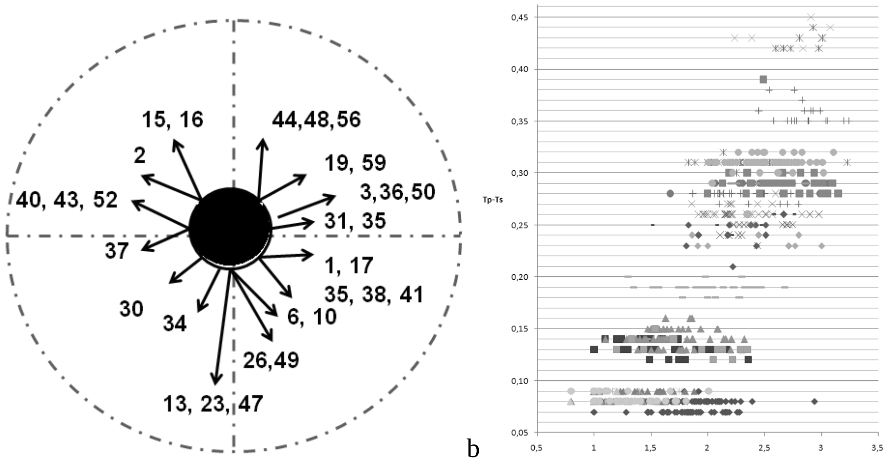

a b

Fig. The azimuthal distribution of the main permanently recorded signals (a) and the dependence of the travel time difference of seismic waves arrivals (b) from recorded signals in 2013 with magnitude range (0.5<M<3.5) by small aperture antenna "Mikhnevo"

References:

1. Sanina I.A., Volosov S.G., Chernykh O.A., Riznechenko O.Ju. Small aperture seismic antenna "Mikhnevo": new opportunities to study seismicity of the East European platform // DAN. 2009. T. 428. No. 4. p. 536-541.
2. Sanina I.A., Kishkina S.B. Complex geophysical monitoring of geodynamic as the basis for security monitoring // Science and safety. 2014. No. 1 (13). p. 14-21.
3. Kulikov V.I., Sanina I.A., Goncharov I.A., Chernykh O.A., Nesterkina M.A., Volosov S.G.,
4. Konstantinovskaya N.L. Peculiarities of propagation of seismic waves from quarry blasts on the Russian Platform // Local and global impacts on the geospheres. M.: GEOS. 2008. p. 89-97.
5. Kitov I.O., Sanina I.A., Nepeina K.S., Konstantinovskaya N.L. The method using a matched filter on a small aperture seismic antenna "Mikhnevo" // Seismic instruments. 2014. T. 50. No. 3. p. 5-18.

Composition of olivine as the primary source of information about the origin of basalts of volcano menshiy brat, Iturup Island, Southern Kurile Islands

Nizametdinov I.R.[1]

1 – Novosibirsk state university, Sobolev IGM SB RAS, iskander642@gmail.com

Holocene volcano Menshiy Brat is located within the Medvezhya Caldera in the north-western part of Iturup island at the front of the Kuril-Kamchatka island arc. The history of this caldera is divided into three stages. Pre-caldera stage, which is manifested by formation of basaltic shield volcano. Caldera stage of destruction of shield volcano and extrusion of rhyolite-dacite domes. Post-caldera stage is characterized by formation of intracaldera shield volcanoes [2]. The caldera has Middle Pleistocene age [3]. Development of volcano Menshiy Bratis related toncaldera stage. The volcano is composed of isolated dacitic dome, covered by post-caldera Vostochny and Korotyshka cinder cones and their flows. These flows are composed of tholeitic olivine-pyroxene-plagioclase basalts and andesite.

Up to 1 mm olivine crystals are dispersed within hyalopilitic groundmass. These phenocrysts do not form aggregates with plagioclase and pyroxene. They have xenomorphic resorbed morphology, sometimes with outermost rim made up of magnetite-pyroxene symplectites. Scarcely olivine forms isometric faceted grains, sometimes with small skeletal outgrowths.

The composition of the olivine phenocrysts studied is typical for island-arc basalts. Forsterite content ranges from 84,5 to 89,5 mol. % (Fig. 1). Olivines have normal zoning, manifested in decreasing of Fo content from the center to the periphery. However, some of these olivines show abrupt increase of Fo content up to 91 in the outer most parts. This increase was explained by olivine oxidation in lava flow under atmospheric conditions [1].

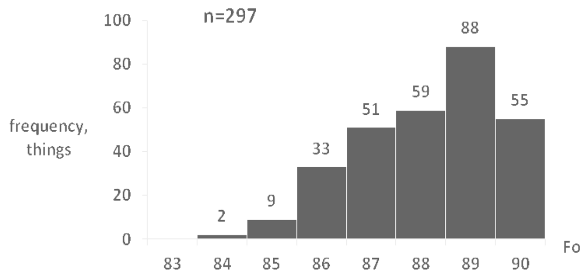

Fig. 1 Histogram forsteritic content of olivine Phenocrysts from basalt Menshiy Brat volcano. Forsteritic content in mol. %.

Olivine crystals contain numerous inclusions of spinel (Cr# - 0,34-0,85). The compositions of the spinel and coexisting olivine were determined by EPMA with special focus to the accuracy of trace element measurements.

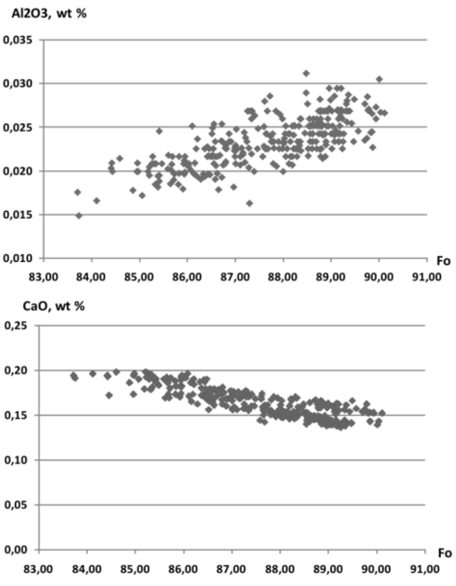

Fig. 2 The composition of the olivine phenocrysts of Menshiy Brat volcano. Forsteritic content in mol. %.

Positive correlation of Al_2O_3vs Fo of the studied olivines and negative for CaO vs Fo (Fig. 2) implies that olivine + spinel assemblage was formed prior to pyroxene and plagioclase. Thus, olivine and spinel are the liquidus phases of the Menshiy Brat basalts, which give information about the parameters and composition of initial melts. It is suggested that olivine-spinel paragenesis crystallizing deep intermediate chamber at temperatures 1070-1260^{o}C and oxygen fugacity NNO ±1,5.

References:

1. Stefano Del Moro, Alberto Renzulli, PatriziaLandi, Sonia La Felice, Mauro Rosi, Unusual lapilli tuff ejecta erupted at Stromboli during the 15 March 2007 explosion shed light on the nature and thermal state of rocks

forming the cratersystem of the volcano // Journal of Volcanology and Geothermal Research.2013.№254. P. 37–52.
2. Ermakov V.A., Steinberg G.S., Kydrjavy, Volcanism and evolution the MedvezhyaCaldera (Iturup Island, Kuril Islands) // Volcanology and seismology. 1999. № 3. P. 19-40.
3. Piskunov B.N., Rybin A.V., Sergeev K.F.Petrogeochemicallyof the MedvezhyaCaldera (Iturup Island, Kuril Islands) // Doklady Earth Sciences. 1999. V. 368. № 3. P. 380-384.

Assessment of yield point of metal nanoparticles

Makat D.K.[1], Orazbayeva Zh.M.[2], Mukasheva L.S.[3], Maratova A.G.[4]
1- KSTU, dastankgtu90@mail.ru; 2 – KSTU, zhupik.m.1@bk.ru; 3 – KSTU, mukasheva@mail.ru; 4 – KSTU, maratova9393@bk.ru

Increased strength and hardness with decreasing grain size up to a certain critical size is typical for virtually all crystals. This follows from the Hall-Petch equation that yield strength σ_T depends inversely on the average size of grain d [1]:

$$\sigma_T = \sigma_M + kd^{-1/2}, \quad (1)$$

where σ_M- the strength limit of the single crystal, k - some dimension factor.

Equation (1) is performed quite well over a wide range of d up to 1 mcm. σ_T values obtained by extrapolation in the region of size d <100 nm is 2-3 times higher than those of traditional materials. Experimental results obtained on nanocrystals show that they are much stronger than coarse grained analogues.

Hall-Petch relation (1) holds for a large part of the studied only up to a certain grain size, while at lower values it is bucking the effects: hardness (strength) decreases with decreasing of grain size. In the work [2] for the yield point it is obtained:

$$\sigma_T = \sigma_M + C\sigma d^{-1/2}. \quad (2)$$

Equation (2) coincides in shape with the Hall-Petch equation (1). However, the coefficients of proportionality differ in both formulas. In this case, the behavior of the yield point of small particles is also determined by the size of their surface tension σ. For small d ones A.I. Russanov got asymptotic linear relationship:

$$\sigma = Kd. \quad (3)$$

Here K - coefficient of proportionality. Formula (3) is obtained on the basis of thermodynamic consideration and should be applicable to small objects of various nature. In this case, the equation (2) takes the form:

$$\sigma_T = \sigma_M + CKd^{1/2}. \quad (4)$$

Equation (4) represents the opposite effect of Hall-Petch.

Let us now consider the question of the amount of metal nanoparticles from which the direct effect of the Hall-Petch is replaced by the reverse, that is hardening of the nanoparticles changes to their softening.

Equation (2) shows that the Hall-Petch equation begins to violate from the moment when the size dependence of surface tension begins to appear.

Experimentally critical radius of nanoparticles can be determined by size dependence of its melting point [3] or any other physical property [4].

The picture shows the dependence of HP for copper and nickel.

Processing of drawing curves with the help of relation (2) gave the value of the constant C:

$$C \approx 102 \text{ MPa}\cdot\text{m}^{1/2}. \quad (5)$$

The following should be noted: the constant C has the same value for most metals of the periodic system of elements. This helps to explain the observed dependence of the coefficient K in HP equation type of metal by the difference in the value of the surface tension for different metals.

Using table values σ_M and determining the value of the surface tension by the method of [6], we can calculate the yield point for those metals when the value σ_M is known.

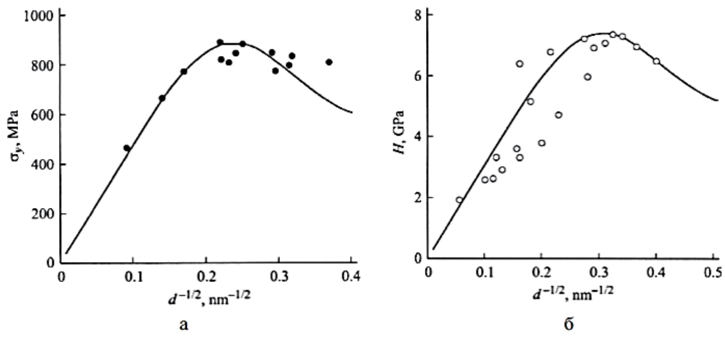

HP Value for yield point of nanocrystalline copper (a) and microhardness nickel (б) [5]

The calculations for a number of metals indicate that the yield point for the particles with size of 0.3-0.5 microns is practically identical with the corresponding value for the massive sample.

Given in this paper approach is not applied to micro-mechanisms of the processes of hardening and softening of nanostructures. However, it may be useful for engineered nanomaterials, as the connection between mechanical properties of nanostructures with their surface tension (surface energy) is explicitly defined.

References:

1. Malygin G.A. Strength and plasticity of nanocrystalline materials and nanosized crystals // UFN, 2011 T.181, №: 11. 1129-1156.
2. Yurov V.M., Laurynas V.C., S.A. Guchenko. Some problems of the physics of strength of metal nanostructures // Intercollege. Sat. scientific. works "Physical and chemical aspects of the study of clusters, nanostructures and nanomaterials. - Tver: Tver. state. University Press, 2013, Vol. 5. 408-412.
3. Yurov V.M., Ibraev N.H., Guchenko S.A. Experimental determination of the surface tension of the nanoparticles and nanofilms // Proceedings of the universities. Physics. - 2011. - T. 54. number-third. 335-340.
4. Yurov V.M., Portnov V.S., V.C. Laurynas et al. Size effects and physical properties of small particles and thin films. - Karaganda: Publishing house of the Kazakh-Russian University Press, 2013. - 116 .p.
5. Vakhrushev A.A., Vakhrusheva L.L., A.A. Shushkov. Numerical analysis of changes modulyauprugosti crystalline nanoparticles of metal under the influence of different load types // Izvestiya of the Tula State. Univ. Natural Sciences. - 2011. - Vol. 3. - P. 137-150.
6. Yurov V.M., Ibraev N.H., Guchenko S.A. An experimental determination of the surface tension of nano-particles and Nanofilms // Proceedings of the universities. Physics. - 2011. - V. 54. - № 1/3. - S. 335-340.

Influence of fault compositon on its activity (laboratory experiments)

A.A. Ostapchuk, D.V. Pavlov, V.K. Markov

Institute of Geosphere Dynamics of Russian Academy of Sciences, Moscow, Russia, ostapchuk@idg.chph.ras.ru

Models of different slip mode nucleation and transformation can be developed basing on laboratory experiments, in which regularities of shear deformation of gouge-filled faults are studied. It’s known that the spectrum of slip modes is defined by both macroscopic deformation characteristics of the fault and mesoscale structure of fault filler. Small variations of structural parameters of the filler may lead to a radical change of slip mode.

This study presents results of laboratory experiments investigating regularities of shear deformation of discontinuities filled with multicomponent granular material. The experiments were carried out in the classical “slider model” statement. A granite block slides under shear load on a granite substrate. The contact gap between rough surfaces was filled with a layer of discrete material, which simulated the principal slip zone of a fault. The filler components were quartz sand, salt, glass beads, granite crumb, corundum, clay and pyrophyllite.

An entire spectrum of possible slip modes was obtained – from stable slip to slow-slip events and to regular stick-slip. Mixing several components in different proportions, it became possible to trace the gradual transition from stable slip to regular stick-slip, from slow-slip events to fast-slip events. Depending on specific filler component content, increasing the portion of one of the components may lead to both a linear and a non-linear change of slip event moment (a equivalent of the seismic moment). For different filler compositions durations of equal-moment events may differ by more than two orders of magnitude.

The primary result of the research is experimental proof that small variations of material composition of the fracture filler may lead to significant change of the slip mode and the portion of energy radiated during dynamic unloading of enclosing rock massif.

The work was supported by the Council for Grants (under RF President) and State Aid of Leading Scientific Schools (grant NSh-7230.2016.5).

Proskurov massif of Alkaline Rocks (Ukrainian shield): new geochemical database and its quality estimation

Osypenko V.Yu.[1], Shnyukov S.E.[1]
Institute of Geology, National Taras Shevchenko University of Kiev
E-mail: victoria.osipenko@gmail.com

Proskurov massif (PM) of alkaline rocks since its discovery (I.D. Tsarovsky, P.F. Bratslavsky, 1978 [6]) was studied by many scientists [1-6] and had been attributed to the alkaline-ultramafic (carbonatite) formation, despite the absence of carbonatites. Partial similarity of PM with well-known Chernigovka carbonatite massif (ChCM) was indicated [4] in rocks composition (alkaline and nepheline syenites, jacupirangites, ijolite-meltejgites), their minerals (alkaline feldspar, albite, nepheline, biotite, aegerine-bearing pyroxene, amphibole, calcite; titanite, apatite, zircon, ilmenite), and wide fenitization halo presence. Based on preliminary geochemical data [1, 4, 5] PM differs from the ChCM and other typical massifs of alkaline-ultramafic formation by low TiO_2 and Cr, Ni, Co, Nb (23-35 ppm), Zr (25-95 ppm), LREE (85-219 ppm) contents. These geochemical features of the PM rocks were the basis of the estimation of element specific and (or) mineral composition of upper mantle as a level of corresponding melts generation [5]. But the modern geochemical data sets [1, 4, 5 etc.] are not complete. Hence, the verification of the PM rocks geochemical composition via forming the modern and representative database is a main goal of this article.

Modern (preliminary) geochemical data set for PM rocks were obtained during the 1980-90s [2-4, 6]. They cover a wide range of rock types, but are representative only in a case of major elements. Data sets obtained during the last 15 years [1, 5] also include the modern analitical results, first of all the results of ICP-MS determination of trace-element rocks composition. But they are not fully characterize all range of PM rock types (fig. 1) and need a significant supplement.

PM alkaline rocks were studied by authors with a help of a set of boreholes and its representative sampling. Concentrations of all major and representative set of trace elements (SiO_2, TiO_2, Al_2O_3, $Fe_2O_3^{total}$, MnO, MgO, CaO, Na_2O, K_2O, P_2O_5, S, Cl, Zr, Sr, Ba, Rb, Y, La, Ce, Pr, Nd, Nb, Th, U, Ga, As, Pb, Ni, Zn, Cu) were detereminated by quantitative XRF uniformly for all samples (n=304).

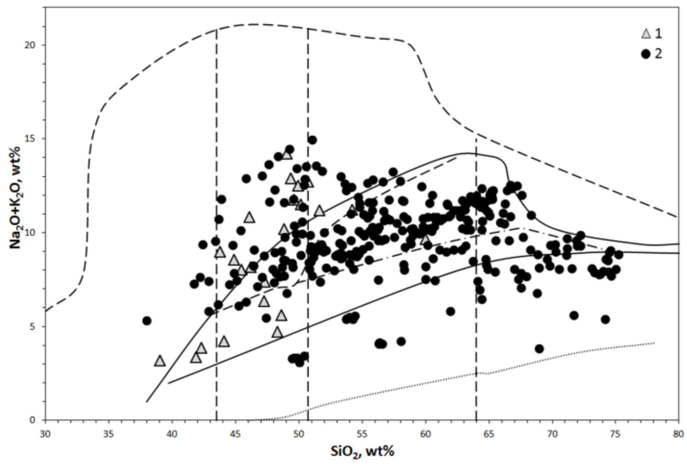

Fig. 1 Our new data in comparison with reference data set (a case of uniform list of major and trace elements): 1 – reference data [1, 5], 2 – our data.

Selected set of standard samples were used for internal and external quality control of analytical estimations. Samples of external control were measured as unknown ones. Measurements results showed that the precision and accuracy of our determinations are within the permissible range (fig. 2).

Newly obtained geochemical data: (1) cover massif rock types as fully as possible; (2) have the complementary set of elements to other authors the most reliable data [1, 5]; (3) significantly supplement them both qualitatively and quantitatively; (4) may be integrated to the single geochemical database, representative for PM and useful for solving the further interpretation.

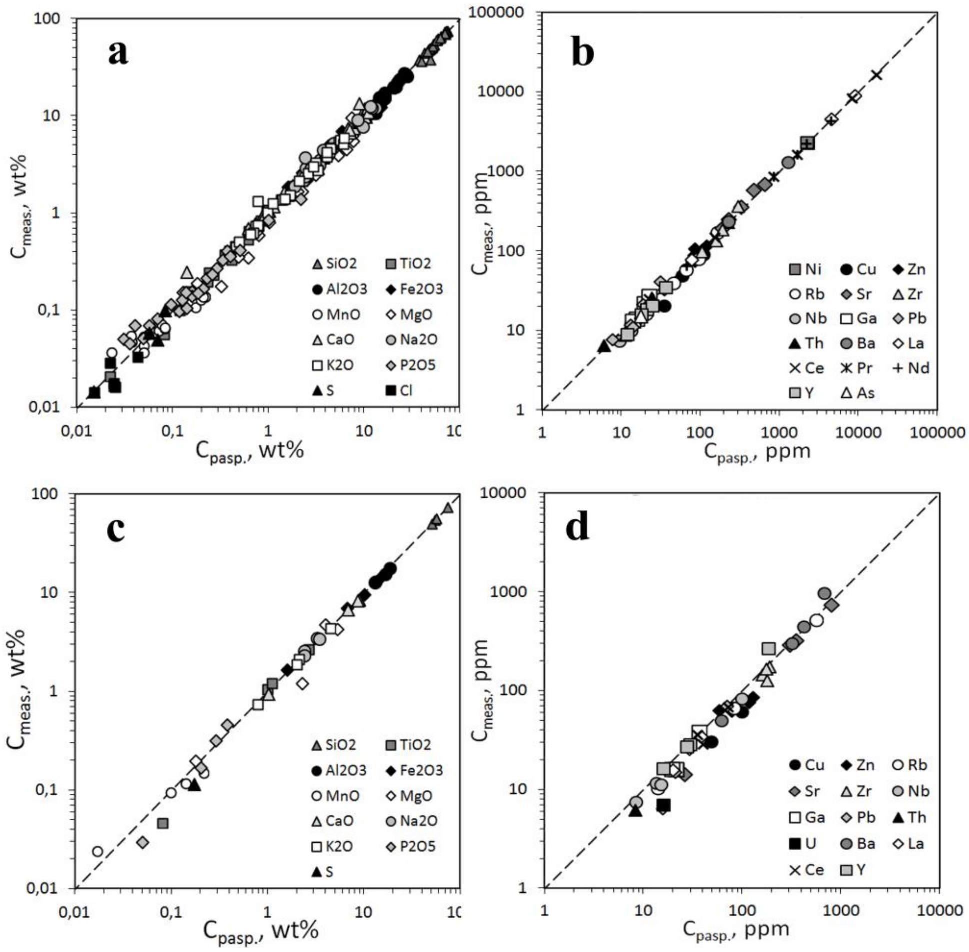

Fig. 2 Plots of the analytical results vs. reference element concentrations for a set of reference samples analyzed as an unknown ones: *a, c* – major elements, *b, d* – trace elements; *a, b* – internal control, *c, d* – external control.

References:

1. Dubyna O.V. Geochemistry of Ukrainian Shield alkaline rocks. Doktoral thesis. – Kyiv. – 2015. (In Ukrainian).
2. Kryvdik S.G., Bratslavsky P.F. Nepheline rocks of Proskurov massif (Dnister area) and their formational belonging // Geol. Journal. – V. 47. – № 1. – 1987. – P. 105-116. (In Russian).
3. Kryvdik S.G., Bratslavsky P.F. Fenites of Proskurov massif (Dnister area) // Geol. journal. – V. 47. – № 2. – 1987. – P. 111-124. (In Russian).
4. Kryvdik S.G., Tkachuk V.I. Petrology of Ukrainian Shield alkaline rocks. – K. : Nauka, 1990. – 406 p. (In Russian).
5. Kryvdik S.G., Dubyna O.V. Dnister-Bug alkaline rocks of Ukrainian Shield geochemical features // Mineralogical journal. – V. 28. – № 4. – 2006. – P. 32-42. (In Ukrainian).
6. Tsarovsky I.D., Bratslavsky P.F. Dnister-Bug nepheline rocks (geology, age and material composition). – Preprint. – K., 1980. – 46 p. (In Russian).

Genesis of apatite-carbonate ores at the seligdar deposit (Central Aldan, Russia): based on the present data on melt and fluid inclusions

Prokopyev I.R. [1,2]
1 – VS Sobolev Institute of Geology and Mineralogy SB RAS, prokop@igm.nsc.ru
2 – Novosibirsk State University

Introduction. The Seligdar apatite deposit is located in the Central Aldan region in Russia. It is situated about 30 km south of the Aldan town of Yakutia, and is a typical object of the Nimnyrskaya apatite zone of the Aldan-Stanovoy shield (Entin, Tyan 1984). The Seligdar ore field contains a single round ore-body with parameters of 1.6x2.2 km at the surface, which is traced to the depth of 1660m by drilling (Boyarko 1983). The ore-body consists of several ore-bearing ring-zones of silicate-apatite- carbonate composition. The ore-body is located in the surrounding Archean metamorphic rocks. The age of apatite-carbonate mineralization at the Seligdar is ~1750 Ma (Smirnov et al. 1976).

There are several hypotheses of the origin of apatite-carbonate ores at the Seligdar deposit: sedimentary-metamorphic hypothesis (Egin, Kichigin 1973), the basic model that there is a potassium-alkaline mafic intrusion at a depth, which was a source of phosphorus (Boyarko 1983), and the formation from the mantle-crust carbonatites (Smirnov 1977), but because of the lack of association of the apatite-dolomite carbonatites with any ultra-basic alkaline rocks this hypothesis had not found a decent support at that time. In this contribution, I present melt and fluid inclusion data, which suggest that the Seligdar ores are probably a product of carbonatite melt.

Methods. The first studies of the conditions of the formation of apatite-carbonate ores at the Seligdar deposit are described in the works of LS Puzanov et al. (1978), VB Vasilenko et al. (1982) etc. Data on the presence of melt inclusions in the minerals of apatite-carbonate rocks have not been subsequently confirmed. To study melt and fluid inclusions in minerals, traditional and modern methods were used, such as thermo-cryometry (TC-1500 and a Linkam THMSG-600), Raman spectroscopy (JobinYvon LabRAM HR800), EPMA, SEM (LEO1430VP, OXFORD detector), and LA-ICP-MS (NexION 300D with a laser ablation system NewWave UP213). To calculate element concentrations in the inclusions by means of LA-ICP-MS, the algorithm proposed by H. Longerich et al. (1996) was used, and Mg concentration determined by means of the SEM analysis of uncovered inclusions was used as an internal standard.

Melt and fluid inclusion data. The ores of the Seligdar deposit consist of idiomorphic crystals of red apatite (with hematite inclusions), as well as magnetite, and secondary quartz in dolomite matrix. Monazite is crystallized as rare mineral in dolomite and in the rim around apatite as a result of metamorphic processes. The silicate phases are represented by plagioclase, K-feldspar, and biotite.

Primary melt inclusions of silicate-carbonate composition were determined in the prismatic crystals of apatite from the core samples of the Seligdar deposit ores (Fig *a, b*). Melt inclusions have a shape of elliptical vacuoles; they occur as a swarm in the central parts of the crystals and trace the crystal growth zones. Melt inclusions are highly susceptible to the secondary hydrothermal-metasomatic processes; they are often opened and filled with secondary fluid inclusions. Non-opened melt inclusions contain daughter phases of dolomite (80-95 vol%), silicate and salt (K, Na, Ca, Fe, Mg, Al, Si, O, Cl, F, S - composition was determined by only qualitative SEM analysis because of the small size of the crystal phase), and fluid phase (1-2 vol%). The average size of inclusions is 10-30μm. Homogenization temperatures of melt inclusions in apatite vary from 820 to 1100°C. According EPMA and SEM analyses of uncovered inclusions, the melt inclusions contain (wt%): Mg - 13.3-13.5, Ca – 21-35, Mn – 0.42-0.3, and Fe – 9-0.15; by LA-ICP-MS (ppm): Sr – 6900, Ba – 960, Th – 100-9010, U – 52, Y – 2180, Nb – 7, K – 47-3.8, Na – 0.72-29, Si – 6.9-9000, and Al – 10-9700.

Apatite, dolomite and secondary quartz of the apatite-dolomite Seligdar ores are full of fluid inclusions of different composition and generation (Fig *c, d*). According to the composition of fluid inclusions, their kinds were established: (i) primary crystal-fluid water-salt inclusions of H_2O±NaCl/KCl-CO_2(L) composition with homogenization temperature intervals of 465-415 and 385-315°C. Primary fluid inclusions are arranged along or as cloud-like bunching in the central parts of the minerals, and the shape of the vacuoles of primary inclusions in apatite and quartz is ellipsoid. Healed cracks and cleavage planes in idiomorphic minerals (apatite, quartz, and dolomite) are traced by numerous pseudo-secondary and secondary fluid inclusions. Secondary inclusions have vacuoles of irregular shapes, often unlaced, and are characterized by various volume phase ratios. Secondary fluid inclusions of H_2O±NaCl/KCl-CO_2±N_2(g) composition (ii) have the homogenization temperature of 300-180°C, secondary CO_2(g)-liquid (iii) – 220-100°C. The average size of inclusions is 5-25μm.

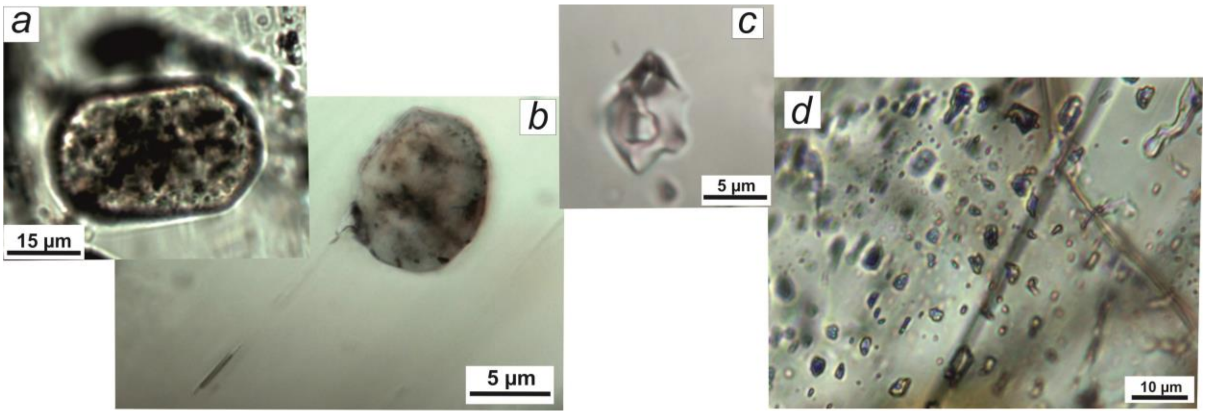

Fig. Melt silicate-dolomite inclusions (i) in apatite (*a*, *b*), primary crystal-fluid (ii) (*c*) and secondary gas-liquid (iii) (*d*) fluid inclusions in apatite and quartz of the Seligdar deposit ores.

Conclusion. Preliminary data on the melt and fluid inclusions show that apatite-carbonate Seligdar deposit ores were formed from carbonate melt of dolomite composition at the temperatures of 800-1100°C. Because of the ancient age, the apatite-carbonate rocks had been exposed to intense processes of metamorphism and hydrothermal-metasomatic alterations, which is reflected in the composition of heterogeneous fluids. Saline fluid-saturated solutions contain sodium and potassium chlorides, the fluid phase is characterized by variation of CO_2(L)-CO_2(g)-N_2(g) in its composition at the temperature decreasing from 465-415 and 385-315°C to 220-100°C. To confirm the carbonatite genesis of the Seligdar deposit, additional mineralogical, geochemical, and isotopic studies are necessary.

This work is supported by the Russian Science Foundation (RSF), Project № 15-17-20036.

References:

1. Boyarko GYu Geological and geochemical features of the Seligdar apatite deposits. – PhD thesis [in Russian]. - Tomsk. - 1983. - 121 p.
2. Entin AR Tyan OA Before-carbonatite step of formation of apatite deposits of Seligdar type (Aldan) [in Russian]. - Yakutsk, USSR SB RAS, 1984. - 28 p.
3. Egin VI, Kichigin LN Characteristics and prospects of apatite mineralization in the Central Aldan [in Russian]. – News of Yakutia Geology. - 1973. V. 3. - P. 75-80.
4. Longerich H P, Jackson S E and Günther D. Laser ablation inductively coupled plasma mass spectrometric transient signal data acquisition and analyte concentration calculation. J. Anal. At. Spectro. – 1996. – V. 11. - # 9. – P. 899–904.
5. Puzanov LS, Partsevsky AI About genetic type of the Seligdar apatite deposit (Central Aldan) [in Russian]. – Doklady USSR RAS. – 1978. – V. 243. - # 1. – P. 163-179.
6. Smirnov FL, Marshintsev ZK, Moskvitina AV et al. Typomorphic features of apatite deposits and occurrences of the Aldan Shield. - Book: Phosphorus geochemistry and mineralogy characteristics of apatite [in Russian]. – Yakutsk, USSR SB RAS, 1976. - P. 5-31.
7. Smirnov FL The role of liquation in the formation of magmatic deposits. Apatites of Aldan shield [in Russian]. – Yakutsk, USSR SB RAS, 1977. - P. 33-53.
8. Vasilenko VB, Kuznetsova LG, Kholodova LD et al. Apatite rocks of the Seligdar [in Russian]. – Novosibirsk: Nauka – 1982. – 213 p.

Gps/glonass observations in geodynamics, seismology, tsunami early warning systems

Pupatenko V.V.
Yu.A. Kosygin Institute of Tectonics and Geophysics, Far Eastern Branch, Russian Academy of Sciences, Khabarovsk, pvv2.dv@gmail.com

The first Global Navigation Satellite Systems (GNSS) – GPS and GLONASS – were designed as a meter-level precision positioning tools for military purposes, but now they allow users to determine hundreds times more precise coordinates. In static mode, the accuracy of the GNSS antenna average daily coordinate determination can attain mm-level. In kinematic mode, the instantaneous coordinates can be determined with

1 cm-level precision, and also in real-time. Nowadays, a great variety of applications exist for which GNSS coordinates are useful, starting from geodesy and navigation to seismology and climatic researches.

The capability of GNSS to determine daily coordinates with mm-level precision makes it possible to measure coseismic slips, i.e., GNSS station permanent position variations caused by an earthquake. The first calculations of coseismic deformations produced by strong earthquakes have been performed since the 1990s. Using coseismic slips recorded by a number of GNSS stations, one can determine the size and orientation of the earthquake source and slip distribution. It is very important for studying earthquakes that do not rupture the surface, because seismic data do not often clearly determine the rupture geometry. The earthquake source parameters can also be used for seismic moment and moment magnitude M_w calculation.

To date, GNSS-based earthquake source modeling becomes a relatively routine processing strategy for strong shallow earthquakes. It has been recently applied even for the strongest deep (up to 600 km) earthquakes such as the May, 24, 2013, $M_w = 8.3$ Okhotsk Deep Focus Earthquake. This earthquake caused relatively small coseismic slips up to 20 mm in the vertical direction and up to 15 mm in the horizontal plane, which was sufficient for developing a reliable source model (Shestakov et al., 2014, Abubakirov et al., 2015). In (Shestakov et al., 2014), we use the regional filtration for improving the precision of coseismic slips estimation.

Coseismic slips can be determined not only during data post-processing several days after the earthquake occurrence, but also from GNSS near real-time data kinematic processing results. Therefore, GNSS can be part of earthquake early warning systems. The earthquake early warning system using seismic and GNSS data is being now tested in California. Grapenthin et al. (2014) show that earthquakes with $M \geq 6$ can be successfully registered and processed within several tens of seconds using real-time data obtained from GNSS stations. Independent GNSS-derived magnitude estimates can be obtained faster than magnitudes based on S- or surface waves, and they are more precise as compared to magnitudes based on P-wave first arrivals. These results have been obtained in the continental region from one of the densest GNSS networks with the absence of the azimuth gaps in the GNSS station distribution. We can expect that a reliable source model parameters for $M > 7$ earthquakes can be obtained in several minutes in most other regions with sufficient number of GNSS-stations installed, including some offshore areas. This is important for solving two main problems of tsunami early warning systems.

The first problem is related to rapid estimation of the strongest earthquake magnitudes. Since 2004, several catastrophic earthquakes with $M > 8.5$ have occurred around the world. Two of these, the 2004 $M = 9.2$ Sumatra-Andaman earthquake and the 2011 $M = 9.0$ Tohoku-Oki earthquake, have produced giant tsunami waves killing tens of thousands of people. In both cases, the magnitudes derived from seismic data were underestimated to a greater extent, which resulted in great tsunami hazard disparaging. Blewitt et al. (2006) show that for the Sumatra-Andaman earthquake, even the existing sparse GNSS network allowed determination of $M = 9.0$ 15 min after the earthquake occurrence, while using the seismic data $M = 8.0$ and $M = 8.5$ were obtained 11 min and 1 hour after the earthquake, respectively. The same situation happened with magnitude estimation of the Tohoku-Oki earthquake (Wright et al., 2012). In spite of this fact, presently, none of the official agencies use GNSS data in tsunami early warning systems.

The second problem is associated with false tsunami alarms. A great number of strong earthquakes with $M > 7$ may cause dangerous tsunami. In the coastal regions close to the earthquake epicenter (within several hundred km), the seismic technique is the only method for tsunami hazard estimation, but it can solely provide the criterion of exceeding the threshold magnitude. This leads to inadequate amount of false alarms. During 1994–2010, the Russian Far East Tsunami Warning Service produced 28 warnings, but only 3 of them (11%) were true. The earthquake source model based on GNSS data can be used for determining tsunami probability and even as the initial data for tsunami modeling. The earthquake magnitudes are not principally limited, and only a few requirements must be fulfilled: the coseismic slips recorded at a number of relatively well-distributed stations must be determined reliably and fast.

In this work we have considered one of the aspects of solving the second problem concerned with reliable coseismic slip detection in near real-time mode. We have developed a new method for increasing the coseismic slip estimation accuracy based on simultaneous GNSS data processing using two approaches: Precise Point Positioning (PPP) and relative positioning. PPP allows obtaining the absolute station coordinates, whereas relative positioning gives coordinates with respect to some base station, i.e., the difference between the coordinates of two stations. Both methods allow us to achieve high accuracy, but they have different main error sources. For the local GNSS network of N stations, we can calculate coseismic slip for each station by N different ways using PPP and relative positioning processing results. In the first approximation, these N slip measurements are uncorrelated, so we can calculate their weighted average value which will be more precise than any of the initial measurements.

We have tested the suggested method on two datasets of 6 stations located in different areas of the world. More than 2000 test slip errors have been calculated for statistical analysis. BKG Ntrip Client (BNC, http://igs.bkg.bund.de/ntrip/download) was used for GNSS real-time data processing in PPP and TRACK module of GAMIT/GLOBK (http://www-gpsg.mit.edu/~simon/gtgk/) was used for data processing in relative positioning in near real-time mode.

For the first dataset of the Benin GNSS local network (Central Africa), the accuracy improvement (at 95% confidence level) vary from 17% to 61% with 41%, on average. Errors in five of six stations have become almost similar (17.4–17.9 mm). The second dataset of the Spanish GNSS local network (Red GNSS de Castilla y León) has initial PPP-derived slip errors twice lower, and the average accuracy improvement is only 15%.

Thereby, the suggested method allows appreciable improving of the coseismic slip accuracy calculation, especially for stations with low-quality PPP processing results.

Analysis of the variations in the geomagnetic field at the mid-latitude observations

Riabova S.A.

IDG RAS, ryabovasa@mail.ru

Now there is quite a lot of evidence of the influence of the magnetic field variations in the biological and physiological processes in living organisms. In particular, the influence of the magnetic field on the blood-vascular system of humans and animals was established [1]. In this context, study of the structure of the natural magnetic field of the Earth in different frequency bands and the study of it dynamics as a function of the changing geophysical conditions is an important problem of modern geophysics.

In this communication, we present the results of joints analysis of local long-period (with periods exceeding one day) geomagnetic variations at the mid-latitude observatories (geophysical observatory «Mikhnevo» (IDG RAS), geophysical observatory «Borok», magnetic observatory «Kiev»)

Measurements of the local variations of the magnetic field at geophysical observatory «Mikhnevo» (IDG RAS) were carried out in special geomagnetic pavilion using fluxgate magnetometer LEMI-018 (The measurement range is ± 68 000 nT, the resolution capacity is 10 pT). Measurements of the variations of the geomagnetic field at the geophysical observatory "Borok" were carried out by the three-magnetometer with measuring range of ± 70000 nT and bandwidth 0 - 1 Hz. The magnetic field at the magnetic observatory «Kiev» was measured by using fluxgate magnetometer LEMI-008 (the resolution of the analog channel is 5000 nT, the breadth of the channel analog output DC is 1 Hz; the analogue output transmission factor is 2 mV / nT).

Foremost the data of the instrumental observations carry to equidistant form. Also gaps and outliers were removed by using linear interpolation and by using forward and inverse Fourier transforms (The outliers we indentified by box-and-whisker plot and Tietjen-Moore test). Then the data were check up to the fortuitousness and stationary. The possibility of correct using of statistical methods was examined on the base of the Benford law [2]. Moreover, the registration data at the geophysical observatory "Borok" have been converted from the geomagnetic coordinate system (in which registration were carried) in the geographic system. Analysis of the periodicities was carried out on the base of the wavelet transform with using wavelet Morlet [3] and weighted wavelet z-transform.

Data analysis testifies complex magnetic field variations. As a example same results of the wavelet-analysis (amplitude and phase) are shown at the Fig. 1, which demonstrate presence variation of periodicities such as 1, 6, 14, 27 and ~ 150-200 days. We can see it better on the Fig.2. Periodicity of ~ 14 days connect with large probability with characteristic period connecting with motion of the Earth-Moon system around there centre of gravity. Similar mechanism is not excluded due to forming periodicity of 27 days (presence of this periodicity explains traditional only by the Sun motion around its axis). It is known that motion of the Moon around the Earth characterized by periodicity of about 27 days too. It allows supposing that periodicity of 27 days caused by two factors: Sun motion around its axis and the Moon motion around the Earth [4].

The intensity of the geomagnetic variations is not constant in time, and for some periods even it has been sporadic. For example, in 2011, the variation with a period of 6 - 8 days we clearly see in February - early March, the first half of April, partly in the second half of May, during the week of July and first half of August, but it virtually absents in the second half of March, in the third week of April, early May, completely in June and in the second half of August.

The feature of the observed periodicities geomagnetic variations is their fractal nature. The wavelet spectrum (Figure 2) shows the hierarchical structure of the geomagnetic field variations. Each scale crushing is marked by the appearance characteristic «forks» in the distribution of coefficient module - a split of local maxima. This is repeated with increasing scale that shows self-similarity of the process, as well as its proximity to the monofractal. Completion of the above analysis on the basis of self-similar properties of wavelet coefficients picture signal is mainly qualitative. Successive quantitative analysis of scaling based on the method of maxima of the module of the coefficients of the wavelet transform proves monofractality.

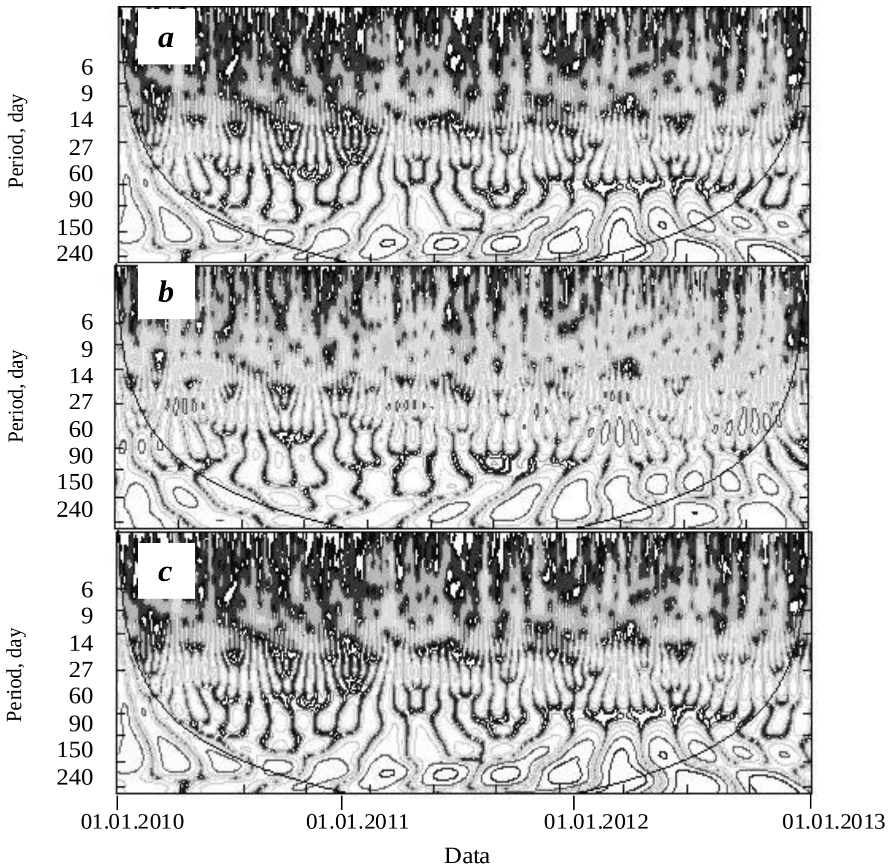

Fig. 1 Results of wavelet-analysis of horizontal component B_x of geomagnetic variations (2010 – 2012) at the mid-latitude observatories:

a) geophysical observatory «Mikhnevo» (IDG RAS),

b) geophysical observatory «Borok»,

c) magnetic observatory «Kiev».

The black line is cone of influence.

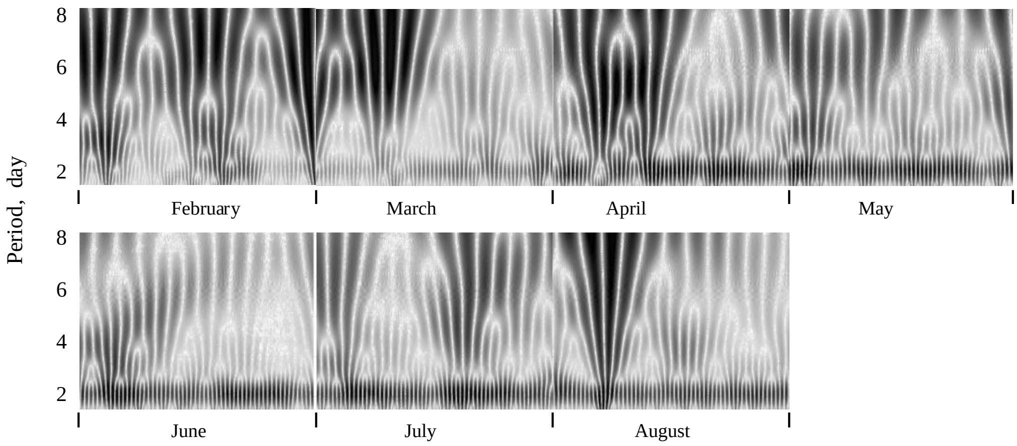

Fig. 2 Results of the wavelet analysis of geomagnetic field variations during the period from February to August 2011 at the geophysical observatory «Mikhnevo» (IDG RAS) within the cone of influence.

References:

1. Baule G.M., McFee R. Detection of magnetic fields of the heart //Amer. Heart J. - 1963. - V. 66, - P. 95-96.
2. Durtisch C., Hillison W., Pacini C. The effective use of Benford's law to assist in detecting fraud in accounting data// J. of Forensic Accounting. 2004. Vol. 5. P. 17 – 34.
3. Meyer Y. Wavelets: Algorithms and Applications, SIAM, Philadelphia, 1993, 134 p.
4. Adushkin V.V., Spivak A.A., Kharlamov V.A. Peculiarities of geomagnetic variations in the central part of the Russian platform// Izvestiya, Physics of the Solid Earth. 2014. Vol. 50. No. 2. P. 215 – 221.

Analysis of relationship between seismic oscilations and geomagnetic field

Riabova S.A.
IDG RAS, ryabovasa@mail.ru

The Sun, interplanetary medium, the magnetosphere, the ionosphere and the Earth with processes taking place in it are a physical system. It is known that change in solar activity causes a chain of interrelated phenomena in interplanetary space, magnetosphere, ionosphere and neutral atmosphere. It is expected that there is a relationship between variations of the geomagnetic field and processes in the solid Earth, for example, seismic oscillations.

We investigate the possible association between geomagnetic disturbances on Earth's surface and the seismic background in terms of mid-latitude Geophysical Observatory "Mikhnevo" of the Institute of Geosphere Dynamics. The peculiarity of the area of the Observatory "Mikhnevo" is the presence of watery deep tectonic structure (Nelidovo-Ryazan suture zone).

We use the result of synchronous records of magnetic field induction at the Earth's surface and seismic oscillations at the Mikhnevo Geophysical Observatory IDG RAS (54.959 N, 37.766 E) in the period from February 1, 2008, to December 31, 2013, as the initial data. The measurements of the geomagnetic field variations at the observatory "Mikhnevo" were carried by using a three-component flux-gate magnetometer LEMI-018 (The measuring range is ± 68000 nT and the resolution is 10 pT). The seismic oscillations were measured by using seismometers SM-3KV and STRECKEISEN STS-2. Collection and storage of data is carried out by using programmable registers QUANTERRA-380 and REFTEK-130.

In order to analyze the relationship between geomagnetic variations and variations of the seismic background the amplitude of positive peaked pulse have chosen as the characteristics of geomagnetic variations and the maximum amplitude of the oscillation velocity V_m have chosen as a characteristic variation of the seismic background.

Analysis of geomagnetic observations showed that at the observatory "Mikhnevo" a significant number of days are characterized by high geomagnetic activity. Visual inspection of the geomagnetic field data was found out that all of the observed geomagnetic variations on the mid-latitude observatory can be divided into 7 types: a) single "spiked" geomagnetic variations when local geomagnetic variations don’t develop; b) so-called magnetic storms with severe sudden onset; c) pulse variation on the background of formed local geomagnetic variations; d) train of multiple disturbances; d) geomagnetic variations, starting with reduced induction of the geomagnetic field; e) magnetic storms with the sudden onset of train vibrations; g) magnetic storm with several single pulses of sudden onset.

Analysis of registration data has shown that the most pronounced response of seismic background is observed in the types a), b) and c), the number of which has reached a total of about 50%. For this reason, at this stage of the research we examined only those types.

The graph between the amplitudes of the two fields is shown in Figure 1. It is clear that stronger geomagnetic variations correspond to more intense variations in the oscillations velocity of the seismic background. In the range of 20 - 100 nT the response of seismic field almost linearly increases with B and for the values of more than 100 nT the dependence $V_m(B)$ becomes flatter, which may indicate that the response level of seismic background to geomagnetic perturbations as the latter become intense.

The analytical dependence $V_m(B)$ is :

$V_m =$ [illegible] m / s,

where B is in nT.

The correlation analysis confirms the significant correlation between variations in the magnetic field and variations in the oscillations velocity of the seismic background (in our case, Spearman’s coefficient of determination is equal to 82.3 %, Pearson’s coefficient of determination is equal to 80 %, Kendall’s coefficient of determination is equal to 58%).

When considering the possible mechanisms of energy conversion of geomagnetic variations in the energy of seismic waves it has been found that under the conditions of the observatory "Mikhnevo" magnetostriction does not provide efficient conversion of energy. Analysis of the real and imaginary parts of the magnetic tipper [1], which reflect the change in the electrical conductivity of the Earth's crust, reveals that perhaps the mechanism of energy conversion between these fields in this case are induced electrical currents which are concentrated in the flooded, and therefore highly conductive zones Nelidovo-Ryazan structure.

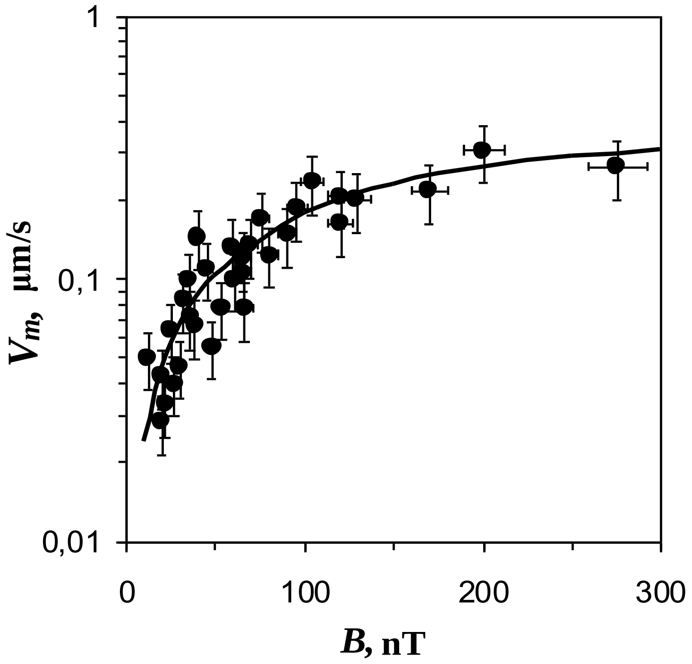

Fig. 1 The relationship between the amplitude of the magnetic pulse B and maximum amplitude variations in the oscillations velocity of the seismic background V_m .

References:

1. Larsen J.C. Transfer functions: smooth robust estimates by least-squares and remote reference methods. // Geophys. J., 1989, V. 99, pp. 645-663.

Karymshina Caldera – the first Kamchatka supervolcano.
New data on the geological structure of the area, the stages of volcanism and pyroclastic volumes (based on field work in 2012-2015)

Rogozin A.N., Leonov V.L., Leonova T.V., Klyapitsky E.S., Rylova S.A.
Institute of Volcanology and Seismology FEB RAS, alekseiras@yandex.ru

The work presents new data on the giant caldera discovered in 2006 in southern part of the Kamchatka peninsula. The caldera was formed during Eopleistocene (1.2 to 1.5 Ma). The caldera boundaries were reconstructed and its dimensions appeared to be approximately 15-25 km. The area of study covers several groups of thermal springs: the Bol'she-Bannaya, Mal. Bannaya, Karymchina, Karymshina, and Verkhne-Paratunka ones. The largest group is the Bol'she-Bannaya springs; which were investigated extensively by many different methods during the 1970s. The reconstruction of the large caldera boundary in this area [1] yields a different location of the present-day hydrothermal systems, in particular, of the Bol'she-Bannaya system. The caldera boundary has been found to pass through the Bol'she-Bannaya springs area. It was also found that numerous outcrops of acid lavas (domes, dikes, short lava flows) occur along the caldera boundary, these formations are relatively young, being formed less than 0.5–0.8 Ma. This data leads to the suggestion that the present-day hydrothermal activity in this area is related, on the one hand, to high crustal permeability at the caldera boundary (due to existing faults), while on the other hand, to the large magma chamber probably existing in the area which retains its heat and continues to supply fluids and water that are circulating around it to overlying hydrothermal system. This chamber cased the caldera generation in the Eopleistocene followed by a resurgent dome growth in the Lower/Middle Pleistocene.

We have reconstructed the boundaries of a large lacustrine basin that was formed in the caldera after the resurgent uplift appearance as well as the boundaries of thick pyroclastic flow protruding out of the caldera. Three complexes are distinguished according to consecutive stages of the caldera development: pre-calderian, caldera-forming (calderian) and post-calderian.

The pre-calderian stage (complex I) is assumed to have mid-Pleiocene age (3.4 – 2.6 myr). During the field work done in 2012, the volcanic edifices which existed just before the caldera formation were revealed and described for the first time. The data on the geochemistry and oxigen isotopism for rocks which build up pre-calderic volcanoes, were obtained in the laboratory of stable isotopes or the Oregon State University, USA. This data allowed to make a preliminary conclusion that the supercaldera was formed at the region where for long time (during whole Pleiocene) the high-siliceous volcanism took place [2].

The caldera-forming stage (complex II) has Eopleistocene age (1.78 – 1.2 myr). It is mainly represented by ignimbrites and crystalloclastic tuffs related to the caldera-formation, which side with volcanic relics shaped the border of the structure at the pre-calderic stage. At the central part of the depression the total observed thickness of ingimbrite deposits reaches 1000 m. During fieldwork in 2012-2014 a vast field of ignimbrites, traces of a large pyroclastic flow associated with caldera Karymshina, was mapped for the first time. Ignimbrites were found at a distance up to 35-40 km from the edge of the caldera [3]. The maximum thickness of the flow exceeds 500 m, the area of the pyroclastic flow deposits is about 298 km^2, and their total volume is about 84 km^3.

The post-calderic stage (complex III) is dated to Lower and Middle Pleistocene (0.5 - 0.8 myr). The extrusions and high-siliceous lavas were studied. The size and thickness of some extrusions and lava flows were specified. It was found during the field works that there are thick lava flows slightly sloped from the central part of the depression towards the rim, which are related to some of extrusion domes. The total volume of high-siliceous extrusions was estimated. The comparison study of volumes of high-siliceous extrusions and lava flows was done for three regions of Kamchatka: the Karymshina caldera (the post-calderic stage, Southerm Kamchatka), the Geiser Valley (Eastern Kamchatka) and the Chashakonja volcano (the Sredinny ridge). The Karymshina caldera is found to have the largest scale in high-siliceous volcanism. Total volume and area of extrusions and related lava flows reaches 2.68 km^3 and 26.44 km^2, correspondingly [4].

It is shown that the caldera-forming eruption was a major one in Kamchatka in regard to its volume of ejected material (approximately 825 km^3 or 2x10^{15} kg by its mass), and ranks as a major eruption worldwide [5].

Conclusions:

(1) A new large caldera (15×25 km), the Karymshina caldera, has been discovered in southern Kamchatka.

(2) An approximate **volume of material erupted** during the caldera generation was estimated to be **about 825 km^3**, which makes **a weight of 2×10^{15} kg**. This eruption should therefore be considered as the largest so far known to have occurred in Kamchatka and to be among the great eruptions worldwide.

(3) A tectonic uplift (4 × 12 km × 200 m) interpreted as a resurgent dome has been reconstructed in the northwestern part of this caldera, bounded by straight northeast and northwest trending faults. Also **the boundary of a lake**, which had existed in the caldera to the South from the resurgent uplift, has been reconstructed.

(4) During fieldwork in 2012-2014 **a vast field of ignimbrites**, **traces of a large pyroclastic flow** associated with caldera Karymshina, **was mapped for the first time**. Ignimbrites were found at a distance up to 35-40 km from the edge of the caldera. The maximum thickness of the flow exceeds **500 m**, the area of the pyroclastic flow deposits is **about 298 km^2**, and their total volume is **84 km^3**.

(5) It has been unambiguously established that the volcanoes of mounts Goryachaya, Yagodnaya, Levaya Karymchina, etc., located out of the caldera, but close to the boundaries of the caldera, are older and must be considered as **evidence of a major volcanic phase that proceeded the caldera generation**. It proved by the fact that the Karymshina rocks (mostly acid tuffs and ignimbrites) that fill the caldera in some cases lay on the lavas that compose the above volcanoes.

(6) New data were obtained on the setting of the rhyolite domes widely abundant in the area of study. It was shown that they are mostly confined to the boundaries of the caldera and to the boundary of the resurgent dome situated in it. Most of the domes were emplaced much later following caldera generation, they have ages of 0.5--0.8 Ma, and they should be regarded as **a consequence of postcaldera volcanism**.

(7) The structural setting of the **present-day hydrothermal systems** in the area of study has been revised. It was observed that all larger hydrothermal systems (the Bol'she-Bannaya, Karymshina, and Verkhne-Paratunka ones) **are confined to the boundaries of the Karymshina caldera**.

This work was carried out within the projects of the Far Eastern Branch, Russian Academy of Sciences (project no. 15-I-2-031), and was supported by the Russian Science Foundation (project no. 16-17-10035).

References:

1. Leonov V.L., Rogozin A.N. Karymshina, a giant supervolcano caldera in Kamchatka: boundaries, structure, volume of pyroclastics // J. Volcanology and Seismology. 2007. V. 1. № 5. P. 14-28.
2. Leonov V.L., Bindeman I.N., Rogozin A.N. New data on volcanism before super-eruption and formation of Karymshina caldera (South Kamchatka) // Proceedings of XV Annual Conference, the Day of Volcanology, March 29-30, Petropavlovsk-Kamchatsky city: IVS FEB RAS, 2012. P. 56-63. (in Russian).

3. Leonov V.L., Rogozin A.N., Klyapitsky E.S., Rylova S.A., Leonova T.V. Reconstruction of a giant pyroclastic flow associated with caldera Karymshina, South Kamchatka // Proceedings of XVIII Annual Conference, the Day of Volcanology, March 30 – April 1, 2015. Petropavlovsk-Kamchatsky city: IVS FEB RAS, 2016. In press (in Russian).
4. Rogozin A.N. New data on acid extrusions in the Banno-Karymshinskii area, Kamchatka // J. «Bulletin of Kamchatka Regional Association «Educational-Scientific Center». Earth Sciences». № 10, 2007. P. 156-164. (in Russian).
5. Bindeman I.N., Leonov V.L., Izbekov P.E., et al. Large-volume silicic volcanism in Kamchatka: Ar-Ar, U-Pb ages, isotopic, and geochemical characteristics of major pre-Holocene caldera-forming eruptions // J. Volcanol. Geotherm. Res. 2010. V. 189. № 1-2. P. 57-80.

Geochemistry of eruptive products of Bulganak mud volcano (Kerch Peninsula): Preliminary data and their interpretation

Samoilov D.A.[1], Virshylo A.V.[1]
1-Taras Shevchenko National University of Kyiv, Educational and Scientific Institute «Institute of Geology»,
dmitry.a.samoilov@gmail.com

Studied the geochemical characteristics of volcanic products (mud breccia) of mud volcano Bulganak (Kerch Peninsula). Due to the interpretation and comparison of the received data with the existing data on the stratigraphic complexes was defined level of stratigraphic mobilization for clay material of breccia and established a quantitative assessment of the contribution of various units of section in its formation. The results confirm the current understanding of the intensity of the drainage Maikop deposits (Neogene-Paleogene) and assume the penetration and drainage by root system of volcano the deposits of Cretaceous. Using the method of determining the level of the material by its geochemical features was identified indications and prospects for further application of this method.

Mud volcanoes are common in the Azov-Black Sea, Caspian and other regions of the world, most of which contain oil and gas deposits. The products of their eruptions (mudvolcanic breccia) are derived from substances of different sections of sedimentary complexes. Identifying the roots of mud volcano at a large depth (about 10 km) determine the large vertical area of drainaging sections of sedimentary complexes and gives grounds to believe that the mud volcano's it is the "free exploratory drills" (D.V.Holubyatnikov, 1923). As sources of information about the deep structure of cuts traditionally considered three components of mudvolcanic breccias: 1) matrix (clay fraction with small fragments of rock and single mineral grains), 2) coarse clastic material (large fragments of rock) and 3) small clastic material (individual mineral grains) [1, 3, 4, 5].

The main obstacle to the use of these components as carriers of information about the features and conditions of occurrence of rocks is their integral nature - they were formed as a result of mixing substances of all departments of cut that is drained. Evaluation of the contribution of different sedimentary horizons in the formation of breccia's is an urgent task that previously solved repeatedly [1, 3, 5, 6], but mainly on quality level (was defined belonging of component to one or another sedimentary horizon).

Attempting to assess the quantitative contribution of different sections of sedimentary complexes in the formation of breccia made by us on the example of the component (1) of Bulganak mud volcano eruptive material, that is represented by clay matrix material with small fragments of rock and single mineral grains.

To determine the quantitative contribution of each unit of the sedimentary horizon in the formation of breccia's cones Andrusov and Central Lake (mudvolcanic field Bulganak) were investigated series of samples that characterizing the last eruptions of these cones (the number of samples, respectively, 75 and 25).

For all samples of the material were identified (XRF) concentration of petrogenic and a wide range of microelements, which were matched with existing geochemical data for the sections of Cretaceous and Paleogene-Neogene (Maikop series). In qualitative terms comparable were only data of contents Zn, Zr, Nb, Ga, Sr.

In order to quantify the contributions of each of the sections of sedimentary complexes, that available for comparison, in the formation of the mudvolcanic breccia was solved system with a system of five equations which type is:

$$C_{n1}V_1 + C_{n2}V_2 + C_{n3}V_3 + C_{n4}V_4 + C_{n5}V_5 = 100C_n,$$

one equation for each chemical element, where on indicators of the concentration of each element in five sections of sedimentary complexes (one for Paleogene-Neogene, 4 for Upper Cretaceous), C_{n1}, C_{n2}, C_{n3}, C_{n4}, C_{n5}, and concentrations of the same elements, but only in the mud volcanic breccia (C_n), determined percentage of the material each of the five layers (V_1, V_2, V_3, V_4, V_5) from which composed of breccia, so:

C_{n1} – the concentration of the element «n» in the sedimentary horizon «1», ppm;

V_1 – volume of material of sedimentary horizon «1», that content in mudvolcanic breccia, %;

C_n – the concentration of the element «n» in the mudvolcanic breccia, ppm.

These estimates of contributions of sedimentary complexes in formation of the component (1) of mudvolcanic breccia, received of the using of available geochemical data on sedimentary complexes, realistic and have the following parameters: for eruptive material from Andrusov cone 100% of the total volume are composed with Paleogene-Neogene sedimentary complex (Maikop series); for the cone Central Lake, material composed of "Maikop series" takes 80% and 20% formed by sedimentary complexes of Upper Cretaceous age.

So, the biggest part in the formation of the component (1), matrix of emissions of mudvolcanic fild Bulganak, takes clays of Maikop series Paleogene-Neogenic age. Estimates of contributions made on the basis of geochemical characteristics of mudvolcanic products, allow the possibility of lowering the mobilization level of stratigraphic substances erupted by cones of mud volcano Bulganak to deposits of Upper Cretaceous age (over 4.5 km). For some mud volcanoes of Kerch peninsula on base of paleontological features of coarse clastic material (large fragments of rock) from mud volcanic emissions vas estimated that the deposits of Cretaceous age are drainaging by root system of volcano [2].

For further use of the proposed method required a valid geochemical data on reference sections of sedimentary complexes of region that draining by mud volcanoes structure. This method can be offered to determine stratigraphic level of mobilization for component (2) of the mudvolcanic breccia - coarse clastic material (large fragments of rocks in mud breccia's matrix). The definition of the stratigraphic lavel of coarse clastic material with further determine of quantitative contribution of each sections of sedimentary complex of the cut in the formation of mudvolcanic breccia's may be complementary to already obtained results.

References:

1. Nesterovsky V.A., Titova N.O. Lithological composition of solid emissions hills Andrusov (Bulganak mud volcano) // Geology and Mineral Resources of the World Ocean. – 2012. – №4. – P. 28–33.
2. Titova N.O. Lithological composition of eruption coarse fragments of Dzhou-Tepe mud volcano // Geology and Mineral Resources of the World Ocean. – 2013. – №3. – P. 110–117.
3. Shnyukov E.F., Ivanchenko V.V., Permiakov V.V. Accessory breccia mineralization knoll mud volcanoes of the Black Sea // Geology and Mineral Resources of the World Ocean. – 2014. – №1. – P. 45–68.
4. Shnyukov E.F., Kobolev V.P., Pasynkov A.A. Gas volcanism of the Black Sea. – Kiev: Logos, 2013. – 384 p.
5. Shnyukov E.F., Gnatenko G.I., Nesterovsky V.A. and others. Mud volcanoes of the Kerch–Taman region. – Kiev: Naukova Dumka, 1992. – 200 p.
6. Shnyukov E.F., Naumenko P.I., Y.S. Lebedev and others. Mud volcanism and mineralization. – Kiev: Naukova Dumka, 1971. – 332 p.

The group *Cyanobacteria* in modern taxonomy of living organisms. Use of terms "Algal" and "Microbial"

Sapurin S.A. [1]

[1] *Zavaritsky Institute of Geology and Geochemistry, RAS, Ural branch, Yekaterinburg, sapurin@igg.uran.ru*

Today in a world academic community there is a great interest to the group *Cyanobacteria* and to the sedimentary rocks, related to their activity. The term *Cyanobacteria* has a large number of synonyms such as Cyanoprocaryota, Cyanobionta, Cyanophyta, Blue-Green algae (obsolete term) due to the long development of ideas about their nature. Nowadays cyanobacteria are considered as the *Phylum Cyanobacteria* in the *Kingdom Bacteria* as part of the *Superkingdom Procaryota* (Ruggiero M.A. et al, 2015). However, the uniformity does not exist in the classifications within the phylum, as latter includes quite diverse representatives of bacteria. That's why its taxonomy based primarily on morphological features. These organisms are widespread in a variety of modern environments and presented by unicellular, colonial and multicellular filamentous (sometimes branched) forms.

Cyanobacteria are characterized by the following main features: the lack of the nucleus and some organelles (prokaryote's feature), the photosynthetic and nitrogen-fixation capability, the availability of phycobilin-pigments in cells (phycocyanin and phycoerythrin) in addition to chlorophyll, the presence of peptidoglycan in the cell wall. The cell size is about 1-2 μm up to 40 μm (Madigan M.T. et al, 2012). Furthermore, many cyanobacteria produce extensive mucilaginous envelopes (which consist of extracellular polymeric substances (EPS)), that bind groups of cells or filaments together. These sheaths may become calcified under certain external conditions (Riding, 2011a), that determines the ability of cyanobionta to be fossilized. Thus, the extracellular calcification is the cyanobacterial hallmark from green and red algae.

Taxonomy, based on these and on the molecular genetic characteristics (Komárek J. et al, 2014), creates some problems with classification of paleocyanobacteria, cause last one is possible only on the basis of morphological features. In this way, it will be impracticable to prove systematic affiliation of ancient cyanobacteria, if they had a form different from the modern representatives. Such formations are problematic and are often included in a special category *Calcibionta* (Luchinina, 1991), or *Calcimicrobes*. Currently, this category taxa (genera) are assumed by most researchers to be cyanobacteria (Riding, 2011a; Knoll, 2008; Wood, 1999). In particular, there is no doubt about the tubular forms nature (eg, *Girvanella, Bevocastria, Stipulella*), as, in fact, they are calcified filamentous forms. At the same time, some scientists (Feng et al, 2010; Zhuravlev, 2013) consider dendritic and multi-chambered (hollow-chambered) forms (*Ortonella, Garwoodia, Renalcis, Izhella, Shuguria, Chabakovia* and etc) as microproblematica, cause they don't have modern analogs.

In paleontological studies, especially in Russia, cyanobacteria are often described in association with green and red algae (Ivanova, 2013). *Sensu stricto* algae are considered as plants, but more often they are recognized as a heterogeneous group of organisms, that includes taxa from different kingdoms (*Bacteria* and *Plantae*) and superkingdoms – respectively, *Procaryota* and *Eucaryota* (Vodorosli v evolyutsii biosfery, 2013). That's why "algae" is a collective term, since it brings together a diverse group of organisms, reflecting the unity of Nature. Indeed, cyanobionta and algae are similar in appearance (notably multicellular individuals) and often occupy the same habitats. Nevertheless, in our opinion, it's not rationally to include prokaryotes in algal category, and, after the foreign scientists (Allaby, 1992; Nabors, 2004), we propose to abandon of using this term in point of cyanobacteria. Only photosynthetic eukaryotes may be called algae.

Currently, "microbial" is more general and convenient term, which is widely used in modern literature and means a genetic link of research objects with microorganisms (microbes). It is a fairly sensitive issue that the term "microorganism" counts. If we examine only organisms not visible to the naked eye (natural border in size is less than 0.1 mm), by no means all organisms of one and the same taxon may be account in this category. So, we hold that microorganisms are any objects of microbiology studies (all single-celled organisms and their phylogenetic relatives). Thereby, this group includes *Bacteria* and *Archaea Kingdoms* taxa; simple eukaryotes (called *Protista* and divided by the new taxonomy (Ruggiero M.A. et al, 2015) to *Protozoa* and *Chromista Kingdoms*); or the most primitive (but not necessary single-celled) representatives of the *Plantae, Fungi* or *Animalia Kingdoms* – in other classification systems; and sometimes viruses (Madigan et al, 2012).

As well known, only some of microorganisms may be fossilized. The geological record preserves mainly bacterial forms and algae (Riding, 2011b). Terms "microbial" and "bacterial" are often considered as synonymous (as a rule, in case of stromatolites). But we should not forget that "microbial" is more extensive term. In particular, *Phyla Chlorophyta* and *Rhodophyta* (green and red algae) also comprise this group. Strictly speaking, according to the classic understanding of the term "microorganism", rocks composed predominantly of, for example, diatom skeletons, or little foraminifera and radiolarians can also be considered as microbial. In conclusion, it is important to say that today there is a popular term "microbialite". In narrow sense it is used for deposits of bentic microbial mats (Burne R.V. & Moore L.S., 1987; Riding, 2011b), but in our opinion it is fully applicable for any significantly microbial sediments.

1. It seems most appropriate at this time to consider the conditional category *Calcibionta* as part of cyanobacteria, at least until there will be available such methods or data that would have allowed to identify certain taxa for them.

2. We recommend not to use an obsolete phrase "blue-green algae" for cyanobacteria (term "algae" should be attributed only to eukaryotes, as was mentioned above). Thus, terms "algal" and "bacterial" are separated quite clearly, and both are included in the concept of "microbial".

The author expresses his gratitude to the supervisor, G.A. Mizens for his endless support and assistance, T.I. Stepanova and R.M. Ivanova for introduction to the world of cyanobacteria and M.P. Pokrovsky for invaluable advice and comments on general and the classification issues.

This work was supported by RFBR (grant № 16-35-00263)

References:

1. Allaby M (ed). Algae. The Concise Dictionary of Botany. Oxford: Oxford University Press. 1992.
2. Burne R.V., Moore L.S. Microbialites: Organosedimentary deposits of benthic microbial communities: Palaios, 1987, v. 2, p. 241–254.
3. Feng, Q., Gong, Y.-M. & Riding, R. Mid-Late Devonian Calcified Marine Algae and Cyanobacteria, South-China // Journal of Paleontology. Vol. 84. 2010. N. 4, pp 569-587.
4. Knoll A.H. Cyanobacteria and Earth history // Cyanobacteria. Molecular Biology, Genomics and Evolution. Herrero, A., and Flores, E. (eds). Norfolk: Caister Academic Press, 2008, pp. 335–382.
5. Komárek J, Kaštovský J, Mareš J, Johansen JR. Taxonomic classification of cyanoprokaryotes (cyanobacterial genera) 2014, using a polyphasic approach // Preslia 86, 2014, pp 295–335.
6. Madigan M.T., Martinko J.M., Stahl D.A., Clark D.P. Biology of microorganisms. 13th ed. Brock. 2012. 1155 p.

7. Nabors M. W. Introduction to Botany. San Francisco, CA: Pearson Education, Inc. 2004.
8. Riding R. Calcified cyanobacteria // Encyclopedia of Geobiology, Encyclopedia of Earth Science Series, Springer, Heidelberg, 2011a, pp. 211-223.
9. Riding R. Microbialites, stromatolites and thrombolites // Encyclopedia of Geobiology, Encyclopedia of Earth Science Series, Springer, Heidelberg, 2011b, pp. 635-654.
10. Ruggiero M.A., Gordon D.P., Orrell T.M., Bailly N., Bourgoin T., Brusca R.C., Cavalier-Smith T., M.D. Guiry, Kirk P.M. A Higher Level Classification of All Living Organisms. PLoS ONE, 2015. 10(4). 60 pp.
11. Wood, R.A. Reef Evolution**.** Oxford University Press. 1999. 414 pp.
12. Vodorosli v evolyutsii biosfery. Pod red. S.V. Rozhnova. M.: PIN RAN. 2014. 230s.
13. Zhuravlev A. Yu. Sistematika i paleoekologiya kembriyskikh obyzvestvlennykh «vodorosley» // Vodorosli v evolyutsii biosfery. M.: PIN RAN. 2014. Ss. 38-39.
14. Ivanova R. M. Izvestkovyye vodorosli karbona Urala. Yekaterinburg: UrO RAN. 2013. 244 s. Luchinina V. A. Kal'tsibionty - izvestkovyye vodorosli venda-fanerozoya. Avtoref. diss. doktora geol. nauk. Novosibirsk. IGiG SO RAN. 1990. 33s.

Textures and mineral chemistry in the platiniferous UG-2 chromitite layer at the Khuseleka and the Northam mines, the Bushveld complex, South Africa

Sedunova A.P.[1], Veksler I.V.[1; 2], Zhdanov V.M.[1], Darin A.V.[3], Kazymov K.P.[1], Reid D.[4]

1 – Perm State University, Russia, sedunova.alena.89@ya.ru

2 – German Research Centre for Geosciences GFZ Potsdam, Germany, veksler@gfz-potsdam.de

3 – V.S. Sobolev Institute of Geology and Mineralogy of the Russian Academy of Sciences, darin@ngs.ru

4 – University of Cape Town, Rondebosch, South Africa, david.reid@uct.ac.za

The Early Proterozoic (2.05 Ga [1]) Bushveld Complex is the largest layered mafic-ultramafic intrusion on Earth, with an area extent of 65,000 km^2. The Bushveld Complex has the bowl-shaped form and contains the world's largest reserves of platinum-group metals (PGM), Cr and V.

The economic PGE-bearing orebodies within the Bushveld Complex are the Merensky Reef, the UG-2 chromitite, and the Platreef. The Merensky Reef and the UG-2 are laterally continuous over hundreds of kilometers [2].

Here we present results of a detailed petrographic and mineralogical study of rock textures and mineral chemistry in a vertical profile across the UG-2 chromitite layer at the Khuseleka mine in the south-western part and at the Northam mine in the north-western part of the Bushveld Complex. The study has been carried out on drill core sections.

The drill core BD14-28 from the Khuseleka mine is 1.5 m long and contains the 80 cm thick main chromitite seam underlain by pegmatoidal plagioclase-bearing harzburgite and overlain by medium-grained pyroxenite, which includes a thin (9 cm) leader chromitite seam.

The drill core section BD15-28 from the Northam mine includes the main chromitite seam, which is 80 cm thick and two leader seams above the main layer, 18 cm and 25 cm respectively. The footwall rock is pegmatoidal plagioclase-bearing pyroxenite, which grades downwards into a medium-grained feldspathic pyroxenite. The two leader chromitite seams are separated by 12 cm thick layer of clinopyroxenite and are overlain by coarse-grained felspathic orthopyroxeniteis.

The whole length of the drill core was scanned by X-Ray computer tomograph (XRCT), cut lengthwise into a set of petrographic thin sections, which were used for electron microprobe analyses of the main rock-forming minerals orthopyroxene, plagioclase and Cr-spinel. The thin sections of the drill core BD14-28 were analysed for whole-rock trace element composition by scanning X-ray fluorescence spectrometry (XRF) with synchrotron radiation source.

At both mines, the main chromitite seam is composed of Cr-spinel (51 vol.%), orthopyroxene (20 vol.%) and plagioclase (29 vol.%), and there are sulfides and platinum group minerals (PGMs) in the subordinate quantity. Chromite grains are generally idiomorphic and have grain sizes averaging from 0.04 to 0.5 mm, with some grains up to 1 mm in size. Plagioclase and orthopyroxene in chromitite form large poikilitic grains cementing chromite crystals.

According to electron microprobe analyses of the drill core samples in the Khuseleka mine, Mg# of ortpyroxene from footwall harzburgites and hanging wall pyroxenites is about the same (83-84 and 81-83 respectively) and it is lower than the Mg# of poikilitic orthpyroxene cementing chromite crystals in chromitite seams (89-91). The composition of plagioclase in silicate cumulates and chromitite varies broadly from An_{30} to An_{85}. Poikilitic plagioclase cementing chromitite tends to be depleted in potassium (0.03-0.2 wt.% K_2O) in comparison with plagioclase from pyroxenite (0.15-0.35 wt.% K_2O). Compositions of disseminated chromite crystals from footwall harzburgite and hanging wall pyroxenites vary broadly (Mg# 19-41; Cr# 45-71). Spinel compositions within chromitite seams are much less variable (Mg# 49-53; Cr# 63-65).

Microprobe analyses of the thin sections from Northam shows Mg# of ortpyroxene from footwall and hanging wall pyroxenites is different (66-67 and 68-75 respectively). Ortpyroxene cementing chromite crystals in the chromitite seams have generally lower Mg# (72-89) than Mg# of ortpyroxene in the thin sections of the drill core BD14-28.

Poikilitic plagioclase cementing chromitite tends to be depleted in potassium (0.02-0.19 wt.% K_2O) in comparison with plagioclase from pyroxenite (0.08-0.65 wt.% K_2O). In the upper part of the section alkali feldspar appears (9.9-12.3 wt.% K_2O, up to 3 wt.% NaO). The composition of disseminated chromite grains in the pyroxenites varies broadly (Mg# 8-39; Cr# 45-72). Spinel compositions within chromitite seams are much less variable (Mg# 33-41; Cr# 60-65).

According to our synchrotron-source XRF data for the Khuseleka profile, Zn, Ti, and V are compatible with chromite. Concentrations of incompatible elements Rb, Zr and Y are higher in the hanging wall pyroxenite than in pegmatiodal harzburite below the UG2 layer.

The concentrations of Pd, Cu and Ni show a peak at the top of the main chromitite seam (up to 0.2 wt.% Cu, up to 0.5 wt.% Ni). The peak is associated with local accumulation of sulfide minerals. We observe a distinct covariance between Pd, Cu and Ni, which reflects association of platinum group metals with sulfides (pentlandite is known to be an important mineral host for Pd). Ruthenium has a different distribution compared to palladium. The maximum Ru concentration is observed below the peak of Pd. Ruthenium is known to form a separate phase – laurite (RuS_2), which tends to form inclusions in chromite.

The collected data will hopefully help to develop the understanding of the roles of cumulus and post-cumulus processes in shaping the UG2 chromitite layer and its mineralisation. The project has been sponsored by RSF grant No. 14-17-00200.

References:

1. Scoates, J.S. & Friedman, R.M. (2008). Precise age of the platiniferous Merensky Reef, Bushveld Complex, South Africa., by the U-Pb zircon chemical ID-Tims abrasion technique. Economic Geology, 103, 465-471.
2. Cawthorn R.G. The Bushveld Complex, South Africa // Layered Intrusions. New York, Springer Dordrecht Heidelberg, 2015, pp. 517-588.

Mineralogy of pyroxenite and peridotite xenoliths from magnesian basalts of the Kharchinsky volcano, Kamchatka

Sekisova V. S.

Novosibirsk State University, V. S. Sobolev's Institute of Geology and Mineralogy, vikasekisova@mail.ru

Mantle xenolith study is very important because it provides rare opportunity for insight into composition and structure of the Earth lithosphere. Xenoliths of ultramafic rocks supply information about different processes in the upper mantle and the crust basement.

This work is devoted to xenoliths from the Kharchinsky volcano, located on the eastern part of Kamchatka peninsula. The Kharchinsky volcano is situated in the north of the Central Kamchatkan Depression, which is adjacent to the junction between Kuril-Kamchatka and Aleutian island arcs. The Kharchinsky is late Pleistocene extinct stratovolcano, which is almost entirely composed of magnesian basalts (MgO up to 12.3 wt.%) (Volynets et al., 1998; 1999). Dyke-like body with numerous different xenoliths is observed in the central part of the strongly destroyed summit. This study was based on the representative xenolith samples from this body.

According to mineral composition the studied xenoliths can be subdivided into two groups: peridotites and pyroxenites (Fig. 1). The ultramafic xenoliths exhibit a coarse-grained, granular texture.

Peridotite xenoliths (Fig. 1a) include spinel wehrlite, olivinite in spinel-amphibole wehrlite, spinel harzburgite and amphibole lherzolite. They are mainly composed of olivine, orthopyroxene and clinopyroxene, with accessory spinel varying in composition. Some of them comprise small amounts of apatite, magnetite and sulfides. Moreover the xenoliths have assemblages composed of chlorite, plagioclase, orthopyroxene, potassium feldspar, barite, rarely amphibole, anhydride, phlogopite, etc. They form interstitial segregations and veinlets, which seem to have crystallized in cracks and along olivine grain boundaries.

Pyroxenite xenoliths (Fig. 1b) are represented by olivine-bearing, plagioclase-ore-rich and amphibole species. Clinopyroxenites are characterized by widely varying amounts of hornblende. Besides clinopyroxene and amphibole they comprise plagioclase, potassium feldspar, chlorite, apatite, orthopyroxene, titanite, ilmenite and Ti-magnetite with solid solution break-up lamellas. Large (up to 1 cm) patches containing plagioclase, minor garnet (andradite), epidote, chlorite, magnetite, wollastonite, etc. are presented in one metasomatized clinopyroxenite xenolith and are compositionally similar to calcic skarn.

Therefore in addition to primary minerals (olivine + clinopyroxene ± orthopyroxene + spinel) most of the studied xenoliths have metasomatic assemblages (amphibole + plagioclase + potassium feldspar + magnetite + barite + phlogopite, etc.) as well as secondary mineral such as chlorite.

Common primary mineral of both types of xenoliths is olivine. Olivine is coarse-grained in the peridotite xenoliths and finer in the pyroxenite ones. No compositional zoning was noted. Olivine has Mg# values ranging within 79.0-90.0 in the peridotite xenoliths and 60.2-77.1 in the pyroxenite xenoliths. Both peridotitic and pyroxenitic olivines have low MnO and CoO contents (0.2-0.3 and 0.02-0.03 wt.%, respectively) and are considerably depleted in NiO, CaO, Al_2O_3 and Cr_2O_3. Surprisingly, NiO is almost constantly low, ranging from 0.1 to 0.3 wt.%. This effect is probably related to presence of sulfide minerals in particular pyrrhotite.

Chemical composition of xenolithic clinopyroxene is $En_{23\text{-}46}Fs_{3\text{-}43}Wo_{34\text{-}61}$ with Na_2O up to 1 wt.% in peridotite and $En_{3\text{-}38}Fs_{5\text{-}44}Wo_{39\text{-}61}$ with Na_2O up to 20 wt.% in clinopyroxenite. These compositions fall within the diopside field. The clinopyroxene is characterized by Mg# values of 66.1-91.9 in the peridotite xenoliths, which is slightly higher than those of the pyroxenite xenoliths. Cr# varies widely, reaching values of 55.9 and 40.6 (in peridotite and clinopyroxenite xenoliths, respectively). Clinopyroxene from the skarn-like patches of the clinopyroxenite xenolith has higher FeO content, compared to this mineral in other parts of the xenolith.

Primary orthopyroxene forms large euhedral crystals in spinel harzburgite and amphibole lherzolite. In other xenoliths orthopyroxene is present in veinlets and patches of intensive recrystallization, which is produced due to metasomatism. Orthopyroxene ($En_{53\text{-}84}Fs_{12\text{-}41}Wo_{0\text{-}9}$, Na_2O up to 0.6 wt.%) is represented by enstatite to enstatite-pigeonite compositions (Mg# = 61.5-88.4) with high CaO (up to 2.9 wt.%) contents. Cr# varies widely, reaching values of 36.6 and 1.8 in peridotite and clinopyroxenite xenoliths, respectively.

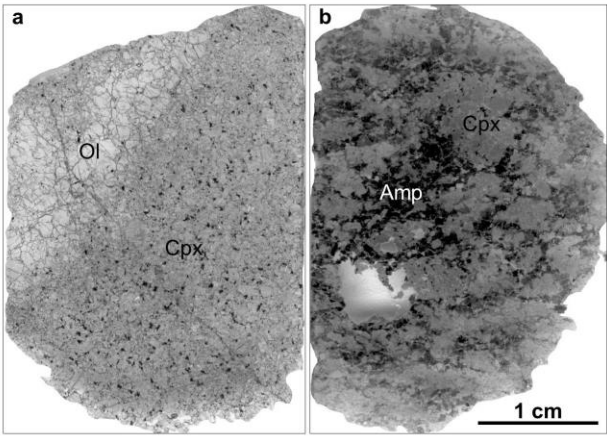

Fig.1 Thin sections of two xenolith groups from the Kharchinsky volcano: a) spinel-hornblende wehrlite with olivinite veinlet; b) hornblende-rich clinopyroxenite.

Oxide crystals can be subdivided into three groups: very large crystals, interstitial grains and relics included in olivine. As a rule several groups can be presented in the same sample. Their compositions vary widely, and oxides form chromite, magnetite, rarely ulvospinel and Al_2O_3-rich hercynite. Chromite occurs predominantly in peridotites, while magnetite prevails in pyroxenites. Chromite and hercynite are sometimes replaced by magnetite. Values of Cr# and Mg# are strongly variable in chromite (up to 75.1 and 61.1), magnetite (up to 84.8 and 26.5) and hercynite (up to 65.5 and 9.8, respectively).

Thus, the studied xenoliths contain two mineral assemblages: primary and secondary. Secondary minerals replace primary assemblages, indicating a metasomatic overprint. Moreover, large sized primary minerals such as olivine and rarely clinopyroxene are intensively fractured, and healed fractures contain abundant fluid and melt inclusions. According to Raman spectra fluid inclusions in clinopyroxene contain CO_2 and H_2O, scanning SEM EDS analyzes indicate presence of silica, calcite, etc. as daughter phases. In addition secondary melt inclusion was found in olivine from the olivinite vein. Its chemical composition is extremely unusual, because silicate glass is characterized by high alkali contents ($Na_2O + K_2O$ = 13.2 wt.%) with relatively low SiO_2 57.3 wt.%, that is similar to alkaline intermediate melts, which nature need to be established.

The majority of the rocks represented by the studied xenoliths are probably cumulates crystallized on intermediate levels, probably at the Moho boundary. Peridotites belong to spinel facies. Both peridotites and pyroxenites experienced intensive metasomatic alteration. Presence of fluid and melt inclusions allow to propose that there was influence of metasomatic media, containing appreciable water and alkali contents.

References:

1. Volynets, O. N., Melekestsev I. V., Ponomareva V. V. and Yogodzinski J. M. (1998) Kharchinsky and Zarechnyi volcanoes, unique centers of Late Pleistocene magnesian basalts in Kamchatka: Tectonic setting, Morphology, Age and Geologic Structure // Volcanology and Seismology. *V*. 20, № 4-5, pp. 383-400.
2. Volynets, O. N., Melekestsev I. V., Ponomareva V. V. and Yogodzinski J. M. (1999) Kharchinsky and Zarechnyi volcanoes, unique centers of Late Pleistocene magnesian basalts in Kamchatka: Composition of erupted rocks // Volcanology and Seismology. *V*. 21, № 1, pp. 45-66.

Isotope-geochemical Nd-Sr evidence of paleoproterozoic magmatism in Fennoscandia and mantle-crust interaction on stages of layered intrusions formation

Serov P.A., Bayanova T.B., Kunakkuzin E.L., Steshenko E.N.

Geological Institute KSC RAS, Apatity, serov@geoksc.apatity.ru

Palaeoproterozoic Fennoscandian layered intrusions belong to the pyroxenite-gabbronorite-anorthosite formation and spread on a vast area within the Baltic Shield. Based on isotope U-Pb, Sm-Nd, Rb-Sr and Re-Os data the duration of this formation can be to 100-150 Ma (2.53-2.39 Ga by U-Pb and Sm-Nd data) [1].

We have studied rocks of layered PGE-bearing Fedorovo-Pansky, Monchetundra, Burakovsky, Olanga group intrusions and Penikat intrusion. According to recent and new complex Nd-Sr-REE data magma source of the vast majority of these intrusions was a mantle reservoir with unusual characteristics (Fig. 1): negative values of εNd (from 0 to -4) and ISr = 0.702-0.706, flat spectra of REE (value of (La/Yb)N ~ 1.0-5.8) with positive Eu-anomalies (Bayanova et al., 2014; Bayanova et al., 2009; Serov, 2008). However, the distribution of REE for ore-bearing gabbronorite intrusions Penikat (Sm-Nd age is 2426±38 Ma (Ekimova et.al., 2011)) has a negative Eu-anomalies. This may be due to the formation of plagioclase and its removal from the magma chamber.

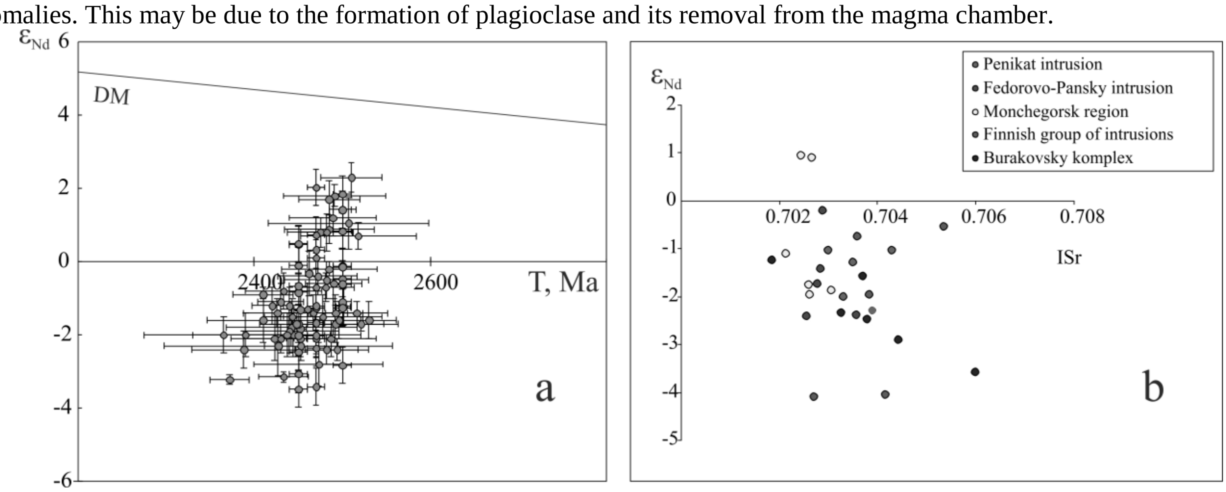

Fig. 1 Variatons εNd(T)-T and εNd(T)-ISr for Palaeoproterozoic Fennoscandian layered intrusions

Numerous publications about sources of a layered intrusions (for example Amelin, Semenov, 1996; Hanski et. al., 1990, Huhma et. al., 1990, 1996; Bayanova et al., 2014; Bayanova et al., 2009; Serov, 2008) as conclusions are two main hypotheses, according to which the studied intrusions could be formed either directly from the anomalous mantle source or there is a negative parameter εNd (T) are related to process of crustal contamination. To estimate the contribution of crustal component the binary mixing model was used (Jahn, Wu, Chen, 2000). As the mantle components we used data for CHUR: εNd = 0, [Nd] = 1.324 (Palm H, O'Neil, 2003) and for crustal components were used host-rocks Nd-data.

The proportion of mantle component for the studied intrusions was 77-99% (Fig. 2). Also, data were obtained for the Monchetundra dike complex and amphibolized gabbro, for which the proportion of mantle material was 20-40%. For these rocks a significant crustal contamination is most likely. This process resulted in low values of εNd, a direct relationship between εNd and Nd concentration, and significant differences between the U-Pb and Sm-Nd model ages. A characteristic feature is that in most cases, the proportion of mantle component decreases from the central parts of intrusions to their boundary zones. This may indicate a slight degree of contamination of the magma intrusion by crustal material near the contacts with the frame- rocks.

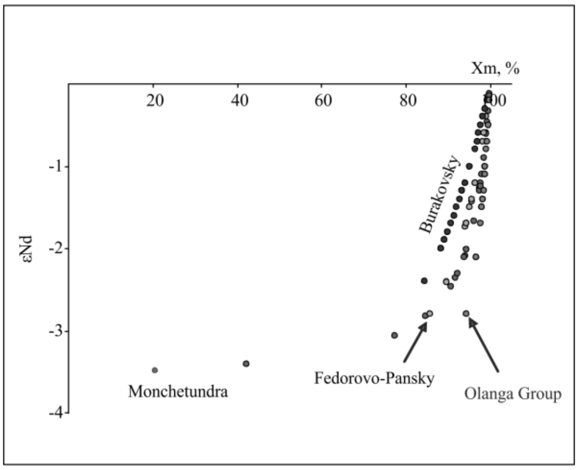

Fig. 2 Mantle component proportion in Palaeoproterozoic Fennoscandian layered intrusions

Thus, our investigations show that Palaeoproterozoic layered PGE-bearing intrusions in the N-E Fennoscandian Shield were derived from intraplate magmatism. The same Palaeoproterozoic layered intrusions are known on the Fennoscandian Shield, Superior and Wyoming provinces of the world, and according to (Heaman, 1997), they were derived from the mantle source which caused the breakup of the oldest supercontinent.

These studies were supported by the RFBR 15-35-20501 mol_a_ved. State assignment theme - № 0231-2015-0005.

Interstitial mineral assemblages in peridotites from cratonic lithospheric mantle roots

Sharygin I.S.[1], Golovin A.V.[1]

1 – V.S. Sobolev Institute of Geology and Mineralogy SB RAS, Novosibirsk, Russia, igor.sharygin@gmail.com

Studies of mantle rocks fragments (i.e. mantle xenoliths) brought to the surface by alkali- basalt and kimberlite magmas provide an unique opportunity to look into the Earth's interior and indicate that the lithospheric mantle has undergone many stages of depletion and enrichment of various elements due to extensive partial melting and metasomatism. It was demonstrated that mantle xenoliths often contain mineral phases which were introduced between rock-forming minerals. The models of formation of interstitial mineral phases in mantle xenoliths may include: 1) decompression melting of primary minerals of xenoliths after trapping by host magmas; 2) partial melting of primary minerals in mantle *in situ*; 3) metasomatic events in mantle before trapping by host magma (i.e. mantle metasomatism); 4) infiltration of the host melt into xenoliths during transport to the surface or at the subsurface conditions. Thus, interstitial mineral phases can be useful for understanding the compositions of mantle fluids or melts and their role in modifying of mantle rocks *in situ* and during transport to the surface.

Peridotites of cratonic lithospheric mantle (CLM) are represented by two texturally distinct types: granular and sheared (porphyroclastic). In contrast to granular type sheared peridotites displays a bimodal grain size with large porphyroclasts resides in fine neoblasts matrix. Sheared peridotites usually have higher *P-T* conditions of equilibrium than granular type and it is suggested that they originated from the lower part of CLM. The evidences of partial melting and metasomatism in sheared peridotite are recorded in their major and trace element signatures (Schmidberger and Francis, 2001; O'Reilly and Griffin, 2010; Agashev et al., 2013). However, the studies of interstitial mineral phases in sheared peridotites are rare.

Here we provide preliminary report on detailed study of the interstitial mineral assemblages in the sheared peridotites from the uniquely fresh kimberlites of Udachnaya-East pipe (Siberian craton). The xenoliths have rounded, ellipsoidal shapes and are large, 10-25 cm in size. The sheared peridotites show porphyroclastic to fluidal-mosaic-porphyroclastic textures. The rock-forming (primary) mineral assemblages of the sheared peridotites are olivine (Fo_{86-91}) + orthopyroxene + garnet ± clinopyroxene. The porphyroclasts and neoblasts of both olivine and pyroxene have identical composition for a certain sample. The primary mineral assemblages of the sheared peridotites were equilibrated in the mantle at 1150-1400 ^{o}C and 6.0-7.5 GPa, corresponding to depths of 180-230 km. Primary mineral assemblages of the sheared peridotites also include blebs of Fe-Ni-Cu sulfides enclosed in rock-forming minerals (Fig. 1a) and in intergranular regions.

In the sheared peridotite we have found interstitial mineral assemblages which include olivine (Fo_{93-94}), clinopyroxene, monticellite, mica, humite, clinohumite, calcite, zoned spinel, calcite, pentlandite, pyrrhotite and djerfisherite ($K_6(Na,Cu)(Fe,Ni,Cu)_{24}S_{26}Cl$). These late interstitial minerals are mostly localized in triple-junctions between both porphyroclasts and neoblasts of rock-forming minerals; less frequently they occur along grain boundaries. Djerfisherite was also observed as rims around blebs of primary Fe-Ni-Cu sulfides. Interstitial olivine and clinopyroxene notably differs in composition from primary ones. Spinel are usually zoned, the core is chromite and the rim is magnetite. Interstitial mica is represented by phlogopite and tetraferriphlogopite.

The interpretation of deformation features suggests that porphyroclastic texture of sheared peridotites results from the recrystallization of granular peridotites under a very high-stress and high strain-rate deformation; the preservation of deformation features implies that recrystallization was essentially contemporaneous with the entrainment of xenoliths by kimberlite magma (O'Reilly and Griffin, 2010). The presence of the studied interstitial minerals between both porphyroclasts and neoblasts of rock-forming minerals indicates their close connection with kimberlite magmatism. Relationship between the interstitial minerals demonstrates that they most likely crystallized during the same process. Mineralogy of the interstitial assemblages, except some minerals, resembles the groundmass of host kimberlites (Sharygin et al., 2007; Kamenetsky et al., 2012). Moreover, compositions of the some minerals from the interstitial assemblages are similar to those of the kimberlite groundmass of the Udachnaya-East pipe. These facts suggest that the origin of the studied interstitial mineral assemblages in the sheared peridotite is the result of infiltration of transporting kimberlite melt into xenoliths. The majority of interstitial minerals crystallized directly from kimberlite melt, but djerfisherite rimming primary Fe-Ni-Cu sulfides is the product of their reaction with kimberlite melt.

In the sheared peridotites interstitial perovskite is a main storage of LREE, Nb and Ta, calcite – Sr, djerfisherite – K, mica – K, Rb and Ba. The presence of these kimberlite-related interstitial minerals may have an essential influence on the bulk trace-elements composition of mantle xenoliths. This fact should be considered when we use bulk geochemical characteristics of mantle xenoliths for interpretation of processes in CLM.

This work was supported by grants from the Russian Foundation for Basic Research (16-35-60052 mol_a_dk) and the President of the Russian Federation (MK-4534.2016.5).

References:

1. Agashev, A.M., Ionov, D.A., Pokhilenko, N.P., Golovin, A.V., Cherepanova, Y., Sharygin, I.S., 2013. Metasomatism in lithospheric mantle roots: Constraints from whole-rock and mineral chemical composition of deformed peridotite xenoliths from kimberlite pipe Udachnaya. Lithos 160-161, 201-215.
2. Kamenetsky, V.S., Kamenetsky, M.B., Golovin, A.V., Sharygin, V.V., Maas, R., 2012. Ultrafresh salty kimberlite of the Udachnaya-East pipe (Yakutia, Russia): A petrological oddity or fortuitous discovery? Lithos 152, 173-186.
3. O'Reilly, S.Y., Griffin, W.L., 2010. The continental lithosphere-asthenosphere boundary: Can we sample it? Lithos 120, 1-13.
4. Schmidberger, S.S., Francis, D., 2001. Constraints on the trace element composition of the Archean mantle root beneath Somerset Island, Arctic Canada. Journal of Petrology 42, 1095-1117.
5. Sharygin, V.V., Golovin, A.V., Pokhilenko, N.P., Kamenetsky, V.S., 2007. Djerfisherite in the Udachnaya-East pipe kimberlites (Sakha-Yakutia, Russia): paragenesis, composition and origin. European Journal of Mineralogy 19, 51-63.

New data on mineralogy of alnöitic rocks from Malaita, Solomon Islands

Sharygin I.S.[1], Litasov K.D.[1,2], Gryaznov I.A.[1,2], Ishikawa A.[3]
1 V.S. Sobolev Institute of Geology and Mineralogy SB RAS, Novosibirsk, Russia, igor.sharygin@gmail.com,
2 Novosibirsk State University, Novosibirsk, Russia, 3 – The University of Tokyo, Tokyo, Japan

The island of Malaita, Solomon Islands, is the exposed SW margin of Ontong Java Plateau, and represents locations of 34-Ma deep mantle-derived magmatic rocks, alnöites, emplaced in essentially oceanic environment. The alnöites form pipe-like bodies and sills, and contain a rich and varied suite of mantle xenoliths which are similar to those found in kimberlites. The PT-estimates on the mantle xenoliths constrain the formation depth of alnöitic magma as > 120 km. Despite mantle xenoliths have been investigated by many authors, there are only three paper focused on magmatic mineralogy (phenocrystic and groundmass) of Malaitan alnöites (Allen and Deans, 1965; Dawson et al., 1978; Nixon et al., 1980).

To date, mineralogical studies were done for alnöitic rocks from Babaru'u locality (Allen and Deans, 1965; Dawson et al., 1978; Nixon et al., 1980). Two types of alnöitic rocks were defined: aphanitic and fragmental ones. The former are compact black rocks. The latter was interpreted as tuffs or breccias, containing fragments of alnöites (lapilli) cemented by cream calcite matrix. Nixon et al. (1980) summarized primary mineralogy of alnöitic rocks from Babaru'u: olivine (Fo_{85}), clinopyroxene (diopside-sahlite), natro-melilite (1/3 melilite – 2/3 akermanite), phlogopite, perovskite, spinel (ulvospinel-magnetite series) and accessory nepheline, melanite, and apatite. This magmatic assemblage almost resembles term ALNÖITE from glossary of IUGS – an ultramafic rock with phenocrysts of phlogopite-biotite, olivine and augite in a groundmass of melilite (often altered to calcite), augite and/or biotite with minor perovskite, garnet and calcite.

Here we present preliminary results of the study of magmatic mineralogy of alnöites from other locality along the Auluta river, obtained by scanning electron microscopy combined with energy-dispersive microanalyses. Studied samples represent fragmental alnöitic rocks and consists of discrete mineral grains (xenocrysts or large phenocrysts) and fragments of alnöites set in calcite matrix. Calcite matrix also contains barite and chlorite. Olivine, melilite, nepheline and melanite were not found in alnöitic fragments. Olivine is probably completely altered. Euhedral fragments of calcites containing magnetite veins were interpreted as pseudomorphs after melilite phenocrysts; these fragments host amphibole inclusions. Among other phenocrystic minerals augite, phlogopite-biotite mica, and amphibole were identified. Groundmass consists of amphibole, mica, apatite, zoned spinel (ulvospinel-magnetite-spinel-chromite series), perovskite, calcite and chlorite.

Basically, the primary mineralogy of studied samples are similar to alnöitic rocks from Babaru'u. The new findings of our study is the detection of amphibole as phenocrystic and groundmass mineral in Malaitan alnöites. Phenocrystic amphibole contains crystalline inclusions of augite and Ti-Cr-magnetite whereas groundmass zoned spinels hosts amphibole inclusions. These observations suggest magmatic origin of amphibole. Additionally, amphibole phenocrysts display complex zoning pattern (from core to rims: Ti, Al, Fe and Ca increase; Si, Cr, Mg and Na decrease). Amphibole is uncommon in alnöites worldwide. The origin of both calcite matrix and groundmass calcite (magmatic or secondary) in Malaitan alnöites is unclear from our observations and requires further studies.

The work is supported by the Russian Foundation for Basic Research (grant no. 16-05-01079 a) and the Ministry of education and science of the Russian Federation (project no. 14.B25.31.0032).

References:

1. Allen, J.B., Deans, T., 1965. Ultrabasic eruptives with alnöitic-kimberlitic affinities from Malaita, Solomon Islands. Mineralogical Magazine 34, 16-34.
2. Dawson, J.B., Delaney, J.S., Smith, J.V., 1978. Aspects of the mineralogy of alnöitic breccia, Malaita, Solomon Islands. Contributions to Mineralogy and Petrology 67, 189-195.
3. Nixon, P.H., Mitchell, R.H., Rogers, N.W., 1980. Petrogenesis of alnöitic rocks from Malaita, Solomon Islands, Melanesia. Mineralogical Magazine 43, 587-596.

Determination of redox conditions for Island-arc magmas using partitioning of vanadium between olivine and silicate melt: experimental and natural data for Mutnovsky volcano (Kamchatka)

T.A.Shishkina T.A., Portnyagin M.V.
GEOKHI RAS (Moscow), t.shishkina@geokhi.ru

Redox conditions have strong effect on fractionation processes in magmatic systems since they affect the order of appearance, proportions and composition of liquid, crystal and volatile phases by affecting the valent state of a number of elements such as Fe, S, V, Cr, C and others. A number of oxygen geobarometers have been proposed to quantify the redox conditions (oxygen fugacity, fO_2) in basaltic systems. The barometers are based on various mineral-mineral or mineral-melt equilibria [e.g. Ballhaus et al., 1991; Spencer&Lindsley, 1981; Sato, 1989; Ryabchikov&Kogarko, 2010] or speciation of polyvalent elements (Fe, S etc) in silicate melts/glasses [e.g. Sack et al., 1980; Jugo et al., 2010].

A promising method for fO_2 determination in basalts, which might be applied to quenched melt inclusions in olivine, exploits the partitioning of vanadium between olivine and coexisting silicate melt ($D_V^{Ol\text{-}M}$). A number of experimental works (Canil, 1997; 2002; Canil&Fedortchouk, 2001; Mallmann&O'Neill, 2009; 2013; and others) showed that $D_V^{Ol\text{-}M}$ for mafic or ultramafic melts correlates strongly with fO_2 and can be used for oxybarometry.

Most published vanadium partitioning data were obtained for high MgO-melts (komatiites, primitive martian basalts, CMAS etc.) at pressures of 1 atm and 0.5 – 2 GPa. The investigated range of oxygen fugacity is between ΔQFM = -13.5 to +10 (ΔQFM is oxygen fugacity deviation from quartz-fayalite-magnetite buffer expressed in $\lg fO_2$ units. The temperature range is mostly between 1200 to 1530°C. Only a few melt compositions with MgO < 11 wt.% equilibrated with olivine at T< 1200°C were studied so far. These experiments were performed using Hawaiian tholeiitic basalt (Canil and Fedortchouk, 2001), MORB and island-arc-type basaltic andesite (Laubier et al., 2014). Although it was shown that melt composition, pressure and temperature have negligible (Canil, 1997; Canil and Fedortchouk, 2001) or small effect (Mallmann&O'Neill, 2013) on $D_V^{Ol\text{-}M}$, more data is required to extend the calibration of the oxybarometer to low-temperature field corresponding the prevailing conditions in island arcs.

This study presents new data on $D_V^{Ol\text{-}M}$ in the products of phase relations experiments performed with high-Al basalt from Mutnovsky volcano (Kamchatka) at various aH_2O, 0.1 and 0.3 GPa, 1025-1150°C and ΔQFM= -0.5 to +3.2. Concentrations of vanadium in experimental and natural glasses and olivine were analyzed by LA-ICP-MS using Agilent 7500s quadrupole mass-spectrometer coupled with 193nm Excimer Laser-Ablation system GeoLasPro (Coherent) at the Institute of Geosciences of the Christian-Albrechts University of Kiel. $D_V^{Ol\text{-}M}$ were estimated to vary between 0.007 and 0.079 and showed a strong linear correlation with ΔQFM in experiments (Fig. 1).

The compilation of previously published experimental data shows well pronounced temperature effect on $D_V^{Ol\text{-}M}$ (Fig. 1). At given ΔQFM, $D_V^{Ol\text{-}M}$ increases with decreasing temperature. Therefore, for calibration of oxybarometer for low temperature basaltic magmas, we selected 65 experiments performed at T <1275°C and with MgO < 14 wt.% and Na_2O < 6 wt.% including our data. Resulting linear correlation between $D_V^{Ol\text{-}M}$ and ΔQFM can be described with an equation

(1): $\Delta QFM = -4.05 * lgD_V^{Ol\text{-}M} - 4.82$ ($R^2 = 0.93$, n=65). The equation reproduces experimental ΔQFM conditions within ± 0.55 log units for 70% of experiments.

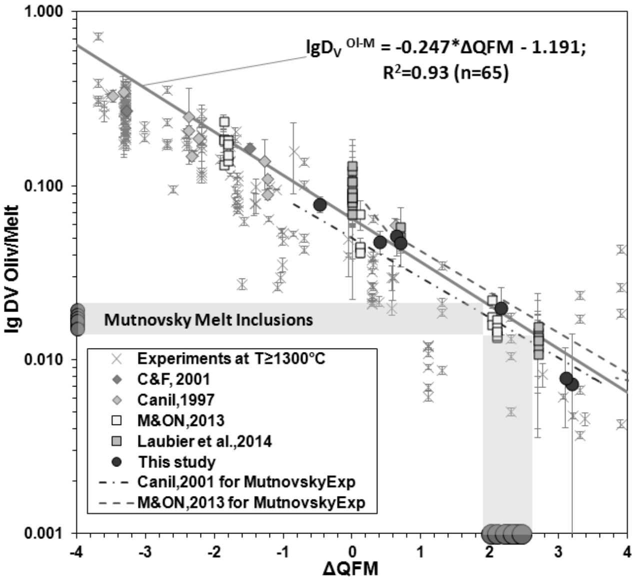

Fig. 1 Covariation of $D_V^{Ol\text{-}M}$ and ΔQFM according to published experimental data and data from this study. ΔQFM estimate for Mutnovsky melt inclusions in olivine is shown by shadowed bar.

The equation was applied to estimate the redox conditions of crystallization for Mutnovsky volcano magmas. With this goal, we have analysed melt inclusions in olivine from basaltic tephras erupted from the late Pleistocene cone on the southern slope of Mutnovsky volcano. Vanadium concentrations vary between 266 and 382 ppm in naturally quenched glassy inclusions and between 4.2 and 6.1 ppm in their host olivines. This corresponds to $D_V^{Ol\text{-}M}$ = 0.0152 - 0.0185 (Fig. 1). The calculated ΔQFM values range from +2.0 to +2.4. The estimates are within 1 log unit of fO_2 and lie between those obtained using oxybarometers proposed by Canil and Fedortchouk (2001) and Mallmann and O'Neill (2013) (Fig. 1).

The new formulation of the V-in-olivine oxybarometer proposed in our study uses all published and also new experimental data relevant for island-arc magmas and can be applied to estimate the redox conditions of their crystallization.

The work was supported by the Russian Science Foundation grant no. 14-17-000582.

References:

1. Canil, D. (1997). Nature, v.389, p.842-845;
2. Canil, D. & Fedortchouk, Y. (2001). Canadian Mineralogist, v.39, p.319-330;
3. Laubier M., Grove T.L., Langmuir C.H. (2014) EPSL, v.392, p.265-278;
4. Mallmann, G. & O'Neill, H. St.C. (2009). Journal of Petrology, v.50, p.1765-1794;
5. Mallmann, G. & O'Neill, H. St.C. (2013) Journal of Petrology, v.54 (5) , p.933-949;
6. Ryabchikov, I.D. & Kogarko, L.N. (2010) Petrology, v.18 (3), p.239-251;

7. Ballhaus C., Berry R.E., Green D.H. (1990) Nature, v.348, p.437-440;
8. Jugo P.J. (2009) Geology, v.37, p.415-418;
9. Sato, H. (1989) Proc. Ocean Drill. Prog. Sci. Res., v.11, p.17-26;
10. Spencer, K. J. and Lindsley, D. H. (1981) American Mineralogist, v.66, p.1189-1201;
11. Sack RO, Carmichael ISE, Rivers M, Ghiorso MS (1980) Contrib Mineral Petrol, v.75, p.369-376.

Cr-rich phases in the MgO-SiO2-Cr2O3 system at 10-24 GPa: composition, solid solutions, and structural features

E. A. Sirotkina1,2*, A. V. Bobrov1,2, L. Bindi3, T. Irifune4

*1 -Moscow State University, Russia (*correspondence: katty.ea@mail.ru, archi3@yandex.ru)*

2 -Vernadsky Institute of Geochemistry and Analytical Chemistry of Russian Academy of Sciences, Moscow, Russia

3 -University of Florence, Italy (luca.bindi@unifi.it)

4 -Ehime University, Japan (irifune@dpc.ehime-u.ac.jp)

Despite significant interest of experimentalists to the study of geophysically important phase equilibria in the Earth's mantle and a huge experimental database on a number of the model and multicomponent systems, incorporation of minor elements in mantle phases was studied only on a qualitative level. The influence of such elements on structural peculiarities of high-pressure phases is poorly investigated, although incorporation of even small portions of them may have a certain influence on the PT-parameters of phase transformations. Chromium is one of such elements with the low bulk concentrations in the Earth's mantle (0.42 wt % Cr_2O_3) [Ringwood, 1966], although some mantle phases are characterized by significant Cr content. Our experiments were aimed on the study of phase relations in the MgO-SiO_2-Cr_2O_3 system at 10–24 GPa and 1600 °C. The experiments were performed using a 2000-t Kawai-type multi-anvil high-pressure apparatus at the Geodynamics Research Center (Ehime, Japan).

The ***Maj–Knr system*** was selected because an association of Knr-garnets with natural diamonds is quite abundant. The main phases obtained in experiments were pyroxene, Knr-Maj garnet, Cr-bearing akimotoite and bridgmanite, eskolaite, $MgCr_2O_4$ with the calcium titanate-type structure, and stishovite.

Our interest to experimental study of the ***Fo – MChr system*** is explained by wide abundance of $(Mg,Fe)_2SiO_4$ polymorphs in the Earth's mantle. The phases synthesized in system include Cr-bearing olivine (*Ol*), wadsleyite (*Wad*), ringwoodite (Rgw), bridgmanite, $Mg_2Cr_2O_5$ with the modified ludwigite-type structure, $Mg(Mg,Cr)(Mg,Si)O_4$ with the distorted calcium titanate-type structure [9], *Knr-Maj* garnet, $MgCr_2O_4$ with the spinel-type (*MChr*) and calcium titanate-type (*Ct*) structures [10], eskolaite, and periclase (*Per*).

Single-crystal X-ray diffraction studies were carried out to determine the symmetry and study the structural peculiarities of the synthesized Cr-rich phases. All garnets synthesized at 10-21 GPa are characterized by a silicon surplus over 3.0 a.p.f.u. and high chromium content (up to 90 mol. % *Knr*). Cr is incorporated in garnet via the scheme: $Mg^{2+}+Si^{4+}=2Cr^{3+}$. All garnets have cubic symmetry (space group *Iad*) and the lattice parameter linearly increases with increasing the *Knr* content. Cr-*Ak* has the chemical composition of $(Mg_{1-x}Cr_x)(Si_{1-x}Cr_x)O_3$ (with x = 0.015, 0.023 and 0.038) and trigonal symmetry. Compared with $MgSiO_3$-*Ak*, the occurrence of Cr leads to a general expansion of the unit cell (*a* from 4.7284(4) to 4.7380(1) and *c* from 13.5591(16) to 13.5611(2) Å). *Brd* synthesized at pressures above 20 GPa have a composition of $(Mg_{1-x}Cr_x)(Si_{1-x}Cr_x)O_3$ with x=0-0.07, orthorhombic symmetry (space group *Pbnm*) and the following lattice parameters for x=0.07: a = 4.8213(5), b = 4.9368(6), c = 6.9132(8) Å. For both Cr-minerals (Cr-*Ak* and Cr-*Brd*), chromium was found to substitute for both Mg and Si, according to the reaction $Mg^{2+}+Si^{4+}=2Cr^{3+}$.

Rgw has the *Sp*-type structure and, that is why, we suggest the following mechanism of Cr incorporation in this phase: Mg substitutes Si in the tetrahedral site, whereas all Cr enters Mg-octahedrons by the following scheme: $2^{VI}Cr^{3+}+^{IV}Mg^{2+}=2^{VI}Mg^{2+}+^{IV}Si^{4+}$. Gudfinnsson and Wood (1998) proposed the same mechanism of Cr incorporation in Wad. We may suggest the different mechanism: $^{VI}Cr^{3+}+^{IV}Cr^{3+}=^{VI}Mg^{2+}+^{IV}Si^{4+}$. Both of these mechanisms are supported by the negative correlation of Cr with Si and Mg in *Wad* with a slope of -0.5.

Experimental study of the simplified model systems *Maj–Knr* and *Fo–MChr* allowed us to consider the influence of chromium on crystallochemical peculiarities of the major mantle phases and on the phase transformations. We established significant changes in cell parameters with increasing Cr concentrations and cordially different reactions of akimotoite and bridgmanite polyhedrons on Cr incorporation. Because of this, while modeling of the composition and properties of the Earth's mantle we should account for the influence of Cr on mantle phases, since even very low concentrations of this element may change the cell volumes significantly and a number of other physical properties, such as density and thermoelastic properties of deep minerals.

This study was supported by the Russian Foundation for Basic Research (project no. 16-35-00171)

Petrography and mineralogy of ultramafic lamprophyre from the Ilbokicheskaya Occurrence, SW Siberia

Smirnova M.D.[1]

1 – Lomonosov MSU, petitmx@gmail.com

This paper will be discussed ultramafic lamprophyre (UML) samples from the Ilbokicheskaya occurrence, which is located in Ilbokicheskoe gas condensate field of the Irkineevo-Chadabets rift of the Siberian platform (fig.1). In previous work (Kargin et al., 2016), the rocks were dated as 391.7±1.9 Ma, which is middle Devonian. All economic-importance kimberlite pipes of the East Siberia are Devonian in age. The Ilbokicheskaya occurrence is the first manifestation of Devonian UML magmatism in SW Siberia. Hence, the origin of the rocks is very important to predicting of diamond-bearing rocks.

Our studies allow us to classify the dike's rocks as aillikites (Tappe et al., 2005; Le Maitre et al., 2002, Francis et al., 2009) according to their mineral and chemical composition. There is no classification name for rock with mineral composition like Ilbakicheskaya's rocks in Russian Petrographic Codecs, but the most suitable are olivine-phlogopite carbonatites, alnoites or orangeites .

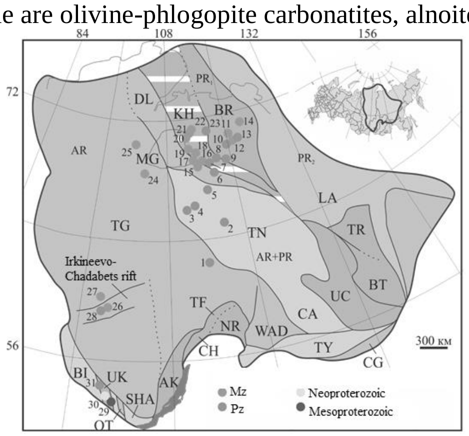

Fig. 1 The geological map of SW Siberia with ages of kimberlites. After Kargin et al, 2016.

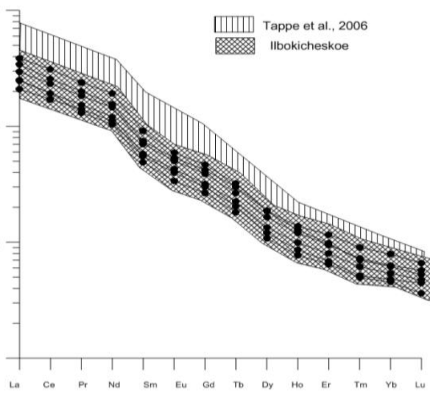

Fig. 2 C_I-normalized REE element diagrams for aillikites from Ilbokicheskoes, and (Tappe et al., 2006). C_I values are after (Sun and McDonough ,1989).

Bulk rock composition is characterized by high content of CO_2 (up to 20 wt. %), CaO (12-22 wt.%), low silica content (up to 35 wt.%). Depending on the amount of carbonate is a relatively wide concentration range of MgO (10-20 wt.%), Fe_2O_3t(7-12 wt.%) and SrO (600-4000 ppm). REE pattern (fig.2) is similar to UML and particularly aillikite distribution of REE (Tappe et al., 2006). In a few samples there is a Zr-Hf minimum, which is characterized aillikites.

The rocks have different texture and mineral composition. The samples from contact zone between aillikites and host rock (limestones) normally have altered olivine phenocrysts, which substituted by calcite and metasomatic pyroxenes, with rims (up to 0.5 mm) of phlogopite, celadonite, perovskite, and calcite as a groundmass. Rarely metasomatic garnet can be found, and it substitutes calcite in groundmass. The contact zone consists of calcite (50%), olivine (30%), phlogopite (15%), other about 5% in sum. Spheroidal structures caused by immiscibility are observed in narrow part of the contact zone directly adjoining the host rock.

Central part of dykes is characterized by partly or fully altered olivine phenocrysts, more phlogopite in ground mass, fewer amount of carbonate, which contents more Mg, Fe, Mn (up to 25 wt.% in sum.). Apatite can be presented in rock up to 5%, pyroxenes – 3%.There are no celadonites, garnets and spheroidal carbonates, but there is rare K-feldspar in groundmass. The compounds of central zone are olivine (35%), phlogopite (35%), calcite and Fe-Mg-Ca carbonate (25%), other about 5% in sum.

Olivine has microinclusions of (Fe, Ni)S_2 in every sample, either altered olivine. Perovskite is substituted by ilmenite and TiO_2. The garnet is androdite with high Ti content (up to 16 wt. %). The calcite spheroidals appear only in rims around altered olivine.

In this work we describe the very first data about petrological and mineralogical features of Devonian UML from the Irkineevo-Chadabets rift of the SW Siberia. As shown by our research the rocks from the Ilbokicheskaya occurrence are magmatic, and the rocks have to be classified as aillikites .They were altered by autometasomatic process at late magmatic stage.

Reference:

1. Francis D., Patterson M. Kimberlites and aillikites as probes of the continental lithospheric mantle //Lithos. – 2009. – T. 109. – №. 1. – C. 72-80.

2. Kargin et al. Devonian ultramafic lamprophyre from the Irkineevo-Chadabets rift of SW Sideria: age, composition and meaning for prediction of diamondiferous.//Geology of Ore Deposits. – 2016. In press.
3. Le Maitre R. W. et al. Igneous rocks. A classification and glossary of terms. Recommendations of the IUGS Subcomission on the Systematics of Igneous Rocks. – 2002.
4. Tappe S. et al. Integrating ultramafic lamprophyres into the IUGS classification of igneous rocks: rationale and implications //Journal of Petrology. – 2005. – T. 46. – №. 9. – C. 1893-1900.
5. Tappe S. et al. Genesis of ultramafic lamprophyres and carbonatites at Aillik Bay, Labrador: a consequence of incipient lithospheric thinning beneath the North Atlantic craton //Journal of Petrology. – 2006. – T. 47. – №. 7. – C. 1261-1315.
6. Sun S. S., McDonough W. F. Chemical and isotopic systematics of oceanic basalts: implications for mantle composition and processes //Geological Society, London, Special Publications. – 1989. – T. 42. – №. 1. – C. 313-345.

Equation of state of fayalite at high temperature and pressure

Sokolova T.S.[1], Dorogokupets P.I.[1], Litasov K.D.[2,3]

1 – Institute of the Earth's Crust SB RAS, sokolovats@crust.irk.ru , dor@crust.irk.ru

2 – V.S. Sobolev Institute of Geology and Mineralogy SB RAS, klitasov@igm.nsc.ru

3 – Novosibirsk State University

The (Mg,Fe)-silicates are minerals of olivine group with general formula X_2SiO_4, which have a major mineralogical and geophysical significance for high-temperature and high-pressure studies. Forsterite (α-Mg_2SiO_4) and fayalite (α-Fe_2SiO_4) are magnesium and ferrous end-members of olivine, which are the most abundant phases in the Earth's upper mantle. It was found that alpha olivine phases undergo transition to spinel structure at high pressure. The ringwoodite or gamma phase of olivine is a stable modification up to lower boundary of the upper mantle at the depth ~670 km. Our recent study of transition ringwoodite into the mixture of bridgmanite and magnesiowüstite in magnesium system only ($MgSiO_3$–MgO) does not explain jumps of density and bulk modulus within this depth interval [Dorogokupets et al., 2015]. Therefore, it is needed to study olivine solid solutions with a Fe content.

Numerous experimental studies of fayalite (review in [Jacobs et al., 2001]) have shown that transition of α-Fe_2SiO_4 into γ-Fe_2SiO_4 appears at pressures higher than 4–5 GPa and at temperatures 700–1300 K [Yong, 2008]. The recent paper has predicted the following structural change in γ-Fe_2SiO_4 under very high pressure up to 64 GPa [Yamanaka et al., 2015]. There is a transition of the cubic spinel structure to a body centered orthorhombic phase I-Fe_2SiO_4. The main idea of this work is to provide reliable thermodynamic properties of fayalite at high temperature and pressure, which would be the base for future calculations of the high-pressure phases in the system $FeSiO_3$–FeO.

Equation of state of fayalite is constructed using the modified thermodynamic model based on the Helmholtz free energy [Dorogokupets et al., 2014, 2015]. The pressure at the reference isotherm 298.15 K is determined from Kunc equation [Kunc et al., 2003]:

$$P_{298}(V) = 3K_0 X^{-k}(1-X)\exp[\eta(1-X)], \quad (1)$$

where $X = (V/V_0)^{1/3}$, $\eta = 1.5K' - k + 0.5$.

The thermal part of the Helmholtz free energy can be represented as a sum Einstein temperature contribution and contribution of intrinsic anharmonicity [Zharkov, Kalinin, 1971]:

$$F_{th}(V,T) = m_i RT\ln[1-\exp(-\Theta_i/T)] + (-3/2nRa_0x^mT^2), \quad (2)$$

where, $m_1 + m_2 = 3n$ (i = 1, 2), n is the number of atoms in the chemical formula, R is the gas constant, $x = V/V_0$, a_0, and m are fitted parameters.

We use two Einstein temperature in eq. (2) because it allows more accurately approximation of the heat capacity of fayalite to the molten temperature. The low temperature λ transition in the heat capacity of fayalite is fixed by calorimetric measurements. It can be considered in our model by the magnetic contribution to the Helmholtz free energy, according [Dinsdale, 1991]:

$$F_{mag}(T) = 2RT\ln(B_0+1)(g(\tau)-1), \quad (3)$$

where B_0 is the average magnetic moment per atom, $\tau = T/T_C$, and T_C is the Curie temperature.

The characteristic temperature Θ_i in eq. (2) is depended on volume and obtained by integration of the Grüneisen parameter, which expressed as [Al'tshuler et al., 1987]:

$$\gamma = \gamma_\infty + (\gamma_0 - \gamma_\infty)x^\beta. \quad (4)$$

Summing the corresponding functions, we have obtained a complete thermodynamic description of equation of state. We are simultaneous optimized experimental measurements of heat capacity, thermal expansion, adiabatic bulk modulus, and *P-V-T* properties of fayalite and obtained the following parameters of EOS: V_0 = 46.27 cm^3mol^{-1}, K_0 = 134.9 GPa, K' = 5.26, Θ_{o1} = 754 K, m_1 = 11.5, Θ_{o2} = 225 K, m_2 = 9.5, γ_0 = 1.112, β = 0.4, a_0 = 69.5, m = 1, B_0 = 1.56, and p = 0.18. The difference between observed and calculated pressure from equation of state is consistent with *P-V-T* measurements within $\Delta P/P = \pm$ 4% up to 1273 K (Fig. 1).

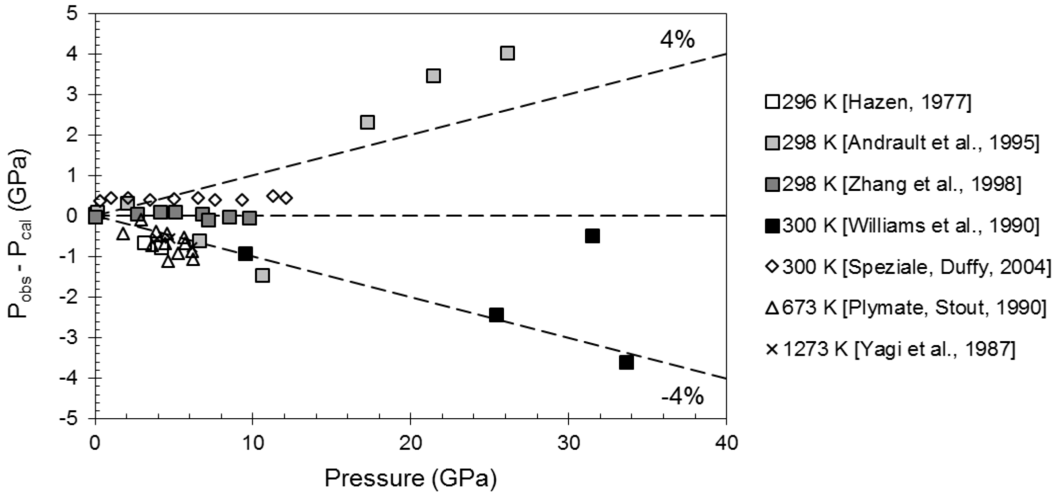

Fig. 1. Difference between observed pressure (P_{obs}) and calculated pressure (P_{cal}) from the equation of state of fayalite at the isotherms 296 to 1273 K.

The work was supported by the Russian Foundation of Basic Research (project no 16-35-00061) and the Russian Scientific Fund (project no 14-17-00601), and conducted under the program of the Ministry of Education and Science of the Russian Federation (project no 14.B.25.31.0032).

References:

1. Al'tshuler L.V., Brusnikin S.E., Kuz'menkov E.A. Isotherms and Grüneisen functions for 25 metals // Journal of Applied Mechanics and Technical Physics. 1987. V. 28 (1). P. 129–141.
2. Dinsdale A.T. SGTE data for pure elements // CALPHAD. 1991. V. 15 (4). P. 317–425.
3. Dorogokupets P.I., Dymshits A.M., Sokolova T.S., et al. The equations of state of forsterite, wadsleyite, ringwoodite, akimotoite, $MgSiO_3$-perovskite, and postperovskite and phase diagram for the Mg_2SiO_4 system at pressures of up to 130 GPa // Russian Geology and Geophysics. 2015. V. 56. P. 172–189.
4. Dorogokupets P.I., Sokolova T.S., Litasov K.D. Thermodynamic properties of bcc-Fe to melting temperature and pressure to 15 GPa // Geodynamic and Tectonophysics. 2014. V. 5 (4). P. 1033–1044.
5. Jacobs M., Jong B., Oonk H. The Gibbs energy formulation of α, γ, and liquid Fe_2SiO_4 using Grover, Getting, and Kennedy's empirical relation between volume and bulk modulus // Geochimica et Cosmochimica Acta. 2001. V. 65 (22). P. 4231–4242.
6. Kunc K., Loa I., Syassen K. Equation of state and phonon frequency calculations of diamond at high pressures // Physical Review B. 2003. V. 68. P. 094107.
7. Yamanaka T., Kyono A., Nakamoto Y., et al. New structure of high-pressure body-centered orthorhombic Fe_2SiO_4 // American Mineralogist. 2015. V. 100. P. 1736–1743.
8. Yong W. Thermodynamic studies of minerals under mantle conditions. A dissertation submitted in partial fulfillment of the requirements for the degree of Doctor of Philosophy (Geology) in The University of Michigan. 2008. 155 p.

Zharkov V.N., Kalinin V.A. Equations of State of Solids at High Pressures and Temperatures. New York: Consultants Bureau. 1971. 257 p.

Ree distribution in rocks and zircon and u-pb age for Kandalaksha Anorthosite masssif (Baltic shield): new data

Steshenko E.N.[1], Bayanova T.B.[1], Serov P.A.[1]
1 -GI KSC RAS, steshenko@geoksc.apatity.ru

Kandalaksha-Kolvitsa complex located in the N-E part of Baltic shield and consists of three parts. Marginal zone (mesocratic metanorite) lies at the base of the massif. Main zone is composed of leucocratic metagabbro. The upper zone is alteration of mataanorthosite and leucocratic metagabbro. All rocks were subjected to granulate metamorphism.

Age of magmatic crystallization of the massif was determined for the first time, using the U-Pb isotope method for single zircon grains. Three fractions of single zircons from anorthosite of the Kandalaksha massif gave U-Pb age 2450± 3 Ma.

For major groups of species concentration of rare-earth elements were measured. REE content in the rocks determined using a quadrupole mass spectrometer Agilent 7500 ce ICP-MS in the laboratory of isotope analytical methods IGM SB RAS (analyst Travin AV). The measurement results are shown in Table 1, Fig. 1.

Table 1 - Content of rare earth elements in rocks of Kandalakshsky array, ppm.

chemical elements	**sample number**		
	183	**220/1**	**225/1**
	leucogabbro	**orthoamphibolite**	**anorthosite**
La	11.29	4.42	7.74
Ce	8.54	2.97	5.82
Pr	6.92	2.75	5.00
Nd	5.00	1.85	4.17
Sm	2.51	0.92	2.46
Eu	8.30	5.03	8.16
Gd	1.74	0.46	1.93
Tb	1.60	0.42	1.71
Dy	1.34	0.40	1.43
Ho	1.25	0.38	1.39
Er	1.29	0.39	1.38
Tm	1.48	0.43	1.54
Yb	1.53	0.43	1.58
Lu	1.46	0.43	1.55
total amount	54.25	21.29	45.87
(La/Yb)n	7.37	10.26	4.90
(Sm/La)n	0.22	0.21	0.32
(Eu/Eu*)n	3.91	7.26	3.72

Anorthosite and leucocratic metagabbros (main zone) is characterized by a flat spectrum distribution of heavy rare earth elements.

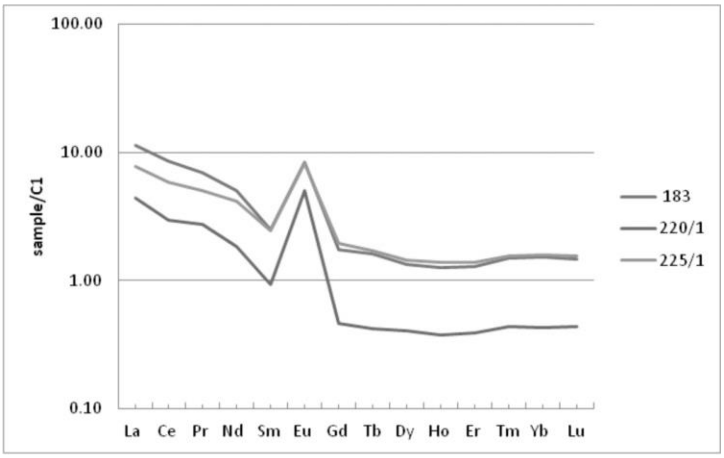

Fig.1 - REE distribution in rocks of Kandalaksha array normalized to chondrite C1 (Sun., McDonough, 1989).

For whole massif is characterized by significant positive anomalies of Eu ((Eu / Eu *)$_n$ = 3.72-3.91) in anorthosite and leucogabbros and 7.26 - in ortoamfibolitah. General content of individual elements that are common to this type of rock: Ce_n = 5.82-8.54, Yb_n = 1.54-1.58, which indicates that the process of crystallization of the rock occurred with predominant accumulation of plagioclase. Based on these data the primary basaltic magma for anorthosite have rift nature and crystallization occurred at primary fractionation and subsequent separation of plagioclase.

Distribution of REE (ICP-MS) in zircon have a typical magmatic nature: a positive Ce, negative Eu anomaly and HREE flat spectrum (fig.2). Titanium content in zircons was measured for the calculation (Watson, Wark, Thomas, 2006) of their crystallization temperature with 869^{0}C. These data are evidence of magmatic origin of zircon.

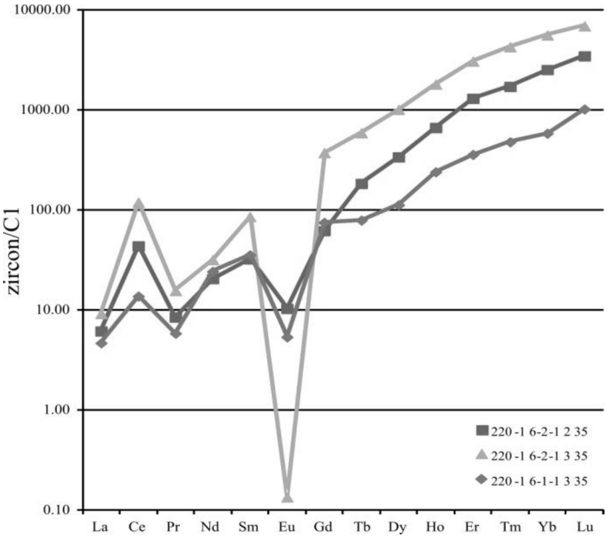

Fig.2 - REE distribution in zircon from Kandalaksha massif normalized to chondrite C1. C1 values given in (Sun., McDonough, 1989).

All investigations are devoted to memory of academician RAS F. Mitrofanov.

The scientific researches are supported by the Russian Foundation of Basic Research (projects № 15-35-20501, 16-05-00305, 16-05-00367). The theme of state assignment № 0231-2015-0005.

New geochemical data set for terrigenous deposition areas of the North-Western part of the Ukrainian shield and some neighboring regions as a potential source of the data for the continental growth history modelling

Tegkaev E.T.
Kiev National University of Taras Shevchenko, tegkaev@ukr.net

Investigation of continental crust is one of main task of geological science. Continental crust has a large signification of life evolution via abundant supply of biophil elements from continent to ocean. Distribution of continents also is an important climate-forming factor because continent has bigger albedo than ocean. Continental growth study is very popular research that has created by lot of scientist around the world. The aim of this study is to add a new geochemistry data from concrete aria of earth's crust to our knowledge box and assess their suitability for further use.

Introduction. When we investigate an evolution of continental crust we use U-Pb, Sm-Nd, Lu-Hf methods of age calculation and spread distribution of according geological formation. It should be noted that standard information about areal extent (mapping results) in a varying degree is subjective and it is a characteristic of earth's crust only on it level of erosion that reduced the accuracy and representativeness our conclusions.

For this task we use methods that based on geochemical investigation of large detrital population of most distributed ("ubiquitous") accessory minerals (UAM ─ zircon, monazite etc.) from modern alluvial and fluvial products of drainage of large earth's crust section. This products (and UAM populations) is objective reflected the compound, age and volume ration of rocks from erosion crust volume. It method eliminate the problem of spatial correlation between types of rocks that was spot dated, and allow to get information about upper part of crust that yet destroyed by erosion and unavailable to research by any other methods.

Implementation of this approach with using modern local (LA-ICP-MS, SEEMS) and sublocal (XRF) analytical methods for UAM study allow us: (1) utilization of most effective isotope systems for single-grain evaluation their crystallization and model ages, (2) identification of parental rock types for each of investigated grains UAM, (3) determination of main stages of continental crust evolution and restoration their petrological content, (4) construction of crustal growth curves with subsequent transition to geochemical modeling of system crust-mantle.

Samples. We systematically collected river sand samples at four points of the Teterev, Irsha, Uzh and Zherev Rivers. These rivers are right tributaries of Dnepr River, drained rocks of North-West part of Ukrainian Shield, and covered the territory of catchment about 17 000 sq.km. In addition, we collected river sand at the mouths of Dnepr, Danube, Southern Bug, Obitochnaya and Molochnaya Rivers, and coastal marine deposits from Berdyanskaya, Belosarayskaya and Krivaya forelands. Terregenous deposits of Obitochnaya and Molochnaya Rivers, Berdyanskaya, Belosarayskaya and Krivaya forelands are rocks destruction products of Priazovsky'smegaterrain of Ukrainian Shield. Deposition of Southern Bug River is characteristic of Dniester-and-Bug megaterrain of Ukrainian Shield. And deposition of Dnepr River is representative characteristic of whole Ukrainian Shield. All sample materials are well sored fine-grained and medium-grained sands with minor impurity of clay material for river sands and shelly material for coastal marine sands.

Tasks. To achieve main goal of our investigation we should perform staged studying of all samples: (1) determination of chemical composition (a wide range of major and trace elements); (2) detail research of mineral composition; (3) typing of sampling deposits, grading of samples with determination the most representativeness; (4) determination the large volume representative single-grain samples of UAM for each of lasted; (5) analytical research (XRF, EPMA, LA-ICP-MS) of selected samples grains; (6) interpretation of all created bank of geochemical data.

For today we made research of first stage that allows us to assess the suitability of determined deposition samples for the tasks.

Analytical methods. We used X-Ray fluorescence analysis with energy-dispersive and wave-length dispersive variants. We determined such elements (compounds): SOi2, TiO2, Al2O3, $Fe2O3_{total}$/FeO_{total}, MnO, MgO, CaO, Na2O, K2O, P2O5, S, Cl, LOI, Zr, Sr, Ba, Rb, Y, La, Ce, Nd, Nb, Th, Ga, Pb, Zn, Cu.Detection limits: Zr, TRCe (LREE) — 10—20, Y — 5—10 ppm; P2O5 — 0,00nweight%; other major and trace elements ─ 0,01-0,1 weight% и 5-20 ppm. The bias is always controlled by multiple analysis of rational set of standard samples (SS). Results of current metrological control present on figure 1.

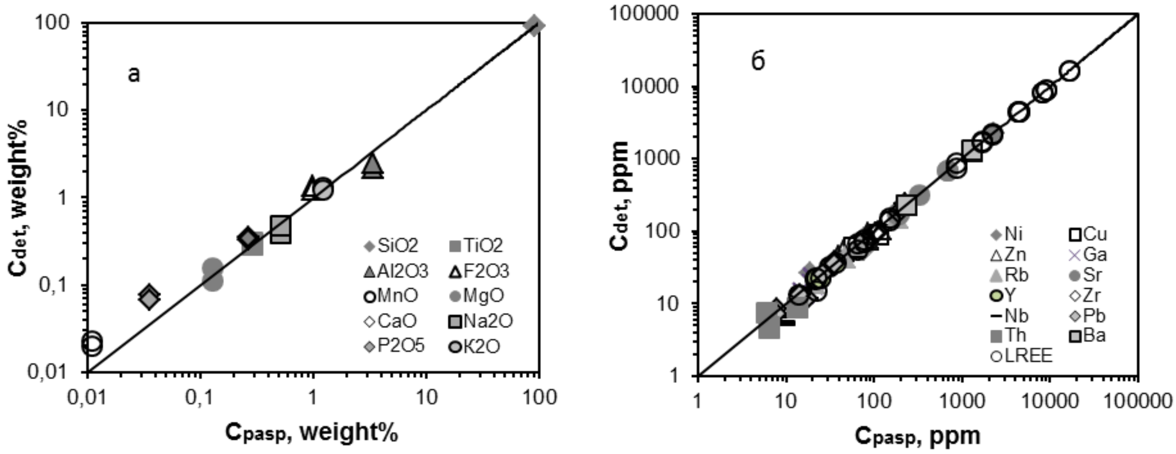

Fig. 1 Comparison of results determination of elemental concentration in control standard samples (C_{det}) with passport concentration (C_{pasp})

Conclusions. New created bank of geochemical data is available for our task that formulated above. Representation and quality level of new geochemical data bank is minimally sufficient for general goal.

References:

1. Shnyukov S.E., Cheburkin A.K., Andreev A.V. Geochemistry of wide-spread coexistent accessory minerals and their role in investigation of endo- and exogenous geological processes // Geol. Magazine – 1989. - №2. – p. 107-114. (In Russian).
2. Shnyukov S.E., Cheburkin A.K., Andreev A.V. perspectives, problems and possible method of terrigenous-mineralogical investigation with using typochemical features of "ubiquitous" terrigenous minerals // Geol. Magazine – 1991.- №6. – p. 100-115. (In Russian).

3. Shnyukov S.E. Geochemistry of wide-spread accessory minerals in terrigenous-mineralogical and forecast-search investigations. // Geological problems of Black Sea – 2001 – p. 55-78. (In Russian).
4. Shnyukov S.E. Geochemical models of evolution of magmatic systems and earth crust: potential sources of petrophysical and ore genetic information // Geophysical magazine – 2002 - №6 – p. 201-219. (In Russian).
5. McCulloch M.T., Bennet V.C. Progressive growth of the Earth's continental crust and depleted mantle: Geochemical constraints // Geochim. etCosmochim. Acta. – 1994. – Vol. 58,No 21. – P. 4717-4738.
6. Rino S., Komiya T., Windley B.F., Katayama I., Motoki A., Hirata T. Major episodic increases of continental crustal growth determined from zircon ages of river sands: implications for mantle overturns in the Early Precambrian // Physics of the Earth and Planetary Interiors. –2004. – 146. – P. 369-394.

New information on the mineralization agate Kuzbass

Tokareva E.V.[1]
1 - Tomsk State University, zmei7772006@mail.ru

The central part of the territory of the Kemerovo region, part of the border of Kuzbass (Kuznetsk coal basin) is renowned among experts, collectors and fans of the presence of agate stone mineralization and has long been known as one of the regions of Siberia having agates. Prior to her active learning local geologists West - Siberian Geological Survey (the second half of the twentieth century), it attracted the attention of such famous scientists as the A.E. Fersman and M.A. Usov. Nevertheless, this mineralization in the area is very poorly understood, and the set of published literature on agatam Kemerovo region are mostly purely descriptive. The nature of the host rocks (basalts) Kuzbass is also still debatable. The interesting thing is that now different researchers have proven the correlation Kuznetsk basalts with a Permian-Triassic trap structures Siberia.

Within the territory of the Kemerovo region known two age forming system agate mineralization: 1 - more ancient - Devonian; 2 - younger - Triassic. Beginning in 2012, the work on the study of quartz - chalcedony formations Kuzbass continued by the author. Work began with the collection of stone material with various manifestations, namely: 1) placer manifestations agate and onyx from Dr. Keys (Kemerovo region, Krapivinskii area). 2) a radical manifestation of vein quartz-chalcedony formations at p. Zelenogorskiĭ (Kemerovo region, Krapivinskii district). The second stage of work was the treatment of the collected samples and sample preparation for X-ray and fluorescent analysis. It should be noted that the analysis conducted for this type of raw material Kuzbass were made for the first time. Accordingly, the processing of the data was the final stage of work.

The two above-mentioned symptoms, from which samples were taken for laboratory tests, are a part of the Mid-Tomsk area.

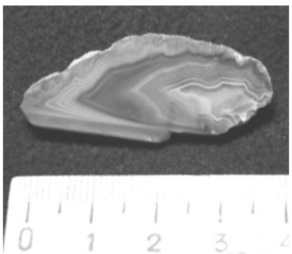

Fig. 1 agate. Russia, Kemerovo region, V. Klutchi

Deposit in V. Klutchi (the left bank of the r. Mungat). Placer manifestation is localized in the Quaternary deposits of the buried terraces. Quartz – chalcedony material made from indigenous basalt of Triassic age Taradanovsky Uval and spread almost to the mouth of the river Mungat. The main colors observed in agates and onyxes: yellow, brownish, brown, honey, interspersed with reddish stripes milky color (Fig. 1), and rare bluish – gray color. Tonsils are composed mainly chalcedony, a subordinate role is quartz (clear to smoked).

Deposit of V. Zelenogorsk (the left Bank of the Tom river). A very peculiar expression, which revealed the vein quartz – chalcedony formation refers to a radical type. Is part of the so-called Krapivinsky dome, composed of sediments of Devonian age. Semiprecious stone material identified in greenish-black basalt in the form of veins, reaching a length of three meters with a width of no more than 7-8 see the majority of these vein formations filled with chalcedony, and the colors vary widely, there are veins filled with chalcedony reddish, bluish (Fig. 2), gray or even green. In some instances there is a quartz portion in the mixture with crystals of calcite. Many instances are characterized by a distinct pattern.

Fig. 2 Vein agate. Kemerovo region, V. Zelenogorsk

The samples collected with the manifestations have been prepared for conducting two different laboratory tests: x-ray diffraction and luminescent.

Sample preparation for x-ray analysis was received and specimens with grain size of 0,1-0,25 mm. Of this fraction were selected under the binocular microscope the grains of quartz agate and chalcedony zone. The measurements were performed on the diffractometer X*Pert PRO. The values of crystallinity index (Kci) was calculated by the formula K=10 F a/b proposed by Murata&Norman [3]. The analysis of the data showed that the quartz-chalcedony formation of Kuzbass, on the index of crystallinity conventionally divided into three groups: high, medium and low degree of crystallinity. As you might expect, a good crystallinity is characteristic of all quartz crystals internal areas of the tonsils and the agate veins. Moreover, it is noticed that the high crystallinity index of quartz is correlated with a sufficiently high value and chalcedony parts of one and the same sample, although K_{ci} chalcedony is always much lower than quartz. Agate amygdales and veins, possessing a high degree of crystallinity as quartz and chalcedony are different from the rest of the samples saturated in color white and gray-blue color, resonatory in them clearly visible. Low rate X have agates and onyxes yellow, brown, reddish color, apparently due to the occurrence of iron in them.

Sample preparation for conducting luminescent analysis are the same as for the previous type of analysis. Overall, we obtained and analyzed 20 samples of quartz-chalcedony formations. RL spectra of the initial samples presented by a series of overlapping bands of radiation in the range of 200-800 nm, which may be responsible for the following centers (λ, nm): 280-290 – O*, 330-360 – (?) AlO_4^{4-}/Na^+, Li^+; H^+ [3], 360-370 – O*[2], 380-400 – SiO_4^{3-}; 450-470 – matrix intrinsic defects SiO_2; 460-510 - AlO_4^{4-}/Li^+; 600-620 – O*.

Analyzing the obtained curves, the samples can be divided into 2 groups: 1 – samples with impurity defects (centers associated with the excitation of O2). To include impurity atoms of those elements that form solid solutions of substitution or introduction into the mineral structure. The second group is the samples who have their own defects. They are imperfections of the lattice mineral, composed of silicon and oxygen. Although some of the samples fall in both the first and the second group, as they have both types of defects.

It should be noted that the samples with their own defects is correlated with a sufficiently high and medium degree of crystallinity of the same samples that may be associated with the genetic bases of formations of quartz-chalcedony formations [1]. It is frequently observed in the spectra of samples РЛ2 the luminescence with λ – 330-360 nm, which may be due to isomorphic substitution of silicon by aluminum in the tetrahedra of silica oxide. The influence of this substitution is a mode of acidity-alkalinity of hydrothermal solutions characterized by neosystem silica and high concentration of alkali metal ions (Na+, Li+). Correlation between color of samples and parameters of the luminescence is not yet clear. We believe that the method of x-ray crystallography and luminescence of minerals can be used as typomorphic sign and search for definition (or refinement) of the conditions of mineral formation and further transformation.

The author is grateful to N. N. Boronowsky and T. S. Nebera for assistance in the analysis and discussion of experimental results.

References:

1. Antsiferova A. A. study of the degree of conversion of quartz by infrared spectroscopy // Successes of modern natural science. – 2012. - No. 4. – C. 17-18.
2. Boroznovskaya N. N., Butaeva N. G. Luminescence as an indicator of microdefects in assessing the quality of quartz raw material / Ore deposits, Mineralogy, Geochemistry. - Tomsk: TSU, 2003. P. 12-27.
3. Murata K.J., Norman M.B. An index of crystallinity for quartz // American Journal of Science. – 1976. – V. 276. – P. 1120-1130.

Chromitite layers of the middle group, Thaba mine, Western Bushveld, South Africa

Tomilina E.M.[1], Veksler I.V.[1,2] and Trumbull R.B.[2]

[1] Perm State University, Russia, tomilinaelena.psu@yandex.ru

[2] German Research Centre for Geosciences GFZ Potsdam, Germany, veksler@gfz-potsdam.de

Here we present first results of a detailed petrographic and mineralogical study of rock textures and mineral chemistry in a vertical profile through the Middle Group chromitite layers at the Thaba mine in the north-western part of the Bushveld Complex, South Africa. The Middle Group includes four main layers numbered from the base upwards: MG1, MG2, MG3 and MG4. The MG4 layer comprises three separate seams labelled as MG0, MG4A and MG4B. Plagiocalse becomes a cumulus phase between the layers MG2 and MG3, but silicate cumulates and chromitite seams below that level contain interstitial plagioclase in minor amounts. Average thicknesses of each layer are around 1 m. Silicate rocks between the layers are mostly feldspathic pyroxenite but also include minor norite and anorthosite.

Our samples come from a drill core which was cut lengthwise into a continuous set of 90 petrographic thin sections, which were used for electron microprobe analyses of the main rock-forming minerals orthopyroxene, plagioclase and Cr-spinel. The electron microprobe results for the MG4A seam show that the orthopyroxene Mg# in footwall and hanging wall pyroxenites is around 70 and 88, respectively. The composition of intercumulus plagioclase in footwall pyroxenite decreases upwards towards the chromitite contact from An_{82-96} to An_{45-49}. The Cr# of chromite within massive chromitite seams is 58-66, whereas the Cr# of disseminated chromite crystals in pyroxenite varies in the range of 48-61.

Crystal size distribution (CSD) diagrams were constructed for chromite in the MG1, MG3 and MG4A seams on the basis of 2D image analysis using ImageJ software and 2D-3D conversion using steric corrections by Higgins (2000). Chromite grains within massive chromitite seams form two distinct textural populations. The first population is represented by smaller idiomorphic crystals with the median Ferret diameter of about 0.06-0.08 mm enclosed in large oval pokilitic grains of orthopyroxene and plagioclase (5-7 mm along the greater axis). The second population consists of closely intergrown groups of texturally equilibrated chromite crystals with Ferret diameters from 0.5 to 1.8 mm and average dihedral angles at triple junctions close to 120 degrees.

Some pyroxenite layers contain sulphide-rich horizons, 20-25 cm thick, e.g., directly above the MG1 and MG4A seams. These horizons were scanned by X-Ray computer tomography for 3D textural study of the sulfides and to search for platimum-group minerals (PGM). In the studied samples, the sulfides (mainly pyrrhotite, pentlandite, chalcopyrite) mostly occur between chromite and silicate crystals. Sulfide aggregates range in sizes from 2.5 to 0.1 mm or less. Most PGM are below 15 microns in size.

Work is ongoing in the other middle-group chromite seams. Our results will provide new insights into the processes responsible for the formation of Bushveld chromitite layers and the mechanisms of platinum-group element concentrations within them.

This study has been sponsored by RSF grant No. 14-17-00200.

References:

1. Higgins, M.D. (2000). Measurement of crystal size distributions. *American Mineralogist*, 85, 1105-1116.

The Mwanubi occurrence: an example of atypical intrusion-hosted gold-molybdenum mineralization in the Lake Victoria Goldfields, Tanzania

Tsikin A.[1], Utenkov V.[1]

1- Russian State Geological Prospecting University, alex_tsikin@yahoo.com

The Mwanubi gold–molybdenum occurrence is situated in the Shinyanga-Mwadui granite-greenstone belt within the Lake Victoria Goldfields (LVG) at the northern part of Archean Tanzania Craton [2]. High-grade quartz veins mined by local artisanal miners from discovery in 2007. Gold mineralization is hosted by deformed and altered medium-grained equigranular to porphyritic granodiorite at north-eastern margin of elliptical (8x3 km) granodiorite-syenogranite intrusion with swarm of aplite and leucogranite parallel dykes.

Granodiorites are characterized by signs of melt flowing – primary banding and distinctly sloping gneissic expressed in the orientation of mafic minerals. Sometimes gneissic banding (Dip.az 190-210 ∟ 20-30˚) is confined to the primary banding, which may not be available at any of the minerals (hornblende, rarely - biotite, microcline). The overall composition of the typical granodiorite without metasomatic alteration: hornblende (10-15%), biotite (5-20%), quartz (15-20%), plagioclase (50-60%) and microcline (5-10%), titanite (2-3%), orthite, zircon, apatite. There is always the secondary minerals are sericite, calcite, epidote, zoisite. The observed asymmetric structure with a gentle dipping to the southwest, suggests the shape of intrusion as harpolith.

Reconnaissance drilling and trenching within artisanal mining site and Au-Cu-Mo-Bi soil anomaly defined a few types of gold mineralization:

Disseminated low-grade gold-molybdenum mineralization occurs to the K-alteration zones and porphyritic lithologies of granodiorite. Gold (780-950 ‰) in association with pyrite, arsenopyrite and chalcopyrite is localized at the boundary of grains of colored minerals (Fig. 1a) and within large phenocrystals of strongly altered plagioclase (Fig. 1b). Gold grains size usually below 0.1 mm.

Low-grade stockwork zone composed by variously oriented stringers and thin veinlets ranging from 0.5 to 15 cm with gold grades from 0.1 to 0.8 g/t. Gold grains (800-900 ‰) in association with chalcopyrite, pyrite and molybdenite occurs in veins and stringers composed mainly by quartz, rarely carbonate and mafic minerals. The primary fluid inclusions in quartz are two-phase gas-liquid, with homogenization at temperature range 290-410˚C and salinity of more than 20 wt. % NaCl eq.

High-grade sheeted veinlets and veins up to 30-50 cm width, composed mainly by quartz and carbonate, rarely actinolite, albite, epidote and chlorite, steeply dipping to N and S and controlled by shear-zone (striking E-NE 70-80˚) Pyrite, molybdenite, rarely chalcopyrite and native gold occurs in deformed and altered granodiorite filling by quartz breccia. Gold (920-980 ‰) consist dodecahedral shape meta-crystals ranging in size from 0.1

up to 2-3 mm. Primary inclusions in quartz are two-phase gas-liquid with homogenization at temperature range 130-260˚C and salinity less than 20 wt. % NaCl eq.

The granodiorite-hosted Au-Mo mineralization of the Mwanubi occurrence shows some signs, which are typical for relatively new Archean porphyry-type, described at the Messegay gold deposit in the Abitibi Greenstone Belt by M.Jebrak [1]. Archean intrusions at Tanzanian Craton can host a range of styles of alteration and mineralization, including Nyabirama and Buzwagi gold deposits, shows excellent potential for discovery industrial-size deposits.

References:

1. Jebrak M., Doucet P. (2002): Geology and gold–molybdenum porphyry mineralisation of the Archean Taschereau–Launay plutons, Abitibi, Quebec // Precambrian Research V.115 P. 329–348
2. Kabete J.M., Groves D.I., McNaughton M.J. and Mruma A.H. (2008): A New Tectonic Subdivision of the Archean Craton of Tanzanian and its Significance to Gold Metallogeny. // SEG-GSSA Abstracts, 2008, p. 21-23.

Comparison megacrysts and basanite of lunar crater monogenetic field (Nevada, USA)

Turova M.A.[1], Plechov P.Y.[2], Larin N.V.[3]

1 - Lomonosov MSU, mary261015@yandex.ru

2 - Lomonosov MSU, pplechov@gmail.com

3 - Institute of Physics of the Earth, larin.hydrogen@gmail.com

Continental rifts are important source of information on sublithospheric magma generation area. Monogenic volcanic fields are common manifestations of intracontinental rift magmatism and are the object of the study. Basin and Range Province (USA) can be regarded as the place where the oceanic plate dives under the mainland (Zoback et all, 1981) and creates tension on the territory of an area of about 1.5 mln km2. Lunar Crater volcanic field (Nevada, USA) is located inside this area and especially in zone of anomalously low heat flow (Eureka Low). The youngest flows (<50 ka) are consists of basanites which bearing in megacrysts (3-10 cm in size) of Olivine, Clinopyroxene and Sanidine. Megacrysts have irregular shape and doesn't contain any inclusions. There are several hypotheses of megacrysts formation, such as 1) megacrysts were seized and recrystallized from ultramafic rocks or gabbro (Shaw, Eyzaguirre, 2000), 2) megacrysts crystallized at high pressure conditions in the same magma (Irving, 1974), 3) crystallization of megacrysts from high-density mantle fluids, which differ significantly in composition from the surrounding lava (Kovalenko et al., 1986). We studied olivine and pyroxene megacrysts as well as rock-forming minerals in the host lava. Megacrysts have highest Mg-number, and could corresponds to early stage of basanite evolution. Basanites contain two generations of phenocrysts and groundmass assemblage. Temperature and oxygen fugacity conditions were estimated for phenocrysts and groundmass crystallization only. We are planning a numerical modeling of magma crystallization to check possibility of megacrysts and phenocrysts crystallization from the same magma.

References:

2. Irving A. J. Megacrysts from the Newer Basalts and other basaltic rocks of southeastern Australia //Geological Society of America Bulletin. – 1974. – Т. 85. – №. 10. – С. 1503-1514.
3. Kovalenko V.I., Solovova I.P., Naumov V.B., Ryabchikov I.D., Ionov D.A., Tzepin A.I. The mantle mineral-formation with participation of carbon dioxide-sulfide-silicate fluid. Geochimiya-1986.- 3:289–303
4. Shaw C. S. J., Eyzaguirre J. Origin of megacrysts in the mafic alkaline lavas of the West Eifel volcanic field, Germany //Lithos. – 2000. – Т. 50. – №. 1. – С. 75-95.
5. Richter K., Carmichael I. S. E. Mega-xenocrysts in alkali olivine basalts; fragments of disrupted mantle assemblages //American Mineralogist. – 1993. – Т. 78. – №. 11-12. – С. 1230-1245.
6. Zoback M. L., Anderson R. E., Thompson G. A. Cainozoic evolution of the state of stress and style of tectonism of the Basin and Range province of the western United States //Philosophical Transactions of the Royal Society of London A: Mathematical, Physical and Engineering Sciences. – 1981. – Т. 300. – №. 1454. – С. 407-434.

Ore potential of magmas with increased alkalinity: the results of petrographic studies, mineralogical and geochemical characteristics of Chuya complex

Vasyukova E.[1,2]
1 -Institute of Geology and Mineralogy SB RAS, Novosibirsk
2 -Novosibirsk State University, lenav@inbox.ru

Lamprophyres are one of the most mysterious of igneous rocks. For a hundred years, since they have extracted into a separate family, the researchers have not reached a consensus on their classification, genesis and role in the ore formation. As of yet, the calc-alkaline lamprophyres, according to the classification of Rock [Rock, 1991], genetically associated with syenites, diorites, granites. In terms of mineralization, the proximity of gold mineralization and lamprophyres is the most frequently observed all over the world in spatio-temporal aspects [Rock, 1991].

However, in recent years according to published sources another types of mineralization became more common and have paragenetic or genetic connection with lamprophyres.

The Chuya complex consists of more then 400 early Mesozoic lamprophyre dikes that occur in the vast territory in the structures of the Gorny and Mongolian Altay. Based on the irregular distribution of the dikes, various researchers have distinguished from 3 to 6 separate dike swarms or areas. In the field of Chuya complex three different areas (South Chuya, Yustyd, Aktash) were studied on the examples of 30 dikes and breed related Tarhata intrusion located within the South-Chuya field (fig.1).

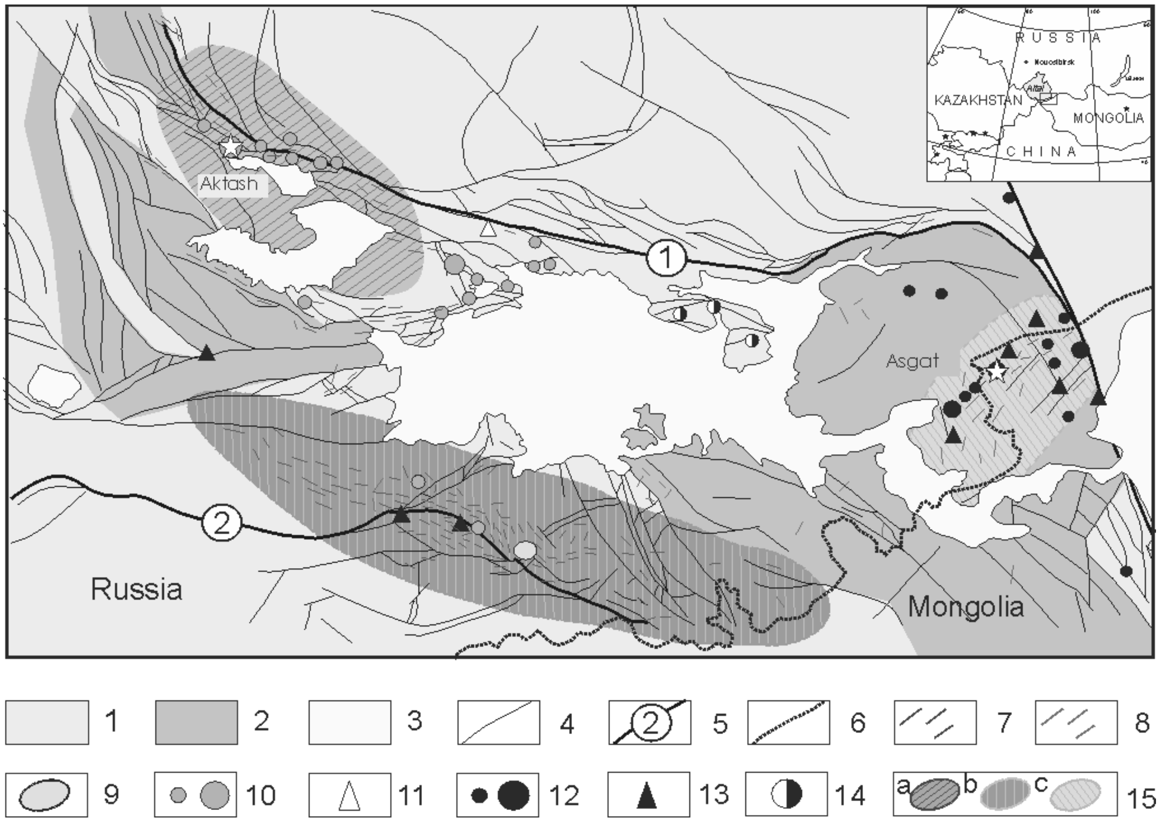

Fig.1 Schematic map of major occurrences of Early Mesozoic magmatism and mineralization in southeastern Altai and northwestern Mongolia. 1 - Cambrian-Ordovician deposits; 2 — Devonian deposites; 3 - Cenozoic deposites; 4 - faults; 5 - fault zones (1-Kurai-Kobdo, 2-Terekta-Tolbonur); 6 - Russia–Mongolia frontier; 7 - lamprophyre dikes of Chuya complex; 8 – gabbro-dolerite Terekhta complex; 9 - Tarkhata granosyenite-monzodiorite complex; 10-14 - mineralization: 10 — Hg, 11 — fluorite, 12 - Ag-Sb, 13 - Ni-Co-As, 14 - Cu-Hg; 15 - Chuya complex dike swarms: a - Aktash, b - South Chuya, c - Yustyd .

The ore potential of Chuya lamprophyres could be considered into 3 aspects. The first one is well described [Borisenko et all., 2010; Pavlova et all., 2009] space-temporal connection between lamprophyres with a specific simultaneous ore deposit. For example, in the field of Aktash dike swarm there are the Aktash, Chagan-Uzun and other Sb-Hg deposits, in the territory of the South-Chuya area there are the Kalguta Mo-W and Chagan-Burgasy Ag-Pb deposits and within the Yustyd area there are the Askhatin-Gol Ni-Co-As deposit, Asgat, Ozernoe and Tolbonour Ag-Sb deposits (fig.1). But our new investigations show, that there is very slightly elevated concentrations of ore components in the rocks, insufficient for the formation of mineralization.

The second aspect of the ore potential – is high LREE and CaO, P2O5 concentrations. Interpretation of the literature with geochronological, geochemical and isotopic studies of recent years has shown not only close relation, but also the possibility of a single source for lamprophyres and carbonatites [J. Woodard, 2010; I.M.Coulson et al., 2003]. In the district of Chuya lamprophyre complex and associated intrusions carbonatites were not found yet.

Petrographic studies have provided incontrovertible evidence of segregation of carbonate-silicate melt. They consist in a special ocellar texture of rocks, where ocelli composed predominantly of silicate minerals and interglobular space is filled with mainly carbonates, with ore segregations and non-metallic minerals. One of them is barytocelestite. In addition, it performs pseudomorphs over silicate mineral phenocrysts and small veins in the rock in association with carbonates (calcite and dolomite), apatite, quartz, iron-magnesia oxide (magnetite, goethite, chromite), chlorite. At the same time, on practically all geochemical multielement spectra built for different rock spices Chuya complex show the coincidence of the slope, the absolute contents of element values, position anomalies HFS elements but clearly manifested anomaly by Sr, and Ba for the rocks of South Chuya field and their absence or weak expression for lamprophyres of Yustyd and Aktash field. Their similar source implies that the Ba and Sr did not be introduced into the system by hydrothermal process. And presence of barytocelestite is an indication of liquid separation enriched Ba, Sr and Ca. So, analysis of geochemical data suggests that on one of the evolution stages of the melt occurred separation of Ba, Sr enriched carbonate containing liquid.

The third aspect is U-Th mineralization. Chuya lamprophyres are enriched in that elements (table 1). But Th/U ratio varies according to the dike swarm – normal for magmatic rocks (3.6-6) in Yustyd dikes, and much higher for South Chuya rocks (5-17). The concentrations are also high as for bulk rock and more over for the inclusions in magmatic accessory apatite (Table 1).

Table 1. Mean U, Th values and Th/U ratio in bulk rock analyses of Chuya complex lamprophyres and melt inclusions in apatite from the same lamprophyres.

		U, ppm	**Th, ppm**	**Th/U**
Inclusions		up to 643	up to 1900	1-10
Lamprophyre fields	**Aktash**	8	47	5,9
	South Chuya	10,6	82,3	8,1
	Yustyd	6	29	4,83

Following conclusions could be formulated due to the vast amount of factual material based on petrography, petro- and geochemistry, mineralogy and isotopic data. Lamprophyres being formed from water-saturated melts with high oxidation activity, served as extracting agent and for the redeposit contributing to the formation of ore mineralization. In addition, at a certain stage (or stages) of melt evolution liquid (or liquids) enriched with Ca, Ba, Sr, U, P was separated and form some veins under the surface.

Work was supported by grant funds 15-17-20036.

References:

1. J. Woodard Genesis and Emplacement of Carbonatites and Lamprophyres in the Svecophennian Domain, Academic Dissertation, University of Turku, Finland, 50 p., 2010
2. I.M. Coulson, K.M. Goodenough, N.J.G. Pearce, M.J. Leng Carbonatites and lamprophyres of the Gardar Province – a "window" to the sub-Gardar mantle? // Mineralogical Magazine, October 2003, Vol. 67(5), pp. 855-872.
3. Pavlova G.G., Borisenko A.S., Seifert Th. Relationships between Sn-W(Mo) and Ag-Sb-base metal mineralization in the Sn-Ag ore districts of Eurasia. In: Large Igneous Provinces of Asia, Mantle Plumes and Metallogeny. Proceedings of International Symposium. Novosibirsk, Russia. 2009. Sibprint. P. 238-242.
4. Rock, N.M.S., 1991, *Lamprophyres,* Blackie, Glasgow, UK ISBN 978-0442303969
5. Borisenko, A.S., Borovikov, A.A., Vasyukova, E.A., Pavlova, G.G., Ragozin, A.L., Prokop'ev, I.R., Vladykin, N.V., 2011. Oxidized magmatogene fluids: metal-bearing capacity and role in ore formation. Russian Geology and Geophysics (Geologiya i Geofizika) 52 (1), 144–164 (182–206)

Structure of the Tsetserleg seismogenic fault (North Mongolia)

Voskresenskii A.G.[1], Sankov V.A.[1,2], Parfeevets A.V.[2]
1 -Irkutsk State University, voskres42@gmail.com
2 -Institute of Earth Crust SB RAS, sankov@crust.irk.ru

On the basis of an interpretation of a satellite images available on the resource Google Earth, and field observations the regularities of seismogenic ruptures associated with the activation of movements along Tsetserleg strike-slip fault during the Tsetserleg earthquake (09.07.1905, Mw = 8.0) in northern Mongolia were obtained. Collection of the information about the spatial distribution, the strike and the length of seismogenic dislocations and the creation of a database were made using the ArcGIS, calculations were done by using OpenOffice Calc.

Tsetserleg earthquake is characterized by left lateral strike-slip displacements along the main seismogenic rupture with reverse component on the surface (Voznesensky, 1908; Khilko et al., 1985). On the right side of the Tesiin-Gol river valley, near the earthquake epicenter (Fig. 1), the amplitude of the left lateral displacement is about 2.0-3.0 m and vertical amplitude reached of up to 1.5 m.

The fault zone with a NE (Az. 65°) general strike formed by complex sublatitudinal and submeridional seismogenic fractures (Fig. 2). The folded structures are presented by pressure ridges of a latitudinal strike. Generally the complex of seismogenic fractures in the investigated area is represented in the bedrock by main fault trace, and sometimes by several parallel ruptures and typical strike-slip parageneses of leading disjunctive and plicative structures in the Quaternary sediments. The latter corresponds to the generalized parageneses en echelon structures in the left lateral strike-slip zone (Sylvester, 1988; Seminsky et al., 2005). Along with the primary seismogenic structures were formed due to the rapid movement along the main fault, in the earthquake epicenter zone the secondary fractures were generated as a result of shaking effects in the gravitationally unstable sediments on the slopes and on the flooded areas of valley bottoms.

Using the collected data on the tectonic fractures and displacements in the fault zone the palaeostress state was reconstructed. The last stage of tectonic deformation, which is associated with the Late Cenozoic movements, characterized by a strike-slip type of tectonic stress field with submeridional axis of compression and sublatitudinal axis of extension. The paleostress reconstruction corresponds with the system of stresses calculated for the focal mechanism of Tsetserleg earthquake (Schlupp, Sisternas, 2007).

The relationships of the obtained regularities of orientation fractures in the zone of Tsetserleg fault and relief in the deformation zone with the published result of physical modeling on equivalent materials are studied (Sherman et al., 1983; Le Guerroue, Cobbold, 2006 и др.). Our data are consistent with published results on the structures of left lateral strike-slip in the elastic-plastic and brittle (sand) materials. General regularities of the formation Riedel shears, opening fractures and compression folds are well revealed in the natural object and models. In both cases the direct relationship between the width of the deformation zones and the thickness of the model layer and the thickness of the unconsolidated sediments in nature is revealed. As in the models and that is in the natural analogue the process of forming the positive relief on fault zone associated with the dilatation of the sediments is well manifested.

The obtained regularities can be used for the diagnostic of the conditions of seismogenic structures formation in seismically active regions.

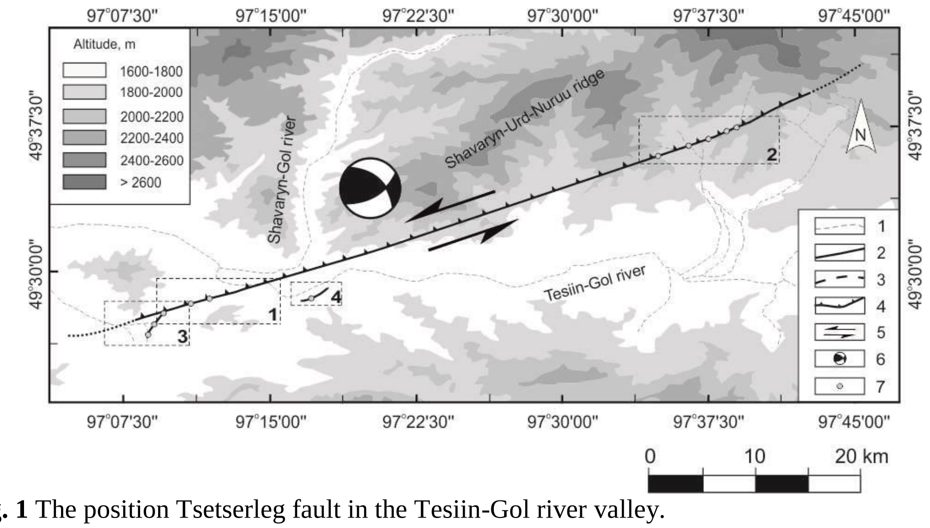

Fig. 1 The position Tsetserleg fault in the Tesiin-Gol river valley.

1 - main watercourses; 2-3 - faults: 2 – estimated; 3 - expected; 4-5 – fault kinematics: 4 - reverse faults; 5 – strike-slip faults; 6 - the focal mechanism of the Tsetserleg earthquake (09.07.1905, Mw = 8.0) (after Schlupp, Sisternas, 2007). The rectangles show areas of detailed research; 7 – observation point.

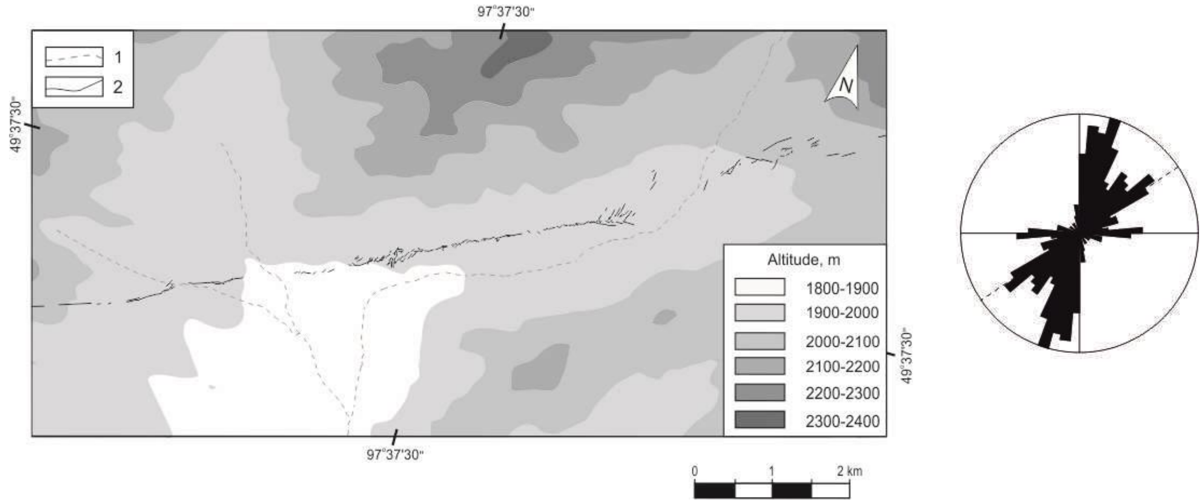

Fig. 2 Seismogenic structures on the surface in the Tsetserleg fault zone on the right side of the Tesiin-Gol river valley. 1 - watercourses; 2 – fractures, visible on the satellite image. The dotted line shows the position of the main fault on the diagram of seismogenic fractures orientation.

Uranium isotopes in kimberlites and enclosing rocks the kimberlite pipes of Arkhangelsk diamondiferous province

G.P. Kiselev[1], E.Yu. Yakovlev[1], S.V. Druzhinin[1]

1 -Institute of Ecological Problems of the North, UB RAS, yakovlev_eu@inbox.ru

Since the discovery of the first kimberlite pipe in the Arkhangelsk diamondiferous province many traditional geophysical methods have been tested for purpose of searching new kimberlite bodies. But aeromagnetic methods have been showed as the most effective. However, at the present time crisis of the efficiency aeromagnetic survey to searching kimberlite bodies influences on the searches results increasingly. Thus, in the early eighties of the last century the efficiency verification magnetic anomalies was about 20 %; at the end of the eighties - 12.5 %; in the nineties it was already below 1 % [5]. Today, this figure is less than 0.5% for the whole territory of the Arkhangelsk diamondiferous province. It is connected with decrease of contrast magnetic anomalies which are tending to geological noise. Therefore, development of new approaches to exploration and prediction kimberlite pipes is important task.

One such approach is identification in drill samples of explaratory wells a signs of near-ore enclosing rocks changes, such as tectonic deformation in rocks, near-contact rock alteration, increased concentrations of radiation defects in various minerals and others [6]. During previous studies on diamond pipes Mir and Sputnik (Yakut diamondiferous province) it was found that near-contact zone contains an increase in excess of the uranium-234 in relation to the uranium-238 [3]. The theoretical model of radioactive decay for ancestor and its daughter products foresees the oncoming of the secular equilibrium consisting in nuclide activity equation after a lapse of time (in comparison with duration of geological processes). For under consideration uranium series (isotopes ^{238}U and ^{234}U) this period is about 1 million years. Accordingly, in natural compounds occurred more than 1 million years ago in uranium series the secular equilibrium should be observed. Numerous studies of the isotopic composition of uranium of various rocks and minerals demonstrate significant deviation ratio of $\gamma={}^{234}U/{}^{238}U$ from equilibrium [1]. As a rule, recent beds, such as peat, bottom sediments, soils, are significantly enriched by U-234. This is due to the fact that the ^{234}U atoms remote from bed rock accumulate in the re-deposited rocks exposed to natural waters [2]. Uranium-234 enrichment is also characteristic for the recent volcanic deposits. For the ancient rocks the activity ratio of even uranium isotopes for the above reasons, comes close to the equilibrium. The research of the uranium isotopic composition of solids within the Northern Tien Shan ore beds allowed to reveal the spatial trends of γ-value, consisting in excess reduction of ^{234}U from the center in a distal direction of the ore fields, to background levels closed to 1 [4].

We studied the uranium-isotopic composition of sample series of diamond and enclosing rocks of Arkhangelskya and Pionerskya kimberlite pipes from M.V. Lomonosov field of the Arkhangelsk diamond province. The purpose of this study was to analyze the isotopic composition of uranium in diamond and enclosing rocks and to estimate degree and potential reasons of fractionation in «ores- enclosing rocks» system. The total uranium isotopes of samples were studied for this.

Uranium-isotopic data indicates at significant differences in the uranium content and γ value ($\gamma = {}^{234}U/{}^{238}U$) in the studied samples. Uranium isotope ratio in autolithic breccias and enclosing rocks that removed from the pipes contains the equilibrium value of the ratio ${}^{234}U/{}^{238}U$. Equilibrium value of the ratio of even uranium isotopes alpha activity indicates a stable condition of these rocks for a long time and absence of the influence of modern exogenous processes that could lead to isotopic fractionation. The isotopic equilibrium in the solid phase of samples located in near-contact zone is anomalous. Uranium isotopic disequilibrium in enclosing rocks of near-contact zone shows at the active uranium fractionation processes during interaction of ore matter and enclosing formations. Results of the study of uranium isotopes in kimberlites and enclosing are as follows:

1. The kimberlites and enclosing rocks at a distance from the boundaries of the pipes contains an equilibrium uranium isotopic composition;
2. There is disturbed equilibrium isotope uranium series in the enclosing sediments in near-contact zone;
3. Increase the isotope indicator ${}^{234}U/{}^{238}U$ ratio in enclosing rocks indicates the existence in near-contact zone the interaction area of kimberlites and enclosing sediments;
4. Near-contact changes in rocks stand out clearly on the increase in excess of the isotope ${}^{234}U$, which in our opinion is the new search criteria manifestation of kimberlite magmatism in the Arkhangelsk diamondiferous province.

References:

1. Chalov P.I. Izotopnoe fraktsionirovanie prirodnogo urana. – Frunze: Ilim, 1975. – 236 s.
2. Cherdyintsev V.V. Uran-234. – M.: Atomizdat, 1969. – 299 s.
3. Kiselev G.P. Chetnyie izotopyi urana v geosfere. (Institut ekolog. Probl. Severa UrO RAN). Ekaterinburg. 1999. – 220 s
4. Kiselev G.P. Prognoz mestorozhdeniy poleznyih iskopaemyih i zagryazneniya geologicheskoy sredyi uran-izotopnyimi metodami. Avtoreferat dis. na soisk. uch.st. d. g-m n., Arhangelsk, IEPS UrO RAN, 2005. – 50 s.
5. Stogniy V.V., Korotkov Yu.V. Poisk kimberlitovyih tel metodom perehodnyih protsessov. Novosibirsk: Izdatelstvo «Malotirazhnaya tipografiya 2D», 2010. - 121 s.
6. Vasilev I.D. Geologicheskie strukturyi v okolotrubochnom prostranstve trubki Arhangelskaya i ih ispolzovanie dlya poiskov korennyih mestorozhdeniy almazov v Zimneberezhnom rayone. Dis. … kand. geol.-min.nauk. M.: MGRI-RGGRU, 2010.

Randomness test of LIP (Large Ignieos Provinces) temporal distribution

Zaitsev V.A.

Vernadsky Institute of Geochemistry and Analytical Chemistry RAS, Moscow

va_zaitsev@inbox.ru

Large igneous provinces are results of specific events during which large volumes of magmas were generated during short time. From the LIPs definition, it was clear that LIPs has a specific significance for Earth history and it was widely believed that, LIPs are result of plume events, as well as other intraplate magmatic provinces. Following the mantle plumes concept, the most part of the Earth radius were involved in the LIPs generation process, therefore analysis of LIPs age record must be a key to understanding the Earth mantle history. There have been numerous attempts to identified cycles and trends in the LIPs age distribution, but there were not publications, there distribution of LIPs age was examine as result of some stochastic process.

To fill this gape, author use database, published by Large Igneous Provinces Commission of International Association of Volcanology and Chemistry of the Earth's Interior (http://www.largeigneousprovinces.org/downloads).

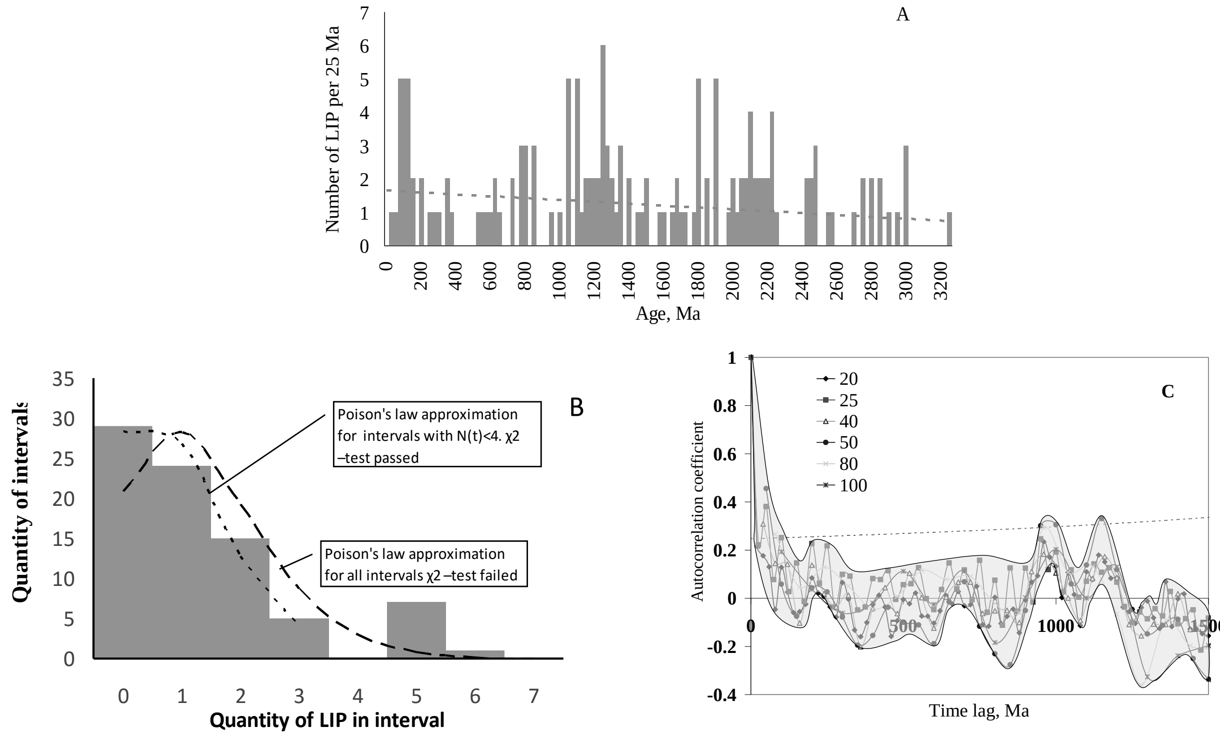

Fig. 1 A- Histogram of LIP ages (25 Ma splitting), and its statistical characteristics: B- distribution of time intervals by number of LIPs (splitting 25Ma), C – Summary of corellograms (dotted line show limit of 95% significance level).

The most popular way to analyze of LIP record is histogram of ages (diagram, where quantity of events in each time interval – N(t) plotted vs. the age of thus interval-t). To verify concept of random LIPs age distribution, author count intervals, containing 1, 2, 3… LIPs (intervals with N(t)=1, 2, 3…). It is possible to estimate these quantities of intervals from the Poisson’s law, on the assumption of random distribution of LIP events in geological time. χ^2 –test was used to determine whether there is a significant difference between the observed and expected quantitys of time intervals containing 1, 2, 3…n LIPs.

Quantities of LIP in time intervals depend on the splitting (time step and shift). Author has tested all splitting with time-steps from 9 to 40 Ma, and some splitting with bigger time-steps (up to 500 Ma).

On the fig. 1B showed example of LIP number distribution for 25 Ma time-step. In all tested cases of splitting with time step from 10 to 100 Ma observed distributions are quite close to the Poisson’s law, especially if only the best known part of geological history is taken into account (1-1,5-2 Ga).

There are only few exclusions: 75-150 Ma, 1000, 1100, 1250 1800 and 1900 Ma. First of they may be explaned by presence of contain oceanic LIPs, which mainly do not preserve for older parts. The excesses of 1000, 1100 and 1250 Ma looks to be attributed to the effect of rounding of poorly dated events (like 1Ga, 1.1Ga, 1-1.5 Ga) the nature of 1800 and 1900 Ma excesses need to be understood.

One of the very popular ideas is cycling of geological processes cycles with periods 30, 100, 170,330, 550-700. For strict validation whether Earth activity in LIP generation in time have regular recurrence, autocorrelation coefficients (correlation coefficients N(t) vs N(t+Δt)) with Δt (time lag) 0-1500 Ma for LIP histograms with 20, 25, 40, 50, 80, 100 Ma splitting were calculated. Autocorrelation coefficients, plotted against time lag (correlogram) showed on the fig. 1. Autocorrelation coefficients quickly decrease, significant values found only for lags<100 Ma. It shows that there is no regular repetition of plume activity of the Earth. High autocorrelation coefficients for small lags connected with obvious trend of LIP quantity grown during geological time (see dotted line on the fig 1A).

This growing looks like a result of effect of LIP destruction by erosion and fragmentation processes. Fig 2 show that observing LIP size dramatically decrease with age incensement. This evident that some (but not many) of ancient provinces might be not recognized as LIPs now.

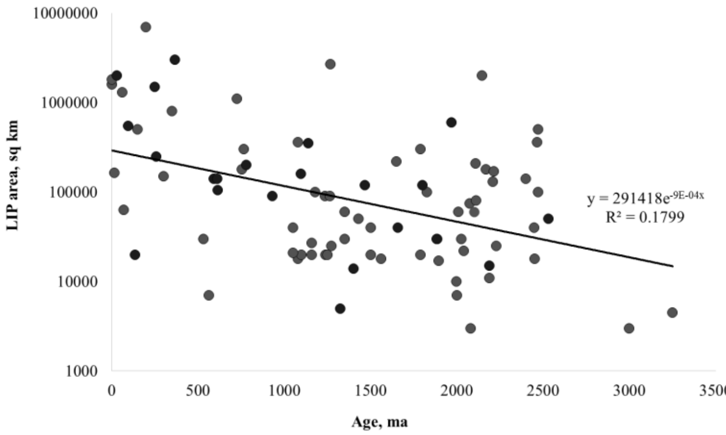

Fig.2 Dependence of observing LIP area from the LIP age.

Summary:

Statistical tests evident that LIP formation must be considered as a stochastic process of rare events, continuous in all time, well observed by rocks record.

This result give strong limitation for plume origin models: plume generation trigger (process, event or they combination) must be insignificant for energy and material balance in plume-generating system, but must be rare (for example, must be a result of some rare combination of conditions).

On the nature of possible protolith of the aduy granite massif, the largest in the Middle Urals

Zamyatina M.D.

Institute of Geology and Geochemistry, Ural Branch of RAS, Yekaterinburg city,

abu-sembella@mail.ru

The Aduy granite massif, which is situated in the northwest paleocontinental zone of the Middle Urals, has a long history of study, which deepenes as new geological data are receved and research methods are improving. Recent studies have shown that formation of essentially magmatic biotite and two-mica orthoclase-microcline granites of Aduy massif occurred in 2 stages - 290 and 256 Ma. For granite with age 290Ma, migmatized tonalites and granodiorites of located to the south Kamensk massif could serve a protolith - age generations of migmatites zircon are 331 and 298 Ma. The younger granites corresponding to the maximum of 256 Ma, probably were formed by heating of the pre-Paleozoic basement in the course of 30-35 Ma before the temperature of granite formation and further melting , as it is supposed for Mursinsk massif placed in the same structural zone [1].

The Kamensk migmatite pluton consists of tonalites, granodiorites and granites, rocks in some places are intensively migmatized. Partial melting zones are presented by banded and spotted migmatites, similar in bulk composition to tonalite, leucosomes in them are granite or adamellite, generally poor in potassium, and melanosomes are the more basic rocks with hornblende and biotite. Dikes of microgabbro and microdiorites migmatized in varying degree intrude banded migmatites. In the formation of dikes, several stages are distinguished, marked geologically. These stages are recorded in the migmatized quartz diorites and granodiorites by presence of earlier xenoliths of migmatites.

The complex and long-term evolution of the Kamensky massif migmatites is reflected in zircon obtained from them, which form 4 age generation with age 331 ± 3,7 Ma, 298,4 ± 2,8 Ma, 280,8 ± 5,1 Ma and 250,3 ± 1,6 Ma. The first generation, presumably, is the relict zircon of diorite or granodiorite protolith, the second one corresponds to the main stage of migmatization, and the third and fourth ones - evolutione stages of secondary anatectic melt. Granites, similar to rocks of the third and fourth generations, are the leading ones in the Aduy massif [2].

Banded texture of migmatites with a thickness of individual layers not more than 2-3 cm indicates that on the whole, movement of the anatectic melt was limited by a small distance and controlled by shear thrust determining the type of banded texture. As the leucosome composition approaches to the granite one, forms of its isolation more and more resemble the vein, and the rock gets the features of intruded rocks; in particular, its limits intersect the direction of migmatites banding. Granites form clear veins in banded migmatites and by chemical composition are similar to the granites of the southern and eastern parts of Aduy massif.

Granites of western part of the Aduy massif are formed, apparently, as a result of partial melting and migmatization of Krutiha massif. The massif is located in the village of Krutiha, 58 km from Ekaterinburg. Here in the career, quartz diorites and products of their partial melting - gray, fine-grained granites and intruding them coarse-grained pink granites, are disclosed. The quartz diorites representing protolith of fine-grained granites form steeply dipping bodies intruded by numerous granite veins of low-angle and steep bedding forming a migmatite – like structure. Contacts of the veins with quartz diorites are both sharp and gradual. Veins contain numerous diorite and granodiorite xenoliths, granitizated in varying degrees. The quartz diorites and enclosing them fine-grained granites (ie migmatites) are intruded by a quartz diorite sinplutonic dyke, which in turn is divided into a number of blocks, separated by the fine-grained granites, similar to those that are associated with quartz diorites and are intruded by dike itself. These ratios are typical for intra- intruzive dikes intruding into not fully hardened rocks.

Considered rocks form a unified trend on diagram Ab-Qz-Or (Fig. 2), built on mezonormam rock in which dark minerals are not pyroxene, but biotite and amphibole. The trend is characterized by approximately the same Ab-Qz ratio close to that in the corresponding eutectic at P_{H2O} 2-3 kbar. Quartz diorites are located in the part of the trend, which is adjacent to the Ab-Qz edge of the triangle, and the Aduy massif granites finish the trend. This situation is caused by the predominance of biotite in quartz diorites, which is the main carrier of potassium. Mineralogy and resulting characteristics of rock chemical composition (in particular, composition of quartz-plagioclase cotectic that contains more quartz than quartz - K-feldspar cotectic) are caused, apparently, a by reduced water pressure and an elevated process temperature, respectively. Most of the potassium in quartz diorites and granodiorites of Kamensk massif concentrate in K-feldspar, and this is due to by their different position on the diagram (Fig. 2). Fine-grained and coarse-grained krutiha granites are located in the central part of this trend together with western part of Aduy massif granites. In accordance with the foregoing geological observations, such a configuration of the trend suggests that the granites of the Aduy massif are formed by melting diorite protolith at higher temperatures and low water pressure compared to Kamensk massif.

References:

1. Fershtater G.B. Paleozoic intrusive magmatism of the Middle and South Urals. Ekaterinburg, IGG of UB of RAS, 2013. 365 p.
2. Krasnobaev A.A., Fershtater G.B., Bea F., Montero P. Polygenic zircons of Aduy batholith (The Central Urals) // Proceedings Russian Academy of Sciences, 2006b. T. 410, №2. P. 244-249.

Illustrations

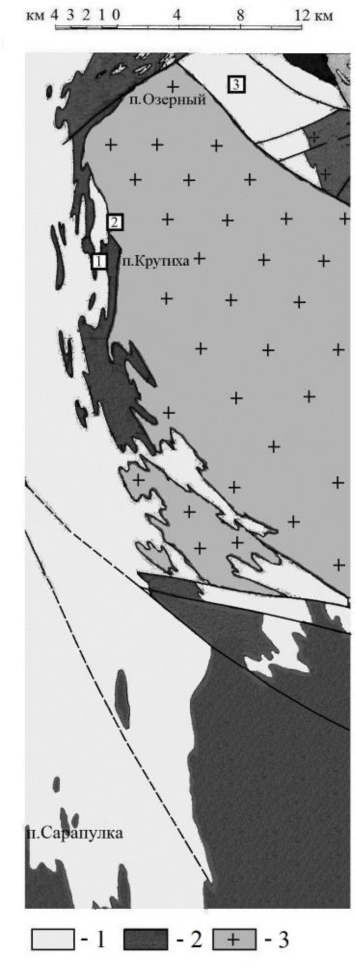

Fig. 1 Scheme of the geological structure of the Aduy massif area. It compiled on the basis of geological maps of the Urals, ed. VV Shalaginov, 1983.
1 - middle- upper Riphean (?). Crystalline schists and biotite, biotite-hornblende, hornblende plagiogneisses amphibolites, quartzites, marbles. 2 - biotite, orthoclase, antiperthitic granites. 3 - two – mica orthoclase-microcline granites. Squares: 1 - Quarry Krutiha, 2 - granitoids of the Western exocontact of Aduy massif, 3 - Quarry Village Lake.

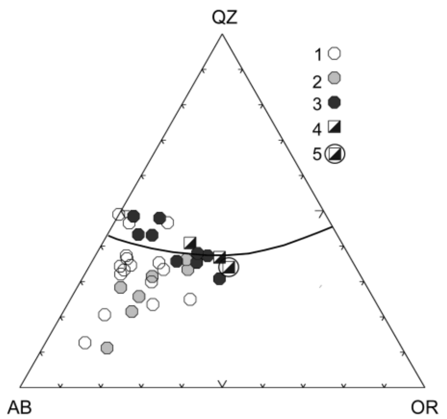

Fig.2 Ab-Qz-Or diagram for CIPW mezofarm rocks of the Kamensk and Aduy massifs.
1 – migmatite of the Kamensk massif, 2 - massive rock of the Kamensk massif, 3 - The Krutiha rock quarry, 4 - granites of the western part of the Aduy massif, 5 - average composition of the Aduy massif granite.

Carbon isotopes in the Earth

Cartigny P.
Institut de Physique du Globe de Paris
cartigny@ipgp.fr

Primarily on the basis of C (but including also N, S, and O) stable isotope systematics, we will review recent achievements in understanding diamond formation and growth in Earth's mantle.

Diamond is a metasomatic mineral that results from either the reduction or oxidation (with associated C-isotope fractionation) of mobile C-bearing liquids (fluids or melts) that intrude preexisting lithologies (eclogites, peridotites, and metamorphic rocks). This process seems ubiquitous, as it occurs over a large range of depths and extends through time.

Diamond-forming carbon derives mainly from the convective asthenosphere. Most of its isotopic *anomalies* reflect fractionation processes in the lithospheric mantle, which are attributed to diamond precipitation itself and/or a mineralogical control occurring prior to diamond precipitation. Evidence for a mineralogical control would be the decoupling of the 15N/14N ratios in eclogitic diamond from other tracers of subduction in inclusions in the same diamond.

C-isotope anomalies related to subduction are rare and are probably best seen in diamonds from the transition zone.

Geochemistry of Carbon, Oil and Diamond.

E.M.Galimov
V.I.Vernadsky Institute of geochemistry and analytical chemistry, Russian Academy of sciences, Moscow, Russia.
galimov@geokhi.ru

Geochemistry of carbon is a broad scientific discipline covering such different fields as, oil and diamond. I will talk about Precambrian oil and cavitational diamond.

Occurrences of oil and gas in ancient Precambrian deposits have been discovered in many parts of the world. In East Siberia the major petroleum occurrences are related to the Lena-Tunguska petroleum province, which occupies almost entire East Siberian platform. The whole hydrocarbon potential is estimated to be about 20 trillion m3 for gas and more than 5 bln ton for oil. The question arises what is origin of such huge amount of hydrocarbons occurring in ancient Precambrian rocks that was not even expected few decades ago. Precambrian hydrocarbons in East Siberia have some peculiar geochemical features, which shed light to the origin of the petroleum accumulations. Overwhelming majority of the petroleum fields in the Lena-Tunguska province are gas-condensate accumulations. Carbon isotope composition of oils varies mostly in the δ13C-range from -33 to -36‰. They are significantly isotopically lighter when compared to oils in the Phanerozoic deposits. The peculiar hydrocarbon chemistry and unusual carbon isotope composition, for a few exceptions, are characteristics of the Precambrian oils from different parts of the world as well.

The phenomenon of unusual enrichment of organic matter in the light isotope in Precambrian deposits was first reported in our work with A.B.Ronov and A.A.Migdisov of 1973, owing to the isotope study of the unique Ronov's sample

collection. Organic matter, lighter than - 35‰, occurred only in Precambrian. In the same work carbonates unusually enriched in the heavy isotope were first to be discovered. Carbonates enriched up to +8 to +10‰ of δ13C-values have been found only in the Precambrian. Later the phenomenon of the enrichment of Precambrian carbonates in heavy carbon isotope confirmed by M.Shidlovski (1975) and many researchers: Veizer, Melezhik and other. We argued that variations of the carbon isotope composition are correlated with periods of tectonic activity.

In general the bio productivity is limited by availability of nutrients, first of all – phosphorus. Volcanism is a source of nutrients. Increase of inflow of nutrients increases bio-productivity, and, in turn, increases the flow of organic carbon to the bottom. It leads to anoxic conditions. As a result organic material of the bacterial origin enriched in the light carbon isotope (12C) is deposited in the layers of the Precambrian. This explains specific isotope and the hydrocarbon composition of the Precambrian oils.

Removing of organic carbon in the Precambrian was apparently huge. This reflected in the anomalous enrichment of carbonate carbon in the heavy isotope. And this may result in catastrophic decrease of concentration of CO2 in the atmosphere. Many authors (Halverson et al,2006; Khabarov and Izokh, 2014; Pokrovski et al, 2014) relate periods of 13C - carbonate deposition to periods of a glaciation.

Thus I conclude that proliferation of the biosphere in periods of volcanic activity resulted in accumulation of great amount of bacterial type of organic matter and subsequent hydrocarbon generation. And the same phenomenon was a cause of CO_2 outflow from atmosphere and triggering glaciation.

The next narrative is about diamond. This story dates back to the late 1960's or early 1970's, when we began studying carbon isotope composition of diamonds from just discovered at that time Siberian kimberlite deposits. We had measured $\delta^{13}C$-values of more than eight hundreds diamond crystals. We have found a broad range of $\delta^{13}C$ variation. This suggested that diamonds do not originate from a homogeneous source.

Existence of the diamonds enriched in the light isotope created a question about their carbon source, in particular under condition of lower pressure and carbon concentration. I suggested that cavitation is an appropriate mechanism.

Experimentally cavitation diamonds were first to be obtained by excitation of cavitation in a carbon-containing liquid (benzine). Then diamond has been synthesized from different liquids, including toluene and ethanol. Different liquids yield diamonds of different shape and size. Recently microcrystalline diamonds have been discovered in products of eruption of volcano Tolbachik in Kamchatka. We attribute genesis of these microdiamonds from lava and ash of Tolbachik volcano eruption to phenomenon of cavitation. The assumption of cavitation mechanism of diamond synthesis allows a plausible explanation for a number of hard-interpreted geochemical features of the Tolbachik's diamond formation. The diamonds were discovered in the porous fluidized lava, but absent in the dense lava of the same mineral composition. The diamonds occurred only in the first explosive portion of the lava and in the pyroclastic material ejected with great speed that is evidence of the active role of a fluid dynamics in formation of the Tolbachik's diamonds. We have measured the $\delta^{13}C$ values of the diamond and in the dispersed carbon in lava and ash. Their isotopic compositions are coincide. It is likely that the dispersed carbon played the role of a substrate for formation of diamond in the process of cavitation in the Tolbachik's conditions.

This mechanism, in our opinion, has general significance. It may provide explanation of origin of so-called non-traditional diamonds described in situations where sources of high pressure are invisible.

Thus, the discovered cavitation mechanism may produce diamond in nature and may be used in technology.

VANADATE GARNETS FROM OLD METALLURGICAL SLAGS OF LAVRION, GREECE: SOLID SOLUTIONS AND CRYSTAL STRUCTURE

N. N. Koshlyakova[1], N. V. Zubkova[1], I. V. Pekov[1], G. Giester[2], D. Yu. Pushcharovsky[1], N. V. Chukanov[3], P. Voudouris[4], A. Magganas[4], A. Katerinopoulos[4]

1 Faculty of Geology, Moscow State University, Vorob'evy Gory, GSP-2, Moscow, 119991, Russia. e-mail: nkoshlyakova@gmail.com

2 Institute of Mineralogy and Crystallography, University of Vienna, Althanstrasse 14 (UZA 2), A-1090 Vienna, Austria.

3 Institute of Problems of Chemical Physics, Chernogolovka, Moscow Region, 142432, Russia.

4 Dept. of Mineralogy and Petrology, Faculty of Geology and Geoenvironment, National and Kapodistrian University of Athens, Panepistimioupolis 15784 Athens, Greece.

Majority of compounds with the garnet-type structure are cubic, space group *Ia*3*d*. This structure type is characterized by three cation sites, *X*, *Y*, and *Z*, and an anion site *O*; the crystal structure is based upon alternating isolated ZO_4 tetrahedra and YO_6 octahedra which share corners to form a three-dimensional framework. Extra-framework cavities contain the *X* cations. The generalized formula of garnets is $\{X_3\}[Y_2]\ (Z_3)O_{12}$ (Z = 8). The current IMA-accepted nomenclature of garnet–supergroup minerals was published by Grew et al. (2013).

The dodecahedral *X* position in garnet-type vanadates is known to be occupied by Li^+, Na^+, K^+, Cu^+, Ag^+, Tl^+, Ca^{2+}, Mn^{2+}, Sr^{2+}, Cd^{2+}, Pb^{2+}, Y^{3+}, Pr-Lu^{3+}, Bi^{3+} and vacancies and the octahedral *Y* position by Li^+, Na^+, Mg^{2+}, Ca^{2+}, Mn^{2+}, Co^{2+}, Ni^{2+}, Cu^{2+}, Zn^{2+}, Cd^{2+}, Al^{3+}, Sc^{3+}, V^{3+}, Cr^{3+}, Fe^{3+}, Ga^{3+}, In^{3+}, and vacancies. Reviews on crystal chemistry and isomorphous substitutions in vanadate garnets were presented by Ronniger & Mill (1971), Mill & Ronniger (1973), Neurgaonkar & Hummel (1975), and Iishi & Ikuta (2006). Only two natural vanadate garnets are known: palenzonaite $\{Ca_2Na\}[Mn^{2+}_2](V^{5+}_3)O_{12}$ (Basso 1987) and schäferite $\{Ca_2Na\}[Mg_2](V^{5+}_3)O_{12}$ (Krause et al. 1999). This paper reports new data on the chemistry and crystal structure of anthropogenic vanadate garnets found in old metallurgical slags near the village of Agios Konstantinos (formerly Kamariza), Lavrion district, Attica, Greece.

Vanadate garnets in the slags occur as well-shaped crystals with different colours: brown, greenish or reddish brown, dark brown to almost black, or, rarely, brownish red. Crystals formed by the {211} faces are up to 2 mm in size. Vanadate garnets are associated with anthropogenic counterparts of olivine belonging to the forsterite–liebenbergite series, trevorite, albite, nosean, haüyne, bannermanite, and other vanadates, silicates and oxides.

The crystal structures of two crystals with different Mg:Ni ratio were studied. Both crystals are cubic, *Ia*3*d*. Unit cell data are: a = 12.388(3) Å, V = 1901.1(14) $Å^3$ for crystal (*1*) and a = 12.387(3) Å V = 1900.6(14) $Å^3$ for (*2*). Final R values are 0.0245 for (*1*) and 0.0237 for (*2*). Due to significant chemical variations, site occupancies for *X* and *Y* were determined mainly based on the structural data, the *R* value was taken as the main criterion with allowances made for electrical neutrality of the formula, refined numbers of electrons and thermal displacement parameters. The formulae are:

(*1*) greenish-brown garnet: $\{Na_{1.5}Ca_{1.5}\}_{\Sigma3}[Mg_{1.1}Fe^{3+}_{0.5}Ni_{0.4}]_{\Sigma2}(V_{2.8}P_{0.2})_{\Sigma3}O_{12}$

(*2*) reddish-brown garnet: $\{Ca_{1.7}Na_{1.3}\}_{\Sigma3}[Ni_{1.0}Mg_{0.7}Fe^{3+}_{0.3}]_{\Sigma2}(V_{2.8}P_{0.2})_{\Sigma3}O_{12}$

Chemical composition was determined by electron microprobe analysis and the empirical formulae were calculated on the basis of 12 O atoms per formula unit (*apfu*). Cation distribution was assumed taking into account the results of structure refinement. Na and Ca occupy the *X* site, Mg, Fe^{3+}, Ni^{2+}, Zn, Al, Mn, Ti and Cu are located in *Y* and V, P, Si and S in *Z*.

The content of Na in the studied garnets varies between 0.9 and 2.0 *apfu* and the content of Ca is between 2.1 and 1.0 *apfu* (Fig. 1). The *Z* site is mainly occupied by V, with P admixture up to 0.4 *apfu*, Si up to 0.2 *apfu* and S <0.01 *apfu*. Mg, Ni and Fe^{3+} are the main cations occupying the *Y* position. The Mg content ranges between 0.4 and 1.2 *apfu*, Fe between 0.0 and 0.8 *apfu* and Ni between 0.1 and 1.5 *apfu* while the sum of other *Y*-components does not exceed 0.2 *apfu*.

The studied vanadate garnets belong to a solid-solution system lying between three major end-member components: $\{NaCa_2\}Mg_2(VO_4)_3$ (schäferite), $\{NaCa_2\}Ni^{2+}_2(VO_4)_3$ and $Na_3Fe^{3+}_2(VO_4)_3$ (Fig. 2). Such system was not reported in literature for synthetic vanadates although the compounds $\{NaCa_2\}Ni_2(VO_4)_3$ and $\{NaCa_2\}Mg_2(VO_4)_3$ were synthesized and reported by several authors (Bayer 1965, Mill & Ronniger 1973, Iishi & Ikuta 2006, etc.). The existence of a vanadate garnet of $Na_3M^{3+}_2(VO_4)_3$-type was reliably proven only for the relatively large M^{3+} cation Sc (Mill & Ronniger 1973, Belokoneva et al., 1974). Iishi & Ikuta (2006) mention the synthesis of $Na_3Fe^{3+}_2(VO_4)_3$ but do not report the synthesis conditions and crystal data for this phase. However, the Fe^{3+} cations may occupy at least a half of octahedral *Y* sites: Mill & Ronniger (1973) have synthesized two Fe^{3+}-bearing vanadate garnets related to schäferite, namely yellowish orange $\{Na_{1.5}Ca_{1.5}\}[Mg_{1.5}Fe^{3+}_{0.5}](VO_4)_3$ (a = 12.422 Å) and orange-brown $\{Na_2Ca\}[MgFe^{3+}](VO_4)_3$ (a = 12.409 Å) and Iishi & Ikuta (2006) synthesized $\{Na_2Ca\}[NiFe^{3+}](VO_4)_3$ (a = 12.386 Å).

In the studied vanadate garnets from Lavrion, the Fe^{3+} content reaches 0.8 *apfu* that corresponds to 40% of *Y* cations. The Ni content in *Y* ranges between 6 and 75 at.%, and that of Mg is between 20 and 60 at.%. Mg and Fe exhibit a positive correlation (Fig. 2).

In the *X* site the Na:Ca ratio correlates with the Fe^{3+} content in the *Y* site. The main scheme of heterovalent isomorphous substitutions in these compounds is $Na^{+} + Fe^{3+} \leftrightarrow Ca^{2+} + M^{2+}$, where M^{2+} = Mg, Ni. Thus, the generalized formula of these garnets can be written as $\{Na_{1+x}Ca_{2-x}\}[Fe^{3+}_{x}M^{2+}_{2-x}](VO_4)_3$.

V^{5+} strongly prevails in the *Z* site. The main admixtures are P^{5+} and Si^{4+} (in average 0.2 *apfu* each). Substitution of V^{5+} for P^{5+} and Si^{4+} is known in natural vanadate garnets: schäferite from Bellerberg contains 0.02 *apfu* P and 0.01 *apfu* Si (Krause et al. 1999). Palenzonaite described by Basso (1987) and Nagashima & Armbruster (2012) contains up to 0.3 *apfu* Si.

This study was supported by the Russian Foundation for Basic Research, grants nos. 15-05-02051 and 14-05-00276-a (crystal chemical analysis and chemical data), and by the Foundation of the President of the Russian Federation, grant no. NSh-1130.2014.5 (crystal structure refinement and XRD analysis).

References:

Basso, R. (1987): (Northern Apennines, Italy). – Neues Jahrb. Mineral., Monatsh., **3**: 136-144.

Bayer, G. (1965): Vanadates $A_3B_2V_3O_{12}$ with garnet structure. – J. Am. Ceram. Soc., **48**(11): 600-600

Belokoneva, E. L., Mill, B. V., Simonov, M. A. & Belov, I. V. (1974): Refinement of the crystal structure of vanadate garnet $Na_2Sc_3V_3O_{12}$. – Kristallografiya, **19**: 374-375 (in Russian).

Grew, E. S., Locock, A. J., Mills, S. J., Galuskina, I. O., Galuskin, E. V. & Hålenius, U. (2013): Nomenclature of the garnet supergroup. – Am. Mineral., **98**(4): 785-811.

Iishi, K. & Ikuta, Y. (2006): Isomorphous substitutions in vanadate garnets. – N. Jb. Miner. Abh., **182**(2): 157-163.

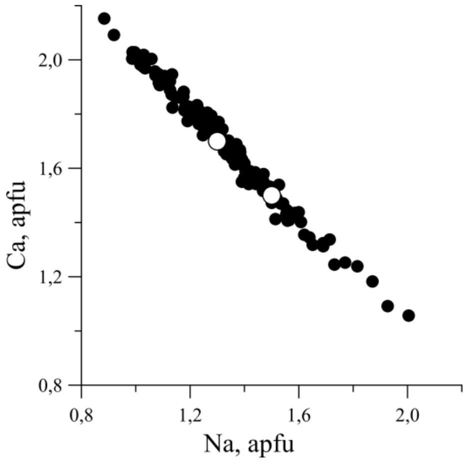

Fig.1 *X* site content of vanadate garnets from Lavrion

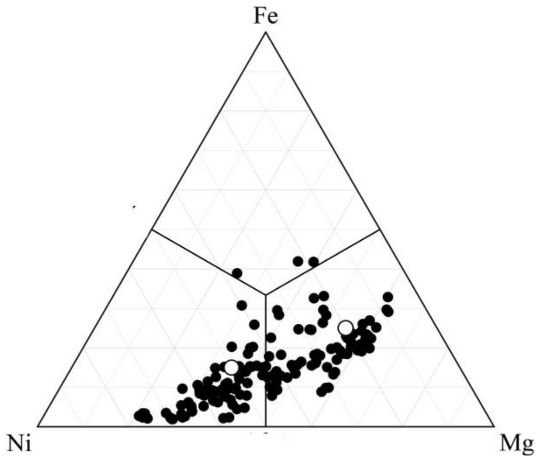

Fig. 2 *Y* site content of vanadate garnets from Lavrion

Krause, W., Blass, G. & Effenberger, H. (1999): Schäferite, a new vanadium garnet from the Bellberg volcano, Eifel, Germany. – Neues Jahrb. Mineral., Monatsh., **3**, 123-134.

Mill, B. & Ronniger, G. (1973): Vanadates with garnet structure. – Physics and Chemistry of Ferrites: 98-115 (in Russian).

Neurgaonkar, R. R., & Hummel, F. A. (1975): Substitutions in vanadate garnets. – Mater. Res. Bull., **10**(1): 51-55.

Ronniger, G.& Mill B. V. (1971): New vanadates with garnet structure. – Kristallografiya, **16**: 1035 (in Russian).

Научное издание

Московская международная школа по наукам о Земле – 2016

Тезисы международной конференции, 23-18 мая 2016 г.

Москва, издательство «ГЕОХИ РАН», 2016

На английском языке

Scientific edition

Moscow International School of Earth Sciences - 2016.

Abstracts of International conference. 23-28 May 2016

Moscow, “GEOKHI RAS”, 2016

Editor-in-chief Academician L.N. Kogarko.

Art editor V.E. Kulikovsky.
Technical editor I.P. Petrov.
Proofreaders V.N. Ermolaeva, N.V. Sorokhtina, V.A. Zaitsev.

Typesetting:
V.I.Vernadsky Institute of Geochemistry and Analytical Chemistry of RAS
(GEOKHI RAS)

Signed to print 10.05.2016
Format of 60x84/8
Offset paper. Headset "Times." Conv. pr. sh. 15.8.
Pressrun 150 copies.
Order № 16-1

Printing: V.I.Vernadsky Institute of Geochemistry and Analytical Chemistry of RAS
(GEOKHI RAS)
Kosygin Street, 19, 119991, Moscow, Russian Federation.